Ph. D. Thesis

NIRMALYA KUMAR CHAKI

June 2005

SYNTHESIS, CHARACTERIZATION AND ELECTROCHEMICAL STUDIES OF METAL NANOCLUSTERS AND THEIR POSSIBLE APPLICATIONS

NIRMALYA KUMAR CHAKI

PHYSICAL AND MATERIALS CHEMISTRY DIVISION

NATIONAL CHEMICAL LABORATORY

PUNE – 411 008

INDIA

June 2005

SYNTHESIS, CHARACTERIZATION AND ELECTROCHEMICAL STUDIES OF METAL NANOCLUSTERS AND THEIR POSSIBLE APPLICATIONS

A THESIS

SUBMITTED TO THE

UNIVERSITY OF PUNE

FOR THE DEGREE OF

DOCTOR OF PHILOSOPHY

IN

CHEMISTRY

BY

NIRMALYA KUMAR CHAKI

PHYSICAL AND MATERIALS CHEMISTRY DIVISION

NATIONAL CHEMICAL LABORATORY

PUNE – 411 008

INDIA

June 2005

Dedicated To

My Parents. . .

DECLARATION

I hereby declare that the thesis entitled "**SYNTHESIS, CHARACTERIZATION AND ELECTROCHEMICAL STUDIES OF METAL NANOCLUSTERS AND THEIR POSSIBLE APPLICATIONS**" submitted for the degree of Doctor of Philosophy in Chemistry to the University of Pune has been carried out by me at Physical and Materials Chemistry Division, National Chemical Laboratory, Pune, 411008, India, under the supervision of Dr. K. Vijayamohanan. The work is original and has not been submitted in part or full by me for any degree or diploma to this or any other University.

Date: **NIRMALYA KUMAR CHAKI**

Physical and Materials Chemistry Division
National Chemical Laboratory
Pune – 411 008

Dr. K. Vijayamohanan
Scientist

Physical and Materials
Chemistry Division
National Chemical Laboratory
Pune – 411008
INDIA

Tel: 91-020-25893300
Extn: 2270/2276
Res: 91-020-25893307
Fax: 91-020-25893044
Email: vk.pillai@ncl.res.in

CERTIFICATE

This is to certify that the work incorporated in the thesis "**SYNTHESIS, CHARACTERIZATION AND ELECTROCHEMICAL STUDIES OF METAL NANOCLUSTERS AND THEIR POSSIBLE APPLICATIONS**" submitted by **NIRMALYA KUMAR CHAKI** was carried out by him under my supervision at Physical and Materials Chemistry Division, National Chemical Laboratory, Pune, 411008, India. All the materials from other sources have been duly acknowledged in the thesis.

Date :
Place : Pune

Dr. K. Vijayamohanan
(Research Guide)

Acknowledgements

There are so many people, whose support, encouragement and inspiration are very much obligatory to accomplish major achievements in life, especially, if it involves elements of fulfilling one's cherish dreams. For me, this thesis is such an important destiny and I am indeed indebted to lot of people for their well wishes and blessings for completing this journey. A sense of appreciation automatically comes into mind at this stage to show my sincere gratitude to all of them, who played a pivotal role and without whom this thesis would not have been possible.

I would like to take this opportunity to pay first my sincere admiration to Dr. K. Vijayamohanan, whose motivation, guidance, inspiration, advice and encouragement have lead me to bring my dream to reality. He has not only introduced me to my research problem, but taught too many other exciting areas and subjects, sometimes more than science. His knowledge is like an ever-expanding encyclopedia, which has all possible answers to help me out of any problem. In this respect, I must mention that he is also a very good teacher and a wonderful research guide, which is often quite rare. I am very much privileged to work under his esteemed guidance. Last but not least, he is a very good human being, whose life's sole motto is to help others, this automatically makes him as my Idol.

I would also like to offer my sincere admiration to Dr. I. S. Mulla for all his help, support and advice during the course of my research as he is like our family member, who is always very kind and considerate.

It gives me great pleasure to thank Prof. C. V. Dharmadhikari, from the Department of Physics, University of Pune and Dr. C. Ramesh from the Polymer Science and Engineering Chemistry Division, NCL, for their invaluable suggestions and making all the lab facilities available to perform certain crucial experiments. Special thanks to both Ms. Poonam Singh and Dr. E. Boje Gowd for their help to accomplish such experiments. I also would like to thank Dr. S. K. Haram from the Department of Chemistry, University of Pune, for his help, advice, and encouragement.

I wish to thank Dr. S. Sivaram, the Director, NCL for providing me the infrastructural facilities and CSIR for financial support. I am also grateful to Dr. P. Ganguly, Dr. S. K. Date and Dr. S. Pal, former and present heads of Physical and Materials Chemistry Division for allowing me to use all the available facilities in the division and for their constant encouragement.

My heartfelt gratitude to Drs. Anil Kumar, P. A. Joy, Murali Sastry, B. L. V. Prasad, Prakash Ghosh, V. Ravi and K. Shreedhar for their advice and help. I am also highly indebted to

Drs. Sainkar, Mandale, Mohan Bhadbhade, Mrs. Renu Pasricha and Mr. A. Gaikwad, who were very helpful during my doctoral work for characterizing my samples. Timely help from Mr. Koshy, Mr. Dipak and Mr. Punekar and the entire library staff for excellent facilities are gratefully acknowledged. I also take this opportunity to thank glass blowing, stores, purchase, workshop and administrative groups for their support during my study.

I can never forget the help from my seniors, Drs. Varsha, Sudrik, Sushama and Aslam for their mentoring during my initial research days. A special thanks to all my labmates, Jadab, Niranjan, Trupti, Gopu, Girish, Deepali, Bhalu, Mahima, Mandar, Mukta, Kannan, Meera, Vivek, Mrudula, Praveen, Sugapriya and Murugan, who created a pleasant atmosphere to work truly in a group. I thank again Dr. Vijayamohanan for his constant efforts to imbue us with several most essential habits, like weekly seminars and group meetings, monthly reports and daily planning, which make me now confident to start an independent scientific carrier.

I wish to thank all my fellow colleagues in my division, Saikat, Kannan, Joly, Anand, Ashavani, Rohini, Suvarna, Sanjay, Sumant, Deka, Shekhar, Anita, Shankar, Debu are few among them. I would like to extend my thanks to several other friends in NCL, Easwar, Sambhaji, Subramaniyam, Subbu, Pai, Amit, Dhananjoy, Gadai, Bibhash, Roopa, Suman, Ghota, Dinuda, Prabalda, Sidhuda, Debdutda, Smiritidi, Mukul, Chanchal, Chinmoy, Soumitra, Prabhas, Pradeep, Sugata, Nilanjan. My sincere appreciation to Senapati, Tickla, Nupur, Amrita, Ranjanda and my other friends for making my stay at NCL a very comfortable and memorable one.

I find no words to express my feelings for my parents and my younger brother 'Babai', whose moral support, love and constant encouragements have helped me to complete this journey. Their patience and sacrifice were always a main source of my inspiration and will remain throughout my life, motivating me to pursue higher goals. I wish to extend my sincere gratitude to my grand mothers, grand fathers, uncles, aunties, cousins and all other relatives for their blessings.

My thesis is also a culmination of a dream for my late mother-in-law, who had a very noble soul and always encouraged everyone for higher studies. I also extend my sincere appreciation to my father-in-law, dada, boudi and little 'Pukki Bui' for their love, constant encouragement and timely help.

Finally, heartfelt thanks to my wife Nabanita, without whose constant support and inspiration this would never have been possible.

The thesis would be useful, if my efforts are ever be of any use for the welfare of mankind and the advancement of science.

Nirmalya Kumar Chaki

List of Abbreviations

Abbreviation	Expansion
2D	Two-Dimensional
3D	Three-Dimensional
AC	Alternating Current
AFM	Atomic Force Microscope
BE	Binding Energy
bcc	Body Centered Cubic
CE	Capillary Electrophoresis
CMOS	Complementary Metal Oxide Semiconductor
CNLS	Complex Nonlinear Least Square
CV	Cyclic Voltammetry
DBTJ	Double Barrier Tunnel Junction
DDAB	Dodecyldimethylammoniumbromide
DDT	Dodecanethiol
DLVO	Derjaguin-Landau-Verwey-Overbeek
DPV	Differential Pulse Voltammetry
DSC	Differential Scanning Calorimetry
ECL	Electrochemiluminescence
EELS	Electron Energy Loss Spectroscopy
PZC	Potential of Zero Charge
ET	Electron Transfer
fcc	Faced Centered Cubic
FET	Field-Effect Transistors
FTIR	Fourier Transform Infrared
FWHM	Full Width at Half Maximum
GMR	Giant Magnetoresistance
hcp	Hexagonal Closed Packed
HOMO	Highest Occupied Molecular Orbital

HOPG	Highly Oriented Pyrolytic Graphite
HPLC	High-Pressure Liquid Chromatography
HREELS	High-Resolution Electron Energy Loss Spectroscopy
HRSEC	High-Resolution Size Exclusion Chromatography
HRTEM	High-Resolution Transmission Electron Microscopy
IEC	Ion Exchange Chromatography
K	Kelvin
LB	Langmuir Blodgett
LFM	Lateral Force Microscope
LRRT	Long Range Resonant Energy Transfer
LUMO	Lowest Unoccupied Molecular Orbital
MEMS/NEMS	Micro/Nano-Electromechanical Systems
MFM	Magnetic Force Microscope
MIM	Metal-Insulator-Metal
MINIM	Metal–Insulator–Nanocluster–Insulator–Bulk Metal
MIS	Metal-Insulator-Semiconductor
MIT	Metal-to-Insulator Transition
MOSFET	Metal Oxide Semiconductor Field-Effect Transistor
MPCs	Monolayer Protected Nanoclusters
MR	Magnetic Resonance
MRFM	Magnetic Resonance Force Microscope
MRI	Magnetic Resonance Imaging
NHE	Normal Hydrogen Electrode
NLO	Nonlinear Optical
NMR	Nuclear Magnetic Resonance
NSOM	Near-field Scanning Optical Microscope
OCP	Open Circuit Potential
QDL	Quantized Double Layer Charging
Q-dots	Quantum Dots
QTM	Quantum Tunneling of Magnetization
SAED	Selected Area Electron Diffraction
SAM	Self-assembled Monolayer
SAXS	Small Angle X-ray Scattering

SCE	Saturated Calomel Electrode
SEC	Size Exclusion Chromatography
SECM	Scanning Electrochemical Microscopy
SET	Single-Electron Transistors
SIMS	Secondary Ion Mass Spectroscopy
SPM	Scanning Probe Microscope
SPR	Surface Plasmon Resonance
SPS	Surface Plasmon Spectroscopy
STM	Scanning Tunnelling Microscope
STS	Scanning Tunnelling Spectroscopy
TBAHFP	Tetrabutylammoniumhexaflurophosphate
TDA	Tridecylamine
TEA	Triethylamine
TEM	Transmission Electron Microscopy
TG	Thermogravimetry
TOAB	Tetraoctylammoniumbromide
TOP	Trioctylphosphine
TOPO	Trioctylphosphineoxide
VRH	Variable Range Hopping
XANES	X-ray Absorption Near-Edge Structure
XPS	X-ray Photoelectron Spectroscopy
XRD	X-ray Diffraction

Table of Contents

Chapter 1

Synthesis, Characterization, Properties and Applications of Monolayer Protected Metallic Nanoclusters *1-71*

1.1	Introduction	2
1.2	What is Nanoscience and Nanotechnology?	5
1.3	Why and How Properties Change in Reduced Dimensions?	7
1.4	Monolayer Protected Metallic Nanoclusters	15
1.5	History	15
1.6	Preparation Procedures	16
1.6.1	Brust's Synthesis	16
1.6.2	Synthesis in Reverse Micelles	18
1.6.3	Other Methods	19
1.7	Purification and Size Tuning	19
1.7.1	Solvent Extraction	20
1.7.2	Chromatography	20
1.7.3	Digestive Ripening	21
1.8	Characterization	21
1.8.1	UV-visible Spectroscopy	22
1.8.2	X-ray Diffraction (XRD)	23
1.8.3	Transmission Electron Microscopy (TEM)	23
1.8.4	Fourier Transform Infrared Spectroscopy (FTIR)	24
1.8.5	X-ray Photoelectron Spectroscopy (XPS)	25
1.8.6	Nuclear Magnetic Resonance (NMR)	25
1.8.7	Thermogravimetry/Differential Scanning Calorimetry (TG/DSC)	26
1.8.8	Scanning Probe Microscopes (SPM)	26
1.8.9	Electroanalytical Techniques	28
1.8.10	Other Characterization Techniques	29
1.9	Salient Features of MPCs	29
1.9.1	Core of MPCs	29
1.9.2	Capping Monolayer of MPCs	30
1.9.2.1	Functionality and Length Scale Control: Tailoring Property	31
1.9.2.2	Place Exchange Strategy: Control of ω-Functionality	32
1.10	Organization of MPCs	32
1.11	Properties	34
1.11.1	Optical Properties	34
1.11.2	Electronic Properties	35
1.11.3	Magnetic Properties	36
1.11.4	Electrochemical Properties	36
1.11.5	Other Properties	38

1.12	Applications of MPCs	39
1.12.1	Novel Optical Devices	39
1.12.2	Miniaturized Electronic Devices	40
1.12.3	Medical Diagnostics and Sensors	42
1.12.4	Other Applications	43
1.13	Conclusions and Perspectives	43
1.14	Motivation, Scope and Organization of the Thesis	44
1.15	Objective of the Present Study	44
1.16	References	49

Chapter 2

72-103

Synthesis and Characterization of Monolayer Protected Gold Nanoclusters: Temperature Effect on Au Nanoparticles Superstructures

2.1	Introduction	73
2.2	Experimental Section	75
2.2.1	Materials	75
2.2.2	Size Selective Synthesis of Au MPCs	75
2.2.3	Techniques Used for the Characterization of MPCs	77
2.2.3.1	UV-visible Spectroscopic Analysis	77
2.2.3.2	Transmission Electron Microscopic (TEM) Analysis	77
2.2.3.3	(a) X-ray Diffraction (XRD) Analysis *(b) In-situ* Temperature Controlled XRD Analysis	77
2.2.3.4	Nuclear Magnetic Resonance (NMR) Analysis	78
2.2.3.5	(a) Fourier Transform Infrared Spectroscopic (FTIR) Analysis (b) *In-situ* Temperature Controlled FTIR Analysis	78
2.2.3.6	Thermogravimetric (TG) Analysis	78
2.2.3.7	Differential Scanning Calorimetric (DSC) Analysis	79
2.3	Results for the Characterization of Au MPCs	79
2.3.1	UV-visible Spectroscopic Analysis	79
2.3.2	TEM Analysis	81
2.3.3	XRD Analysis	84
2.3.4	NMR Analysis	85
2.3.5	FTIR Analysis	87
2.4	Effect of Temperature on 3.72 nm Sized Au MPCs Superstructures	89
2.4.1	TEM Analysis	90
2.4.2	*In-situ* XRD and TG-DSC Analysis	91
2.4.3	*In-situ* FTIR Analysis	94
2.5	Discussion	97
2.6	Conclusions	98
2.7	References	100

Chapter 3

104-137

Single Electron Charging Features of Monolayer Protected Gold Clusters

3.1	Introduction	105
3.2	A Simplified Model to Understand the Charging Behaviour in Coulomb Blockade Nanostructure	107
3.3	Experimental Section	110
3.3.1	Materials	110
3.3.2	Synthesis of Au MPCs	111
3.3.3	Scanning Tunneling Microscope/Spectroscopic (STM/STS) Measurements	111
3.3.4	Electrochemical Measurements	111
3.4	Single Electron Charging Features of $Au_{1415}(DDT)_{328}$	112
3.4.1	STM/STS Measurements	112
3.4.2	Electrochemical Behaviour	116
3.4.2.1	Quantized Double Layer Charging	116
3.4.2.2	Adsorption features	129
3.5	Conclusions	134
3.6	References	135

Chapter 4

138-169

Interactions of Charged Monolayer Protected Gold Clusters in Electrolyte Solution

4.1	Introduction	139
4.2	Experimental Section	141
4.2.1	Materials	141
4.2.2	Synthesis of Au MPCs	141
4.2.3	Scanning Tunneling Microscope/Spectroscopic (STM/STS) Measurements	141
4.2.4	Electrochemical Measurements	142
4.3	Single Electron Charging Features of $Au_{2869}(DDT)_{541}$	142
4.3.1	STM/STS Results	143
4.3.2	Voltammetric Results	147
4.4	Interaction of Au MPCs	153
4.4.1	Chronoamperometric Results	155
4.4.2	Impedance Results	157
4.4.3	Effect of Charge Steps on Diffusion Coefficient	164

4.5	Conclusions	166
4.6	References	167

Chapter 5

170-199

Electrochemical Investigation of Monolayer Protected Silver Nanoclusters

5.1	Introduction	171
5.2	Experimental Section	172
5.2.1	Materials	172
5.2.2	Synthesis of Different Sized Ag MPCs	172
5.2.3	Characterization Techniques	173
5.3	Size Dependent Redox Features of Ag MPCs	174
5.3.1	Particle Characterization	174
5.3.2	Electrochemical Measurements	180
5.4	Synthesis of Ag Nanoparticles Using Triethylamine	186
5.4.1	Synthetic Procedure	187
5.4.2	Characterization of Ag Nanoparticles	187
5.4.3	Electrochemical Properties	192
5.5	Conclusions	195
5.6	References	196

Chapter 6

200-205

Conclusions and Future Prospects

List of Publications

206-207

Erratum

208

Chapter 1

Synthesis, Characterization, Properties and Applications of Monolayer Protected Metallic Nanoclusters*

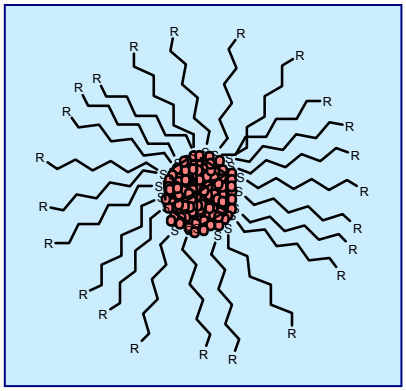

This chapter presents a critical summary of the monolayer protected metallic nanoclusters (MPCs). The scope for these particles in nanotechnology along with several fundamental issues related to their origin and the evolution of size and shape dependent properties at nano scale and their potential applications are discussed. Particular emphasis has been placed on the synthesis, characterization, properties and diverse applications of MPCs of silver and gold. The objective of the present study and abstract of the overall investigation are also mentioned at the end of this chapter.

* A part of the work has been published in "***Encyclopedia of Nanoscience and Nanotechnology (ENN)***: *American Scientific Publishers, Vol. 5*, 861" and another part in "***Proc. Indian Acad. Sci. (Chem. Sci.)*** **2001**, 113, 659".

1.1 Introduction

Science and technology in the upcoming decades is forecasted to be revolutionized based on the knowledge of its ability to create, measure, manipulate and organize matter at the nanoscale — 1 to 100 billionths of a meter, which is expected to have major implications for health, wealth and peace, widely known as nanotechnology.[1,2] The knowledge will be jointly contributed from chemistry, physics, materials science, biology and several branches of engineering, where quantum size effects and other confinement phenomena are expected to be dominated along with other physical laws.[1,2]

The properties of matter change at nano scale and more specifically, they become size and shape dependent at this size regime, often due to their size being equal or smaller than the characteristic length scales that define the physical properties.[3-12] In particular, several interesting quantum (electron confinement,[3] near-field optical effects,[4] quantum entanglement,[5] electron tunneling[6-8] and ballistic transport[9]) or subdomain (superparamagnetism,[10,11] overlapping double layers in fluids[12]) phenomena are observed, which may be absent either in bulk or in molecular systems. These unique size and shape dependent properties of nanometer sized particles render them as potentially important building blocks for nanotechnology.[13,14] Accordingly, several applications, such as solar cells, controlled drug-delivery systems, selective chemical sensors, light emitting diodes, single electron transistors and memory devices, have been demonstrated in the recent past.[13,14]

Size tunable inorganic nanostructures of metallic, semiconducting and insulating materials have been extensively investigated in recent years, while several related nanosized objects, such as dendrimer, carbon nanotubes, polymer nanocomposites and several organic-inorganic hybrid materials, also have drawn considerable importance due to their novel properties.[15,16] Consequently, one of the major themes of present day research is based on our ability to create these building blocks along with the understanding of their properties, so that the manipulation can be carried out at nanoscale in a prerequisite manner.[3-16]

Aside from organizing interesting molecules in low dimensions, development of nanotechnology also necessitates suitable functional units for the fabrication of nanoarchitectures that are several orders of magnitude smaller than presently available lithographically fabricated devices. For example, transistors are one of the most basic electronic components of present day computer chips with feature size of ~200-300 nm, where their numbers get doubled in every two years (Moore' Law) by shrinking their feature size.[17] However, the conventional fabrication techniques, like lithography, do not allow further size reduction as quantum restrictions will interfere with their operation.[18] Interestingly, the recent success of the "Bottom-Up Engineering" approach for creating nanoarchitectures using self-assembly as compared to "Top-Down Engineering" strategy has tempted many of the nanotechnologists to focus more on electronic applications.[19] In particular, the "Bottom-Up Engineering" is suitable for this purpose as it ascertains chemical control on the individual nano/molecular/atomic components.[19]

Self-assembly is the coordinated action of independent functional units under distributed control to produce organized structures or superstructures with certain specific patterns.[20] For instance, widely investigated self-assembled supramolecular systems have been designed for performing electronic operations, like switching, gating, rectification, amplification and this interdisciplinary area is known as molecular electronics.[13,14] Accordingly, the integration of nanosized building blocks in a predefined fashion can also generate novel properties and functions, which may be achieved through the interaction of atom-by-atom, molecule-by-molecule or may be nanostructure-by-nanostructure.[15,21,22] The primary objective is thus to design and synthesize suitable building blocks with novel and potentially useful electronic properties depending on the ability of organic molecules to control the electron flow as elegantly illustrated in several self-assembled systems in biology and chemistry.[13,14,21-23] More specific cases, like a molecular switch using an organic molecule sandwiched between a nanocluster and a gold tip, have been reported recently, with a remarkable ability to tune electron transfer depending upon its redox state.[24] This and several such recent examples have illustrated the potential of chemical tailoring of suitable mesoscopic structures to accomplish the fabrication of ordered arrays of nanoelectrodes and nanoclusters.[13,14, 21-26]

Since the introduction of Brust's method for synthesizing thiol protected gold nanoclusters in 1994, the emerging area of monolayer protected nanoclusters (MPCs) has rapidly become a topic of intense activity in the field of nanotechnology.[26a] This is mainly due to its simplistic approach in achieving size and shape control for a large number of materials with enhanced stability, especially, for a variety of applications.[26,27] More specifically, the monolayer formation provides a unique opportunity to stabilize nanoparticles by isolating them from their environment, where particle growth and agglomeration through different mechanisms, like Ostwald ripening and air oxidation, can be prevented.[26,27] The capping of organic molecules on colloidal particles is comparable with the widely studied self-assembled monolayer (SAM) on flat surfaces, like gold, silver or silicon[23,27] and is often known as three-dimensional (3D) SAM.[26,27] More specifically, the word SAM generally means a monomolecular thick film of organic compounds on two-dimensional substrates due to the strong chemisorption between substrate head group of the desired compounds on the surface, leading to the formation of a thermodynamically stable monolayer.[23,27-31] Apart from enhancing the stability of MPCs, SAM method also provides flexibility to tune the functionality for their manipulation of structure and properties. [26-32]

Self-assembly of similar sized MPCs in crystalline arrays of one, two or three dimensions to form superlattice structures is of particular interest for fundamental and technological importance.[26,32] The characteristic features of such nanoscale architectures, includes size and shape dependent quantum effects, where collective properties often produce interesting phenomena, perhaps vastly different from individual features.[13,14,26,32]. Some of the major advantages of these self-assembled systems arise due to their ability to control interparticle distance, interaction and directional electron transfer arising from the multifunctional nature of organic capping ligands.[13,14,26,32] Further, these systems also provide opportunities to modulate their physicochemical behaviour by controlling the spatial confinement of electrons smaller than the electron delocalization length in bulk materials, generating interesting optical and electronic applications.[13,14,33]

The primary objective of this chapter is to summarize basic aspects of MPCs with their relevant characterization data, properties and applications with special emphasis on

metallic nanoparticles of Au and Ag. A brief description of the promising area of nanoscience and nanotechnology is given in section 1.2 along with their proposed applications and potential limitations. Since fundamental and technological interests of these small particles are due to their size dependent properties, the theoretical basis for such behaviour is discussed in section 1.3. Other sections are devoted to describe few of the recent developments of metallic MPCs for nanotechnological applications. However, an exhaustive description is difficult, since innumerable reports do appear regularly about MPCs and their applications. Major developments of Au and Ag MPCs are mentioned in the text, while few other important contributions are cited in the references. We hope that this brief summary will be helpful to understand the importance of MPCs for future technological developments.

1.2 What is Nanoscience and Nanotechnology?

Nanoscience comprises of manipulating and developing materials at nanoscale level (0.1 to 100 nm) to endow them with novel size dependent properties (e.g. optical, electrical, magnetic and chemical) for diverse set of applications in various fields of science and engineering.[1] Accordingly, ***nanotechnology*** is the technology to generate structures or devices less than 100 nanometers in size for performing complex functionalities using the knowledge of nanoscience and is expected to make a significant impact on the society.[1]

Some of the initial ideas of nanotechnology came from Richard Feynman's lecture in 1959 at the annual meeting of the American Physical Society at California Institute of Technology (Caltech), entitled "*There's Plenty of Room at the Bottom"*, where he discussed the possibilities of the direct manipulation of individual atoms to develop and operate next generation machine tools and so forth.[34] The term *Nanotechnology* was first coined by Norio Taniguchi of Tokyo Science University in 1974 as *"Nano-technology' mainly consists of the processing of separation, consolidation and deformation of materials by one atom or one molecule"* to describe the precise manufacturing of materials with nanometer tolerances,[35] while during 1980s the term was re-invented and expanded by Eric Drexler.[36,37] However, the invention of the Scanning Tunneling Microscope (STM) by Gerd Binnig and Heinrich Rohrer in 1981 at

IBM's Zurich Research Laboratory and the Atomic Force Microscope (AFM) in 1986 by Gerd Binnig, Christoph Gerber and Calvin Quate, made it possible to realize the essence of nanotechnology due to their uncanny ability to image and manipulate matter with atomic level precision.

Some of the benefits of nanotechnology have been exaggerated to include all kinds of amazing applications, like a tiny, yet powerful computers, earthquake resistant building materials, advanced systems for drug delivery and custom-tailored pharmaceuticals as well as the elimination of invasive surgery due to intrinsic repair possibility.[1,2] Nanotechnology is also expected to have considerable impact on the field of miniaturized electronic devices, manufacturing of chemicals, health and energy sectors; as an "one word" to solve all problems of our daily life.[1,2] The transformative and convergent nature of nanotechnology can enrich the existing technologies, like bio or information technologies.[1,2] Accordingly, the nanotechnology is not just a way to have further miniaturization but would lead to a dramatic change in materials, devices and thus, to the society, as defined by Richard Smalley "***Nanotechnology holds the answer, to the extent there are answers, to most of our pressing materials needs in energy, health, communication, transportation, food, water, etc."***.[38]

A new technology is always dangerous in some ways, especially, if adequate precautions are not taken in the beginning itself, like the case of nuclear energy or cloning technology. Since nanotechnology deals with a variety of both living and anthropogenic systems, utmost care must be taken at early stages and at all levels.[39] For example, since reactivity increases at the nanoscale, accordingly the toxicity is also expected to increase, especially, if these materials are confined to living cells or immune systems.[39] Further, the activity of the commonly used materials (non toxic) have to be critically rechecked at nanoscale to avoid their unknown toxicity. A popular endanger of nanotechnology is defined by the "*grey goo",* which introduced by Eric Drexler as the hypothetical end of all life of the world due to the formation of out of control self-replicating robots (*esophagy*) due to nanotechnology;[36] although such worst scenario is possible only in science fiction. Nevertheless, adequate strategies ("*precaution is always better than cure!*") must be applied to scrutinize effects on environment before adopting this new technology for creating a better future. The word "anti-nanotechnology" already

contains some of the growing oppositions to the widespread use of nanotechnology, which obviously helps to formulate regulatory measures for their applications.

1.3 Why and How Properties Change in Reduced Dimensions?

There are numerous reasons why size reduction can in principle, affect behaviour of materials, including catalytic, thermal, mechanical, optical, electronic, magnetic and electrochemical properties.[40,41] The increment of catalytic activity with size can be rationalized on the basis of the increasing surface to volume ratio with decreasing particle size, since the surface atoms are more active due to the presence of unsaturated co-ordinations or dangling bonds.[40,41] Further, due to higher surface to volume ratio, considerable lattice contraction is observed in nanoparticles, which increases with the decrease of particle size.[40,41] The lattice contraction or lattice strain is generated due to the hydrostatic pressure on the surface induced by the intrinsic surface stress.[40] As most of the atoms are situated on the surface for smaller particles and they have an excess free energy due to the large number of unsaturated bonds, the melting point also decreases with decreasing particle size. Since the surface energy of liquid is less as compared to the corresponding solid, the depression of melting point occurs by minimizing the surface energy (Figure 1.1).

The electronic structure of a metal particle in reduced dimension critically depends on its size and is drastically different from its bulk and atomic or molecular analogues, however, the definition of the dimensionality of a system often depends upon the interest. This can be generally defined by the electron movement in a restricted environment such that the particle size is of the order of mean free path at least in one dimension, which also commonly known as quantum confinement.[13d,14b,42] The important length scale can be electron mean free path, length of the effective Bohr radius or phase coherence length. More specifically, mean free path of the electrons dictates the property of the metallic nanoparticles, whereas semiconducting particles are mainly governed by Bohr's radius (the electron-hole separation as characterized by the excitonic diameter).[42,43] Accordingly, if any one, two or three dimensions of the material are less than any of these aforementioned length scales, the system can be said as zero (quantum dot), one (quantum wire) and two dimensional system (quantum well).[42]

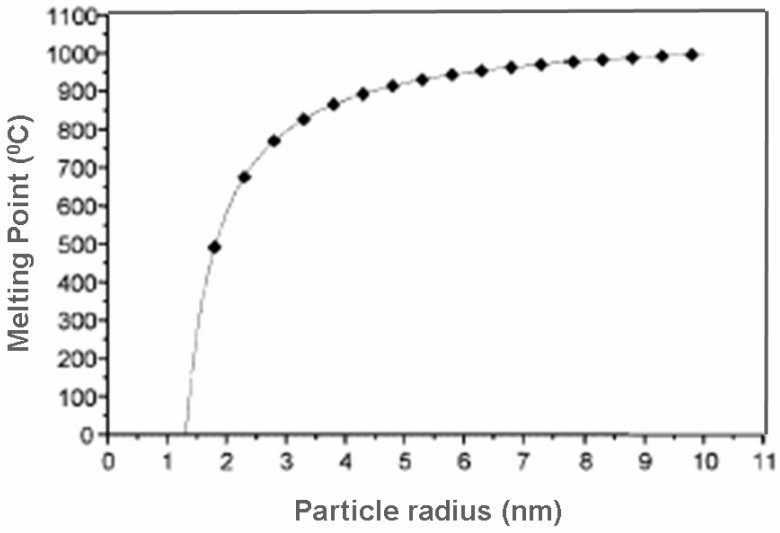

Figure 1.1 Relationship between particle size and melting point of gold nanoparticles. (Adopted from Ref. 44)

The size reduction causes the electrons to be confined within a small region of the spherical potential well (for nanoparticles), where these electrons occupy discrete energy levels given by particle-in-a-box solution.[42,44] However, molecules have well separated energy levels (explained by molecular orbital theory), while solids posses well defined band structures due to the overlap of the energy levels of infinite number of atoms having translational symmetry.[44] More specifically, the average spacing of successive quantum levels, known as Kubo gap; ($\delta = 4E_f/3n$; E_f is the Fermi energy of bulk metal and n is the number of valence electrons in the nanoclusters), can be controlled to make a system either metallic or nonmetallic.[14b,44-46] For example, for an Ag particle of 3 nm diameter containing ~10^3 atoms, the value of δ would be 5–10 meV. Since at room temperature, k_BT ~ 25 meV (k_B is Boltzmann's constant), the 3 nm particle would be metallic ($k_BT > \delta$).[14b,45,46] At low temperatures, the level spacing, especially, in small particles, may become comparable to k_BT, rendering them nonmetallic.[14b,45,46] Most importantly, the change in the spacing between the energy levels as a function of the number of atoms can be used to understand the electronic, optical or magnetic properties.[13e,45-47] Since "δ" depends on "n", size tuning can lead to the control of "δ" as compared to the value of thermal energy, which in turn can control the properties of materials. For example, "δ" can vary with "r^{-3}" for spherical particles (r is the radius of the

particles), as their density of states is proportional to volume. The low temperature behaviour of these systems will be more interesting as the spacing "δ" may become larger than k_BT and the life time (τ) of the electronic states will be much larger than $\hbar/\delta$ ($\hbar = h/2\pi$, where h is the Plank's constant), thus making the system insulating.[47]

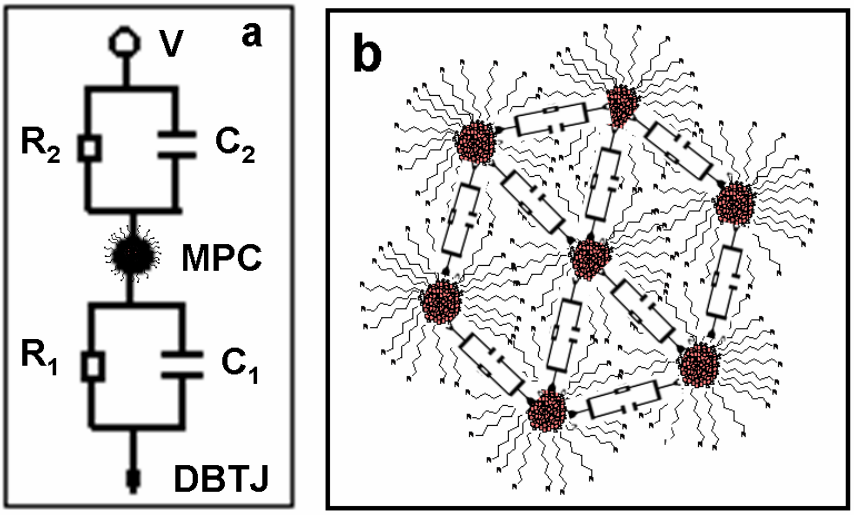

Scheme 1.1 (a) Schematic representation of the equivalent circuit for the double barrier tunnel junction (DBTJ) for an attached MPC on a solid surface, while (b) several tunnel junctions are possible for MPC superlattices. R_1, C_1 and R_2, C_2 represent the resistance and capacitance of the first and second tunnel junctions respectively.

The discreteness of energy levels in these nanoparticles causes the single electron tunneling to be feasible at room temperature, which is believed to be one of the most important phenomena for future electronic devices.[13,48] Nanoparticles, with a dielectric coating (tunnel barriers) are ideal in this respect as they have very tiny capacitance (~ 10^{-18} F). In comparison, if we want to observe single electron charging effect in a typical capacitor (pF), we need to apply a very small amount of voltage (10^{-8} V). Further, the capacitor would have to be cooled to a temperature such that 10^{-8} V > k_T (k_T is the critical temperature to observe single electron tunneling) to suppress the thermal effects, which turn out to be a temperature of 0.0005 K, this is quite unfeasible

for any practical use. In comparison, if we apply a 100 mV potential increments in these systems, it will lead to store 10^6 electrons at room temperature, diminishing the possibility of single electron charging.[48b] The single electron charging effects generally exhibit by nanoparticles or their assembled structures often forming metal–insulator–nanocluster–insulator–bulk metal (MINIM) double barrier tunnel junction (DBTJ) systems.[13,48] The equivalent circuits as DBTJ constructed for organized MPCs (a) on surface or (b) interconnected systems are shown in Scheme 1.1, which shows several tunnel junctions are possible for the later case.

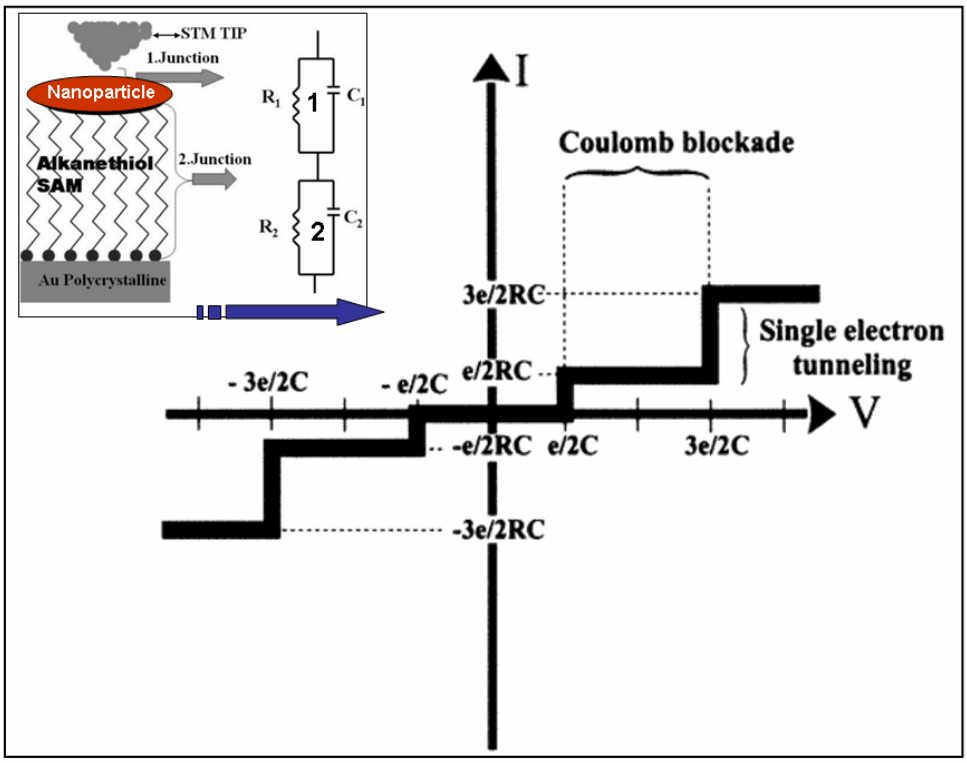

Figure 1.2 The ideal Coulomb blockade phenomenon is depicted in current–voltage (I-V) graphs, often known as Coulomb staircase due to its resemblance with stairs; inset showing a widely investigated nanoparticles based MINIM system to illustrate such behaviour.

One of the best illustrations of the single electron tunneling through nanoparticles is known as “Coulomb blockade effect”, which is the energy necessary to place an extra

electron on a nanoparticle, arising due to the Coulombic repulsion among electrons.[48b] This electrostatic energy can be simply viewed as the difference between the electron affinity and the ionization potential of the nanoparticle, which is termed as the charging energy ($E_C = e^2/2C >> C$ is the capacitance of the particle). Further, to observe single electron tunneling, E_C should be greater than k_BT, in order to restrict the thermal motion of electrons.[48b] The ideal Coulomb blockade phenomenon is depicted in current–voltage (I-V) graphs as shown in Figure 1.2, also known as Coulomb staircase due to its resemblance with stairs. Accordingly, for each extra electron to be tunneled an "e/C" amount of voltage is required for an increase of "e/R_TC" amount of tunneling current (R_T is the tunnel resistance). The Coulomb blockade effect has been initially observed for metal islands at low temperature, while all the features could be easily viewed for passivated nanoparticles attached on electrode surface (Inset of Figure 1.2).[48]

A few theoretical attempts have been made earlier to study the electronic structure of monolayer protected clusters (MPCs) in the simultaneous presence of interaction and disorder.[49] The disorder in the monolayer can create localization and this can be responsible for the temperature dependence as explained by Variable Range Hopping (VRH) theory.[50] More specifically, when there is a large interparticle separation ($L_{CC} > 2r$, L_{CC} is the particle core to core separation), the clusters behave, like a Mott insulator with a Coulomb gap described by the charging energies of individual nanoparticle sites. On the other hand when the distance between the adjacent clusters is very small ($L_{CC} << 2r$) compared to their size, strong quantum mechanical exchange coupling can cause the disappearance of Coulomb gap, facilitating metal-to-insulator transition (MIT).[49-51] Since the charging energy scales inversely with particle size, the MIT is experimentally easier to observe in superlattices composed of the larger clusters.[52] This is to be contrasted with transition metal oxides, where MIT is normally accomplished by the variation of charge carrier density through altering the composition using substitution chemistry.[50] Temperature dependence of the conductivity in disordered insulating systems below the percolation threshold can be described by a simple Arrehnius-type formula implying activated charge transport. As the temperature reaches to a critical value (T_c), it fits to the Motts VRH conduction rule,[50] leading to use localization length as the dimensionality of the system and is comparable with the hopping distance or the lattice spacing.[50]

The discreteness of the energy levels of nanoparticles is also the reason for the evolution of their fascinating colors.[43] For semiconductors, if the radius of the nanoparticle (r) is comparable with that of Bohr radius ($r_B = \varepsilon_s \hbar/\mu e^2$, where ε_s is the dielectric constant of the semiconductor and μ is exciton-reduced mass and e is the electronic charge) of the bulk exciton. The change in optical property depends on the nature of quantum confinement as $r >> r_B$, $r \sim r_B$ or $r << r_B$.[43b,53] In particular, for smaller particles the optical property arises due to the transitions between the electron and hole quantum states.[43a] Accordingly, size reduction causes this energy to be increased, thus shifting the excitations to higher energetic sides.[43b,53] On the other hand, the interaction of electromagnetic wave with the coherent motion of the conduction band electrons of metal nanoparticles, known as surface plasmon resonance (SPR), causing several interesting properties.[43a] This is a collective excitation of the electrons at the interface between a conductor and an insulator and is strongly dependent on particle size, shape and surrounding medium. The MPCs are ideal to study the effect of size, medium or functionality on the optical properties in nanodomain, while these features enable them as ideal for several applications, including photonics, bio-molecule detection or medical diagnostics.[26c]

Magnetic nanoparticles provide great opportunities to understand the magnetic properties at the atomic level without the interference from complicated domain wall movements due to their single domain magnetic nature. For example, some fundamental issues, such as quantum tunneling of magnetization (QTM), superparamagnetism and giant magnetoresistance, could be understood by investigating the passivated magnetic nanoparticles.[54,55] The QTM is solely possible due to the discreteness of the energy states and has become a topic of much interest for spintronics and quantum computers.[55] Further, several other phenomena, like giant magnetoresistance (GMR) and spin valve effect, can be seen in nano-multilayer-structures of ferromagnetic transition metals.[55] The magnetic nanoparticles, especially, MPCs provide an opportunity for studying the effect of crystal nature, size, shape and surface state on magnetism.[56-58]

The effect of size reduction causes drastic changes in the electrochemical features of nanoparticles such as the redox potentials (E^0), double layer charging, potential of zero charge (E_{PZC}) as compared to their bulk analogues.[59-62] For example,

unusual catalytic property of smaller metal particles, like Au, Ag and Cu, arises due to the shift in the redox potentials, which has been revealed by pulse radiolysis experiments.[59b-g] Similarly, electrochemical properties of Pt nanoparticles are different than that of bulk Pt, while electrochemistry is also different for Ag nuclei formed in the photographic layers.[61,62] Further, pulse radiolysis experiments also suggested that the Ag clusters are stronger reducing agent than Zinc.[59]

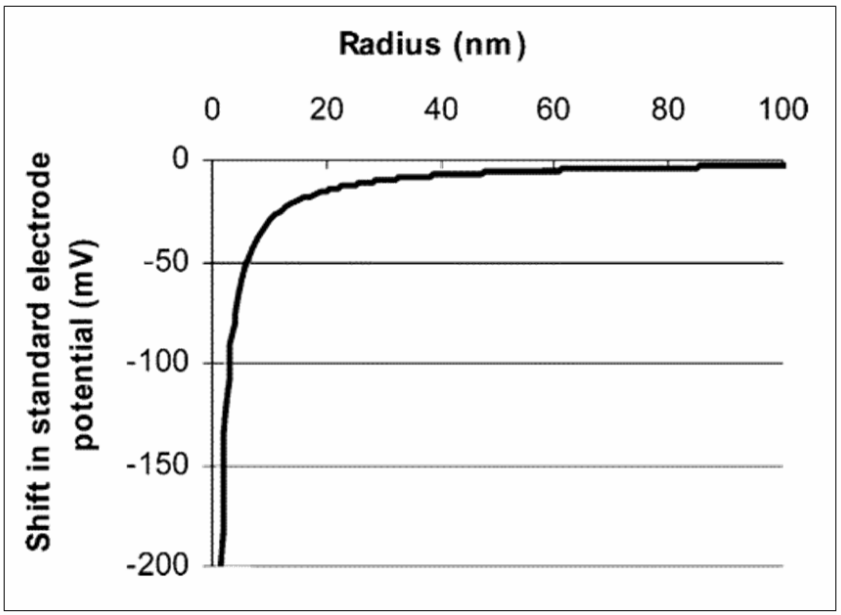

Figure 1.3 Theoretical variation of the shift in standard electrode potential of small silver particles from their bulk value with size. (Adopted from Ref. 64)

The quantitative description of shift in the E^0 has been described by constructing an electrochemical cell consisting two half cells of both bulk metal and in the dispersed states, provided that the surface free energy is the same for both.[62,63] The difference in equilibrium potentials ($\Delta\varepsilon_D$) is calculated by considering spherical dispersed particles as

$$\Delta\varepsilon_D = \varepsilon_p - \varepsilon_b = - (2\gamma\upsilon_M/zFr) \qquad (1.1)$$

Where, ε_p and ε_b are the equilibrium potentials of dispersed nanoparticles and bulk respectively, γ is surface tension, υ_M is the molar volume, *z* is the lowest valance state, F is Faraday's constant and r is the radius of particles.[62] Thus the standard electrode potential (E^0_P) of small particles is,

$$E^0_P = E^0_B - (2\gamma\upsilon_M/zFr) \qquad (1.2)$$

where, E^0_B is bulk standard electrode potential.[62] ***The redox potential is thus predicted to shift negatively for nanoparticles than that of bulk and is proportional to the reciprocal of the radius.***[62] Accordingly, the theoretical variation of the shift in standard electrode potential of small silver particles from their bulk value with the radius is shown in Figure 1.3.[64] Further, the E_{PZC} and work function are also predicted to be decreased with decreasing particle size.[62]

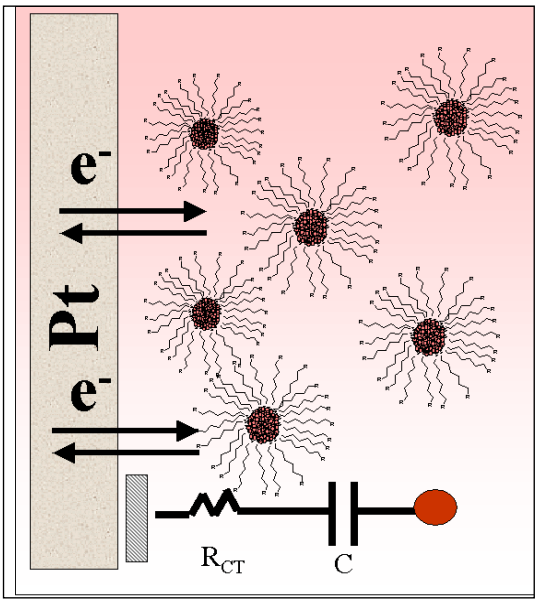

Scheme 1.2 Schematic representation of the QDL process, where the equivalent circuit is also shown. The organic monolayer acts as insulating barrier, whereas the nanoparticle//capping molecule junctions behave, like a capacitor; R_{CT} and C represent charge transfer resistance and capacitance respectively.

Another, important feature of passivated particles is their double layer charging, which arises due to their sub-atto farad capacitance, termed as quantized double layer (QDL) charging.[65] The QDL phenomena observe due to single electron charging, which is analogous to the STM based Coulomb blockade phenomenon.[65] The schematic representation of QDL phenomena has been provided in Scheme 1.2, where an equivalent circuit is also shown to describe the contribution of organic monolayer and the capping//nanoparticles interface. Interestingly, MPCs have great flexibility to tune the size and nature of the capping layer, thus providing opportunity to explore some of the above predictions.[65,66]

1.4 Monolayer Protected Metallic Nanoclusters

The nanoparticles stabilized by monomolecular thick films of aliphatic or aromatic thiols, amines or carboxylic acids are known as monolayer protected nanoclusters (MPCs), due to the structural similarity of the capping monolayer with SAM.[23,26,27] To some extent, MPCs are analogous to single crystals extending their interior periodic arrangement of atoms or molecules up to the surface, which provides a bridge between the properties of metal atoms and those of the infinite metallic solid.[26,27] Thus the way of experimental preparation of MPCs allows a direct comparison of theory and experiment. In the following sections, we discuss several issues related to metallic MPCs with special emphasis on their synthesis, characterization, properties and applications.

1.5 History

The vivid characteristic colors of gold nanoparticles are known since the 17th century and these types of particles have been used for coloring stained glass windows of cathedrals in Europe or vases and other ornaments in China. Further, long ago Michael Faraday and colleagues have indeed investigated the formulation of stabilized Au colloids for several applications.[67] However, the concept of protected nanoclusters probably came from the successful synthesis of the phosphine ligand stabilized Au and other metal nanoparticles by Günter Schmid and his coworkers with empirical formula of $M_{55}L_{12}Cl_x$, where M = Au, Rh, Ru, Co or Pt; L = PPh_3, P(t-Bu_3), PMe_3 or As(t-Bu_3); x = 6, 20.[41,68] Despite their low thermal stability, these nanoclusters have been thoroughly characterized and used for catalysis.[41,68] Accordingly, several other catalytically active

metal nanoclusters were known, including Mosieev's phenanthroline or 2,2'- bipyridine capped palladium clusters, Bönnemann's tetraalkylammonium stabilized particles, Reetz's electrochemical route to synthesize tetraalkylammonium stabilized particles and polyoxoanion or tetrabutylammonium stabilized metal nanoclusters.[41] Although nanoparticles synthesized in several supports (like glass, zeolites, alumina and TiO_2) or stabilized with polymers (e.g. block-copolymers, dendrimers etc.), inorganic shells, poly-ions routinely, Brust technique offers one of the most simple and widely used process for preparing MPCs.[26-32,69,70]

1.6 Preparation Procedures

1.6.1 Brust's Synthesis

Mathius Burst and colleagues have illustrated a convenient method for the preparation of dodecanethiol protected Au nanoclusters, which is commonly known as Brust's Synthesis.[26a] This method produces thermally stable, moderately size dispersed MPCs in the diameter range of 1.5 and 5.2 nm with a predominant presence of cuboctahedral and icosahedral structures.[26a] Although, the stabilization of Au clusters with alkanethiols were known earlier,[71] Brust's method has been used routinely to synthesize various metallic and semiconducting MPCs.[26,27] In particular, the MPCs prepared using this method can be isolated as liquid dispersion as well as solid powders and can be repeatedly redissolved in organic solvents without aggregation or decomposition. In brief, the Brust's synthesis consists of reduction of Au salts in aqueous-nonaqueous interface by $NaBH_4$ in presence of alkanethiols and a phase transfer agent, like tetraoctylammoniumbromide (TOAB), in non-aqueous medium with vigorous stirring.[26] The organic phase changes from yellowish to deep red within few seconds upon the addition of $NaBH_4$, confirming the formation of Au nanoparticles. In particular, thiol ligands strongly bind to the gold surface due to the soft character of both Au and S, which concomitantly stabilizes the nanoparticles by forming 3D SAM on the colloidal surface.[26b,e]

Table 1.1 A summary of different types of gold nanoparticles with various capping agents, size and shape distributions along with their optical (UV-visible) absorption maximum

Size of cluster (nm)	Capping agent	Structure	UV-visible absorption (nm)	Ref.
1.5-3.5	Alkyl Thiolate	fcc	515-518	30.a
2-3.2	2,6-Bis(1'-(8-thiooctyl) benzimidazole-2-yl)pyridine	Hexagonal network	520-523	30.b
2-4	Dodecanethiol	fcc	520-525	30.c
3.5-4	S-Dodecyl thiosulphate in THF and water		516-527	30.d
8-9	Tris-n-octyl Phosphine Oxide	fcc	525-530	30.e
10	Hexadecyl trimethyl ammonium bromide	Nano rod	520 + 600-700	30.f
40- 50	Hexadecyl trimethyl ammonium bromide	Nano rod	520 + 800-850	30.g

There have been enormous efforts to prepare size tunable cores along with the functional group manipulation for a diverse set of applications by modifying this synthetic technique.[25-31,56-58,60b-g,65,66,73-78] For example, smaller monodispersed core sized MPCs can be obtained by either changing the thiol/metal molar ratio, addition time of the reducing agent or controlling the reaction temperature.[26b,27a,f,65,75a,79] Further, the nature of the monolayer forming molecule has also a critical effect on the size and dispersion of these MPCs.[26,73-78,80-90] For instance, shorter chain length thiols produce substantially disordered clusters compared to the case using longer chain thiols,[79f] while smaller core sized particles can be obtained using sterically bulky ligands.[26b,27a,f,65,75a,79] There have been several other methods, like the use of reverse micelles,[72f,91,92] acid or base facilitated transfer[27c,93] and single-phase preparation techniques,[30e,94] for the preparation of MPCs and some of these for gold and silver nanoparticles with their size, structure and nature of capping agents are summarized in Table 1.1 and 1.2 respectively. These data clearly indicate that interesting transformations of nanoparticles to nanorods can be possible by controlling the preparation chemistry, enabling a systematic variation of the

aspect ratio of these structures by changing the nature and the amount of capping agent.

Table 1.2 A summary of different types of silver nanoparticles with various capping agents, size and shape distributions along with their optical (UV-visible) absorption maximum

Size of cluster (nm)	Capping agent	Structure	UV-visible absorption (nm)	Ref.
2-3	3-aminopropyltrimethoxy silane, boron nitride	fcc, hcp	400-410	31.a, 31.b
5-6	dioctyl sulfosuccinate sodium salt, organo sulphur compounds, alkyl thiolate	fcc, hcp	375-380	31.c
6	Alkane thiolate	hcp		31.a-h
7.8	Perfluoropolyether carboxylic acid and aqueous ammonium hydroxide, N-Hexadecylethylenediamine	Hexagonal array	410-415	72.a,b
7.7-8	Dodecane thiol,SN,N dimethyl 2,6 Pyridinediylbis[undecamide	hcp	415-420	72.c,d
10-15	Poly(2,6-dimethyl-1,4-phenylene oxide), Dodecanethiol	Colloidal	425-435 (doublet)	72.e,f

1.6.2 Synthesis in Reverse Micelles

The capped and uncapped nanoparticles have been synthesized in microemulsions, copolymer micelles and reverse micelles long before the emergence of Brust's method.[72f,91,92,95] In particular, reverse micelles have attracted significant attention in last decade for the preparation of MPCs, especially, if it consists of thermodynamically stable mixtures of water, oil and surfactants.[91,92,95] The water regions are separated from oil by a monolayer of surfactants due to its amphiphilic nature, which creates numerous

disordered or partially ordered phases depending on the temperature and the nature of surfactant. These surfactant-stabilized water pools act as microreactors by the preparation of nanoparticles, whereas the aggregation of particles is controlled by the adsorption of surfactants. The particles produced by these methods are generally uniform in size as illustrated for the preparation of metallic (eg. Au, Ag, Cu, Co)[72f,91] or bimetallic (eg. Pt/Pd, Cu/Au Au/Pd) nanoparticles.[92]

1.6.3 Other Methods

Several other methods, like molten salts, supercritical solvents, seed mediated growth, photo irradiation, laser-ablation and sonochemistry, have been used to prepare size controlled nanoparticles.[32,91-97] Further, decomposition or thermolysis of organometallic salts at higher temperature also produces alkyl-chains-passivated MPCs. Several single phase (nonaqueous) methods are also available for the preparation of MPCs, where soluble organometallic compounds are reduced with suitable reducing agents in presence of surface passivating molecules. Other advantages of single-phase techniques are the absence of phase-transfer catalysts (may cause surface contamination), ease of separation/purification and flexibility for large scale preparation (scale-up).[30e,94]

1.7 Purification and Size Tuning

Purification is one of the necessary steps before characterization and further property assessments or applications, since the “as prepared” particles contain excess unbound thiols (often as multilayered), phase-transfer catalysts or several side products, like di-sulfides apart from their polydispersity.[26] Further, the polydispersity often causes irreproducibility of measured properties due to the collective contribution from all components, while multilayered particles also have different properties other than that of monolayer capped particles. In particular, impurities, like excess thiols and phase transfer catalysts, are generally removed by repeated solvent extraction (using polar solvent for hydrophobic MPCs and vice versa) followed by concentrating in vacuum or rotary evaporator.[26] Since the influence of trace ionic impurities might mislead the measured properties useful for various applications, like vapor-sensing, this is an urgent need to remove the phase-transfer catalysts from MPCs completely. For example, the

purification of dodecanethiol stabilized Au MPCs from the contamination of TOAB has been recently reported by Soxhlet extraction.[98] A variety of techniques, like solubility fractionation, chromatography and capillary electrophoresis, are coupled with different analytical techniques for the purification and size selective isolation/detection of various sized MPCs, while post heat treatment (digestive ripening) is also a widely used technique for reducing the size dispersion.[26,30a,87] Few of such techniques for the purification or size tuning are briefly discussed below:

1.7.1 Solvent Extraction

Solvent extraction has been effectively used for the separation of smaller core sized particles, since smaller particles are more soluble in polar solvents compared to larger passivated MPCs.[30a,87] In particular, fractionations are performed by repeated re-precipitation of larger hydrophobic MPCs from toluene dispersion by the addition of more polar solvents, like ethanol and acetone, leading to the precipitation of larger cores. This process could be repeated several times by increasing the volume of polar solvents to successive precipitation of smaller core fractions until insufficient material is left for further precipitation steps. Although this method is quite effective for selective precipitation of smaller sized particles, it is time consuming, tedious and less effective for longer alkane chain capped MPCs. [26,30a,87]

1.7.2 Chromatography

Several chromatographic methods such as the size exclusion chromatography (SEC), capillary electrophoresis (CE) and ion exchange chromatography (IEC) are being used by various groups to improve size dispersion.[89c,99] For example, CE method has been used to separate a number core size/charge state combinations using tiopronin-MPCs and viologen-functionalized tiopronin-MPCs.[89c,99d] However, all these methods have several disadvantages, which prevent their effective use for large scale preparation. For example, the irreversible adsorption in SEC column packing material and inabilities of IEC method for separating neutral nanoparticles are typical disadvantages, while CE is only applicable for very small sized particles. Another method is high-pressure liquid chromatography (HPLC), which is typically used to separate smaller sized particles.[99f] Further, HPLC and high-resolution size exclusion

chromatography (HRSEC) have been used for the investigation of the size distribution of Au and Ag MPCs (1 to 10 nm).[99c,g,h] Several other tools, like TEM, mass spectrometry and voltammetry, have been coupled recently with these chromatographic techniques to precisely assess the size distribution of MPCs.[26b,c,99]

1.7.3 Digestive Ripening

In this technique, heating of colloidal suspension at or near the solvent boiling point in the presence of an excess surface-active ligands is used to reduce the average particle size (digestive ripening), which is very convenient and specially advantageous for large-scale syntheses.[32] In particular, Au colloids are prepared in a miceller solution of dodecyldimethylammoniumbromide (DDAB) in toluene and subsequently reduced by aqueous $NaBH_4$ solution (under vigorous stirring).[32] These colloids are further treated with various alkane-thiols (RSH), -amines (RNH_2), -silanes($RSiH_3$), -phosphines (R_3P), -bromides (RBr), -iodides (RI) etc. with approximate molar ratio of Au/ligand at 1 : 30.[32] These ligand capped particles are separated from the DDAB, excess capping ligands or any other side products and are boiled in same solvent after re-addition of the same proportion of ligands. The solvent extraction using polar solvents can further remove impurities, finally leading to the preparation of highly monodispersed particles.[32]

1.8 Characterization

A variety of characterization techniques have been effectively used to quantify the particle size, shape, distribution, composition and purity. However, combined results from various techniques are necessary to provide complementary information regarding their structure and assemblies as shown by the Scheme 1.3. In general, the individual characterization technique should not be invasive, but should be able to provide all quantative details of the structure or composition. Few of such techniques are discussed below:

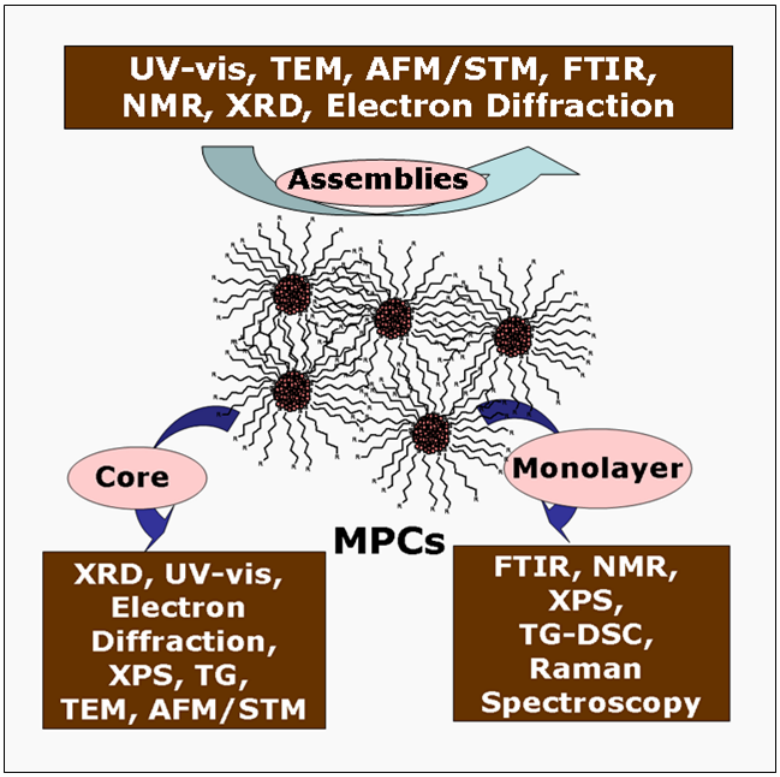

Scheme 1.3 Schematic representation of the use of different analytical tools for the characterization of MPCs and their assemblies; MPCs can be divided into two distinguished part as core and capping monolayer for the convenience of characterizations.

1.8.1 UV-visible Spectroscopy

UV-visible spectroscopy is one of the most common technique to obtain useful information regarding size, shape and the degree of aggregation of MPCs.[43a,c] The characteristic optical absorption in UV-visible region is observed due to the interaction of surface free electrons with electromagnetic radiation (surface plasmon resonance) as mentioned earlier.[43a,c] Further, the SPR absorption maximum (λ_{max}) and band width of metallic MPCs are also affected by the nature of surface capping agent and the nature of the dielectric environment changes around the nanoparticle surroundings.[59b] For example, the UV-visible absorbance spectra of Au MPCs and Ag MPCs show a strong plasmon absorption band around 510-530 and 400-430 nm respectively depending upon the shape, size and protection layer, which decays exponentially into the visible

region.[99c,g,h] The surface plasmon absorbance peak is red shifted for Au MPCs, while blue shifted for Ag MPCs with increasing size along with concomitant increment in their peak full width at half maximum (FWHM).[99c,g,h]

1.8.2 X-ray Diffraction (XRD)

The crystallinity and particle size of MPCs are often determined by X-ray diffraction. For example, XRD studies indicate that thiol protected Au nanoparticles have bulk fcc structure for the majority of larger particles (particle size > 2.6 nm), while some of the smaller particles reveal decahedral (1.7 nm) and icosahedral (≤1.3 nm) structures.[30c] Further, the long range ordering in superlattices can be characterized by XRD analysis. For example, XRD has been recently used to characterize Ag or AuAg alloy MPCs superlattices, where the effect of temperature and the length of the capping molecules are investigated with several other complementary techniques.[100f,101]

1.8.3 Transmission Electron Microscopy (TEM)

Direct visual information of size, shape, dispersion and structure of nanoparticles is generally obtained by TEM and more specifically by employing high-resolution transmission electron microscopy (HRTEM).[102] For example, TEM studies of alkanethiol capped Au MPCs reveal semi-ordered islands with uniform core size distribution and core-core spacing of about two alkanethiol chains.[30a] Further, HRTEM studies are also useful to study the faceting, crystallinity and ordering in these nanocrystals.[102] Interestingly, various complex structures, like spherical to rod like transformation and chain melting, can be studied *in-situ* in a TEM chamber, if suitable capping agents are selected.[102]

Potential drawbacks of this technique include, (a) electron beam-induced structural rearrangements, aggregations or decompositions; (b) the inherent problems in interpreting two-dimensional images of 3D samples and (c) problems with sampling (only a small number of clusters can be analysed and counted, which may not be representative of the sample as a whole). Despite these limitations, TEM has been the technique of choice due to atomic-level resolution and the attendant benefits of possible selected area electron diffraction (SAED).

1.8.4 Fourier Transform Infrared Spectroscopy (FTIR)

The monolayer and its nature, i.e., orientation, packing and density are generally characterized by FTIR spectroscopy. Detailed information about the packing and the functional groups can, in principle, be obtained with polarized light, since the absorption in the vicinity of a molecular vibration frequency is dictated by the relative orientation of the electric field and the dipole transition moment.

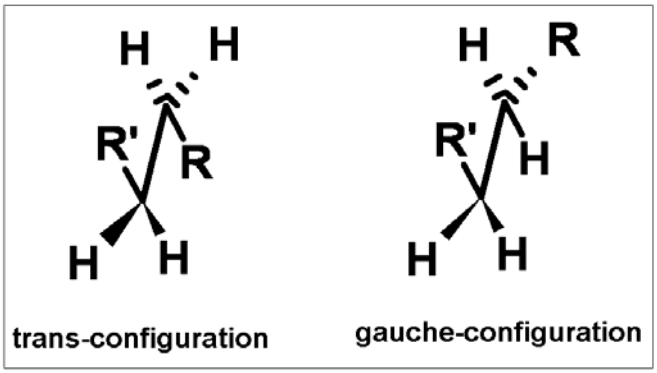

Scheme 1.4 Trans and gauche configurations are shown for unsymmetrical alkanes, where R and R′ represent rest of the aliphatic part around the particular C-C bond.

FTIR studies have shown that alkanethiol chains are typically in all-trans, zig-zag configuration in two dimensional (2D) SAMs,[103] while apart from all-trans configuration, significant (5.25%) gauche configurations at both inner and terminal chain ends are also present for solid-state MPC films.[79b,e,f,104] The trans and gauche configurations are schematically represented in Scheme 1.4 considering unsaturated alkanes. Further, these defects are mostly observed for longer chain above the chain melting temperature and for dissolved MPCs, comparable to that of liquid alkanes. The interdigitation of chain domains (bundles) or neighbouring cluster molecules are also seen for solid state MPC samples.[79b,e,f,104] Several other interactions, like hydrogen bonding and association with other molecules, can also be successfully characterized by FTIR.[79b]

1.8.5 X-ray Photoelectron Spectroscopy (XPS)

Significant qualitative and quantitative information about the chemical state of elements present in MPCs can be obtained from XPS analysis.[27a] For example, a systematic investigation of the nature of alkylthiols in SAM, MPCs and Au(I) thiol complexes (sometimes referred Au(I) thiolate polymers), reveal that S atom in the SAMs and MPCs bears about 0.2 e charge and is easily distinguishable from that in Au(I) complex.[105] In particular, the nature of thiols in 2D SAM is found as RS^- ligand (binding energy (B. E.) = 161.9 eV), while the bond is somewhere between RS-M and $RS^- - M^+$ for 3D SAM.[79f,105,106] The Au $4f_{7/2}$ B. E. appears to be very near to Au(0) (83.9 eV) for both the cases, although increase of B. E. is only observed for smaller core sizes.[79c] Further, the detection of the free/unbound/chemically reacted ligands or any other chemical impurities in the sample can be obtained from XPS analysis, thus providing valuable information regarding the purity of the sample. However, beam-induced damage and carbon contamination from XPS chamber are few limitations of XPS, thus necessitates the need for complementary information from other independent techniques.[106c]

1.8.6 Nuclear Magnetic Resonance (NMR)

The monolayer binding, structure and dynamics of capping molecules within MPCs are generally obtained by NMR spectroscopy. In particular, ^1H and ^{13}C NMR resonances of MPCs are characteristically broadened and shifted relative to those of free alkanethiols upon binding to the core,[79c,104,107] indicative of successful surface capping. For example, ^1H and ^{13}C NMR studies of alkanethiol capped Au particles show that the resonance at the first C next to the sulfur head group disappear upon binding to gold, indicating a strong interaction with the surface. The results of NMR experiments are particularly useful for studying order-disorder transitions of the monolayer of MPCs as revealed by the chain length dependent studies. These studies reveal that the population of gauche conformation is increased than the commonly preferred all-trans configuration of larger chain lengths upon heating. [104a,107] Further, NMR is also useful to assess the purity content of the sample and all these results can be supplemented by the data obtained from FTIR.

1.8.7 Thermogravimetry and Differential Scanning Calorimetry (TG/DSC)

Valuable information regarding the thermal stability as well as the stoichiometry of MPCs is obtained from TG analysis, whereas DSC is particularly useful to understand the change of orientations of monolayer upon heating. For example, TG results of alkanethiol protected Au MPCs reveal stability up to 180-250 °C despite a slight increase with increasing the chain length.[27a] These studies also show for the presence of an average 4.7 ligands/nm^2 in the MPCs, which confirm that MPC/ligand coverage is *ca.* 50% which in turn is greater than the ligand/Au ratio for 2D SAM on Au(111) surface (~33%) as in perfect agreement with the theoretical calculations.[108] The melting of alkanethiol monolayer of MPCs is effectively characterized by DSC. For example, phases of Au MPCs studied in the temperature range of –100 °C to 100 ^{o}C show that for smaller chains ($\leq$ C_8-thiolate MPCs) no phase transition is observed, while for C_{12} and C_{16}-thiolate MPCs a broad endotherm is seen, where the phase transition temperature increases with increasing chain lengths.[79c]

1.8.8 Scanning Probe Microscopes (SPM)

The scanning probe microscopes (SPM) have enormous applications for characterizing MPCs apart from these aforementioned standard techniques due to their atomic resolution capability.[109,110] Like high-resolution electron microscopy, these techniques also have facilities for direct imaging of structures, especially if they are operated at low temperatures or under vacuum due to the ability to focus on the localized zones of interest.[110] The generalized schematic representation of SPM techniques is shown in Scheme 1.5. For example, in scanning tunneling microscopic (STM) experiments, the tunneling current is monitored during the scanning of an atomically sharp tip (like PtIr and PtRh alloy) over the analyzed substrate by generating a small potential difference (~ 1 V) between the surface and the tip, when the tip is brought very close ($\leq$ 10Å) to the surface.[111] The STM experiments can be carried at either in (a) constant current or (b) constant height mode, whereas the samples for STM should have few desirable criteria such as (1) good electrical conductivity, (2) atomically flat surface and (3) limited surface mobility.

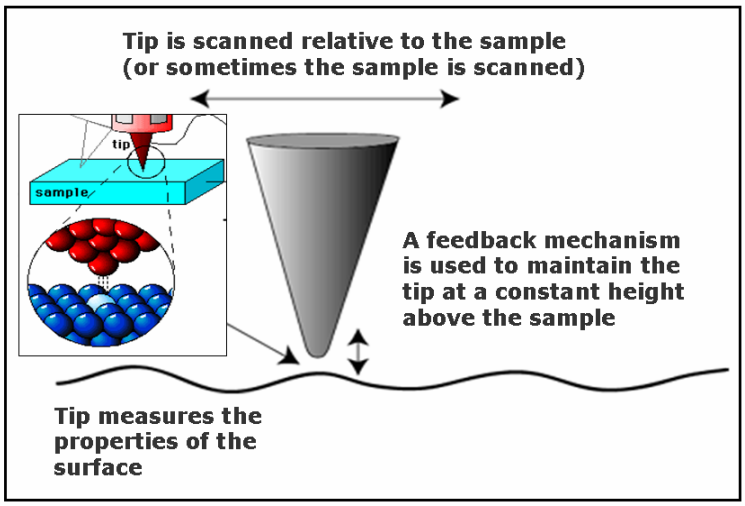

Scheme 1.5 Working principle of scanning probe microscopic techniques.

In general alkanethiolate MPCs and their ordered films on various surfaces have been studied with scanning tunneling microscopy/spectroscopy (STM/STS).[27a,110] Although limitations, like tip-induced artifacts and the possibility of monolayer damage, can complicate the interpretation, while the added advantage of I-V measurements to provide local density of states (STS techniques), distinctly offers several powerful benefits. For example, apart from imaging, STS is a crucial tool to study the electrical properties of MPCs, which reveals the single electron charging features of MPCs (Coulomb blockade behaviour).[48,] However, the scanning probe microscopy data are to be interpreted carefully, because of the possibility of monolayer damage by tip.

Another similar technique is Atomic Force Microscope (AFM) used to measure the surface height profile as a function of distance, where a cantilever tip attached to a spring is dragged across the sample.[13f,112] The chief advantages of AFM are, its ability to carry out measurements on non-conducting substrates, the determination of particles height with atomic level precision and flexibility. However, limitations, like poor capability to determine its diameter, shape differences and difficulties to image spatially separated particles, restricts its independent use.[13f,112] Several other force microscopes, including Magnetic Force Microscopes (MFM), Magnetic Resonance Force Microscopes (MRFM) Lateral Force Microscopes (LFM) and Near-field Scanning Optical Microscopy (NSOM),

are also widely used to investigate nanostructures.[109,113] For example, in MFM a magnetic tip is used to probe the magnetic stray field above the sample surface to sense the deflection of the cantilever for imaging.[109e-g] Accordingly, MRFM, LFM and NSOM are extended version of atomic force microscopy, having greater capabilities of imaging three-dimensional subsurface entities of a broad range of materials with chemical specificity and atomic resolution.[109,113]

1.8.9 Electroanalytical Techniques

Several electroanalytical techniques, like voltammetry, impedance and chronoamperometry, are routinely used to study the electrochemical properties of MPCs and their assemblies.[65,66,84,85b,e,114] Some of the most widely used techniques for MPCs are cyclic and differential pulse voltammetry (CV and DPV respectively), where the current responses is monitored either applying a potential ramp (CV) or a differential of tiny potential pulse (DPV) and is plotted against the applied potentials.[115] Since DPV allows discrimination between the faradaic and charging currents, it is more advantageous for measuring faradic current as compared to that of CV. For example, these studies show that the redox-functionalized nanoclusters (e.g. ferrocene, anthraquinone) in solution are capable of delivering equivalents of redox charge per MPC to electrode surface in a diffusion controlled fashion.[85b,e,f,114] Further, both the CV and DPV have been utilized to assess their single electron charging features (QDL) in solution as described earlier, which is often comparable with STM based measurements.[65] The organized MPCs also have been examined by voltammetry to determine surface coverage, rate of electron transfer or electron transfer diffusion coefficient and interestingly voltammetry also can be used for depositing films on electrode surface.[13a,65,66,114,116] However, adequate precautions have to be taken with the cleanliness of the electrode surface and with monolayer stability under electric field in order to get correct information.

Another important technique involve the use of electrochemical impedance, based on the measurement of the response of an electrochemical cell after applying a small amplitude alternating current (AC) signal.[115] It also can give valuable information about surface coverage, dielectric constant, diffusion-coefficients and electron transfer

behaviour of MPCs assembly both in solution and in solid state.[13a,116g] The response is often analyzed using the complex impedance presentation and the results are interpreted in terms of suitable equivalent circuits. The complex model dependence of the calculated parameters is the major limitation, which may mislead, if incorrect equivalent circuits are used.

1.8.10 Other Characterization Techniques

Apart from these techniques, several other special characterization techniques, such as He, electron and neutron diffraction,[117] surface plasmon spectroscopy (SPS),[118] Raman spectroscopy,[119] magnetoelectrochemistry,[120] secondary ion mass spectroscopy (SIMS),[121] electron energy loss spectroscopy (EELS)[102a,121a,b] and scanning electrochemical microscopy (SECM),[122] have been applied for investigations of nanoparticles.

1.9 Salient Features of MPCs

Diverse classification schemes for MPCs are possible, depending upon the nature of the core and peripheral monolayer. For simplifying the understanding, the MPCs can be divided into core and capping monolayer part and a brief description of each of them is summarized below:

1.9.1 Core of MPCs

The core of MPCs is usually made up of numerous inorganic materials, including metallic (Au, Ag, Cu, Co, Fe_2O_3, Pt, Pd etc.), semiconducting (CdS, CdSe, PbS, CdTe etc.) and insulating (SiO_2, TiO_2, Al_2O_3 etc.) types.[25-31,56-58,60b-g,65,66,72] Similarly, alloy, bi-metal (AuAg, FePt, AgPd etc.) or core-shell (CdS/CdSe, CdS/CuS etc.) structures have also been prepared using different types of inorganic materials.[100,123] The cores are assumed to have full-shell clusters, built up with close-packed atoms on a centre atom by adding one, two, or three dense-packed shells.[40,41] The number of atoms per shell is $N_s = 10n_s^2 + 2$, where n_s is the number of the shell and the total number of all these atoms are known as "Magic Numbers".[40,41]

Since the size tuning of the core typically alters the characteristic electronic

length scales, it is often utilized for the manipulation of properties of these hybrid materials to generate novel functions. Interestingly, the alloy or core-shell morphologies represent a new type of constructional units consisting of two dissimilar compositional and structural domains, which augment new chemical and physical properties, not present in their individual counterparts. For example, a large difference between the intrinsic Fermi levels of the core and the conduction band energies of the n-type shell often generates new properties in core/shell geometry.

1.9.2 Capping Monolayer of MPCs

The capping monolayer of MPCs are usually made up of organic molecules (typically long chain aliphatic or aromatic thiols, amines, acids etc.), which offer several versatile advantages as compared to other types of stabilizers. Advantages, like solubility of nanoparticles in both aqueous and nonaqueous medium depending upon the tail functional groups, binding capability with further inorganic, organic or biomolecules, tunability of physico-chemical properties with controlled length scale and functionality of the capping molecules, have enabled several successful applications. [25-31,56-58,60b-g,65,66,73-78] A large variety of functional molecules other than simple alkane thiols have been utilized, like xanthates, disulfides, di and trithiols, resorcinarene tetrathiols, phosphine, phosphine oxide, amine, carboxylate and isocyanide, for the preparation of MPCs.[73,74] Additionally, by place exchange or coupling reactions it can be further functionalized to get suitable functional groups or mixed functional groups on the organic layer to manipulate functionality and surface energy states of the core.[26b,75] In particular, by changing the functionality the electronic structure of the core can be tailored to modulate the macroscopic properties, like photoluminescence and optical absorption.[73-75] Further, various chemical reactions, like substitution, polymerization and coupling, depending on the functional groups of the monolayer, have been reported for monolayer coated gold nanoparticles.[26b] Interestingly, the reactivity or functional group tunability plays a crucial role for organization of nanoparticles to create nanoarchitectures.[26b-d] Few of such advantages of the manipulation of monolayer of MPCs have been given below with specific examples:

1.9.2.1 Functionality and Length Scale Control: Tailoring Property

The nature of monolayer can be carefully manipulated to tune physical or chemical properties of MPCs. For example, optoelectronic properties of metallic MPCs have been recently tailored by organizing various chromophores of specific properties and functions to generate photo-responsive, organic-inorganic hybrid materials.[73-78,80] For example, chromophores, like pyrene, spiropyran, $Ru(bpy)_3^{2+}$, fluorescenyl derivatives, dansyl derivatives, various dyes (like Rhodamine 6G) and functionalized fullerenes, have been used recently to change their photo-physical properties.[76,77] These chromophore functionalized MPCs offer exciting opportunities for designing novel photon based devises for sensing, switching and drug delivery.[76,77] Further, optical property can also be altered by changing the head group (tethering end) of the capping molecules, like phenylisothiocyanate and benzylamine.[78] The mere presence of a suitable monolayer can make nanoparticles compatible with biological systems, thus suggesting the usefulness of monolayers in designing biomolecular systems.[26d,80-83] For example, the attachment of bio-active precursors, like oligonucleotide molecules labelled with thio group, has been used recently for the selective reorganization and detection of DNA sequence.[80-83] Further, the surface energy of smaller MPCs can also be altered by changing the functionality for the manipulation of electrochemical and optical properties of phosphine and thiol protected 0.8 nm sized Au MPCs.[84] Accordingly, the attachment of various redox active molecules, like ferrocene, bi-ferrocene and phenothiazine, have also generated novel electrochemical properties.[75a,85]

Apart from functionality tuning, another major advantage of MPCs is their capability to control the thickness of the dielectric layer around the core by changing the length of the capping molecule, which has a profound effect on the optical and electron transfer properties. For example, recently our group has shown that a change in the length of the capping molecules can drastically affect the tunneling conductance of Au MPCs while organized on a SAM surface.[86] Further, the effect of chain length has been systematically controlled to change QDL behaviour using various alkanethiols with C_6, C_8, C_{10}, C_{12} and C_{16} chain protected Au MPCs, where the double layer capacitance has been increased with increase of chain length.[87] Accordingly, porphyrin group functionalized Au MPCs with different chain lengths have recently been utilized to

examine the structure and photophysical properties in comparison with SAMs of the porphyrins on a flat gold surface, where weak chain length dependence of the energy transfer quenching has been observed for both the systems.[88] These studies show that the properties of MPCs can be tailored by changing either the head or tail group functionality or changing length scale of capping molecules.[73-78,80-88]

1.9.2.2 Place Exchange Strategy: Control of ω-Functionality

Tail functionalization (ω-functionalization) of MPCs causes a profound impact on their solubility and interactions, especially for superstructure formation.[73-78,80-90] For example, the methyl terminated aliphatic chain protected MPCs are generally hydrophobic and are dispersed in nonpolar solvent, which can be made soluble in polar solvent by introducing ω-terminated alkanethiolate derivatives of acids, amine, amides.[26b,c,75,89] Further, a recent report shows the use of various water soluble thiol ligands for the preparation of water soluble MPCs.[73j] These water soluble MPCs are important for catalysis, biomolecules detection and biosensing, since most of these applications are performed in water. In general, the most widely used technique to insert ω-functionality in MPCs is place exchange reaction, where MPCs with specific capping molecule can be place exchanged with other functional molecules.[75] Accordingly, the mole ratio of molecules of new exchanging molecules to the molecules present on the surface control the rate and equilibrium stoichiometry of this ligand exchange reactions.[90] There are varieties of functionalities, like -Br, -CN, vinyl, ferrocene, -Ph, -OH, -COOH, $-COOCH_3$ and anthraquinone, are incorporated on the MPC monolayer by place exchange strategy.[26b-d,75,89,90]

1.10 Organization of MPCs

MPCs are considered as artificial building blocks for creating nanoarchitectures, where several interesting physical phenomena, arising due to quantum effects, could be conveniently investigated.[13-15,21,26,32,45,124] In particular, these ordered arrays could result in several novel physical and chemical phenomena due to the collective interactions of these MPCs, encompassing several interesting optical, electronic and magnetic properties.[13-15,26,32,45,124-126]

The three dimensional organization or superlattices of MPCs can be formed by 1) self-assembly using simple solvent evaporation,[25-27,32,127] 2) organization at the air-water or water-organic solvent interface or by Langmuir Blodgett (LB) techniques.[14e,19d,64,74c,116f,128] For example, a 3D ordered superlattice formation through the solvent evaporation of iron oxide colloids has been reported.[129] Similarly, 14 nm Au nanoparticles have also been reported to form an ordered hexagonal array through electrophoretic deposition.[130] Furthermore, another report shows the 2D ordering for semiconducting nanoparticles,[14e,128d] while broad size distributed metallic nanoparticles are also reported to form superlattices due to their sufficient size dependent interparticle attractions.[131] In comparison, the assembly of covalently bound particles is not stable, which form irreversible cross linkages driven by the weak dispersion interaction.[131] For narrower particle size distribution, easier is the long-range order.[25-27,32,127,131] Further efforts to enhance the stability of both clusters and ordered arrays also need detailed investigations to improve the application prospects. Anchoring them on suitable polymeric, carbon nanotube and biological substrates have been found to be useful in enhancing their stability.[132]

The organization of MPCs on solid surfaces has been extensively studied in the last decade for designing/tuning the properties of solid surfaces, since the surface properties critically depend on the nature of surfaces and interfaces through which the electron passes.[13a,e,14a,f,23,24,33,86,116,119,133,134] The assembly of nanoclusters on SAM covered substrates is ideal in this respect, where synthetic and property manipulation can be carried out by tuning the nature of organic molecules and MPCs.[13a,e,14a,f,23,24,33,86,116,119,133,134] The organization of these clusters can be accomplished using several interactions, including covalent, electrostatic and hydrophobic. The covalent organization strategy involves the utilization of bifunctional ligand, where a self-assembled monolayer is formed with one end adsorbed on the substrate while the other end is used to anchor particles.[133,134] Alternatively, electrostatic interactions are used to organize nanoparticles by controlling their charge with the help of oppositely charged ligand molecules on surface (e.g. a quaternary amine to bind anionic monolayer coated particles).[133,134] Apart from these two conventional forces, several other interactions, like hydrogen bonding, van der Waal's interaction, hydrophobic and π-π type of interaction can also be used to organize MPCs.[133,134] For

example, aliphatic chain covered MPCs (hydrophobic) have been recently organized on SAM functionalized substrate using weak van der Waals interaction between the methyl terminal ends of thiol molecules of SAM and MPCs.[134a,e] Apart from using SAM substrates, polymers or polyelectrolytes are also routinely used for the preparation of nanoparticle multilayers on surfaces.[116d,135]

1.11 Properties

The reduced dimension often generates novel properties as we have accounted in the previous section, while in this section few examples of such features will be discussed for metallic MPCs.

1.11.1 Optical Properties

Metallic MPCs display fascinating surface plasmon resonance (SPR), depending on the particle size and shape, chemical nature of the passivating ligands, solvent, temperature and also on the core charge.[30,43,136] For example, Au MPCs exhibit a prominent SPR around 510-530 nm, which drastically differs from that of gold oxide or gold chloride,[30,99c,g,h,136] despite the red shift with increasing size or aggregation.[99c,g,h] However, smaller core sized particles (~ < 2 nm) do not show prominent SPR, although decreasing their size causes a slight blue shift along with a concomitant broadening of the plasmon band width.[27e,65b,87,137,138] Interestingly, step like spectral features are observed for < 2 nm sized particles due to the quantum confinement, indicating their semiconducting nature.[27e,65b,87,137,138] Further, Ag MPCs have a characteristic SPR around 380-430 nm, while some of them show interesting luminescent behaviour as a function of size and cluster-cluster spacing.[31,59,72,99c] The bi-metallic, alloy or core-shell AuAg MPCs also show intense SPR, where the band position depends on the core composition as reported recently.[100,139]

The SPR of the metallic MPCs have been nicely correlated with the Mie theory,[43,140] which explains the dependence of SPR maxima and bandwidth with particle size and shape, medium dielectric constant or solvent refractive index, temperature and particle-particle interaction.[27e,65b,87,137,138] Further, the effect of core charge has also been investigated on the SPR, which shows the accumulation of excess electronic charge

causing blue shift of SPR position and vice versa.[136a,b] The nature of ligand has a drastic effect on the SPR position, which could be selectively used for applications in sensors and medical diagnostics.[76-78,141] Apart from the absorption features of MPCs, they are also attractive for fluorescence studies. For instance, the flurophore group functionalized MPCs exhibit resonant energy transfer phenomenon, which is of great interest in biophotonics and materials science.[76-78,142,143] Further, MPCs show visible luminescence possibly due to 5 $d^{10} \rightarrow 6\ (sp)^1$ interband transition.[138,143]

1.11.2 Electronic Properties

Electronic properties of metallic MPCs would be promising for constructing electrical devices superior to presently available semiconductor based integrated circuits and information storage devices. Although their typical resistivity value suggests semiconducting behaviour, especially if the size is < ~2 nm, the I-V curves show Coulomb blockade behaviour that manifests single electron tunneling at room temperature.[13a,27,48,65,66,87,102a,114,116,121a,b,137,138] The thin dielectric layer acting as an insulating barrier for constructing DBTJ geometry, essential for single electron transfer.[26b-d,48] Several investigations have confirmed this phenomenon using STM/STS,[48] although the use of atomic resolution is not essential to get staircase I-V behaviour. Further, organized MPCs (on 2D surface or superlattice) have unique electronic properties due to their collective interactions and for even larger sized particles, the I-V behaviour is strongly affected by the nature of the capping organic molecule.[13,133,134] For example, chain length effects on the electrical behaviour has been compared for hydrophobically organized Au MPCs on various SAM surfaces, shows limiting behaviour of the transmission probability with respect to longer chain length (C_8 or C_{12} aliphatic thiols).[86] Further, although ohmic I-V characteristics are dominated at room temperature for MPC superlattices of larger than 5 nm, the Coulomb blockade effect is observed at low temperature.[13,48] For example, the individual and collective electronic properties of protected silver nanoparticles have been analyzed to explore the electronic properties as a function of the interparticle separation and size dispersion.[74c,124,126d] Apart from these examples, several other experimental reports are also available, illustrating electrical properties for both 2D organized and superlattices of MPCs.[48,144]

There are several other methods, like X-ray absorption near-edge structure (XANES),[145a] high resolution XPS,[145b,c] femtosecond laser pulse techniques[146] and high-resolution electron energy loss spectroscopy (HREELS),[121a] used to understand the electronic properties of MPCs.

1.11.3 Magnetic Properties

Crystal anisotropy of magnetic particles enables the observation of effects of size, shape, crystal structure and surface anisotropy on magnetic properties. For example, various aliphatic acids, amines, sulphonates, phosphonates or trioctylphosphine functionalized hematite (γ-Fe_2O_3),[56] Co[57] and FePt[58] nanoparticles have been recently synthesized and the effect of particle size and shape on the magnetic properties have been studied. The superlattices of capped magnetic nanoclusters are very interesting as both weak van der Waals and dipolar magnetic attractions play crucial role for the stability along with their interesting collective magnetic properties, often different from that of isolated MPCs.[13b,57] For example, Co MPCs are self-organized to form 2D hexagonal networks, while several other types of organizations such as dots or labyrinths deposited on films have been observed upon applying perpendicular magnetic field.[13b,57,147] Interestingly, the magnetic moments of these systems are aligned along an "easy" axis, which act as ferromagnetic upon reduction of temperature below a critical temperature (blocking temperature, T_b).[147] Consequently, above the blocking temperature, thermal fluctuations randomize the moments causing hysteresis, while the width of the hysteresis loop is found to decrease significantly with the decrease in size (i.e., the energy barrier decreases).[147] For example, an hcp array of Co MPCs shows transition from ferromagnetic to superparamagnetic behaviour upon cooling due to the single magnetic domain.[13b,57,147] Apart from these magnetic particles, very small diamagnetic clusters, like Au and Pd, show size dependent paramagnetism, demonstrating complete transformation of properties with size.[148]

1.11.4 Electrochemical Properties

The tunable structure of MPCs has been found to reveal several interesting electrochemical properties depending upon the core size or nature of the

monolayer.[65,66,84,85b,e,114] For example, MPCs with redox-functionality on its monolayer (e.g. ferrocene, anthraquinone) are very interesting, where redox charge equivalents to MPC's can be delivered to the electrode/solution interface in a diffusion controlled manner.[114,116] Further, several other redox functionalized MPCs with thiol ligands containing ferrocenyl,[75a,79d,f,116f] amidoorsilylferrocenyl,[149] biferrocenyl,[150] anthraquinone[151] have been deposited on electrode surface using potential sweeping in electrolyte solution to produce uniform redoxactive MPC films.[149-151] This method has also been used to create hetero-multilayers of palladium and gold nanoparticles connected with biferrocenyl groups.[151] Consequently, C_{60}-modifed MPCs show interesting redox activity upon film formation on an electrode surface due to the mixed-valent nature of C_{60}.[77a,e,152] Such redox active films have several interesting applications, like molecular recognization, photo-current generation and electroctalysis.[77a,e,149-152]

Major emphasis has also been placed on the investigation of the double layer charging properties of these MPCs (< 3 nm) to understand the electron transfer features at nano-dimension apart from the aforementioned electrochemical studies of redox-functionalized particles.[65,66] The freely diffusing or surface attached MPCs on electrode show discrete double layer charging features with respect to one electron, where the capacitance (aF) is associated with the ionic space charge formed around each MPCs dissolved in the electrolyte solution, known as quantized double layer charging (QDL).[65,66] Various voltammetric techniques (CV and DPV) are used to assess their QDL features as mentioned earlier.[65] The double layer capacitance (C_{CLU}) can be calculated from the voltage spacing ($\Delta V=e/C_{CLU,}$ e is electronic charge) in potential axis during voltammetric measurements (especially during DPV), which is found to be size dependent, since capacitance of MPCs are found to be increased with increase of particles size.[66] Further, DPV is particularly useful to assess the HOMO-LUMO gap of very smaller core sized particles (< 2 nm), which is found to be similar with that obtained using standard optical measurements.[65,66,138,143] The QDL phenomenon has been reported for various MPCs and several effects, like core size (< 3 nm), chain length, nature of monolayer, temperature and magnetic field, have been studied, although this property is not known for larger MPCs.[65,66,84,85b,e,114]

Electrochemical features of interlinked or surface organized MPCs are also widely investigated due to their interesting properties. For example, di-thiols containing viologen moieties have been used as redox-active linkers in order to study electron transfer between linked Au MPCs.[153] The advantages for electrochemical studies of organized MPCs are particularly convenient to estimate their surface coverage along with electron transfer rate constants.[13a,65,66,114,116] Further, scanning electrochemical microscopy (SECM) has been used to investigate the kinetics of electron-transfer of organized MPCs,[122] especially involving metal-insulator transition using a Langmuir trough.[122a] Accordingly, electrochemical properties of Ag and Au particles have been investigated recently, which show the retention of redox property despite the formation of an insulating monolayer.[124,154] Apart from these studies, impedance techniques also have been used to understand the electronic properties of an array of Ag MPCs (superlattice) as a function of the interparticle separation, where inductive behaviour has been observed at smaller interparticle separation while the array become insulating at larger separation.[126e] Despite these importances, limitations, like potential induced reorganization of monolayers, reductive desorption of organic molecules,[155] changes due to solvent entrapment and etching of the nanoparticles due to cycling, have to be kept in mind for their future applications.

1.11.5 Other Properties

MPCs also show several other interesting properties, like chemical reactivity,[26b,79e,156] molecular recognition[149,157,158] and the ability to form bioconjugates.[82,134b,159,160] Accordingly, the reactive nature of functionalized MPCs has been utilized for chemical reactions for the introduction of complex functionality, like naphthalene, ferrocene, α-D-glucose,[156] pyrene,[156] fluorescein,[26b,156] carbon nanotubes,[132] C_{60},[77a,e,152] and bio-molecules (like proteins, peptides and oligonucleotides).[79b,82,159,160] Further, cationic polymerization of MPCs have also been reported using typical functionalization with atom-transfer-radical polymerization initiators such as CuBr/tris(2-dimethylaminoethyl)amine[161a] or CuBr/1,4,8,11-tetramehyl-1,4,8,11-tetraazacyclotetradecane.[161b] Interestingly, these functionalized MPCs have been used for catalyzing organic reactions as recently shown by Ti-BINOLate complex (Ti complex of BINOL ligand, ie., chiral (R) 1,1'-bi-2-naphthol) functionalized Au MPCs to assist

catalytic asymmetric alkylation of benzaldehyde with Et_2Zn to afford the adduct formation up to 98% yield with 86% enatiomeric excess (*ee)*.[100a] Further, Pt MPCs also have been utilized recently for catalyzing hydrogenation of maleic acid to succinic acid,[162a] while hydrogenation of allylamine have been performed using cyclodextrin modified Pt and Pd nanoparticles.[162b]

1.12 Applications of MPCs

MPCs have offered several exciting applications due to the quantum confinement and possibility of tailoring chemical functionalities. These features of MPCs have been successfully utilized for evaluating several orthodox theories as well as their existing applications for miniaturized, faster and high speed optical, electrical or magnetic devices, medicinal diagnostics, sensors, molecular recognition and several other related phenomena. Some of these recent applications are briefly summarized below:

1.12.1 Novel Optical Devices

The SPR of MPCs, especially because of its tunable nature, is promising for developing optical devices, like optical switches, sensors and light emitting diodes.[16a,51,149,157,158,163,164] Further, since SPR is dependent on the interparticle separation, it can be used to sense the aggregation of the nanoparticles.[43a,c, 99c,g,h] For example, several biomolecules, like proteins, DNAs and amino acids have already been detected using this procedure.[80-83] Interestingly, the coupling of optical and electronic properties in a material can generate several novel phenomena, like selective sensing and nano-optics, as shown by the incorporation of Ru(II) tris(2,2'-bipyrridine)cyclobis(paraquat-*p*-phenylene) catenane as a photosensitizer to cross-link Au nanoparticles arrays for photo-electrochemical and electrochemical sensing.[165] In another related example, optical fibers coated with a layer of gold nanoparticles to form a ring microelectrode have been used for electrochemiluminescence (ECL) studies.[166]

As nanoparticles have novel nonlinear optical (NLO) properties, it is possible to change the wavelength of laser light through parametric processes. For example, the large third-order nonlinear susceptibility of Au nanoparticles along with the near-resonance nonlinear response is promising for use in nonlinear optical devices dispersed

in a glass matrix.[167] Another interesting application is in photonics as some frequencies of light cannot penetrate through the dielectric periodic structures because photon modes at these frequencies do not exist, recently proposed for the preparation of invisibility shield.[168,] In such photonic crystals, the dispersion of Au nanoparticles in layers as a defect structure could cause NLO effects[169] as demonstrated by the optical limiting behaviour of C_{60}-containing Au nanoparticles.[169d] These applications generate promise for nanoparticles in photonics, since the interaction of photons with nanoparticle arrays can be modulated to generate optical switches.[167-169] Further, organized nanostructures in various geometries are also suitable for performing novel optical devices.[170] For example, self-organization in dense hexagonal packages to form apparently an external ring may be useful for the fabrication of optical devices and may be fruitfully used to design biomaterials with cell-selective properties.[171] For instance, several bio-molecular nanocomposite based devices are already active for medicinal use and will be discussed later. Lastly, the performance of some of these optical devices can be further enhanced by introducing complex metal-semiconductor networks or assemblies and also by providing selective functionality on the surface.

1.12.2 Miniaturized Electronic Devices

Metallic MPCs are promising for several potential applications in the field of electronics, electro-optics and information storage, which could substantially decrease the voltage and power requirements for all types of optical sources typically from high performance communication lasers to general illuminations. In order to realize these benefits, functional nanostructures, however, will have to be fabricated in huge quantities with extremely uniform and controlled size, shape and composition distributions to optimize their properties for a particular application. Since the microelectronic devices based on the complementary metal oxide semiconductor (CMOS) technology have quantum mechanical restrictions for their further miniaturization, the nanoelectronic circuit components have gained considerable attention recently.[48,49] For example, a significant increase in the density of the transistors in both the microprocessor unit (MPU) and the dynamic random access memory (DRAM) of a CMOS chip by next decade is expected.[172] Another, important application is, metal oxide semiconductor field

effect transistor (MOSFET) using single or multiple nanoparticles as charge storage elements, which can also act as sensors or actuators.[173]

Nanoparticles and their organized structures are promising for novel electronic applications due to their single electron tunneling phenomena as discussed earlier. An example of such a molecular electronic component is the nanoscale transistor that can be switched between "on" and "off" states with a single electron, which works efficiently at room temperature leading to the manufacturing of field-effect transistors (FET) or room-temperature single-electron transistors (SET).[48a,e] More specifically, upon organizing nanoparticles on suitably functionalized substrates, metal-insulator-metal (MIM) or metal-insulator-semiconductor (MIS) devices can be created, where single electron tunneling event often generates novel properties.[48] For example, recently we and others have reported several methods to fabricate such MIM devices using MPCs, which show significant nonlinearity in the I-V characteristics, suitable for performing applications of rectifier, diodes and switches.[13a,e,14a,f,23,24,33,86,119,134] Further, Langmuir-Blodgett deposition of Au MPCs have been recently reported to form a MIS device, which exhibits hysteresis in its capacitance versus voltage characteristics, promising for electronic memory structure applications.[174] Another recent study shows the importance of organized gold nanoparticles for the application of resonant tunneling diode using N, N-di-(10-mercaptodecyl)-4,4'-bipyridiniumdibromide molecule as a linker to the substrate, where the potential dependent redox reaction of the bypyridinium molecule controls the current flow.[24] Accordingly, a nanogapped particle film based on dithiolinked Au nanoparticles has been fabricated for a label-free DNA sensing device to acquire nucleotide polymorphism information, which can be subsequently read by electronic protocols.[175]

The assembly of magnetic MPCs can be used to generate information storage or memory systems. For example, polymer-mediated FePt nanoparticle assemblies on a solid substrate has been fabricated for performing such functions.[176] Accordingly, magnetic field dependent properties of the superlattices of Co MPCs are also promising in these respect.[57,147] Apart from these, coupled magnetic and electronic functionalities could also generate novel properties as shown for a Langmuir-Blodgett deposition of a nonmagnetic-magnetic metal-organic bilayer film of Au nanocluster with the magnetic

monolayer of gadolinium stearate.[177] Further, the undecanoate-capped magnetites have been recently used to control and switch the hydrophobic or hydrophilic properties of the electrode surface.[178]

1.12.3 Medical Diagnostics and Sensors

Conjugates of Au nanoparticles-oligonucleotides are of immense importance due to the potential use for the detection of precise DNA sequences, with their attendant applications for medical diagnoses, like disease detection, gene expression, biosensors and forensic applications.[82,83a,b] Further, DNA also has been used as a template for organizing nanoparticles on a single oligonucleotide strand,[82b,c] leading to the formation of biochips. Apart form DNA, MPCs functionalized with cells, biomolecules and other biological components have been extensively used for recognition of amino acids, proteins,[179,134b] antigen detection[180] and biosensors for immunoassays of human serum.[181] For example, gold nanoparticles capped with redox protein, like cytochrome C, have been used for construction of biosensors, where the redox enzymes act as a sensor element and nanoparticle array as a conductive matrix.[182] In yet another example, D-fructose has been sensed by gold nanoparticles encapsulated with D-fructose dehydrogenase on glassy carbon electrode.[183] More interesting is the array constructed using bio-catalytic enzymes and nanoparticles on thiol modified Au (111) surfaces as this shows electron transfer process in the presence of a mediator, like catechol and a conductive spacer.[184] Similarly sensors built with multilayer of horseradish peroxidase and gold nanoparticles are found to be electrocatalytically active for hydrogen peroxide reduction.[185]

One of the fascinating applications of superparamagnetic nanoparticles is in biomedical diagnostics as an excellent magnetic resonance (MR) signal enhancer, especially applicable for gene expression, cancer, angiogenesis imaging and cellular trafficking. This can resolve the weakness of current magnetic resonance imaging (MRI) techniques for commonly used as MR contrast agents. For example, 2, 3-dimercaptosuccinic acid functionalized magnetic Fe_3O_4 nanocrystals have been used to develop a high-performance nanocrystal-antibody probe systems for the diagnosis of breast cancer cells via magnetic resonance imaging.[186] Although several new biomedical

applications are suggested day-by-day, adequate investigations are required to check their effect on the immune systems before any practical use.

1.12.4 Other Applications

Apart from the above applications of MPCs, there are several other interesting uses as catalysts as mentioned earlier; however, the monolayer stability has to be ensured during the reaction conditions. Controlled organization of MPCs in 2D or 3D is also considered as one of the most fascinating applications, since their size dependent properties can be utilized for achieving the desired results. For example, several nanocluster assemblies organized in different length scales have been found to be promising due to their potential applications in many diverse areas such as optoelectronic devices, single electron transistors and chemical sensors as explained earlier. Further, several new applications, like micro/nano-electromechanical systems (MEMS/NEMS), can be envisaged from these organized structures, since the chemical control of the surface functionality and interaction is one of the key issues for the design, fabrication and operation of MEMS/NEMS. For example, an active MEMS/NEMS device has been recently created from nanoparticles using selective deposition of either semiconducting or metallic nanoparticles (100 layers thick) on plastic/glass substrates.[187]

1.13 Conclusion and Perspectives

Thus some of the most recent developments of metallic MPCs have been presented in this chapter with particular emphasis on their preparation, characterization, size-dependent properties and various applications. MPCs are elegant examples of hybrid inorganic-organic nanomaterials, having vast tunabilty with respect to their structure property and application and are expected to lead the prospect of this field for continuing decades with more and more tangible applications. More specifically, both the isolated particles as well as arrays of such clusters act as indispensable building blocks for creating designer materials in the rapidly emerging field of nanotechnology. Although there are varieties of well-established methods to synthesize and understand the properties of MPCs, several daunting challenges of these materials such as time and temperature dependent reorganization, difficulties of scale-up, possibilities of reorientation of the organic monolayer, less thermal/air stability require immediate

attention to fructify their technological processes.

1.14 Motivation, Scope and Organization of the Thesis

The thesis addresses some of the major issues of metallic MPCs such as Au and Ag nanoclusters, the motivation being both fundamental and technological applications in nanotechnology. This includes syntheses, characterization and electrochemical studies of these MPCs to address the size dependent issues on their electrochemical properties. Further, these MPCs are considered as artificial building blocks for creating 1, 2 and 3-D nanoarchitectures (i.e., superlattices or artificial solids) for several potential applications due to the collective interactions. In this regard, the effect of temperature on the Au MPCs superstructures has been evaluated to understand the effect of thermal stress on such ordered assemblies because of their significant relevance for device applications. Accordingly, the electrochemical studies of relatively larger sized Au MPCs reveal that they are capable of single electron charging, which may help to understand the effect of size on the single electron transfer phenomena with its attendant applications in nanotechnology. We have also investigated the interactions of charged MPCs by estimating the diffusion coefficient at various charge steps, since the delicate balance of van der Waals interactions and electrostatic repulsion could change their motion in solution. The effect of size on the redox features of Ag MPCs in aqueous medium has been evaluated to answer the question *"does the redox activity change with size for nanometer scale particles?"* Since silver shows several size dependent properties, like the lattice constant, melting point, electronic properties including the photoelectron yield and the energy of the plasmon resonance absorption, leads to the expectation that the electrochemical properties of silver nanoparticles should also be size dependent. Similar studies for Au particles are also important to explore several critical questions regarding their size dependent features.

1.15 Objective of the Present Study

The foregoing critical review of metallic MPCs shows several methods for their syntheses, characterization, property and applications; although several lacunae are still present for their wide utilization for various electronic applications. For example, most of the Au MPCs synthesized using quaternary-ammonium salts whose removal is very

troublesome, leads to contamination the surfaces due to the presence of ionic species. Accordingly, the size selectivity is a daunting task, involving several complex procedures; thus, the simple preparations of size selective nanoparticles without quaternary-ammonium salts are important for any practical applications. Since the superlattices of Au MPCs are important for device applications, it is necessary to understand the thermal stress on such superstructures. Further, the relatively larger sized Au MPCs (> 3 nm) are always sidelined despite their unique single electron charging features along with their simple preparation techniques, despite their usefulness for nanoelectronics. Hence, it will be interesting to explore the single electron charging features for designing hybrid systems for applications in nanotechnology. Redox activities of MPCs are also major issues to be explored, since their catalytic, electrocatalytic or photocatalytic features vary drastically depending on their redox activity. The specific objectives of the work embodied in this thesis are set out in this perspective as follows:

a) To accomplish size selective synthesis and characterization of Au MPCs;

b) To explore the effect of temperature on the phase behaviour of Au MPC superstructures;

c) To elucidate the single electron charging features of relatively larger sized Au MPCs using electrochemical techniques;

d) To compare the solution based QDL behaviour with STM based single electron charging features

e) To reveal the effective interaction by estimating diffusion coefficients, electron transfer rate constants at various charge state using electrochemical techniques;

f) To examine the size dependent redox activity of Ag MPCs in aqueous medium;

g) To demonstrate the synthesis and characterization of Ag MPCs in single-phase;

h) To understand the redox activity of Ag nanoparticles with or with out capping agents for exploring their electrocatalytic activity.

The present thesis addresses above important questions related to the synthesis, characterization and electrochemical properties of Au and Ag MPCs in **six separate chapters**. The **first chapter** represents a critical review of synthesis, characterization, properties and various strategies for the organization of monolayer protected metallic nanoclusters. The electron transfer features of these nanosized particles have been elaborately discussed to harness their potential applications in electronics, where STM based features are discussed in conjunction with results from electrochemical measurements. The impact of these materials on nanotechnology for diverse applications such as catalysis, optical, electronic and magnetic device construction, medical diagnostics and therapeutics, environmental and pollution control has been briefly discussed. The chapter concludes by specific objectives for the present study, future prospects and finally mentioning some of the existing limitations of these hybrid materials.

The **second chapter** primarily deals with a novel route for the preparation of size selective Au MPCs and their detailed characterization using UV-visible, TEM, XRD, ^{1}H NMR and FTIR. The effect of temperature on the ordered superlattice structure of DDT passivated Au MPCs [approximate composition: $Au_{1415}(DDT)_{328}$] is investigated with the help of *in-situ* temperature controlled XRD and FTIR in conjunction with TG-DSC and TEM analysis. These results indicate the formation of temperature induced, diffusion limited phase transition involving non-equilibrium fractal structures, which is in good agreement with the results available from previous theoretical studies.

The **third chapter** starts with the discussion of the effect of particle size and chain length of the capping molecule on charging energy of MPCs for Coulomb blockade nanostructures using a simple theoretical model. In later sections, the electron transfer features of *ca.* 3.72 nm sized DDT protected Au MPCs [approximate composition, $Au_{1415}(DDT)_{328}$] have been discussed using combined electrochemical and scanning tunneling microscopic (STM) results. Further, various parameters such as capacitance, diffusion coefficient and electron transfer rate constant have been calculated using chronoamperometry and impedance techniques and adsorption phenomena of these MPCs have also been discussed.

The electron transfer features of 4.63 nm sized Au MPCs have been further discussed in **fourth chapter** using electrochemical and STM/STS studies, where these results show clear accessibility of these particles for single electron charging despite their higher capacitance (1.95 aF). The effect of charge steps on various parameters such as diffusion and electron transfer rate has also been discussed using combined results of chronoamperometry and impedance. In particular, these results show that the presence of higher charge enables these particles to diffuse faster along with the concomitant enhancement in their electron transfer rates, which could be useful for understanding the interparticle interactions of charged MPCs.

In **fifth chapter**, the redox features of various sized DDT protected silver nanoparticle film (in the size regime of 2-7 nm) on a Pt electrode have been compared using cyclic voltammetry in aqueous medium. Interestingly, these particles show an irreversible redox feature, which indeed is affected by the size as in agreement with the theoretical calculations of Kubo gap. Further, an alternate one step method of the preparation of Ag MPCs in nonaqueous medium using a reducing agent triethylamine (TEA) has been demonstrated along with their electrochemical features.

Finally, **chapter six** outlines a summary of all the major conclusions of the present study with respect to synthesis, characterization and electron transfer properties of monolayer protected metallic nanoclusters. The major observation is the detection of single electron charging capability of larger sized Au MPCs in ambient condition, which has not been previously addressed. In addition to Au MPCs, the demonstration of the size dependent redox features of Ag MPCs directly relates these experimental results to the previous theoretical predictions. This chapter also outlines some of the limitations of these materials along with probable hazardous effect on the environment and their precautions. Finally, the future prospects of these materials is outlined for next 10-20 years within a broad perspective of both fundamental and technological interest in diverse fields such as chemistry, physics, biology, engineering for these unique hybrid materials.

The results presented in the thesis clearly suggest, that due to the ease of preparation, superlattice formation tendency and single electron features, larger sized Au nanoparticles can act as promising building blocks for nanoelectronic circuit

components. However, several limitations of these materials such as time and temperature dependent reorganization and reorientation of the organic monolayer, less thermal and air stability need improvement for extended use. Further, one should also keep in mind that the electric field may damage and reorient the monolayer and structural changes can perhaps occur at longer time scales. Despite these limitations, the simple chemical method of preparation and the electron transfer properties of such hybrid materials are useful to understand several important issues related to electron transfer features of nanomaterials for possible future electronic applications.

1.16 References

1. (a) *Societal Implications of Nanoscience and Nanotechnology*; Roco, M. C.; Bainbridge, W. S., Eds.; National Science Foundation Report: Arlington, VA, 2001 and also published by Kluwer Academic Publishers: Boston, MA, 2001. (b) http://www.nano.gov.
2. (a) Roco, M. C. *J. Nanopart. Res.* **2003**, *5*, 181. (b) Phoenix, C.; Drexler, E. *Nanotechnology* **2004**, *15*, 869. (c) Whitesides, G. M. *Sci. Am.* **2001**, *285*, 70.
3. (a) Petroff, P. M.; Lorke, A.; Imamoglu, A. *Phys. Today* **2001**, *54*, 46. (b) Julien, F. H.; Alexandrou, A. *Science* **1998**, *282*, 1429. (c) McEuen, P. L. *Science* **1997**, *278*, 1729.
4. (a) Jiang, J.; Bosnick, K.; Maillard, M.; Brus, L. E. *J. Phys. Chem. B* **2003**, *107*, 9964. (b) Levene, M. J.; Korlach, J.; Turner, S. W.; Foquet, M.; Craighead, H. G.; Webb, W. W. *Science* **2003**, *299*, 682.
5. (a) Bao, J.; Bragas, A. V.; Furdyna, J. K.; Merlin, R. *Nat. Mater.* **2003**, *2*, 175. (b) Leuenberger, M. N.; Loss, D. *Nature* **2001**, *410*, 789. (c) Bayer, M.; Hawrylak, P.; Hinzer, K.; Fafard, S.; Korkusinski, M.; Wasilewski, Z. R.; Stern, O.; Forchel, A. *Science* **2001**, *291*, 451.
6. Wang, W.; Lee, T.; Reed, M. A. *Phys. Rev. B: Condens. Matter.* **2003**, *68*, 035416.
7. Binnig, G.; Rohrer, H. *I. B. M J. Res. Dev.* **2000**, *44*, 279.
8. Stroscio, J. A.; Eigler, D. M. *Science* **1991**, *254*, 1319.
9. (a) Torchynska, T. V. *J. Appl. Phys.* **2002**, *92*, 4019. (b) Yanson, A. I.; Bollinger, G. R.; Van Den Brom, H. E.; Agrait, N.; Van Ruitenbeek, J. M. *Nature* **1998**, *395*, 783.
10. (a) Pankhurst, Q. A.; Connolly, J.; Jones, S. K.; Dobson, J. *J. Phys. D: Appl. Phys.* **2003**, *36*, R167. (b) Sun, S.; Weller, D.; Murray, C. B. *Springer Ser. Surf. Sci.* **2001**, *41*, 249.
11. Murray, C. B.; Sun, S.; Gaschler, W.; Doyle, H.; Betley, T. A.; Kagan, C. R. *I. B. M. J. Res. Dev.* **2001**, *45*, 47.

12. (a) Pericet-Camara, R.; Papastavrou, G.; Borkovec, M. *Langmuir* **2004**, *20*, 3264. (b) Leite, F. L.; Riul Jr., A.; Herrmann, P. S. P. *J. Adhes. Sci. Technol.* **2003**, *17*, 2141.

13. (a) Chen, S. *J. Phys. Chem. B* **2000**, *104*, 663. (b) Pileni, M. P. *J. Phys. Chem. B* **2001**, *104*, 3358. (c) Whetten, R. L.; Shafigullin, M. N.; Khoury, J. T.; Schaaff, T. G.; Vezmar, I.; Alvarez, M. M.; Wilkinson, A. *Acc. Chem. Res.* **1999**, *32*, 397. (d) Schmid, G.; Baumle, M.; Greekens, M.; Heim, I.; Osemann, C.; Sawitwoski, T. *Chem. Soc. Rev.* **1999**, *28*, 179. (e) Feldheim, D. L. *Nature* **2000**, *408*, 45. (f) Fendler, J. H. *Chem. Mater.* **2001**, *13*, 3196.

14. (a) Shipway, A. N.; Katz, E.; Willner, I. *Chem. Phys. Chem.* **2000**, *1*, 18. (b) Rao, C. N. R.; Kulkarni, G. U.; Thomas, P. J.; Edwards, P. P. *Chem. Soc. Rev.* **2000**, *29*, 27. (c) Mirkin, C. A. *Inorg. Chem.* **2000**, *39*, 2258. (d) Colvin, V. L.; Schlamp, M. C.; Alivisatos, A. P. *Nature* **1994**, *370*, 354. (e) Murray, C. B.; Kagan, C. R.; Bawendi, M. G. *Science* **1995**, *270*, 1335. (f) Shipway, A. N.; Lahav, M.; Willner, I. *Adv. Mater.* **2000**, *12*, 993.

15. (a) Caminade, A.-M.; Majoral, J.-P. *Acc. Chem. Res.* **2004**, *37*, 341. (b) Crooks, R. M.; Zhao, M.; Sun, L.; Chechik, V.; Yeung, L. K. *Acc. Chem. Res.* **2001**, *34*, 181. (c) Zhou, O.; Shimoda, H.; Gao, B.; Oh, S.; Fleming, L.; Yue, G. *Acc. Chem. Res.* **2002**, *35*, 1045. (d) Andrews, R.; Jacques, D.; Qian, D.; Rantell, T. *Acc. Chem. Res.* **2002**, *35*, 1008. (e) Avouris, P. *Acc. Chem. Res.* **2002**, *35*, 1026. (f) Burda, C.; Chen, X.; Narayanan, R.; El-Sayed, M. A. *Chem. Rev.* **2005**, *105*, 1025.

16. (a) Park, J. H.; Lim, Y. T.; Park, O. O.; Kim, J. K.; Yu, J.-W.; Kim, Y. C. *Chem. Mater.* **2004**, *16*, 688. (b) Danumah, C.; Bousmina, M.; Kaliaguine, S. *Macromolecules* **2003**, *36*, 8208. (c) Murugan, A. V.; Kwon, C. W.; Campet, G.; Kale, B. B.; Mandale, A. B.; Sainker, S. R.; Gopinath, C. S.; Vijayamohanan, K. *J. Phys. Chem. B* **2004**, *108*, 10736. (d) Wu, C.-G.; DeGroot, D. C.; Marcy, H. O.; Schindler, J. L.; Kannewurf, C. R.; Liu. Y.-J.; Hirpo, W.; Kanatzidis, M. G. *Chem. Mater*. **1996**, *8*, 1992.

17. Moore, G. E. *Electronics* **1965**, *38*, 114.

18. (a) Peercy, P. S. *Nature* **2000**, *406*, 1023. (b) Kingon, A. I.; Maria, J.-P.; Streiffer, S. K. *Nature* **2000**, *406*, 1032.

19. (a) Becerril, H. A.; Stoltenberg, R. M.; Wheeler, D. R.; Davis, R. C.; Harb, J. N.; Woolley, A. T. *J. Am. Chem. Soc.* **2005**, *127*, 2828. (b) Tans, S. J.; Verschueren, R. M.; Dekker, C. *Nature* **1998**, *393*, 49. (c) Zhong, Z.; Wang, D.; Cui, Y.; Bockrath, M. V.; Lieber, C. M. *Science* **2003**, *302*, 1377. (d) Collier, C. P.; Wong, E. W.; Belohradsky, M.; Raymo, F. M.; Stoddart, J. F.; Kuekes, P. J.; Williams, R. S.; Heath, J. R. *Science* **1999**, *285*, 391.

20. (a) Lehn, J.-M. *Supramolecular Chemistry: Concepts and Perspectives*; Wiley-VCH: Weinheim, 1995. (b) Terfort, A.; Bowden, N. B.; Whitesides, G. M. *Nature* **1997**, *386*, 162. (c) Whitesides, G. M.; Gryzbowski, B. *Science* **2002**, *295*, 2418 and references therein.

21. (a) Boal, A. K.; Frankamp, B. L.; Uzun, O.; Tuominen, M. T.; Rotello, V. M. *Chem. Mater.* **2004**, *16*, 3252. (b) Murray, C. B.; Kagan, C. R.; Bawendi, M. G. *Annu. Rev. Mater. Sci.* **2000**, *30*, 545. (c) Tripp, S. L.; Pusztay, S. V.; Ribbe, A. E.; Wei, A. *J. Am. Chem. Soc.* **2002**, *124*, 7914.

22. (a) Richter, J. *Physica E* **2003**, *16*, 157. (b) Parak, W. J.; Gerion, D.; Pellegrino, T.; Zanchet, D.; Micheel, C.; Williams, S. C.; Boudreau, R.; Le Gros, M. A.; Larabell, C. A.; Alivisatos, A. P. *Nanotechnology* **2003**, *14,* R15. (c) Saponjic, Z. V.; Csencsits, R.; Rajh, T.; Dimitrijevic, N. M. *Chem. Mater.* **2003**, *15*, 4521.

23. Love, J. C.; Estroff, L. A.; Kriebel, J. K.; Nuzzo, R. G.; Whitesides, G. M. *Chem. Rev.* **2005**, *105,* 1103 and references therein.

24. Gittins, D. I.; Bethell, D.; Schiffrin, D. J.; Nichols, R. J. *Nature* **2000**, *408*, 67.

25. (a) Kiely, C. J.; Fink, J.; Brust, M.; Bethell, D.; Schiffrin, D. J. *Nature* **1998**, *396*, 444. (b) Wang, Z. L. *Adv. Mater.* **1998**, *10*, 13.

26. (a) Brust, M.; Walker, M.; Bethell, D.; Schiffrin, D. J.; Whyman, R. *J. Chem. Soc. Chem. Commun.* **1994**, 801. (b) Templeton, A. C.; Wuelfing, M. P.; Murray, R. W. *Acc. Chem. Res.* **2000**, *33*, 27 and references therein. (c) Daniel, M.-C.; Astruc, D. *Chem. Rev.* **2004**, *104*, 293 and references therein. (d) Shenhar, R.; Rotello, V. M. *Acc. Chem. Res.* **2003**, *36*, 549 and references therein. (e) Brust, M.; Fink, J.; Bethell, D.; Schiffrin, D. J.; Kiely, C. J. *J. Chem. Soc., Chem. Commun*. **1995**, 1655.

27. (a) Terril, R. H.; Postlethwaite, T. A.; Chen, C. H.; Poon, C. D.; Terzis, A.; Chen, A.; Hutchison, J. E.; Clark, M. R.; Wignall, G.; Londono, J. D.; Superfine, R.; Falvo, M.; Johnson Jr., C. S.; Samulski, E. T.; Murray, R. W. *J. Am. Chem. Soc.* **1995**, *117*, 12537. (b) Leff, D. V.; Ohara, P. C.; Heath, J. C.; Gelbart, W. M. *J. Phys. Chem.* **1995**, *99*, 7036. (c) Sarathy, K. V.; Raina, G.; Yadav, R. T.; Kulkarni, G. U.; Rao, C. N. R. *J. Phys. Chem. B* **1997**, *101*, 9876. (d) Porter, L. A.; Ji, D.; Westcott, S. L.; Graupe, M.; Czernuszewicz, R. S.; Halas, N. J.; Lee, T. R. *Langmuir* **1998**, *14*, 7378. (e) Johnson, S. R.; Evans, S. D.; Mahon, S. W.; Ulman, A. *Langmuir* **1997**, *13*, 51. (f) Chen, S.; Murray, R. W. *Langmuir* **1999**, *15*, 682.

28. (a) Cliffel, D. E.; Zamborini, F. P.; Gross, S. M.; Murray, R. W. *Langmuir* **2000**, *16*, 9699. (b) Mitra, S.; Nair, B.; Pradeep, T.; Goyal, P. S.; Mukhopadhyay, R. *J. Phys. Chem. B* **2002**, *106*, 3960.

29. (a) Tsuruoka, T.; Akamatsu, K.; Nawafune, H. *Langmuir* **2004,** *20,* 11169. (b) Peng, Z. A.; Peng, X. *J. Am. Chem. Soc.* **2001**, *123*, 183. (c) Hanus, L. H.; Sooklal, K.; Murphy, C. J.; Ploehn, H. J. *Langmuir* **2000**, *16*, 2621.

30. (a) Whetten, R. L.; Khoury, J. T.; Alvarez, M. M.; Murthy, S.; Vezmar, I.; Wang, Z. L.; Stephenes, P. W.; Cleveland, C. L.; Luedtke, W. D.; Landman, U. *Adv. Mater.* **1996**, *8*, 428. (b) Teranishi, T.; Haga, M.; Shiozawa, Y.; Miyake, M. *J. Am. Chem. Soc.* **2000**, *122*, 4237. (c) Zanchet, D.; Hall, B. D.; Ugarte, D. *J. Phys. Chem. B* **2000**, *104*, 11013. (d) Shon, Y.-S.; Gross, S. M.; Dawson, B.; Porter, M.; Murray, R. W. *Langmuir* **2000**, *16*, 6555. (e) Green, M.; O'Brien, P. *Chem. Commun*. **2000**, 183. (f) Yu, Y.-Y.; Chang, S.-S.; Lee, C.-L.; Wang, C. R. C. *J. Phys. Chem. B* **1997**, *101*, 6661. (g) Dujardin, E.; Hsin, L.; Wang, C. R. C.; Mann, S. *Chem. Comm.* **2001**, 1264.

31. (a) Jackson, J. B.; Halas, N. J. *J. Phys. Chem. B* **2001**, *105*, 2743. (b) Oku, T.; Kusunose, T.; Niihara, K.; Suganuma, K. *J. Mater. Chem.* **2000**, *10*, 255. (c) Bagwe, R. P.; Khilar, K. C. *Langmuir* **2000**, *16*, 905. (d) Chen, M. C.; Tsai, S. D.; Chen, M. R.; Ou, S. Y.; Li, W. H.; Lee, K. C. *Phys. Rev. B: Condens. Matter.* **1995**, *51*, 4507. (e) Remita, S.; Orts, J. M.; Feliu, J. M.; Mostafavi, M.; Delcourt, M. O. *Chem. Phys. Lett.* **1994**, *218*, 115. (f) Wen, J. M.; Evans, J. W.; Chang, S. L.; Burnett, J. W.; Thiel, P. A. *Mater. Res. Soc. Symp. Proc.* **1995**, *355*, 15. (g)

Downes, A.; Welland, M. E. *Appl. Phys. Lett.* **1998**, *72*, 2671. (h) Harfenist, S. A.; Wang, Z. L.; Alvarez, M. M.; Vezmar, I.; Whetten, R. L. *J. Phys. Chem.* **1996**, *100*, 13904.

32. (a) Prasad, B. L. V.; Stoeva, S. I.; Sorensen, C. M.; Klabunde, K. J. *Langmuir* **2002**, *18*, 7515. (b) Prasad, B. L. V.; Stoeva, S. I.; Sorensen, C. M.; Klabunde, K. J. *Chem. Mater.* **2003**, *15*, 935. (c) Stoeva, S. I.; Prasad, B. L. V.; Uma, S.; Stoimenov, P. K.; Zaikovsky, V.; Sorensen, C. M.; Klabunde, K. J. *J. Phys. Chem. B* **2003**, *107*, 7441. (d) Stoeva, S.; Klabunde, K. J.; Sorensen, C. M.; Dragieva, I. *J. Am. Chem. Soc*. **2002**, *124*, 2305.
33. (a) Markovich, G.; Leff, D. V.; Chung, S. W.; Soyez, H. M.; Dunn, B.; Heath, J. R. *Appl. Phys. Lett.* **1997**, *70*, 3107. (b) Peschel, S.; Schmid, G. *Angew. Chem., Int. Ed. Engl.* **1995**, *34*, 1442.
34. http://www.zyvex.com/nanotech/feynman.html
35. Taniguchi, N. *On the Basic Concept of 'Nano-Technology*; Proc. Intl. Conf. Prod. Eng. Tokyo, Part II, Japan Society of Precision Engineering, 1974.
36. Drexler, K. E. *Engines of Creation: The Coming Era of Nanotechnology;* Anchor Press/ Doubleday: New York, 1986.
37. Drexler, K. E. *Nanosystems: molecular machinery, manufacturing and computation;* John Wiley & Sons: New York, 1992.
38. http://www.swissre.com/INTERNET/pwsfilpr.nsf/vwFilebyIDKEYLu/ULUR-5YNGET/$FILE/Publ04_Nanotech_en.pdf.
39. Roco, M. C.; Karn, B. *Environ. Sci. Technol. A-Pages* **2005**, *39*, 106A and reference therein.
40. Schmid, G. In *Nanoscale Materials in Chemistry*; Klabunde, K. J.; Ed.; Wiley-Interscience: New York, 2001.
41. Aiken III, J. D.; Finke, R. G. *J. Mol. Cata. A:Chem.* **1999**, *145*, 1 and references therein.
42. *Nanoparticles: From Theory to Application*; Schmid, G.; Eds.; Wiley-VCH: Weinheim, 2004.

43. (a) El-Sayed, M. A. *Acc. Chem. Res.* **2001**, *34*, 257. (b) El-Sayed, M. A. *Acc. Chem. Res.* **2004**, *37*, 326. (c) Ghosh, S. K.; Nath, S.; Kundu, S.; Esumi, K.; Pal, T. *J. Phys. Chem. B* **2004**, *108*, 13963. (d) Link, S.; El-Sayed, M. A. *J. Phys. Chem. B* **1999**, *103*, 4212.

44. Schmid, G.; Corain, B. *Eur. J. Inorg. Chem.* **2003**, 3081.

45. (a) Henrichs, S.; Collier, C. P.; Saykally, R. J.; Shen, Y.; Heath, J. R. *J. Am. Chem. Soc.* **2000**, *122*, 4077. (b) McConnel, W. P.; Novak, J. P.; Brousseau III, L. C.; Fuierer, R. R.; Tenent, R. C.; Feldheim, D. L. *J. Phys. Chem. B* **2000**, *104*, 8925. (c) Schmid, G.; Chi, L. F. *Adv. Mater.* **1998**, *10*, 515.

46. Kubo, R. *J. Phys. Soc. Jpn.* **1962**, *17*, 952.

47. Halperin, W. P. *Rev. Mod. Phys.* **1986**, *58*, 533.

48. (a) Andres, R. P.; Bein, T.; Dorogi, M.; Feng, S.; Henderson, J. I.; Kubiak, C. P.; Mahoney, W.; Osifchin, R. G.; Reifenberger, R. *Science* **1996**, *272*, 1323. (b) Feldheim, D. L.; Keatig, C. D. *Chem. Soc. Rev.* **1998**, *27*, 1. (c) Dorogi, M.; Gomez, J.; Osifchin, R.; Andres, R. P.; Reifenberger, R. *Phy. Rev. B* **1995**, *52*, 9071. (d) Thomas, P. J.; Kulkarni, G. U.; Rao, C. N. R. *Chem. Phys. Lett.* **2000**, *321*, 163. (e) Harrell, L. E.; Bigioni, T. P.; Cullen, W. G.; Whetten, R. L.; First, P. N. *J. Vac. Sci. Technol. B* **1999**, *17*, 2411.

49. (a) Remacle, F.; Levine, R. *J. Amer. Chem. Soc.* **2000**, *122,* 4084. (b) Lambe, J.; Jaklevic, R. C. *Phy. Rev. Lett.* **1969**, *22*, 1371. (c) Cavicchi, R. E.; Silsbee, R. H. *Phy. Rev. B* **1988**, *37*, 706.

50. Mott, N. F.; Davis, E. A. *Electronic Processes in Noncrystalline Materials*; Clarendon Press: Oxford, UK, 1971.

51. Shiang, J. J.; Heath, J. R.; Collier, C. P.; Saykally, R. J. *J. Phys. Chem. B* **1998**, *102*, 3425.

52. Aslam, M. Ph. D thesis, University of Pune, Pune, Maharashtra, 2002.

53. (a) Alivisatos, A. P. *J. Phys. Chem* **1996**, *100*, 13226. (b) Alivisatos, A. P. *Science* **1996**, *271*, 933.

54. (a) Baibich, M. N.; Broto, J. M.; Fert, A.; Nguyen Van Dau, F.; Petroff, F.; Etiene, P.; Creuzet, G.; Friederich, A.; Chazelas, J. *Phys. Rev. Lett.* **1988**, *61*, 2472. (b) Bean, C. P.; Jacobs, I. S. *J. Appl. Phys.* **1960**, *31*, 1228.

55. (a) Livingstone, J. D.; Bean, C. P. *J. Appl. Phys.* **1961**, *32*, 1964. (b) *Quantum Tunneling of Magnetization;* Gunther, L., Barbara, B., Eds.; Kluwer Academic Publishers: Dodrecht, The Netherlands, 1994.

56. (a) Hai, B.; Wu, J.; Chen, X.; Protasiewicz, J. D.; Scherson, D. A. *Langmuir* **2005**, *21*, 3104. (b) Sun, S.; Zeng, H. *J. Am. Chem. Soc.* **2002**, *124*, 8204. (c) Boal, A. K.; Das, K.; Gray, M.; Rotello, V. M. *Chem. Mater.* **2002**, *14*, 2628.

57. (a) Sun, S.; Murray, C. B. *J. Appl. Phys.* **1999**, *85*, 4325. (b) Wu, N.; Fu, L.; Su, M.; Aslam, M.; Wong, K. C.; Dravid, V. P. *Nano Lett.* **2004**, *4*, 383. (c) Petit, C.; Taleb, A.; Pileni, M. P. *J. Phys. Chem. B* **1999**, *103*, 1805. (d) Puntes, V. F.; Krishnan, K. M.; Alivisatos, A. P. *Science* **2001**, *291*, 2115.

58. (a) Salgueirino-Maceira, V.; Liz-Marzan, L. M.; Farle, M. *Langmuir* **2004**, *20*, 6946. (b) Sun, S.; Murray, C. B.; Weller, D.; Folks, L.; Moser, A. *Science* **2000**, *287*, 1989.

59. (a) Henglein, A. *In Modern Trends of Colloid Science in Chemistry and Biology*; Eicke, H.-F., Eds.; Berkhäuser-Verlag: Basel, Switzerland, 1985. (b) Henglein, A. *J. Phys. Chem.* **1993**, *97*, 5457. (c) Henglein, A. *Top. Curr. Chem.* **1988**, *141*, 113. (d) Henglein, A.; Mulvaney, P.; Linnert, T. *Faraday Dis. Chem. Soc.* **1991**, *92*, 31. (e) Henglein, A. *Ber. Bunsen-Ges. Phys. Chem.* **1977**, *81*, 556. (f) Henglein, A. *Chem. Phys. Lett.* **1989**, *154*, 473. (g) Tausch-Treml, R.; Henglein, A.; Lilie, J. *Ber. Bunsen-Ges. Phys. Chem.* **1978**, *82*, 1335.

60. (a) Rossetti, R.; Nakahara, S.; Brus, L. E. *J. Chem. Phys.* **1983**, *79*, 1086. (b) Haram, S. K.; Quinn, B. M.; Bard, A. J. *J. Am. Chem. Soc.* **2001**, *123*, 8860. (c) Ding, Z.; Quinn, B. M.; Haram, S. K.; Pell, L. E.; Korgel, B. A.; Bard, A. J. *Science* **2002**, *296*, 1293. (d) Chen, S.; Truax, L. A.; Sommers, J. M. *Chem. Mater.* **2000**, *12*, 3864. (e) Bae, Y.; Myung, N.; Bard, A. J. *Nano Lett.* **2004**, *4*, 1153. (f) Kucur, E.; Riegler, J.; Urban, G. A.; Nann, T. *J. Chem. Phys.* **2003**, *119*, 2333. (g) Poznyak, S. K.; Osipovich, N. P.; Shavel, A.; Talapin, D. V.; Gao, M.; Eychmuller, A.; Gaponik, N. *J. Phys. Chem. B* **2005**, *109*, 1094.

61. *Advances in Electrochemistry and Electrochemical Engineering;* Gerischer, H.; Tobias, C. Eds.; Wiley, New York, 1977. Vol. 10.

62. Plieth, W. J. *Surf. Sci.* **1985**, *156*, 530.

63. Fisher, L. R.; Israelachvili, J. N. *J. Colloid Interface Sci.* **1981**, *80*, 528.

64. Werts, M. H.; Lambert, M.; Bourgoin, J.-P.; Brust, M. *Nano Lett.* **2002**, *2*, 43.

65. (a) Ingram, R. S.; Hostetler, M. J.; Murray, R. W.; Schaaff, T. G.; Khoury, J. T.; Whetten, R. L.; Bigioni, R. L.; Guthrie, D. K.; First, P. N. *J. Am. Chem. Soc.* **1997,** *119*, 9279. (b) Chen, S.; Ingram, R. S.; Hostetler, M. J.; Pietron, J. J.; Murray, R. W.; Schaaff, T. G.; Khoury, J. T.; Alvarez, M. M.; Whetten, R. L. *Science* **1998**, *280*, 2098. (c) Guo, R.; Georganopoulou, D.; Feldberg, S. W.; Donkers, R.; Murray, R. W. *Anal. Chem.* **2005**, *77*, 2662.

66. (a) Chen, S.; Murray, R. W.; Feldberg, S. W. *J. Phys. Chem. B* **1998**, *102*, 9898. (b) Quinn, B. M.; Lijeroth, P.; Ruiz, V.; Kaaksonen, T.; Kontturi, K. *J. Am. Chem. Soc.* **2003**, *125*, 6644. (c) Hicks, J. F.; Miles, D. T.; Murray, R. W. *J. Am. Chem. Soc.* **2002**, *124*, 13322.

67. Faraday, M. *Philos. Trans. R. Soc.* **1857**, *147*, 145.

68. (a) Schmid, G.; Pfeil, R.; Boese, R.; Bandermann, F.; Meyer, S.; Calis, G. H. M.; van der Velden. J. A. W. *Chem. Ber.* **1981**, *114*, 3634. (b) Schmid. G. *Struct. Bonding* **1985**, *62*, 51. (c) Schmid. G. *Polyhedron* **1988**, *7*, 2321.

69. (a) Hirai, T.; Okubo, H.; Komasawa, I. *J. Phys. Chem. B* **1999**, *103*, 4228. (b) Xu, W.; Liao, Y.; Akins, D. L. *J. Phys. Chem. B* **2002**, *106*, 11127.

70. (a) Shan, J.; Nuopponen, M.; Jiang, H.; Kauppinen, E.; Tenhu, H. *Macromolecules* **2003**, *36*, 4526. (b) Shon, Y.-S.; Wuelfing, W. P.; Murray, R. W. *Langmuir* **2001**, *17*, 1255. (c) Sun, X.; Dong, S.; Wang, E. *Macromolecules* **2004**, *37*, 7105. (d) Chen, D.; Peng, H.; Jiang, M. *Macromolecules* **2003**, *36*, 2576. (e) Bronstein, L.; Chernyshov, D.; Valetsky, P.; Tkachenko, N.; Lemmetyinen, H.; Hartmann, J.; Forster, S. *Langmuir* **1999**, *15*, 83.

71. Giersig, M.; Mulvaney, P. *Langmuir* **1993**, *9*, 3408.

72. (a) Sun, Y.-P.; Atorngitjawat, P.; Meziani, M. J. *Langmuir* **2001**, *17*, 5707. (b) Manna, A.; Imae, T.; Iida, M.; Hisamatsu, N. *Langmuir* **2001**, *17*, 6000. (c) Kang, S.

Y.; Kim, K. *Langmuir* **1998**, *14*, 226. (d) Fullam, S.; Rao, S. N.; Fitzmaurice, D. *J. Phys. Chem. B* **2000**, *104*, 6164. (e) Kim, H. S.; Ryu, J. H.; Jose, B.; Lee, B. G.; Ahn, B. S.; Kang, Y. S. *Langmuir* **2001**, *17*, 5817. (f) Manna, A.; Kulkarni, B. D.; Bandyopadhyay, K.; Vijayamohanan, K. *Chem. Mater.* **1997**, *9*, 3032.

73. (a) Yonezawa, T.; Yasui, K.; Kimizuka, N. *Langmuir* **2001**, *17*, 271. (b) Stefanescu, D. M.; Glueck, D. S.; Siegel, R.; Wasylishen, R. E. *Langmuir* **2004**, *20*, 10379. (c) Manna, A.; Chen, P.-L.; Akiyama, H.; Wei, T.-X.; Tamada, K.; Knoll, W. *Chem. Mater.* **2003**, *15*, 20. (d) Resch, R.; Baur, C.; Bugacov, A.; Koel, B. E.; Echternach, P. M.; Madhukar, A.; Montoya, N.; Requicha, A. A. G.; Will, P. *J. Phys. Chem. B* **1999**, *103*, 3647. (e) Tan, Y.; Li, Y.; Zhu, D. *Langmuir* **2002**, *18*, 3392. (f) Balasubramanian, R.; Kim, B.; Tripp, S. L.; Wang, X.; Lieberman, M.; Wei, A. *Langmuir* **2002**, *18*, 3676. (g) Shelley, E. J.; Ryan, D.; Johnson, S. R.; Couillard, M.; Fitzmaurice, D.; Nellist, P. D.; Chen, Y.; Palmer, R. E.; Preece, J. A. *Langmuir* **2002**, *18*, 1791. (h) Maye, M. M.; Chun, S. C.; Han, L.; Rabinovitch, D.; Zhong, C.-J. *J. Am. Chem. Soc.* **2002**, *124*, 4958. (i) Tzhayik, O.; Sawant, P.; Efrima, S.; Kovalev, E.; Klug, J. T. *Langmuir* **2002**, *18*, 3364. (j) Ackerson, C. J.; Jadzinsky, P. D.; Kornberg, R. D. *J. Am. Chem. Soc.* **2005**, *127*, 6550.

74. (a) Weare, W. W.; Reed, S. M.; Warner, M. G.; Hutchison, J. E. *J. Am. Chem. Soc.* **2000**, *122*, 12890. (b) Yamamoto, M.; Nakamoto, M. *Chem. Lett.* **2003**, *32*, 452. (c) Heath, J. R.; Brandt, L.; Leff, D. V. *Langmuir* **1996**, *12*, 4723. (c) Heath, J. R.; Knobler, C. M.; Leff, D. V. *J. Phys. Chem. B* **1997**, *101*, 189. (d) Selvakannan, P. R.; Mandal, S.; Phadtare, S.; Pasricha, R.; Sastry, M. *Langmuir* **2003**, *19*, 3545. (e) Kim, H. S.; Lee, S. J.; Kim, N. H.; Yoon, J. K.; Park, H. K.; Kim, K. *Langmuir* **2003**, *19*, 6701. (f) Joo, S.-W.; Kim, W.-J.; Yoon, W. S.; Choi, I. S. *J. Raman Spectrosc.* **2003**, *34*, 271.

75. (a) Hostetler, M. J.; Green, S. J.; Stokes, J. J.; Murray, R. W. *J. Am. Chem. Soc.* **1996**, *118*, 4212. (b) Hostetler, M. J.; Templeton, A. C.; Murray, R. W. *Langmuir* **1999**, *15*, 3782. (c) Shon, Y.-S.; Mazzitelli, C.; Murray, R. W. *Langmuir* **2001**, *17*, 7735. (d) Choo, H.; Cutler, E.; Shon, Y.-S. *Langmuir* **2003**, *19*, 8555. (e) Kell, A. J.; Stringle, D. L. B.; Workentin, M. S. *Org. Lett.* **2000**, *2*, 3381. (f) Kell, A. J.; Workentin, M. S. *Langmuir* **2001**, *17*, 7355. (g) Petroski, J.; Chou, M. H.; Creutz, C.

Inorg. Chem. **2004**, *43*, 1597. (h) Ionita, P.; Caragheorgheopol, A. *J. Am. Chem. Soc.* **2002**, *124*, 9048.

76. (a) Thomas, K. G.; Kamat, P. V. *Acc. Chem. Res.* **2003**, *36*, 888. (b) Hranisavljevic, J.; Dimitrijevic, N. M.; Wurtz, G. A.; Wiederrecht, G. P. *J. Am. Chem. Soc.* **2002**, *124*, 4536. (c) Chandrasekharan, N.; Kamat, P. V.; Hu, J.; Jones, G., II. *J. Phys. Chem. B* **2000**, *104*, 11103. (d) Thomas, K. G.; Kamat, P. V. *J. Am. Chem. Soc*. **2000**, *122,* 2655. (e) Ipe, B. I.; Mahima, S.; Thomas, K. G. *J. Am. Chem. Soc.* **2003**, *125*, 7174. (f) Huang, T.; Murray, R. W. *Langmuir* **2002**, *18*, 7077. (g) Aguila, A.; Murray, R. W. *Langmuir* **2000**, *16*, 5949.

77. (a) Sudeep, P. K.; Ipe, B. I.; George Thomas, K.; George, M. V.; Barazzouk, S.; Hotchandani, S.; Kamat, P. V. *Nano Lett.* **2002**, *2*, 29. (b) Brust, M.; Kiely, C. J.; Bethell, D.; Schiffrin, D. J. *J. Am. Chem. Soc.* **1998**, *120*, 12367. (c) Imahori, H.; Arimura, M.; Hanada, T.; Nishimura, Y.; Yamazaki, I.; Sakata, Y.; Fukuzumi, S. *J. Am. Chem. Soc.* **2001**, *123*, 335. (d) Gu, T.; Ye, T.; Simon, J. D.; Whitesell, J. K.; Fox, M. A. *J. Phys. Chem. B* **2003**, *107*, 1765. (e) Deng, F.; Yang, Y.; Hwang, S.; Shon, Y.-S.; Chen, S. *Anal. Chem.* **2004**, *76*, 6102.

78. Thomas, K. G.; Zajicek, J.; Kamat, P. V. *Langmuir* **2002**, *18*, 3722.

79. (a) Chen, S. *Langmuir* **1999**, *15*, 7551. (b) Templeton, A. C.; Chen, S. W.; Gross, S. M.; Murray, R. W. *Langmuir* **1999**, *15*, 66. (c) Hostetler, M. J.; Wingate, J. E.; Zhong, C.-J.; Harris, J. E.; Vachet, R. W.; Clark, M. R.; Londono, J. D.; Green, S. J.; Stokes, J. J.; Wignall, G. D.; Glish, G. L.; Porter, M. D.; Evans, N. D.; Murray, R. W. *Langmuir* **1998**, *14*, 17. (d) Ingram, R. S.; Hostetler, M. J.; Murray, R. W. *J. Am. Chem. Soc.* **1997**, *119*, 9175. (e) Templeton, A. C.; Hostetler, M. J.; Kraft, C. T.; Murray, R. W. *J. Am. Chem. Soc.* **1998**, *120*, 1906. (f) Hostetler, M. J.; Stokes, J. J.; Murray, R. W. *Langmuir* **1996**, *12*, 3604. (g) Li, D.; Zhang, Y.; Li, J. *Microelectron. Eng.* **2003**, *66*, 91.

80. (a) Pengo, P.; Broxterman, Q. B.; Kaptein, B.; Pasquato, L.; Scrimin, P. *Langmuir* **2003**, *19*, 2521. (b) Nam, J. M.; Park, S. J.; Mirkin, C. A. *J. Am. Chem. Soc.* **2002**, *124*, 3820. (c) Loweth, C. J.; Caldwell, W. B.; Peng, X. G.; Alivisatos, A. P.; Schultz, P. G. *Angew. Chem., Int. Ed. Engl.* **1999**, *38*, 1808. (d) Fischer N. O.,

McIntosh C. M., Simard J. M., Rotello V. M. *P. Natl. Acad. Sci. U.S.A.* **2002**, *99*, 5018.

81. (a) McIntosh, C. M.; Esposito, E. A.; Boal, A. K.; Simard, J. M.; Martin, C. T.; Rotello, V. M. *J. Am. Chem. Soc.* **2001**, *123*, 7626. (b) Boal, A. K.; Rotello, V. M. *J. Am. Chem. Soc.* **2000**, *122*, 734. (c) Briggs, C.; Norsten, T. B.; Rotello, V. M. *Chem. Commun.* **2002**, 1890. (d) Rosi, N. L.; Mirkin, C. A. *Chem. Rev.* **2005**, *105*, 1547.

82. (a) Storhoff, J. J.; Mirkin, C. A. *Chem. Rev.* **1999**, *99*, 1849. (b) Storhoff, J. J.; Mucic, R. C.; Mirkin, C. A. *J. Clust. Sci.* **1997**, *8*, 179. (c) Alivisatos, A. P.; Johnsson, K. P.; Peng, X.; Wislon, T. E.; Loweth, C. J.; Bruchez, M. P., Jr.; Schultz, P. G. *Nature* **1996**, *382*, 609. (d) Mirkin, C. A.; Letsinger, R. L.; Mucic, R. C.; Storhoff, J. J. *Nature* **1996**, *382*, 607. (e) Reynolds, R. A.; Mirkin, C. A.; Letsinger, R. L. *J. Am. Chem. Soc.* **2000**, *122*, 3795. (f) Elghanian, R.; Storhoff, J. J.; Mucic, R. C.; Letsinger, R. L.; Mirkin, C. A. *Science* **1997**, *277*, 1078.

83. (a) Glynou, K.; Ioannou, P. C.; Christopoulos, T. K.; Syriopoulou, V. *Anal. Chem*. **2003**, *75*, 4155. (b) Sandstrom, P.; Boncheva, M.; Åkerman, B. *Langmuir* **2003**, *19*, 6066.

84. Yang, Y.; Chen, S. *Nano Lett.* **2003**, *3*, 75.

85. (a) Green, S. J.; Stokes, J. J.; Hostetler, M. J.; Pietron, J. J.; Murray, R. W. *J. Phys. Chem. B* **1997**, *101*, 2663. (b) Green, S. J.; Pietron, J. J.; Stokes, J. J.; Hostetler, M. J.; Vu, H.; Wuelfing, W. P.; Murray, R. W. *Langmuir* **1998**, *14*, 5612. (c) Dong, T.-Y.; Chang, L. S.; Tseng, I. M.; Huang, S. J. *Langmuir* **2004**, *20*, 4471. (d) Dong, T.-Y.; Shih, H.-W.; Chang, L.-S. *Langmuir* **2004**, *20*, 9340. (e) Pietron, J. J.; Murray, R. W. *J. Phys. Chem. B* **1999**, *103*, 4440. (f) Miles, D. T.; Murray, R. W. *Anal. Chem.* **2001**, *73*, 921.

86. Chaki, N. K.; Aslam, M.; Gopakumar, T. G.; Sharma, J.; Pasricha, R.; Mulla, I. S.; Vijayamohanan, K. *J. Phys. Chem. B* **2003**, *107*, 13567.

87. Hicks, J. F.; Templeton, A. C.; Chen, S.; Sheran, K. M.; Jasti, R.; Murray, R. W.; Debord, J.; Schaaff, T. G.; Whetten, R. L. *Anal. Chem.* **1999**, *71*, 3703.

88. Imahori, H.; Kashiwagi, Y.; Endo, Y.; Hanada, T.; Nishimura, Y.; Yamazaki, I.; Araki, Y.; Ito, O.; Fukuzumi, S. *Langmuir* **2004**, *20*, 73.

89. (a) Johnson, S. R.; Evans, S. D.; Brydson, R. *Langmuir* **1998**, *14*, 6639. (b) Schaaff, T. G.; Knight, G.; Shafigullin, M. N.; Borkman, R. F.; Whetten, R. L. *J. Phys. Chem. B* **1998**, *102*, 10643. (c) Templeton, A. C.; Cliffel, D. E.; Murray, R. W. *J. Am. Chem. Soc.* **1999**, *121*, 7081.

90. (a) Montalti, M.; Prodi, L.; Zaccheroni, N.; Baxter, R.; Teobaldi, G.; Zerbetto, F. *Langmuir* **2003**, *19*, 5172. (b) Donkers, R. L.; Song, Y.; Murray, R. W. *Langmuir* **2004**, *20*, 4703. (c) Song, Y.; Murray, R. W. *J. Am. Chem. Soc.* **2002**, *124*, 7096.

91. (a) Chiang, C.-L. *J. Colloid Surf. Sci.* **2001**, *239*, 334. (b) Boutonnet, M.; Kizling, J.; Stenius, P.; Maire, G. *Colloids Surf*. **1982**, *5*, 209. (c) Petit, C.; Lixon, P.; Pilei, M.-P. *J. Phys. Chem.* **1993**, *97*, 12974. (d) Qi, L.; Ma, J.; Shen, J. *J. Colloid Interface Sci.* **1997**, *186*, 498. (e) Chen, D. H.; Yeh, J. J.; Hung, T. C. *J. Colloid Interface Sci.* **1999**, *215*, 159. (f) Chen, D. H.; Wu, S. H. *Chem. Mater.* **2000**, *12*, 1354.

92. (a) Touroude, R.; Girard, P.; Maire, G.; Kizling, J.; Boutonnet-Kizling, M.; Stenius, P. *Colloids Surf.* **1992**, *67*, 9. (b) Sangregorio, C.; Galeotti, M.; Bardi, U.; Baglioni, P. *Langmuir* **1996**, *12*, 5800. (c) Wu, M.-L.; Chen, D.-H.; Huang, T.-C. *Langmuir* **2001**, 17, 3877.

93. (a) Sarathy, K. V.; Kulkarni, G. U.; Rao, C. N. R. *Chem. Commun.* **1997**, 537. (b) Zhao, S.-Y.; Chen, S.-H.; Wang, S.-Y.; Li, D.-G.; Ma, H.-Y. *Langmuir* **2002**, 18, 3315. (c) Yang, J.; Deivaraj, T. C.; Too, H.-P. Lee, J. Y. *J. Phys. Chem. B* **2004**, *108*, 2181.

94. (a) Jana, N. R.; Peng, X. *J. Am. Chem. Soc.* **2003**, *125*, 14280. (b) Gu, H.; Zheng, R.; Zhang, X.; Xu, B. *J. Am. Chem. Soc.* **2004**, *126*, 5664. (c) Sharma, J.; Mahima, S.; Kakade, B. A.; Pasricha, R.; Mandale, A. B.; Vijayamohanan, K. *J. Phys. Chem. B* **2004**, *108*, 13280. (d) Chen, M.; Liu, J. P.; Sun, S. *J. Am. Chem. Soc.* **2004**, *126*, 8394. (e) Hiramatsu, H.; Osterloh, F. E. *Chem. Mater.* **2004**, *16*, 2509. (f) Aslam, M.; Fu, L.; Su, M.; Vijayamohanan, K.; Dravid, V. P. *J. Mater. Chem.* **2004**, *14*, 1795.

95. (a) Manna, A.; Imae, T.; Yogo, T.; Aoi, K.; Okazaki, M. *J. Colloid Interface Sci.* **2002**, *256*, 297. (b) Arcoleo, V.; Liveri, V. T. *Chem. Phys. Lett.* **1996**, *258*, 223. (c)

Carrot, G.; Valmalette, J. C.; Plummer, C. J. G.; Scholz, S. M.; Dutta, J.; Hofmann, H.; Hilborn, J. G. *Colloid Polym. Sci.* **1998**, *276*, 853. (d) Mandal, M.; Ghosh, S. K.; Kundu, S.; Esumi, K.; Pal, T. *Langmuir* **2002**, *18*, 7792. (e) Jana, N. R.; Gearheart, L.; Murphy, C. J. *Langmuir* **2001**, *17*, 6782. (f) Markowitz, M. A.; Dunn, D. N.; Chow, G. M.; Zhang, J. *J. Colloid Interface Sci.* **1999**, *210*, 73.

96. (a) Jana, N. R.; Gearheart, L.; Murphy, C. J. *Chem. Mater.* **2001**, *13*, 2313. (b) Sau, T. K.; Pal, A.; Jana, N. R.; Wang, Z. L.; Pal, T. *J. Nanopart. Res.* **2001**, *3*, 257. (c) Mallick, K.; Wang, Z. L.; Pal, T. *J. Photochem. Photobiol.* **2001**, *140*, 75. (d) Niidome, Y.; Hori, A.; Sato, T.; Yamada, S. *Chem. Lett.* **2000**, 310. (e) Reed, J. A.; Cook, A.; Halaas, D. J.; Parazolli, P.; Robinson, A.; Matula, T. J.; Griezer, F. *Ultrason. Sonochem.* **2003**, *10*, 285. (f) Henglein, A.; Meisel, D. *Langmuir* **1998**, *14*, 7392.

97. (a) Nakamoto, M.; Yamamoto, M.; Fukusumi, M. *Chem. Commun.* **2002**, 1622. (b) Shimizu, T.; Teranishi, T.; Hasegawa, S.; Miyake, M. *J. Phys. Chem. B* **2003**, *107*, 2719. (c) Teranishi, T.; Hasegawa, S.; Shimizu, T.; Miyake, M. *Adv. Mater.* **2001**, *13*, 1699. (d) Maye, M. M.; Zheng, W.; Leibowitz, F. L.; Ly, N. K.; Zhong, C.-J. *Langmuir* **2000**, *16*, 490. (e) Wuelfing, W. P.; Gross, S. M.; Miles, D. T.; Murray, R. W. *J. Am. Chem. Soc.* **1998**, *120*, 12696. (f) Mafune, F.; Kohno, J.-y.; Takeda, Y.; Kondow, T. *J. Phys. Chem. B* **2002**, *106*, 8555.

98. Waters, C. A.; Mills, A. J.; Johnson, K. A.; Schiffrin, D. J. *Chem. Commun.* **2003**, 540.

99. (a) Wei, G. T.; Liu, F. *J. Chromatogr. A* **1999**, 253. (b) Wei, G.; Liu, F.; Wang, C. R. C. *Anal. Chem.* **1999**, *71*, 2085. (c) Wilcoxon, J. P.; Martin, J. E.; Provencio, P. *Langmuir* **2000**, *16*, 9912. (d) Schnabel, U.; Fischer, C.; Kenndler, E. *J. Microcolumn Sep.* **1997**, *9*, 529. (e) Bos, W.; Steggerda, J. J.; Yan, S.; Casalnuovo, J. A.; Mueting, A. M.; Pignolet, L. H. *Inorg. Chem.* **1988**, *27*, 948. (f) Jimenez, V. L.; Leopold, M. C.; Mazzitelli, C.; Jorgenson, J. W.; Murray, R. W. *Anal. Chem.* **2003**, *75*, 199. (g) Wilcoxon, J. P.; Martin, J. E.; Provencio, P. *J. Chem. Phys.* **2001**, *115*, 998. (h) Wilcoxon, J. P.; Provencio, P. *J. Phys. Chem. B* **2003**, *107*, 12949. (i) Song, Y.; Jimenez, V.; McKinney, C.; Donkers, R.; Murray, R. W. *Anal. Chem.* **2003**, *75*, 5088.

100. (a) Marubayashi, K.; Takizawa, S.; Kawakusu, T.; Arai, T.; Sasai, H. *Org. Lett.* **2003**, *5*, 4409. (b) Shon, Y.-S.; Dawson, G. B.; Porter, M.; Murray, R. W. *Langmuir* **2002**, *18*, 3880. (c) Mallin, M. P.; Murphy, C. J. *Nano Lett.* **2002**, *2*, 1235. (d) Hostetler, M. J.; Zhong, C.-J.; Yen, B. K. H.; Anderegg, J.; Gross, S. M.; Evans, N. D.; Porter, M.; Murray, R. W. *J. Am. Chem. Soc.* **1998**, *120*, 9396. (e) Han, S. W.; Kim, Y.; Kim, K. *J. Colloid Interface Sci.* **1998**, *208*, 272. (f) Sandhyarani, N.; Pradeep, T. *Chem. Mater.* **2000**, *12*, 1755.

101. Sandhyarani, N.; Resmi, M. R.; Unnikrishnan, R.; Vidyasagar, K.; Ma, S.; Antony, M. P.; Selvaam, G. P.; Visalakshi, V., Kumar, N. C.; Pandian, K.; Tao, Y. T.; Pradeep, T. *Chem. Mater* **2000**, *12*, 104.

102. (a) Wang, Z. L. *J. Phys. Chem. B* **2000**, *104*, 1153. (b) Martin, J. E.; Odinek, J.; Wilcoxon, J. P.; Anderson, R. A.; Provencio, P. *J. Phys. Chem. B* **2003**, *107*, 430.

103. Ulman, A. *Chem. Rev.* **1996**, *96*, 1533.

104. (a) Badia, A.; Gao, W.; Singh, L.; Demers, L.; Cuccia, L.; Reven, L. *Langmuir* **1996**, *12*, 1262. (b) Badia, A.; Cuccia, L.; Demers, L.; Morin, F.; Lennox, R. B. *J. Am. Chem. Soc.* **1997**, *119*, 2682.

105. Bourg, M.; Badia, A.; Lennox, R. B. *J. Phys. Chem. B* **2000**, *104,* 6562.

106. (a) Laibinis, P. E.; Whitesides, G. M.; Allara, D. L.; Tao, Y.-T.; Parikh, A. N.; Nuzzo, R. G. *J. Am. Chem. Soc.* **1991**, *113*, 7152. (b) Bain, C. D.; Troughton, E. B.; Tao, Y. T.; Eval, J.; Whitesides, G. M.; Nuzzo, R. G. *J. Am. Chem. Soc.* **1989**, *111*, 321. (c) Colvin, V. L.; Goldstein, A. N.; Alivisatos, A. P. *J. Am. Chem Soc.* **1992**, *114*, 5229.

107. (a) Hasan, M.; Bethell, D.; Brust, M. *J. Am. Chem. Soc.* **2002**, *124*, 1132. (b) Bower, P. V.; Louie, E. A.; Long, J. R.; Stayton, P. S.; Drobny, G. P. *Langmuir* **2005**, *21*, 3002. (c) Kohlmann, O.; Steinmetz, W. E.; Mao, X.-A.; Wuelfing, W. P.; Templeton, A. C.; Murray, R. W.; Johnson, C. S., Jr. *J. Phys. Chem. B* **2001**, *105*, 8801. (d) Song, Y.; Harper, A. S.; Murray, R. W. *Langmuir* **2005**, *21*, 5492.

108. (a) Luedtke, W. D.; Landman, U. *J. Phys. Chem.* **1996**, *100*, 13323. (b) Luedtke, W. D.; Landman, U. *J. Phys. Chem. B* **1998**, *102*, 6566.

109. (a) Nyffenegger, R. M.; Penner, R. M. *Chem. Rev.* **1997**, *97*, 1195. (b) Kossakovski, D.; Beauchamp, J. L. *Anal. Chem.* **2000**, *72*, 4731. (c) Durig, U.; Pohl, D. W.; Rohner, F. *J. Appl. Phys.* **1986**, *59*, 3318. (d) Rugar, D.; Budakian, R.; Mamin, H. J.; Chui, B. W. *Nature* **2004**, *430*, 329. (e) Schonenberger, C.; Alvarado, S. F.; Lambert, S. E.; Sanders, I. L. *J. Appl. Phys.* **1990**, *67*, 7278. (f) Martin, Y.; Wickramasinghe, H. K. *Appl. Phys. Lett.* **1987**, *50*, 1455. (g) Zhong, Q.; Innis, D.; Kjoller, K.; Elings, V. B. *Surf. Sci. Lett.* **1993**, *290*, L888.

110. (a) Durston P. J.; Palmer, R. E.; Wilcoxon, J. P. *Appl. Phys. Lett.* **1998**, *72*, 176. (b) Durston, P. J.; Schmidt, J.; Palmer, R. E.; Wilcoxon, J. P. *Appl. Phys. Lett.* **1997**, *71*, 2940. (c) Yang, W.; Chen, M.; Knoll, W.; Deng, H. *Langmuir* **2002**, *18*, 4124. (d) Rowe, M. P.; Plass, K. E.; Kim, K.; Kurdak, C.; Zellers, E. T.; Matzger, A. J. *Chem. Mater.* **2004**, *16*, 3513.

111. (a) Kaiser, W. J.; Jaklevic, R. C. *Surf. Sci.* **1987**, *181*, 55. (b) Binning, G.; Smith, D. P. E. *Rev. Sci. Instrum.* **1986**, *57*, 1688. (c) Dharmadhikari, C. V. In *Encyclopedia of Analytical Chemistry: Instrumentation and Applications*; Meyers, R. A.; Ed.; John Wiley, UK, 2000.

112. (a) Mulvaney, P.; Giersig, M. *J. Chem. Soc. Faraday Trans.* **1996**, *92*, 3137. (b) Li, X.-M.; Paraschiv, V.; Huskens, J.; Reinhoudt, D. N. *J. Am. Chem. Soc.* **2003**, *125*, 4279. (c) Wang, G.; Zhang, J.; Murray, R. W. *Anal. Chem.* **2002**, *74*, 4320.

113. Hosaka, S.; Koyanagi, H.; Kikukawa, A.; Miyamoto, M.; Imura, R.; Ushiyama, J. *J. Vac. Sci. Technol. B* **1995**, *13*, 1307.

114. (a) Ingram, R. S.; Murray, R. W. *Langmuir* **1998**, *14*, 4115. (b) Pietron, J. J.; Hicks, J. F.; Murray, R. W. *J. Am. Chem. Soc.* **1999**, *121*, 5565.

115. Bard, A. J.; Faulkner, L. R. *Electrochemical Methods, Fundamentals and Applications; 2nd ed.* John Wiley & Sons: New York, 2001.

116. (a) Hicks, J. F.; Zamborini, F. P.; Osisek, A. J.; Murray, R. W. *J. Am. Chem. Soc.* **2001**, *123*, 7048. (b) Hicks, J. F.; Zamborini, F. P.; Murray, R. W. *J. Phys. Chem. B* **2002**, *106*, 7751. (c) Wuelfing, W. P.; Green, S. J.; Pietron, J. J.; Cliffel, D. E.; Murray, R. W. *J. Am. Chem. Soc.* **2000**, *122*, 11465. (d) Hicks, J. F.; Seok-Shon, Y.; Murray, R. W. *Langmuir* **2002**, *18*, 2288. (e) Chen, S. *J. Am.*

Chem. Soc. **2000**, *122*, 7420. (f) Chen, S. *Langmuir* **2001**, *17*, 6664. (g) Chen, S.; Murray, R. W. *J. Phys. Chem. B* **1999**, *103*, 9996.

117. (a) Brown, L. O.; Hutchison, J. E. *J. Phys. Chem. B* **2001**, *105*, 8911. (b) Bodkev, F.; Hansen, M. F.; Koch, C. B.; Leffman, K.; Steen, M. *Phy. Rev. B* **2000**, *61*, 6826.

118. Hutter, E.; Fendler, J. H.; Roy, D. *J. Phys. Chem. B* **2001**, *105*, 11159.

119. (a) Freeman, R. G.; Grabar, K. C.; Allison, K. J.; Bright, R. M.; Davis, J. A.; Guthrie, A. P.; Hommer, M. B.; Jackson, M. A.; Smith, P. C.; Walter, D. G.; Natan, M. J. *Science* **1995**, *267*, 1629. (b) Grabar, K. C.; Smith, P. C.; Musick, M. D.; Davis, J. A.; Walter, D. G.; Jackson, M. A.; Guthrie, A. P.; Natan, M. J. *J. Am. Chem. Soc.* **1996**, *118*, 1148. (c) Schwartzberg, A. M.; Grant, C. D.; Wolcott, A.; Talley, C. E.; Huser, T. R.; Bogomolni, R.; Zhang, J. Z. *J. Phys. Chem. B* **2004**, *108*, 19191.

120. (a) Chen, S.; Yang, Y. *J. Am. Chem. Soc.* **2000**, *124*, 5280. (b) Yang, Y.; Grant, K. M.; White, H. S.; Chen, S. *Langmuir* **2003**, *19*, 9446.

121. (a) Chen, Y.; Palmer, R. E.; Shelley, E. J.; Preece, J. *Surf. Sci.* **2002**, *502-503*, 208. (b) Otsuka, H.; Akiyama, Y.; Nagasaki, Y.; Kataoka, K. *J. Am. Chem. Soc.* **2001**, *123*, 8226. (c) Armelao, L.; Colombo, P.; Fabrizio, M.; Gross, S.; Silvia, T. E. *J. Mat. Chem.***1999**, *9*, 2893.

122. (a) Quinn, B. M.; Prieto, I.; Haram, S. K.; Bard, A. J. *J. Phys. Chem. B* **2001**, *105*, 7474. (b) Liljeroth, P.; Vanmaekelbergh, D.; Ruiz, V.; Kontturi, K.; Jiang, H.; Kauppinen, E.; Quinn, B. M. *J. Am. Chem. Soc.* **2004**, *126*, 7126. (c) Quinn, B. M.; Liljeroth, P.; Kontturi, K. *J. Am. Chem. Soc.* **2002**, *124*, 12915. (d) Ruiz, V.; Liljeroth, P.; Quinn, B. M.; Kontturi, K. *Nano Lett.* **2003**, *3*, 1459. (e) Georganopoulou, D. G.; Mirkin, M. V.; Murray, R. W. *Nano Lett.* **2004**, *4*, 1763. (f) Liljeroth, P.; Quinn, B. M.; Ruiz, V.; Kontturi, K. *Chem. Commun.* **2003**, 1570.

123. (a) Bavykin, D. V.; Savinov, E. N.; Parmon, V. N. *Langmuir* **1999**, *15*, 4722. (b) Wang, W.; Germanenko, I.; El-Shall, M. S. *Chem. Mater.* **2002**, *14*, 3028. (c) Yang, H.; Holloway, P. H. *J. Phys. Chem. B* **2003**, *107*, 9705. (d) Talapin, D. V.; Mekis, I.; Gotzinger, S.; Kornowski, A.; Benson, O.; Weller, H. *J. Phys. Chem. B* **2004**, *108*, 18826.

124. Collier, C. P.; Vossmeyer, T.; Heath, J. R. *Annu. Rev. Phys. Chem*. **1998**, *49*, 371 and references therein.

125. (a) Guzelian, A. A.; Katari, J. E. B.; Kadavanich, A. V.; Barin, U.; Hamad, K. *J. Phys. Chem.* **1996**, *100*, 7212. (b) Nakanishi, T.; Ohtani, B.; Uosaki, K. *J. Phys. Chem. B* **1998**, *102*, 1571. (c) Aslam, M.; Chaki, N. K.; Sharma, J.; Mulla, I. S.; Vijayamohanan, K. *Curr. Appl. Phys.* **2003,** *3*, 115. (d) Yin, J. S.; Wang, Z. L. *Phy. Rev. Lett.* **1997**, *79*, 2570. (e) Kim, S.-H.; Medeiros-Ribeiro, G.; Ohlberg, D. A. A.; Williams, R. S.; Heath, J. R. *J. Phys. Chem. B*, **1999**, *103*, 10341.

126. (a) Ahmadi, T. S.; Wang, Z. L.; Green, T. C.; Henglein, A.; El-Sayed, M. A. *Science* **1996**, *272*, 1924. (b) Tanori, J.; Pileni, M. P. *Adv. Mater.* **1995**, *7*, 862. (c) Lisiek, I.; Pileni, M. P. *J. Phy. Chem.* **1995**, *99*, 5077. (d) Collier, C. P.; Saykally, R. J.; Shiang, J. J.; Henrichs, S. E.; Heath, J. R. *Science*, **1997**, *277*, 1978. (e) Markovich, G.; Collier, C. P; Heath, J. R. *Phys. Rev. Lett.* **1998**, *80*, 3807.

127. (a) Gacoin, T.; Chaput, F.; Boilot, J. P.; Jaskierowicz, G. *Chem. Mater.* **1993**, *5*, 1150. (b) Brinker, C. J.; Lu, Y.; Sellinger, A.; Fan, H. *Adv. Mater.* **1999**, *11*, 579. (c) Connolly, S.; Fullam, S.; Korgel, B.; Fitzamurice, D. *J. Am. Chem. Soc.* **1998**, *120*, 2969.

128. (a) Fendler, J. H.; Meldrum, F. *Adv. Mater.* **1995**, *7*, 607 and references therein. (b) Sastry, M.; Patil, V.; Mayya, K. S.; Paranjape, D. V.; Singh, P.; Sainkar, S. R. *Thin Solid Films* **1998**, *324*, 239. (c) Li, M.; Wong, K. K. W.; Mann, S. *Chem. Mater.* **1999**, *11*, 23. (d) Dabbousi, B. O.; Murray, C. B.; Rubner, M. F.; Bawendi, M. G. *Chem*. *Mater*. **1994**, *6*, 216. (e) Sastry, M.; Gole, A.; Patil, V. *Thin Solid Films* **2001**, *384*, 125. (f) Huang, S.; Tsutsui, G.; Sakaue, H.; Shingubara, S.; Takahagi, T. *J. Vac. Sci. Technol. B* **2001**, *19*, 2045.

129. Bentzon, M. D.; Tholen, A. *Ultramicroscopy* **1990**, *38*, 105.

130. Giersig, M.; Mulvaney, P. *J. Phys. Chem.* **1993**, *97*, 6334.

131. Ohara, P. C.; Leff, D. V.; Heath, J. R.; Gelbart, W. M. *Phy. Rev. Lett.* **1995**, *75*, 3466.

132. (a) Ellis, A. V.; Vijayamohanan, K.; Goswami, R.; Chakrapani, N.; Ramanathan, L. S.; Ajayan, P. M.; Ramanath, G. *Nano Lett.* **2003**, *3*, 279. (b) Wang, G.; Murray, R.

W. *Nano Lett.* **2004**, *4*, 95. (c) Liu, L.; Wang, T.; Li, J.; Guo, Z.-X.; Dai, L.; Zhang, D.; Zhu, D. *Chem. Phys. Lett.* **2003**, *367*, 747. (d) Jiang, K.; Eitan, A.; Schadler, L. S.; Ajayan, P. M.; Siegel, R. W.; Grobert, N.; Mayne, M.; Reyes-Reyes, M.; Terrones, H.; Terrones, M. *Nano Lett.* **2003**, *3*, 275.

133. (a) Baum, T.; Bethell, D.; Brust, M.; Schiffrin, D. J. *Langmuir* **1999**, *15*, 866. (b) Zamborini, F. P.; Hicks, J. F.; Murray, R. W. *J. Am. Chem. Soc.* **2000**, *122,* 4514. (c) Templeton, A. C.; Zamborini, F. P.; Wuelfing, W. P.; Murray, R. W. *Langmuir* **2000**, *16*, 6682. (d) He, H. X.; Zhang, H.; Li, Q. G.; Zhu, T.; Li, S. F. Y.; Liu, Z. F. *Langmuir* **2000**, *16*, 3846. (e) Wuelfing, W. P.; Zamborini, F. P.; Templeton, A. C.; Wen, X.; Yoon, H.; Murray, R. W. *Chem. Mater.* **2001**, *13*, 87.

134. (a) Peng, Z.; Qu, X.; Dong, S. *Langmuir* **2004**, *20*, 5. (b) Sastry, M.; Rao, M.; Ganesh, K. N. *Acc. Chem. Res.* **2002**, *35*, 847. (c) Bandhyopadhyay, K.; Mayya, S.; Vijayamohanan, K.; Sastry, M. *Langmuir* **1997**, *13*, 5244. (d) Pethkar, S.; Aslam, M.; Mulla, I. S.; Ganeshan, P.; Vijayamohanan, K. *J. Mater. Chem.* **2001**, *11*, 1710. (e) Aslam, M.; Mulla, I. S.; Vijayamohanan, K. *Langmuir* **2001**, *17*, 7487.

135. (a) Malikova, N.; Pastoriza-Santos, I.; Schierhorn, M.; Kotov, N. A.; Liz-Marzan, L. M. *Langmuir* **2002**, *18*, 3694. (b) Jiang, C.; Markutsya, S.; Tsukruk, V. V. *Langmuir* **2004**, *20*, 882. (c) Constantine, C. A.; Gattas-Asfura, K. M.; Mello, S. V.; Crespo, G.; Rastogi, V.; Cheng, T.-C.; DeFrank, J. J.; Leblanc, R. M. *Langmuir* **2003**, *19*, 9863. (d) Sarathy, K. V.; Thomas, P. J.; Kulkarni, G. U.; Rao, C. N. R. *J. Phys. Chem. B* **1999**, *103*, 399. (e) Chan, E. W. L.; Lee, D.-C.; Ng, M.-K.; Wu, G.; Lee, K. Y. C.; Yu, L. *J. Am. Chem. Soc.* **2002**, *124*, 12238.

136. (a) Templeton, A. C.; Pietron, J. J.; Murray, R. W.; Mulvaney, P. *J. Phys. Chem. B* **2000**, *104*, 564. (b) Qu, X.; Peng, Z.; Jiang, X.; Dong, S. *Langmuir* **2004**, *20*, 2519. (c) Link, S.; Mohamed, M. B.; El-Sayed, M. A. *J. Phys. Chem. B* **1999**, *103*, 3073. (d) Swanson, N. L.; Billard, B. D. *Nanotechnology* **2003**, *14*, 353.

137. (a) Schaaf, T. G.; Shafigullen, M. N.; Khoury, J. T.; Vezmar, I.; Whetten, R. L.; Cullen, W. G.; First, P. N.; Guttierrez-Wing, C.; Ascencio, J.; Jose-Yacamun, M. J. *J. Phys. Chem. B* **1997**, *101*, 7885. (b) Zaitoun, M. A.; Mason, W. R.; Lin, C. T. *J. Phys. Chem. B* **2001**, *105*, 6780. (c) Melinger, J. S.; Kleiman, V. D.; McMorrow, D.; Grohn, F.; Bauer, B. J.; Amis, E. *J. Phys. Chem. A* **2003**, *107*, 3424. (d) Logunov,

S. L.; Ahmadi, T. S.; El-Sayed, M. A.; Khoury, J. T.; Whetten, R. L. *J. Phys. Chem. B* **1997**, *101*, 3713.

138. (a) Alvarez, M. M.; Khoury, J. T.; Schaaff, T. G.; Shafigullin, M. N.; Vezmar, I.; Whetten, R. L. *J. Phys. Chem. B* **1997**, *101*, 3706. (b) Gutierrez, E.; Powell, R. D.; Furuya, F. R.; Hainfeld, J. F.; Schaaff, T. G.; Shafigullin, M. N.; Stephens, P. W.; Whetten, R. L. *Eur. Phys. J. D* **1999**, *9*, 647. (c) Donkers, R. L.; Lee, D.; Murray, R. W. *Langmuir* **2004**, *20*, 1945.

139. (a) Link, S.; Wang, Z. L.; El-Sayed, M. A. *J. Phys. Chem. B* **1999**, *103*, 3529. (b) Mulvaney, P. *Langmuir* **1996**, *12*, 788.

140. Mie, G. *Ann. Phys*. **1908**, *25*, 377.

141. Nath, N.; Chilkoti, A. *J. Am. Chem. Soc.* **2001**, *123*, 8197.

142. (a) Imahori, H.; Fukuzumi, S. *Adv. Mater.* **2001**, *13*, 1197. (b) Gu, T.; Whitesell, J. K.; Fox, M. A. *Chem. Mater.* **2003**, *15*, 1358. (c) Lakowitcz, J. R. *Principles of Fluorescence Spectroscopy*; Kluwer: New York, 1999.

143. (a) Wilcoxon, J. P.; Martin, J. E.; Parsapour, F.; Wiedenman, B.; Kelley, D. F. *J. Chem. Phys.* **1998**, *108*, 9137. (b) Lee, D.; Donkers, R. L.; Wang, G.; Harper, A. S.; Murray, R. W. *J. Am. Chem. Soc.* **2004**, *126*, 6193. (c) Wang, G.; Huang, T.; Murray, R. W.; Menard, L.; Nuzzo, R. G. *J. Am. Chem. Soc.* **2005**, *127*, 812. (d) Bigioni, T. P.; Whetten, T. P.; Dag, O. *J. Phys. Chem. B* **2000**, *104*, 6983.

144. (a) Ancona, M. G.; Kruppa, W.; Rendell, R. W.; Snow, A. W.; Park, D.; Boos, J. B. *Phy. Rev. B* **2001**, *64*, 033408. (b) Wang, B.; Wang, H.; Li, H.; Zheng, C.; Hou, J. G. *Phy. Rev. B* **2000**, *63*, 035403. (c) Hanna, A. E.; Tinkham, M. *Phy. Rev. B* **1991**, *44*, 5919. (d) Medeiros-Ribeiro, G.; Ohlberg, D. A. A.; Williams, R. S.; Heath, J. R. *Phy. Rev. B* **1999**, *59,*1633. (e) Aslam, M.; Mulla, I. S.; Vijayamohanan, K. *Appl. Phys. Lett.* **2001**, *79*, 689. (f) Brust, M.; Bethell, D.; Schiffrin, D. J.; Kiely, C. J. *Adv. Mater.* **1995**, *7*, 795.

145. (a) Zhang, P.; Sham, T. K. *Appl. Phys. Lett.* **2002**, *81*, 736. (b) Zhang, P.; Sham, T. K. *Phys. Rev. Lett.* **2003**, *90*, 245502. (c) Huang, X.; Huang, H.; Wu, N.; Hu, R.; Zhu, T.; Liu, Z. *Surf. Sci.* **2000**, *459*, 183.

146. Mohamed, M. B.; Ahmadi, T. S.; Link, S.; Braun, M.; El-Sayed, M. A. *Chem. Phys. Lett.* **2001**, *343*, 55.

147. (a) Legrand, J.; Ngo, A. T.; Petit, C.; Pileni, M. P. *Adv. Mater.* **2001**, *13*, 58. (b) Legrand, J.; Petit, C.; Pileni, M. P. *J. Phys. Chem. B* **2001**, *105*, 5643. (c) Germain, V.; Pileni, M. P. *J. Phys. Chem. B* **2005**, *109*, 5548.

148. (a) Volokitin, Y.; Sinzig, J.; de Jongh, L. J.; Schmid, G.; Moiseev, I. I. *Nature* **1997**, *384*, 621. (b) Claus, P.; Bruckner, A.; Mohr, C.; Hofmeister, H. *J. Am. Chem. Soc.* **2000**, *122*, 11430.

149. (a) Labande, A.; Ruiz, J.; Astruc, D. *J. Am. Chem. Soc.* **2002**, *124*, 1782. (b) Daniel, M.-C.; Ruiz, J.; Nlate, J.; Palumbo, J.; Blais, J.-C.; Astruc, D. *Chem. Commun*. **2001**, 2000. (c) Daniel, M.-C.; Ruiz, J.; Nlate, S.; Blais, J.-C.; Astruc, D. *J. Am. Chem. Soc*. **2003**, *125*, 2617. (d) Horikoshi, T.; Itoh, M.; Kurihara, M.; Kubo, K.; Nishihara, H. *J. Electroanal. Chem.* **1999**, *473*, 113.

150. Yamada, M.; Nishihara, H. *Chem. Commun*. **2002**, 2578.

151. Yamada, M.; Kubo, K.; Nishihara, H. *Chem. Lett.* **1999**, 1335.

152. (a) Liu, J.; Alvarez, J.; Ong, W.; Kaifer, A. E. *Nano Lett.* **2001**, *1*, 57. (b) Zhu, D.; Li, Y.; Wang, S.; Shi, Z.; Du, C.; Xiao, S.; Fang, H.; Zhou, Y. *Synth. Met.* **2003**, *133-134*, 679. (c) Fujihara, H.; Nakai, H. *Langmuir* **2001**, *17*, 6393. (d) Shon, Y.-S.; Choo, H. *Chem. Commun.* **2002**, 2560. (e) C. Roth, I. Hussain, M. Bayati, R. J. Nichols, D. J. Schiffrin, *Chem. Commun.* **2004**, 1532.

153. (a) Gittins, D. I.; Bethell, D.; Nichols, R. J.; Schiffrin, D. J. *Adv. Mater.* **1999**, *11*, 737. (b) Sagara, T.; Kato, N.; Toyota, A.; Nakashima, N. *Langmuir* **2002**, *18*, 6995.

154. (a) Ung, T.; Giersig, M.; Dunstan, D.; Mulvaney, P. *Langmuir* **1997**, *13*, 1773. (b) Marcaccio, M.; Margotti, M.; Montalti, M.; Paolucci, F.;Prodi, L.; Zaccheroni, N. *Collect. Czech. Chem. Commun.* **2003**, *68*, 1395. (c) Aslam, M.; Chaki, N. K.; Mulla, I. S.; Vijayamohanan, K. *Appl. Surf. Sc.* **2001**, *182*, 338. (d) Maye, M. M.; Lou, Y.; Zhong, C.-J. *Langmuir* **2000,** *16,* 7520.

155. Quinn, B. M.; Kontturi, K. *J. Am. Chem. Soc.* **2004**, *126*, 7168.

156. Templeton, A. C.; Hostetler, M. J.; Warmoth, E. K.; Chen, S.; Hartshorn, C. M.; Krishnamurthy, V. M.; Forbes, M. D. E.; Murray, R. W. *J. Am. Chem. Soc.* **1998**, *120*, 4845.

157. (a) Boal, A. K.; Rotello, V. M. *J. Am. Chem. Soc.* **2002**, *124*, 5019. (b) Lin, S.-Y.; Liu, S.-W.; Lin, C.-M.; Chen, C.-H. *Anal. Chem.* **2002**, *74*, 330. (c) Obare, S. O.; Hollowell, R. E.; Murphy, C. J. *Langmuir* **2002**, *18*, 10407.

158. (a) Joseph, Y.; Besnard, I.; Rosenberger, M.; Guse, B.; Nothofer, H.-G.; Wessels, J.-M.; Ute, W.; Knop-Gericke, A.; Su, D.; Schlogl, R.; Yasuda, A.; Vossmeyer, T. *J. Phys. Chem. B* **2003**, *107*, 7406. (b) Kim, Y.; Johnson, R. C.; Hupp, J. T. *Nano Lett.* **2001**, *1*, 165. (c) Zhang, H.-L.; Evans, S. D.; Henderson, J. R.; Miles, R. E.; Shen, T.-H. *Nanotechnology* **2002**, *13*, 439.

159. (a) Schroedter, A.; Weller, H. *Angew. Chem., Int. Ed.* **2002**, *41*, 3218. (b) Su, X.; Yau Li, S. F.; O'Shea, S. J. *Chem. Commun.* **2001**, 755. (c) Gole, A.; Dash, C.; Soman, C.; Sainkar, S. R.; Rao, M.; Sastry, M. *Bioconjugate Chem.* **2001**, *12*, 684. (d) Jia, J.; Wang, B.; Wu, A.; Cheng, G.; Li, Z.; Dong, S. *Anal. Chem.* **2002**, *74*, 2217.

160. (a) Gregori, L.; Hainfeld, J. F.; Simon, M. N.; Golbager, D. *J. Biol. Chem.* **1997**, *272*, 58. (b) Burkett, S. L.; Mann, S. *Chem. Commun.* **1996**, 321. (c) Bhattacharya, S.; Srivastava, A. *Langmuir* **2003**, *19*, 4439. (d) Fan, J.; Chen, S.; Gao, Y. *Colloids Surf.* **2003**, *28*, 199.

161. (a) Nuss, S.; Bottcher, H.; Wurm, H.; Hallensleben, M. L. *Angew. Chem., Int. Ed.* **2001**, *40*, 4016. (b) Mandal, T. K.; Fleming, M. S.; Walt, D. R. *Nano Lett.* **2002**, *2*, 3.

162. (a) Eklund, S. E.; Cliffel, D. E. *Langmuir* **2004**, *20*, 6012. (b) Alvarez, J.; Liu, J.; Roman, E.; Kaifer, A. E. *Chem. Commun.* **2000**, 1151.

163. (a) Evans, S. D.; Johnson, S. R.; Ringsdorf, R.; Williams, L. M.; Wolf, H. *Langmuir* **1998**, *14*, 6436. (b) Dabbousi, B. O.; Bawendi, M. G.; Onitsuka, O.; Rubner, M. F. *Appl. Phys. Lett.***1995**, *66*, 1316. (c) Youk, J. H.; Locklin, J.; Xia, C.; Park, M.-K.; Advincula, R. *Langmuir* **2001**, *17*, 4681.

164. (a) Zayats, M.; Kharitonov, A. B.; Pogorelova, S. P.; Lioubashevski, O.; Katz, E.; Willner, I. *J. Am. Chem. Soc.* **2003**, *125*, 16006. (b) Nabika, H.; Deki, S. *J. Phys. Chem. B* **2003**, *107*, 9161. (c) Bakker, E. *Anal. Chem.* **2004**, *76*, 3285. (d) Richter, M. M. *Chem. Rev.* **2004**, *104*, 3003.

165. (a) Shipway, A. N.; Lahav, M.; Blonder, R.; Willner, I. *Chem. Mater.* **1999**, *11*, 13. (b) Lahav, M.; Heleg-Shabtai, V.; Wasserman, J.; Katz, E.; Willner, I.; Durr, H.; Hu, Y.-Z.; Bossmann, S. H. *J. Am. Chem. Soc.* **2000**, *122*, 11480.

166. Szunerits, S.; Walt, D. R. *Anal. Chem.* **2002**, *74*, 1718.

167. (a) Shen, Y. R. *The Principles of Nonlinear Optics*; Wiley: New York, 1984. (b) Antoine, R.; Brevet, P. F.; Girault, H. H.; Bethell, D.; Schiffrin, D. J. *Chem. Commun.* **1997**, 1901. (c) Novak, J. P.; Brousseau, L. C., III; Vance, F. W.; Johnson, R. C.; Lemon, B. I.; Hupp, J. T.; Feldheim, D. L. *J. Am. Chem. Soc.* **2000**, *122*, 12029.

168. Ball, P. *Engineers devise invisibility shield;* news@nature.com, published online: 28 February 2005, doi:10.1038/news050228-1.

169. (a) Inouye, H.; Kanemitsu, Y. *Appl. Phys. Lett.* **2003**, *82*, 1155. (b) Qu, S.; Song, Y.; Du, C.; Wang, Y.; Gao, Y.; Liu, S.; Li, Y.; Zhu, D. *Opt. Commun*. **2001**, *196*, 317. (c) Qu, S.; Du, C.; Song, Y.; Wang, Y.; Gao, Y.; Liu, S.; Li, Y.; Zhu, D. *Chem. Phys. Lett.* **2002**, *356*, 403. (d) Fang, H.; Du, C.; Qu, S.; Li, Y.; Song, Y.; Li, H.; Liu, H.; Zhu, D. *Chem. Phys. Lett.* **2002**, *364*, 290.

170. Mendes, P. M.; Jacke, S.; Critchley, K.; Plaza, J.; Chen, Y.; Nikitin, K.; Palmer, R. E.; Preece, J. A.; Evans, S. D.; Fitzmaurice, D. *Langmuir* **2004**, *20*, 3766.

171. Sommer, A. P.; Ben-Moshe, M.; Magdassi, S. *J. Phys. Chem. B* **2004**, *108*, 8.

172. http://www.public.itrs.net/

173. Streetman, B. G.; Banerjee, S. *Solid State Electronic Devices*; Prentice Hall: New Jersey, 2000.

174. Paul, S.; Pearson, C.; Molloy, A.; Cousins, M. A.; Green, M.; Kolliopoulou, S.; Dimitrakis, P.; Normand, P.; Tsoukalas, D.; Petty, M. C. *Nano Lett.* **2003**, *3*, 533.

175. Shiigi, H.; Tokonami, S.; Yakabe, H.; Nagaoka, T. *J. Am. Chem. Soc.* **2005**, *127*, 3280.

176. Sun, S.; Anders, S.; Thomson, T.; Baglin, J. E. E.; Toney, M. F.; Hamann, H. F.; Murray, C. B.; Terris, B. D. *J. Phys. Chem. B* **2003**, *107*, 5419.

177. Pal, S.; John, N. S.; Thomas, P. J.; Kulkarni, G. U.; Sanyal, M. K. *J. Phys. Chem. B* **2004**, *108*, 10770.

178. Sun, S.; Anders, S.; Hamann, H. F.; Thiele, J.-U.; Baglin, J. E. E.; Thomson, T.; Fullerton, E. E.; Murray, C. B.; Terris, B. D. *J. Am. Chem. Soc.* **2002**, *124*, 2884.

179. Niemeyer, C. M. *Angew. Chem., Int. Ed.* **2001**, *40*, 4128.

180. (a) Natan, M. J.; Lyon, L. A. In *Surface Plasmon Resonnance Biosensing with Colloidal Au Amplification. In Metal Nanoparticles-Synthesis, Characterization and Applications*; Feldheim, D. L.; Colby, A. F. Jr.; Ed.; Marcel Dekker: New York, 2002 pp 183. (b) Thanh, N. T. K.; Rosenzweig, Z. *Anal. Chem.* **2002**, *74*, 1624. (c) Zhang, C.; Zhang, Z.; Yu, B.; Shi, J.; Zhang, X. *Anal. Chem.* **2002**, *74*, 96.

181. (a) Schneider, B. H.; Dickinson, E. L.; Vach, M. D.; Hoijer, J. V.; Howard, L. V. *Biosens. Bioelectron.* **2000**, *15*, 13. (b) Schneider, B. H.; Dickinson, E. L.; Vach, M. D.; Hoijer, J. V.; Howard, L. V. *Biosens. Bioelectron.* **2000**, *15*, 497.

182. Brown, K. J.; Fox, A. P.; Natan, M. J. *J. Am. Chem. Soc.* **1996**, *118*, 1154.

183. Yabuki, S.; Mitzutani, F. *Electroanalysis* **1997**, *9*, 23.

184. (a) Xiao, Y.; Ju, X. H.; Chen, H. Y. *Anal. Chim. Acta.* **1999**, *391*, 73. (b) Katz, E.; Schmid, H. L. *J. Electroanal. Chem.* **1993**, *360*, 337.

185. Zhao, J.; Henkens, R. W.; Stonehuerner, J.; O'Daly, J. P.; Crumbliss, A. L. *J. Electroanal. Chem.* **1992**, *327*, 109.

186. (a) Jun, Y.-w.; Huh, Y.-M.; Choi, J.-s.; Lee, J.-H.; Song, H.-T.; Kim, S.; Yoon, S.; Kim, K.-S.; Shin, J.-S.; Suh, J.-S.; Cheon, J. *J. Am. Chem. Soc.* **2005**, *127*, 5732. (b) Kim, D. K.; Mikhaylova, M.; Wang, F. H.; Kehr, J.; Bjelke, B.; Zhang, Y.; Tsakalakos, T.; Muhammed, M. *Chem. Mater.* **2003**, *15*, 4343.

187. Ridley, B. A.; Nivi, B.; Jacobson, J. M. *Science* **1999**, *286*, 746.

Chapter 2

Synthesis and Characterization of Monolayer Protected Gold Nanoclusters: Temperature Effect on Au Nanoparticles Superstructures*

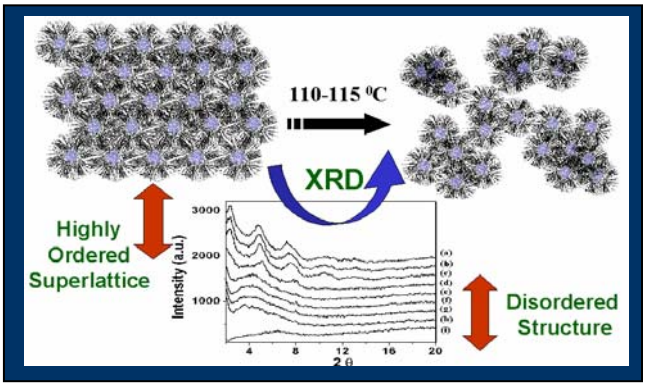

This chapter primarily deals with a novel route to prepare size selective monolayer protected gold nanoclusters (Au MPCs) and their detailed characterization using various analytical techniques. The effect of temperature on the ordered superlattice structure of 3.72 nm sized dodecanethiol (DDT) passivated Au nanoclusters is also investigated. These results indicate the formation of a temperature induced, diffusion limited, irreversible phase transition.

---

* A part of the work has been published in "***J. Phys. Chem. B* 2005**, 109, 2522".

2.1 Introduction

Monolayer protected nanoclusters (MPCs) show novel physico-chemical properties due to size quantization as accounted in greater details in chapter 1. More importantly, when these particles are organized at controlled cluster-cluster separation (spacing) they form superstructures (superlattices), generating several interesting phenomena due to their collective behaviour.[1-5] For example, low temperature studies reveal that the "Coulomb blockade effect" especially governs the electron transport in such assemblies, where the individual site energies, coupling strengths, lattice dimensionality and orders are expected to play a crucial role in the electronic transport and the associated long range resonant energy transfer (LRRT).[2,6-8] Accordingly, both classical and quantum coupling are observed in these structures, where the manipulation of interparticle separation between adjacent MPCs triggers a metal-insulator transition.[4,9] The unique physical properties of these ordered assemblies are especially promising for several potential technological applications.[1-6,10]

Au MPCs have drawn considerable attention as a novel inorgano-organic hybrid materials after the emergence of Brust synthesis due to their enhanced stability, ease of size control and a wide range of applications.[3,11-13] This method has been further used for synthesizing several other metallic or alloy MPCs,[14] although it has several limitations, like ability to synthesize only 1 - 5 nm sized particles, polydispersity, higher costs for the phase transfer agents and tedious methods for purification and size sieving.[11-14] Several other processes have also been used for synthesizing monodispersed MPCs, including the synthesis in reverse micelles, seed mediated growth, digestive ripening and several one-phase methods.[3,5,15-17] For instance, Jana et. al. has reported a single-phase technique for the preparation of larger sized metallic nanoparticles (Au, Ag, Cu and Pt) by reducing organic soluble metal precursors in presence of surfactants.[17a] Most of these synthetic procedures involve the use of quaternary-ammonium salts, whose complete removal from the particle surface is very troublesome.[11-18] Thus, the development of low cost synthetic procedures for the preparation of size selective MPCs by avoiding the use of any quaternary-ammonium salts is important for their practical applications.

There are extensive reports for grooming different types of MPC superlattices of both metals and semiconductors, where various effects, including particle size and their distribution, length of capping molecules and several fundamental issues, like nucleation and the growth kinetics of these ordered assemblies, have been comprehensively discussed.[2-5,11-13,16a,b,19-24] For example, hydrophobic interactions between adjacent hydrocarbon chains lead to the formation of highly ordered, close-packed superlattices from narrowly size distributed alkylthiol or alkylamine passivated MPCs.[19,20] Accordingly, longer alkyl chains favor long range ordering due to the enhancement of the interchain interactions.[19,20] Ohara and coworkers have used Hamaker theory for accounting the cluster-cluster interactions in a superlattice considering the interactions between two finite volume spheres as a function of their separation.[21] In another remarkable study, Landman and his co-workers have used molecular dynamics simulations to understand the structure, dynamics and thermodynamics of these superlattices of smaller MPCs under various conditions, where the interlocking of bundled alkyl chains due to the predominant van der Waal's attractions play a critical role.[22] In particular, their results show that smaller capping length clusters arranged in a bcc superlattice structure, undergoes a remarkable transition to an fcc lattice at higher temperature.[22] Furthermore, these MPCs with longer chain length capping molecules possess tetragonally distorted fcc structure, where the interlocking of these bundling passivating molecules can be enhanced along the direction of the tetragonal distortion.[22] In a series of studies, Heath and his co-workers have shown the detailed phase behaviour of two dimensional (2D) monolayers of Ag MPCs (2-7.5 nm diameters) by pressure-area isotherms in a Langmuir trough to account both the effect of size and interparticle separation on superlattice structure.[23] More interestingly, they have observed three distinct types of phase behaviour, which could be classified in terms of extra classical volume available of the passivating ligands.[23] Another related study by Pradeep and co-workers has shown that Ag MPC and AuAg alloy MPC superlattices posses distinct liquid phase as observed by XRD and calorimetric studies; however, detailed investigation show that Au MPCs are not ideal for superlattice formation.[24] Although there are extensive reports of the effect of temperature on the phase transition of Ag or AuAg Alloy MPC superlattices, there is no such systematic data for Au MPCs.[24,25] The understanding of the effect of temperature

on such ordered assemblies are technologically important, since it would help to predict the effect of thermal stress on nanodevice performance.

In this chapter, we describe a simple synthetic procedure for the size selective preparation of Au MPCs protected with either dodecanethiol (DDT) or tridecylamine (TDA) ligands. In particular, we use DDT or TDA for both simultaneous phase transfer and capping in nonaqueous medium for Au particles during reduction, which upon boiling at 120 °C in toluene produces moderately monodispersed nanoparticles. More importantly, these particles are free from any quaternary-ammonium salts, while various sizes of particles are also obtained by simple tuning of the synthetic conditions. Further, these particles spontaneously form superlattices upon slow evaporation of solvent on solid supports or TEM grids. The effect of temperature on 3.72 nm sized DDT protected Au MPCs has been investigated using *in-situ* temperature controlled XRD and FTIR studies in conjunction with TG-DSC analysis. *In-situ* temperature controlled XRD and FTIR studies reveal that upon thermal heating, these ordered assemblies of Au MPCs transform to a disordered state. This phenomenon has been identified as temperature induced irreversible phase transition from an ordered phase to a disordered state.

2.2 Experimental Section

2.2.1 Materials

Dodecanethiol (99%), $NaBH_4$, tridecylamine and $HAuCl_4.3H_2O$ were obtained from Aldrich, while toluene, acetone and ethanol (AR grade from Merck) were used after further purification; deionized water (16 MΩ) from Milli-Q system was used for all experiments.

2.2.2 Size Selective Synthesis of Au MPCs

Au MPCs of four differently sizes (viz. 3.72, 4.63, 6 and 8.2 nm) have been synthesized using modified Brust synthesis[11] followed by a digestive ripening process.[16a,b]

In brief, particles were synthesized in a bi-phasic mixture of water and toluene (v : v; 1 : 1; 50 ml each) using 1 : 3 mole ratio of gold to thiol in an ice bath. This Au :

thiol ratio was kept constant, since the core size is mainly controlled by the Au : thiol stoichiometry.[12] The biphasic mixture under low temperature (ice bath) was stirred for 30 m and subsequently reduced by dropwise addition of 20 ml 0.1 M aqueous $NaBH_4$ solution. Upon the slow addition of $NaBH_4$, the pale yellow color of gold salt was transformed to reddish-violet indicating Au^0 cluster formation. The Au^o clusters were found to be shifted to the organic phase turning the upper layer reddish-violet upon rigorous stirring for 3 h. After separating the aqueous layer, the non-aqueous layer was collected and this process was repeated 20 times to obtain finally 1 lt of toluene containing both Au MPC and unbound thiol. The non-aqueous layer was then concentrated under vacuum at 40 °C to a final volume of 100 ml, where the ratio of Au to unbound thiols is typically 1 : 30. This procedure will be repeated for the preparation all other particles and will be termed as step (P).

Particle (a) was obtained as violet powder after step (P) by concentrating the toluene layer under vacuum at 40 °C. This was further redissolved in 20 ml toluene and centrifuged to precipitate the agglomerated or bigger fraction particles. The highly toluene soluble fraction (after centrifugation) was precipitated by the addition of copious amount of acetone (500 ml). The particles were allowed to settle and the excess acetone was decanted to reduce the volume to 20 ml, followed by repeated centrifugation (5 times) and decantation to remove the unbound thiol and other unwanted by-products.

Particles (b-d) were synthesized by boiling the reaction mixture after the step (P) at 120 °C in an oil bath and were subsequently cooled slowly at room temperature to form a dark red solution. In particular, Au : thiol/amine ratios were kept at 1 : 30 for the preparation of particles (b) and (d) respectively, which were boiled for 1 h. In contrast, particles (c) was prepared by boiling the reaction mixture for 1.5 h using Au : thiol ratio of 1 : 200. These reaction mixtures were further concentrated (10 ml) and the MPCs were precipitated by the addition of excess acetone (250 ml), followed by the decantation to reduce the volume to 20 ml. These particles were then repeatedly centrifuged (7 times) with excess of acetone for further purifications.

2.2.3 Techniques Used for the Characterization of MPCs

2.2.3.1 UV-visible Spectroscopic Analysis

All the optical measurements were recorded using Shimadzu, UV-2101 PC spectrophotometer using a quartz cell (10 mm path). The spectra were background subtracted using the same solvent as used for nanoparticles dispersion unless mentioned separately.

2.2.3.2 Transmission Electron Microscopic (TEM) Analysis

TEM and high resolution TEM (HRTEM) micrographs were taken on a JEOL model 1200EX instrument operated at an accelerating voltage of 120 kV and a Philips CM 20 FEG instrument operated at an accelerating voltage of 200 kV respectively. TEM samples were prepared by dropcasting highly purified Au MPCs from toluene dispersion on a carbon coated Cu grid (400 mesh) and dried slowly at room temperature.

2.2.3.3 (a) X-ray Diffraction (XRD) Analysis

X-ray diffraction was carried out on a Philip1730 machine using Cu $K\alpha$ radiation (λ_x = 1.54 Å) at a step of 0.02° (2θ) at room temperature. The background was subtracted with the linear interpolation method.

(b) In-situ Temperature Controlled XRD Analysis

In-situ temperature controlled X-ray diffraction experiments were performed using Rigaku Dmax 2500 diffractometer. The system consisted of a rotating anode generator with a copper target and a wide-angle powder goniometer, having a diffracted beam graphite monochromator. Rigaku low-medium temperature attachment was fitted in the goniometer for high temperature measurements. The maximum temperature that could be reached in this attachment was 300 ^{o}C. The generator was operated at 40 kV and 150 mA. All the experiments were performed in the reflection mode. The sample holder was a copper block and a very thin layer of MPCs was dropcasted on this block. The copper block with the sample was heated at the rate of 2 ^{o}C /min. The diffraction pattern was collected while the sample temperature was held constant within 1 ^{o}C of the set

temperature and the data was acquired in 5 min. The sample was kept under vacuum during the experiment to avoid thermal degradation. The diffraction data was collected at room temperature and subsequently at various temperatures as mentioned in the text to monitor the change in structure during heating.

2.2.3.4 Nuclear Magnetic Resonance (NMR) Analysis

NMR spectra were recorded in a Bruker MSL300 MHz in $CDCl_3$ solvent using tetramethoxysilane (TMS) as an internal standard, while concentrations of MPCs were approximately 10-12 mg/ml.

2.2.3.5 (a) Fourier Transform Infrared Spectroscopic (FTIR) Analysis

FTIR spectroscopic measurements of purified powders of Au MPCs were carried out on a Perkin-Elmer FTIR Spectrum One spectrophotometer operating at a resolution of 4 cm^{-1} after mixing with KBr (1 wt % MPCs).

(b) *In-situ* Temperature Controlled FTIR Analysis

Room temperature and high temperature infrared spectra of these samples were taken using a Perkin-Elmer FTIR Spectrometer (model PC 16) at a resolution of 2 cm^{-1} in the range of 450 - 4400 cm^{-1}. A total of 32 scans were used for signal averaging. High temperature spectra were obtained by mounting the sample in the Mettler Toledo FP82HT hot stage and placing it in the sample compartment of FTIR after aligning using a red laser light. The sample was heated at the rate of 5 ^{o}C/min and the spectra were collected while the sample temperature was held constant.

2.2.3.6 Thermogravimetric (TG) Analysis

Thermogravimetric experiment was performed in a TGA-7 unit of the Perkin Elmer thermal analysis system, operated under nitrogen flow in the temperature range of 50 to 800 ^{o}C with a scanning rate of 5 ^{o}C/min.

2.2.3.7 Differential Scanning Calorimetric (DSC) Analysis

The calorimetric measurements were carried out using the DSC-7 unit in a temperature range of -10 °C to 150 °C. The samples were heated at a rate of 10 °C/m under nitrogen environment. The instrument was calibrated using standard procedures but for heating rates other than 10 °C/min indium was scanned at the required heating rate to determine the instrumental lag and the sample data was corrected accordingly.

2.3 Results for the Characterization of Au MPCs

2.3.1 UV-visible Spectroscopic Analysis

The color of the nanoparticles have fascinated scientist over hundreds of years, which originates due to the surface plasmon resonance of the particles.[25] Mie was the first to describe them quantitatively by solving Maxwell's equations with the appropriate boundary conditions for spherical particles.[26] The total extinction cross section (σ_{ext}) composed of absorption and scattering is given as a summation over all electric and magnetic multipole oscillations. For particles with smaller sizes than the wavelength (λ_l) of the exciting light (λ_l »2r, for gold when 2r < 25 nm, where r is the radius),[27] only the dipole absorption of the Mie equation contributes to the extinction cross section (σ_{ext}). The Mie theory then reduces to the following relationship (quasi-static or dipole approximation),

$$\sigma_{ext} = (9V_P\varepsilon_m^{3/2}/c).[\omega\varepsilon_2(\omega)/\{\varepsilon_1(\omega) + 2\varepsilon_m\}^2 + \varepsilon_2(\omega_2)^2] \qquad (2.1)$$

where V_P is the spherical particle volume, c is the speed of light, ω is the angular frequency of the exciting radiation and ε_m is the dielectric constant of the surrounding medium (assumed to be frequency independent).[28] Accordingly, $[\varepsilon(\omega) = \varepsilon_1(\omega) + i\varepsilon_2(\omega)]$, where $\varepsilon_1(\omega)$ and $\varepsilon_2(\omega)$ denote the real and imaginary part of the dielectric function of the material respectively. This shows that the surface plasmon band position strongly depends on the particle size, dielectric function of the materials and its surrounding medium.[25-28]

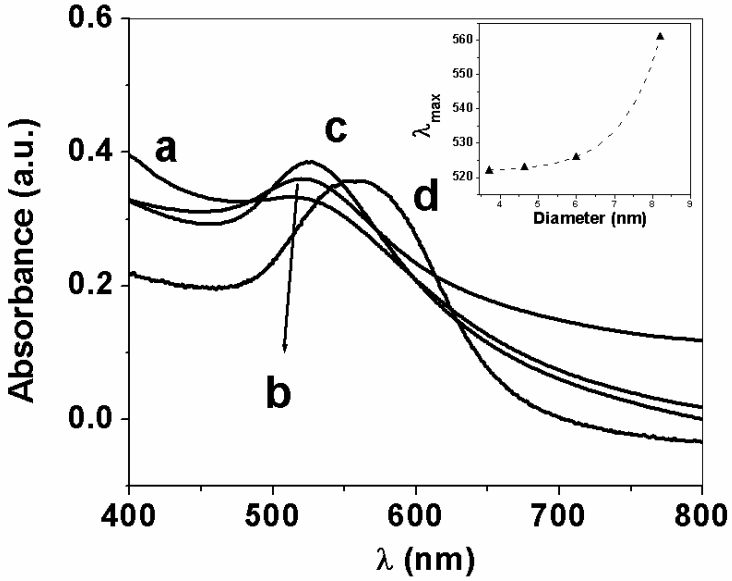

Figure 2.1 (a-d) UV-visible absorption spectra corresponding to Au MPCs (a) 3.72, (b) 4.63, (c) 6 and (d) 8 nm in toluene, where particles (a-c) are capped with DDT and (d) is capped with TDA. These spectra show a red shift and sharpening of surface plasmon peak with increase in particle size, inset showing the exponential variation of peak position with size.

Figure 2.1 shows the superimposed UV-visible spectra of these particles in toluene, where the plasmon peak positions have been found to be red shifted and sharpened with the increase in particle size.[29] Inset shows the variation of the peak positions with particle size (diameter), which could be fitted to a first order exponential growth. Accordingly, Figure 2.2 (a) shows the UV-visible spectra of 3.72 nm sized MPCs in various solvents, such as hexane, heptane, cyclohexane, chloroform, carbontetrachloride and toluene (i-vi) to account the effect of solvent refractive index (dielectric constant), where the absorption maxima have been shown along the arbitrary Y axis. The surface plasmon resonance of these particles are observed between 518-522 nm for the above solvents (i-vi), where the peak position has been red-shifted with increase in solvent refractive index. In particular, Figure 2.2 (b) shows the nonlinear variation of surface plasmon peak position with the refractive index, which is in good agreement with the earlier reports.[30] However, a minor absorption at *ca.* 375 nm has been observed, which might be attributed to the presence of weakly bound Au^{3+} ions on these nanoparticles.

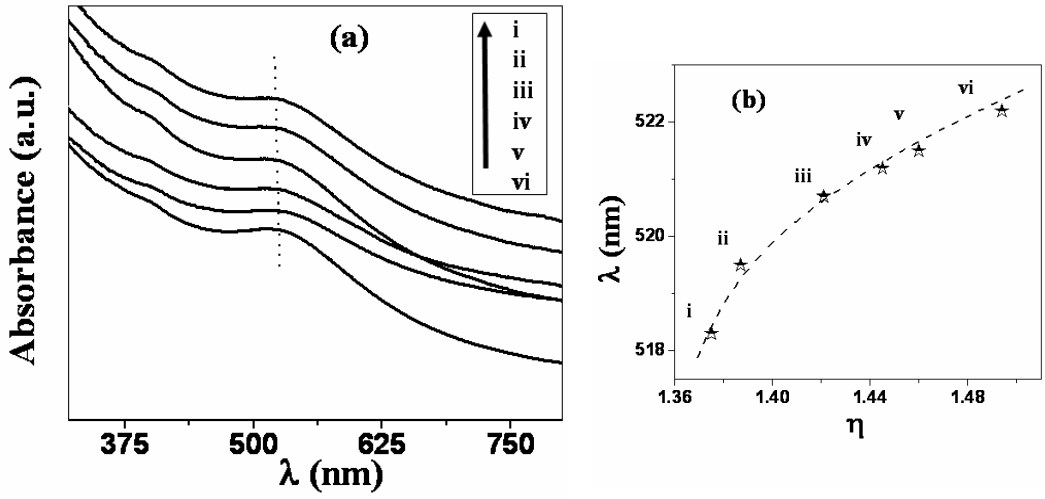

Figure 2.2 (a) UV-visible absorption of DDT protected 3.72 nm sized Au MPCs in hexane, heptane, cyclohexane, chloroform, carbontetrachloride and toluene (i-vi); (b) the nonlinear variation of the surface plasmon peak position with increase in solvent refractive index.

2.3.2 TEM Analysis

Size distributions and periodic arrangements are evident from a comparison of the TEM images of these particles. For example, Figure 2.3 (a-d) shows a high population of uniformly sized particles with an average size of 3.72±0.4 nm along with their statistical distribution (Gaussian) as shown in the inset of Figure 2.3 (b). More specifically, the high-resolution image shown in Figure 2.3 (a), depicts the lattice fringes for these particles, whereas hexagonal closed packed superlattice structure is evident in Figure 2.3 (b-c). Accordingly, Figure (2.4-2.6) shows the respective TEM images of the particles having diameter of 4.63, 6 and 8.2 nm along with their statistical distribution. All of these particles clearly show large area superstructures due to their monodispersed nature, either mono or multi layers at different regions.

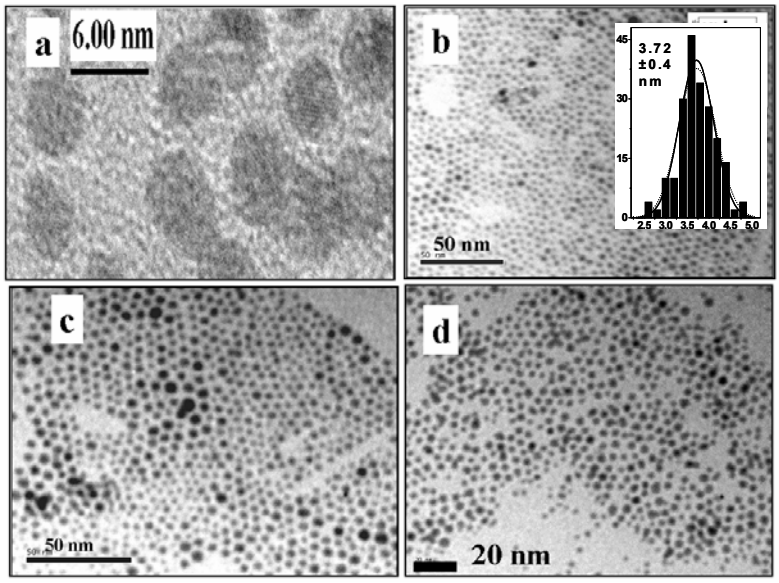

Figure 2.3 (a-d) TEM images of purified Au MPCs corresponding to particle $Au_{1415}(DDT)_{328}$ after repeated solvent extraction and careful fractionation experiments revealing particle size of 3.72±0.4 nm [particle size distribution is shown at the inset of (b)]. The lattice fringes are also visible in micrograph (a) for these particles, whereas ordered structures are seen in (b-c).

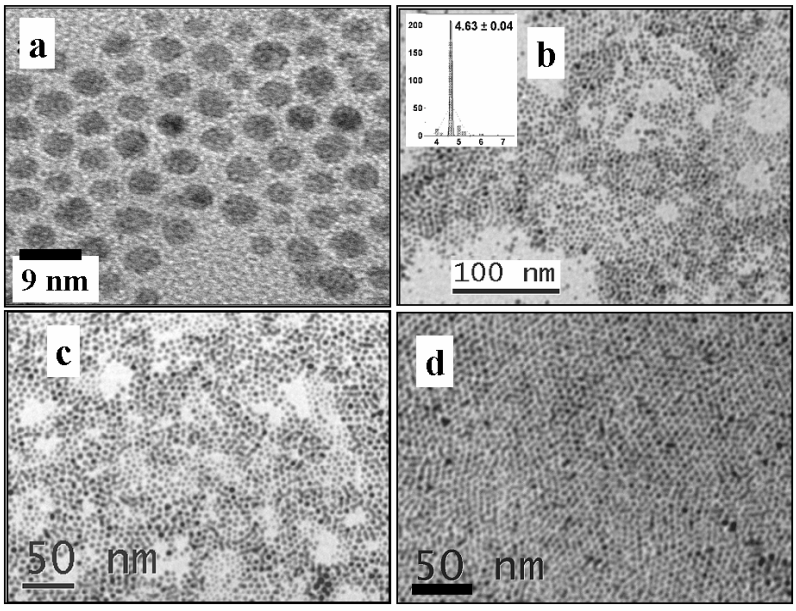

Figure 2.4 (a-c) TEM images of purified Au MPCs corresponding to particle $Au_{2869}(DDT)_{541}$ after purification, revealing particle size of 4.63±0.04 nm [particle size distribution is shown at the inset of (b)]. Both mono and multilayer superstructures are seen in (b-d).

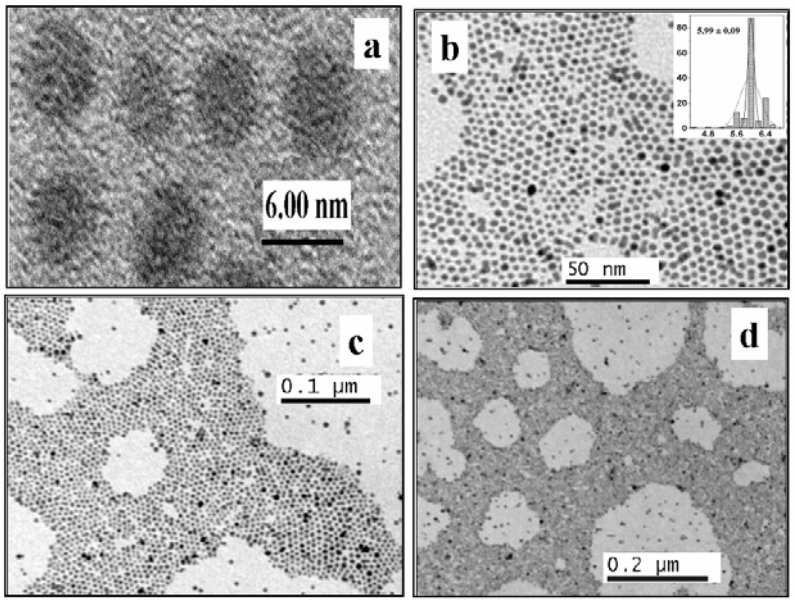

Figure 2.5 (a-c) TEM images of purified Au MPCs corresponding to particle $Au_{6535}(DDT)_{961}$, where highly long-range ordered structures are seen in (b-d) [particle size distribution is shown at the inset of (b)].

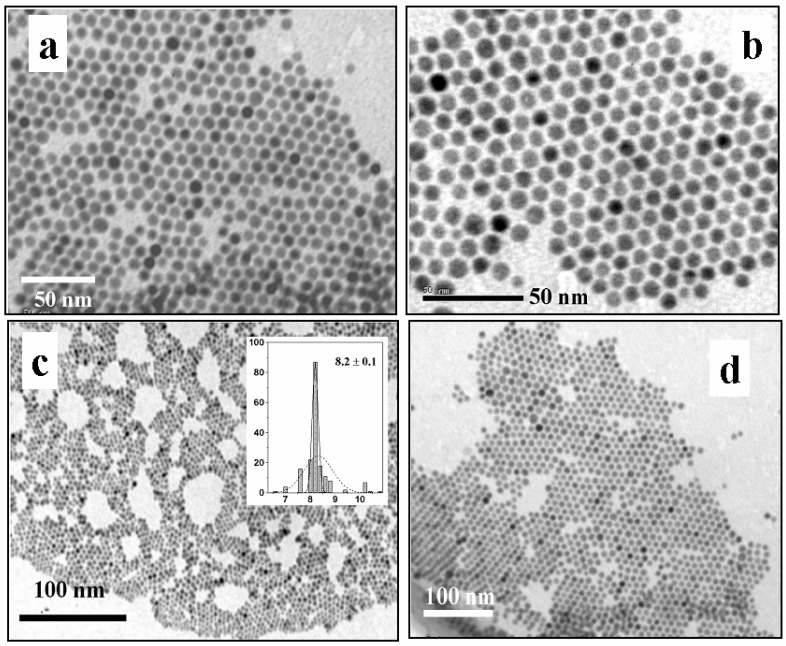

Figure 2.6 (a-d) TEM images of the highly monodispersed Au MPCs corresponding to particle $Au_{17895}(TDA)_{1928}$ along with ordered structures [particle size distribution is shown at the inset of (c)].

The composition of these Au MPCs are also approximated from the TEM results by calculating the nearest stable magic numbers as full shell clusters, since certain magic numbers are known to be stable.[31] The average composition of these MPCs are summarized in Table 2.1 by assuming the shape of these particles as spherical, radius of Au atom is of 144 pm, perfect fcc packing and further considering 2 S atoms per 3 Au atoms on the surface as reported for two dimensional SAMs.[12a,31]

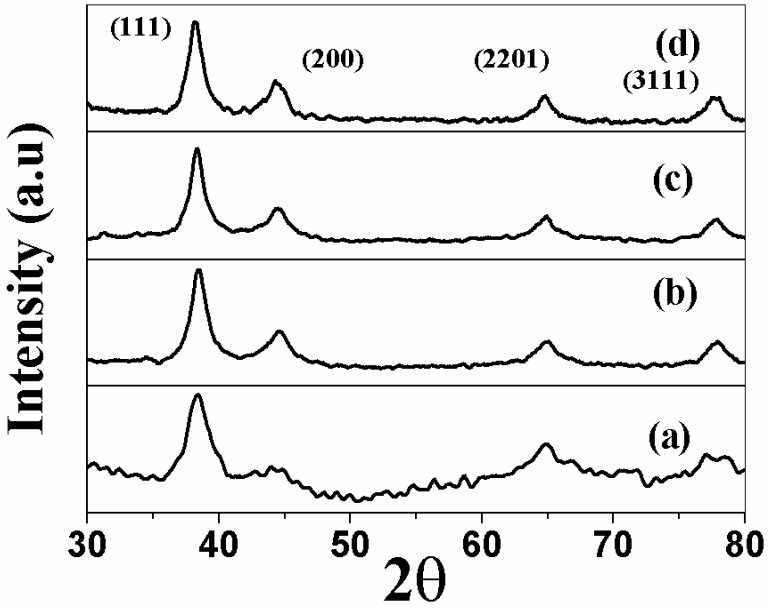

Figure 2.7(a-d) XRD patterns of Au MPCs corresponding to particles (a-d), showing bulk fcc crystal structures, corresponding lattice planes are marked in the figure.

2.3.3 XRD Analysis

XRD analysis was further carried out to investigate the crystallinity of these MPCs and also to evaluate their size distribution. Figure 2.7 (a-d) shows the respective XRD patterns of these MPCs corresponding to particles (a-d). The XRD reveals bulk fcc crystal structure as in agreement with the previous reports[22] and the corresponding

lattice planes are marked in the figure. Particle size is calculated from the full width at the half maxima (FWHM) of the (111) peaks using the Scherrer formula as given by:

$$\text{Particle Size} = K_s\lambda_X / B\text{Cos}\theta \qquad (2.2)$$

where K_s is Scherrer constant (0.9 for spherical particles), λ_X is wavelength of the X-ray diffraction (1.54 Å for Cu K_α), B is the FWHM of the peak and θ is diffraction angle.[32] The calculated particles size is comparable with the corresponding size calculated from TEM analysis and this data is also summarized in Table 2.1 along with approximated particle composition, surface plasmon peak position and size for TEM analysis.

Table 2.1 Variation of surface plasmon peak position with experimentally obtained particle size from both TEM and XRD analysis along with average particle composition

Sample number	Average particle compositions	Plasmon peak position (nm)	Size from TEM (nm)	Size from XRD (nm)
(a)	$Au_{1415}(DDT)_{328}$	522	3.72±0.40	3.82
(b)	$Au_{2869}(DDT)_{541}$	523	4.63±0.04	4.91
(c)	$Au_{6535}(DDT)_{961}$	526	5.99±0.09	5.72
(d)	$Au_{17895}(TDA)_{1928}$	561	8.20±0.10	8.70

2.3.4 NMR Analysis

Surface passivation as well as the purity of these MPCs (a-d) is examined with the help of ^{1}H NMR analysis as shown in Figure 2.8 (a-d). These spectra show three distinct multiplets corresponding to the protons at C_2, $C_{3\text{-}11}$ and C_{12} (C_{13} for particles d) carbons at ~1.56, ~1.26 and ~0.84 ppm respectively. The carbon positions have been marked for DDT in the scheme as shown in the inset of Figure 2.8 (a). The individual peak positions are similar but broadened as compared to that of pure alkanes.[13a] Interestingly, the proton at C_1 position is not observed perhaps due to the inhomogeneity

in the local chemical environment as a consequence of capping through S atom. In particular, the absence of prominent resonance at 2.7 ppm corresponding to the protons at C_1 position indicates strong interaction with the metal surface as well as the purity of the samples.[13a]

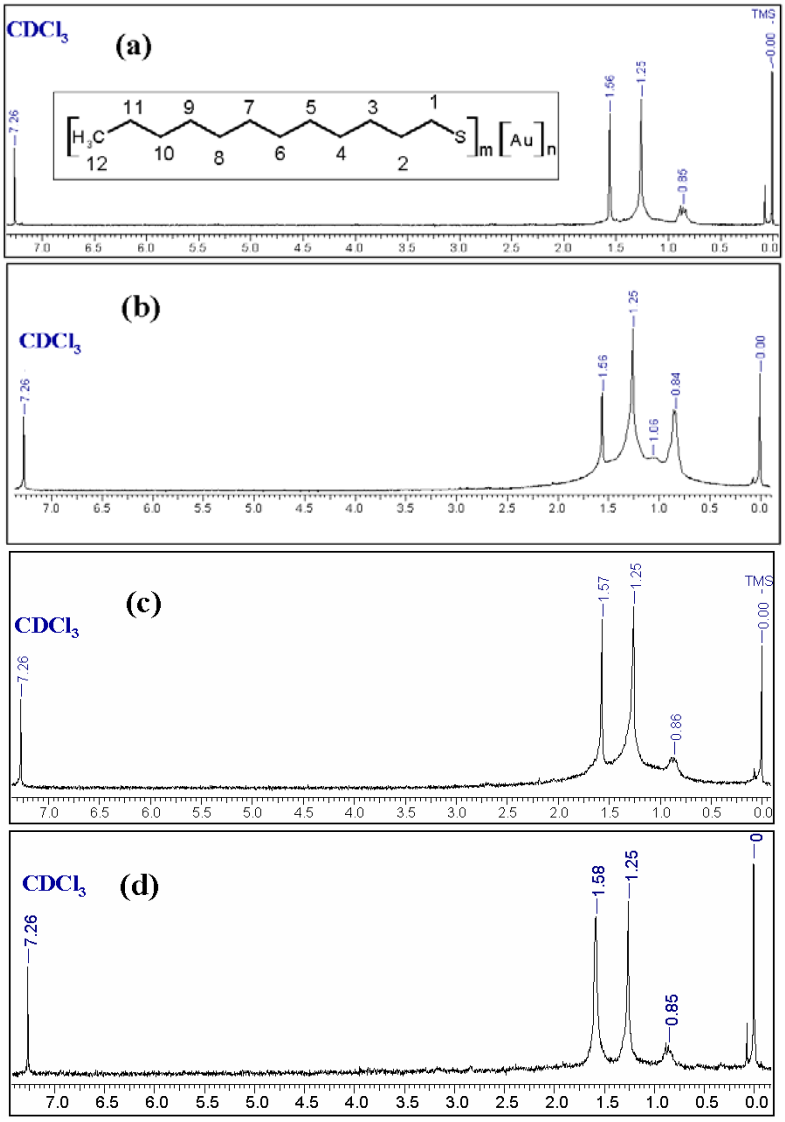

Figure 2.8 (a-d) ^{1}H NMR response of purified Au MPCs (a-d) in $CDCl_3$, revealing that peaks are significantly broadened from their ideal position due to the effective surface passivation of Au core. The carbon positions have been marked for DDT in the scheme as shown in the inset of (a).

2.3.5 FTIR Analysis

The local molecular environment of the passivating ligands on these MPCs can be obtained from FTIR analysis, where the C-H stretching region (2800-3000 cm^{-1}) is particularly informative about the orientation of methylene chains. For example, Figure 2.9 (i) (a-d) shows the superimposed FTIR spectra of C-H stretching region corresponding to particles (a-d), where four peaks are evident corresponding to symmetric (d^+) and asymmetric (d^-) CH_2 stretching modes, asymmetric in plane (r^-) and symmetric (r^+) stretching mode of terminal methyl groups.

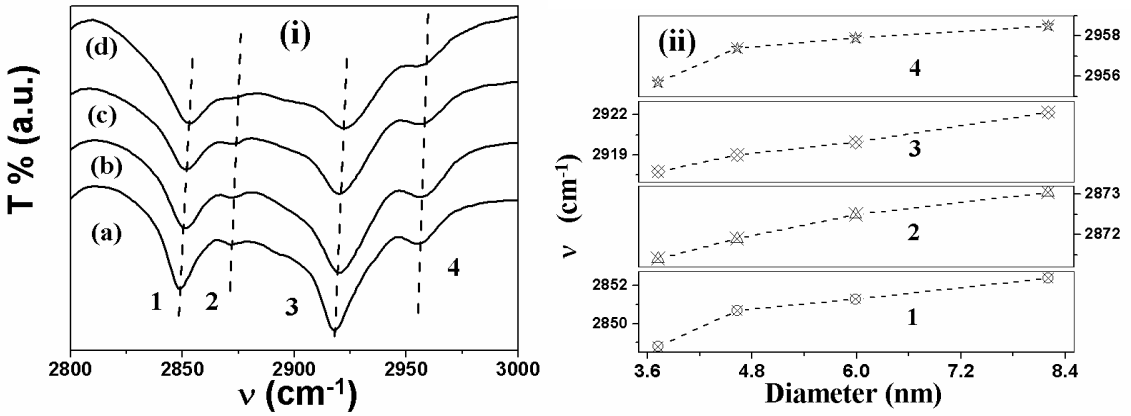

Figure 2.9 (i) The superimposed FTIR spectra of C-H stretching region (a-d) corresponding to particles (a-d), where four peaks are evident corresponding to symmetric (d^+) and asymmetric (d^-) CH_2 stretching modes and symmetric (r^+) and asymmetric in plane (r^-) stretching mode of terminal methyl groups. (ii) Variation of (1) d^+, (2) r^+, (3) d^- and (4) r^- stretching modes with particle size, showing blue shit with increase of size due to the increment of disordering in monolayer.

The ordering of the alkyl chains is best evident by the peak positions of d^+ and d^- CH_2 stretching vibrations, whereas r^+ and r^- stretching modes are indicative of orientational freedom of the chain terminals. The corresponding positions of these stretching modes are summarized in Table 2.2 for Au MPCs (a-d) and are also plotted individually with their size in Figure 2.9 (ii). Most importantly, we find the d^+ and d^- values for particle (a-b) red shifted as compared to the bulk alkanes, whereas a similar blue

shift is observed for particles (c-d). The red shift of d^+ and d^- stretching modes indicates the presence of extremely high percentage of all-trans conformations, characteristic of crystalline alkanes, whereas blue shift corresponds to greater number of gauche defects.[24,33] Interestingly, all these stretching modes are blue shitted with respect to the size as shown in Figure 2.9 (ii), where (1-4) corresponding to d^+, r^+, d^- and r^-. More specifically, this blue shift of stretching modes with increase of size illustrates the decrease of alkyl chain order along with concomitant increment of gauche defects. Thus, our results indicate that the presence of higher number of ligands (as expected to be increase with the size of core) might promote disordering in the capping monolayer.

Table 2.2 Variation of d^+, r^+, d^- and r^- FTIR stretching modes with particle size

Particle Size	(1) d^+ (cm^{-1})	(2) r^+ (cm^{-1})	(3) d^- (cm^{-1})	(4) r^- (cm^{-1})
(a) 3.72	2848.8	2871.4	2917.8	2955.7
(b) 4.63	2850.7	2871.9	2919.0	2957.4
(c) 6.00	2851.3	2872.5	2920.0	2957.9
(d) 8.20	2852.4	2873.0	2922.2	2958.5

All other bands are assigned on the basis of n-alkane vibrations as shown in Figure 2.10, where graphs (a-d) correspond to particles (a-d). The scissoring motion of all-trans methylene chains are apparent at ~1467 cm^{-1}, which is broadened with the increase of size. This may be due to the overlap of other vibration modes, such as scissoring motion of a methylene group next to a gauche bond and the methyl antisymmetric bending vibration. The methylene wagging and rocking bands appearing between 1200 and 1400 cm^{-1}, indicate crystallinity, which is also suppressed for particles (d). The appearance of a prominent band at ~1369 perhaps corresponds to defects, which appears as a very small peak at ~ l367 for particles (a-c). This further, indicates that the disorder in the alkyl chains environment increases with the increase of particle size.

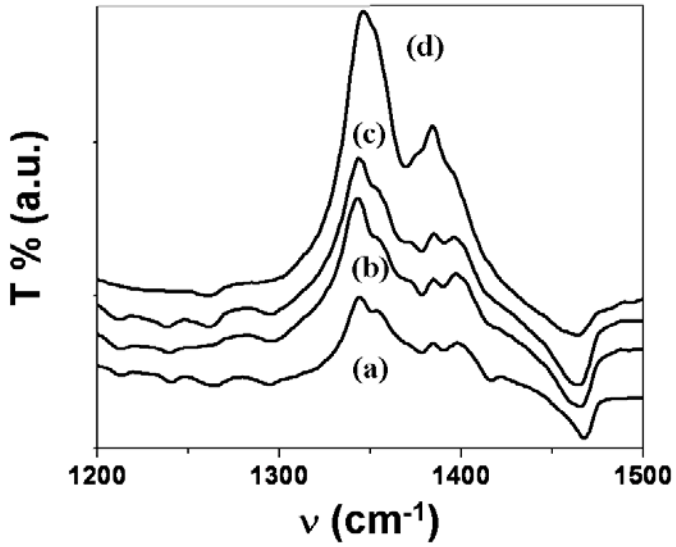

Figure 2.10 (a-d) Superimposed FTIR spectra of Au MPCs in 1200-1500 cm^{-1} region corresponding to particles (a-d), where methylene wagging, rocking and a large number of progression bands are visible.

Thus, we have successfully described the synthesis of size selective Au MPCs in the range of 3.7 – 8 nm excluding either the use of quaternary-ammonium salts or any tedious separation steps. These particles are thoroughly characterized by UV-visible, TEM, XRD, ^{1}H NMR and FTIR to depict their size, crystallinity and surface passivation. Most importantly, we find that the ordering of the passivating alkyl chains decreases with the increase Au core size. Further, the capability of these MPCs for larger superlattice structure along with their simple synthetic techniques could be useful for several applications in nanotechnology.

2.4 Effect of Temperature on 3.72 nm Sized Au MPCs Superstructures

In this part, the investigation of the effect of temperature on the ordered superstructures of 3.72 nm sized Au MPCs is described with the help of *in-situ* temperature controlled XRD and FTIR in conjunction with TG and DSC analysis. Since $Au_{1415}(DDT)_{328}$ particles have relatively ordered, crystalline passivating layer and are capable for superlattice formation, we examine the effect of temperature on their superstructure in detail as described below:

2.4.1 TEM Analysis

The ordered superlattice structure is obtained due to the uniform size distribution of these particles (images a-c in Figure 2.11). Interestingly, the TEM images of the solids precipitated after mixing large excess of acetone in the toluene containing Au MPCs show highly ordered superlattice along with several multilayer (3D ordering) structures [Figure 2.11 (d)]. More specifically, these particles show a tendency to arrange in a hexagonally close packed arrangement, where the average particle edge to edge distance is 2.5 – 2.7 nm. These average spacing is in good agreement with earlier reports, where 3-4 carbon chains are assumed to be interdigitated during the superlattice formation.[12,24]

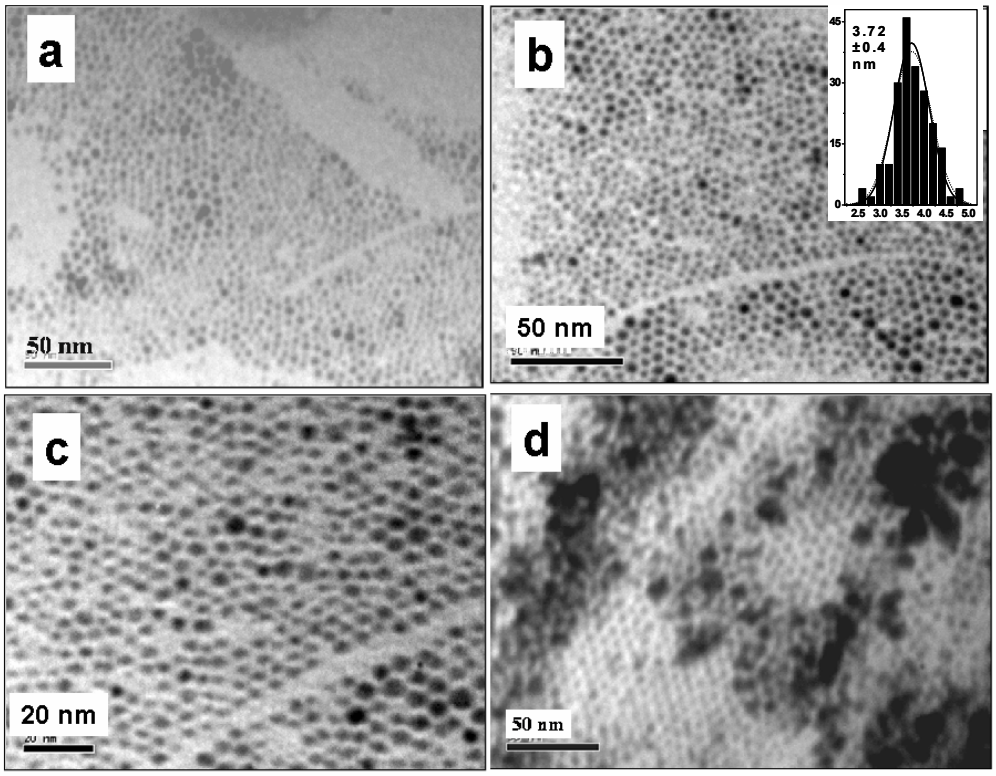

Figure 2.11 (a-c) Ordered superlattice structures of the nearly uniform 3.72±0.4 nm sized Au MPCs; inset (c) shows Gaussian distribution of their size. (d) Ordered superlattice structure along with several multilayers (3D ordering) obtained from the solid precipitated after mixing large excess of acetone in toluene containing Au MPCs.

2.4.2 *In-situ* XRD and TG-DSC Analysis

Long range ordering in these structures can be investigated with the help of low angle XRD measurement, which indicates the enhancement of interplanar spacing (d_{hkl}). We used dropcasted thin films of Au MPCs from toluene at room temperature on a Cu substrate for *in-situ* temperature controlled XRD analysis. This Au MPC containing Cu holder was heated at various (a-i) temperatures and the XRD data were recorded. For example, Figure 2.12 (i) shows the superimposed variation of the low angle XRD peaks of these Au MPCs, where several sharp peaks at regular intervals indicate the long-range superlattice formation. The superlattice is indexed in a bcc phase with (110), (220) and (330) lattice planes as in good agreement with previous results.[22b]

However, the calculated lattice parameter from low angle XRD results (*ca.* 5.25 nm) for the superlattice is smaller than the value obtained from TEM analysis (6.3±1 nm), which indicates that significant overlap is present between neighbouring clusters. More specifically curves (a-i) correspond to 25, 65, 85, 115, 125, 150, 165, 180 and 200 °C, which accounts for a drastic change in the crystallinity of the Au MPC superlattice after 110 °C. In particular, the peak positions are almost unaffected for the curve (a-c), while a shift and an increase in the peak to peak spacing can be seen in curve (d). Interestingly, curves (e-h) depict an amorphous nature, which indicates that the crystallinity is lost at 110-120 °C. However, the room temperature XRD analysis of the previously heated sample at 150 °C retains the amorphous nature, depicting that the transition is irreversible unlike that of Ag MPCs.[24] The thermal stability of these MPCs is also investigated with the help of thermogravimetric (TG) analysis, which shows that partial degradation starts from 175 °C and completes at 270 °C with almost 20 % wt loss as shown in the inset of Figure 2.12 (i). This weight loss is in good agreement with our approximate calculation of MPC's composition. Accordingly, the TG result shows that the degradation of these particles is not the reason for the destruction of the superlattice order, which is further confirmed from the higher angle XRD results.

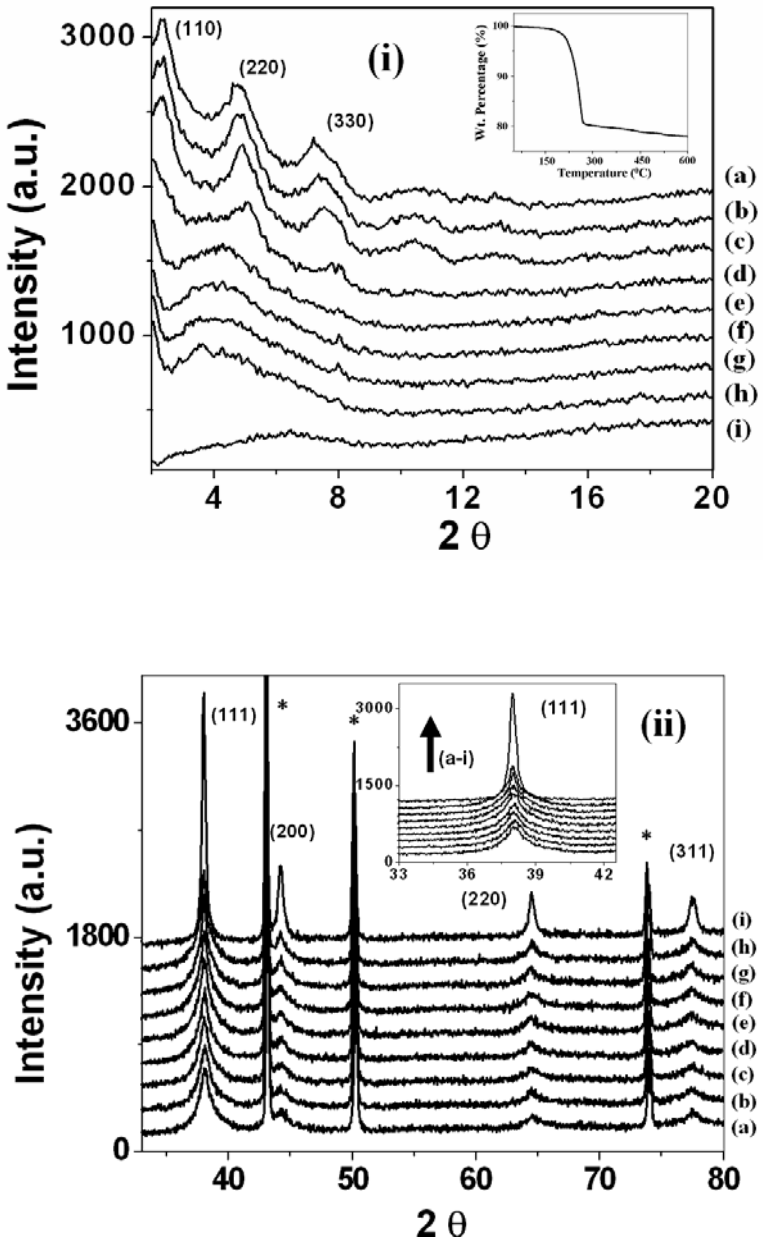

Figure 2.12 (i) (a-i) The superimposed variation of the low angle XRD peaks of Au MPCs at 25, 65, 85, 115, 125, 150, 165, 180 and 200 °C, which reveal a sharp phase transition in a temperature range of 110-120 °C; inset shows thermogravimetric (TG) curve of the corresponding particles. (ii) (a-i) The superimposed variation of the high angle XRD peaks of Au MPCs at 25, 65, 85, 115, 125, 150, 165, 180 and 200 °C, where bulk fcc structure are evident for these particles; inset shows the effect of temperature for the case of (111) peak.

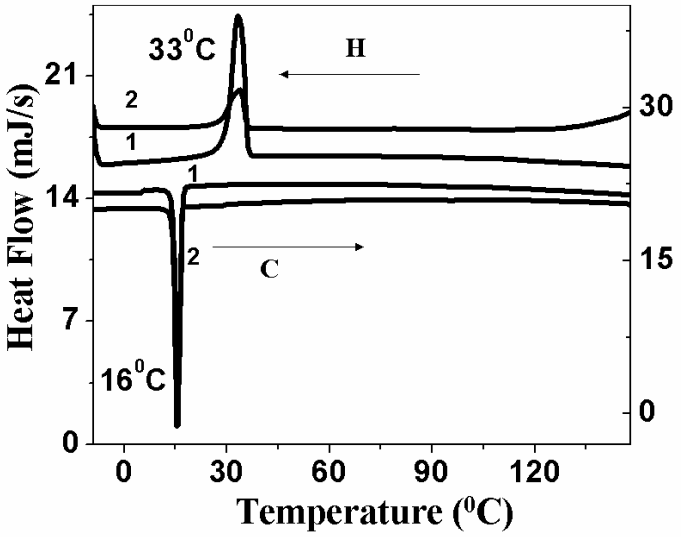

Figure 2.13 Superimposed first two cycles (1 and 2 indicating the number of cycle) of DSC response of Au MPCs, where the alkyl chain melting (H) and cooling (C) are seen at 33 °C and 16 °C respectively as reversible first-order transitions.

The higher angle XRD results reveal that these MPCs have bulk fcc structure as reported earlier for larger MPCs and the planes are identified as (111), (220), (200) and (311).[22] However, Cu sample holder peaks are observed due to the thin nature of the MPC films (marked as ∗), although these do not appear in the low angle region for blank substrate. More importantly, the peak position and the full width at the half maximum (FWHM) of these peaks are not affected up to 165 °C, as shown in Figure 2.12 (ii) corresponding to curves (a-i) for 25, 65, 85, 115, 125, 150, 165, 180 and 200 °C. However, the intensity of these peaks has been slightly increased above 115 °C and a drastic increment along with sharpening is observed above 180 °C as shown in the inset of Figure 2.12 (ii) for the case of (111) peak. The sharpening of the peak positions could be attributed to the partial desorption of the thiol monolayers from the nanoclusters surface. Thus these higher angle XRD results further preclude the possibility of the destruction of monolayer and increment of the particle size as the reason for the phase transition observed in the low angle XRD analysis.

In an attempt to capture this phase transition, we have carried out differential scanning calorimetric (DSC) analysis of the purified powder of these particles in the temperature range of -10 °C to 150 °C. Interestingly, only one distinct first-order transition is observed corresponding to the melting of the alkanethiolate chain assembly, while no other transition is evident, unlike, previously observed for Ag or AuAg alloy superstructure (Figure 2.13) and octadecanethiol protected Au MPCs.[24] The alkyl chain melting and cooling are manifested at around 33 °C and 16 °C respectively. More importantly, the observed chain melting temperature is shifted to higher energy as compared to its smaller analogues as reported earlier due to the increase in particle size.[12b] The reversible hysteresis behaviour is a characteristic of the first-order transitions. The alkyl chain melting transition appears at the same temperature during the second cycle and is comparable to that of the previous cooling curves.[12b,24] However, the absence of superstructure phase transition might be attributed to the higher ordering of the alkyl chains as compared to the Ag and AuAg alloy.[24] Further heating causes more ordering of the alkyl monolayer as evident from the increase of the sharpness and the height of these DSC peaks (particularly in the heating curves), which might also suppress these superstructure phase transition.

2.4.3 *In-situ* FTIR Analysis

The variable temperature infrared analysis was carried out to investigate the exact characteristic of the alkyl chain assembly during the heating. Figure 2.14 (i and ii) shows the high and low frequency region of the infrared spectra of these MPCs in a pressed KBr pellets heated *in-situ* at 40, 60, 95, 120, 140, 160, 180 and 200 °C temperatures corresponding to curves (a-h). The positions of the characteristic peaks are drastically shifted to lower energy side permanently at higher frequency region above 100 °C. The high degree of conformational order in the monolayer is best evidenced by the position of the symmetric (d^+) and antisymmetric (d^-) CH_2 stretching peaks in the room temperature FTIR spectra. Average values of 2852 and 2922 cm^{-1} for these peaks indicate an extremely high percentage of all-trans conformations, characteristic of crystalline alkanes.[24,33] Disordered systems, such as liquid alkanes, display much higher values (2856 and 2928 cm^{-1} respectively), which have been convoluted to higher number of gauche defects.[24,33] The r^- bands for methylene vibrations

have been identified as 2955 cm^{-1}, although the r^{+} mode is not prominent enough in the spectra.

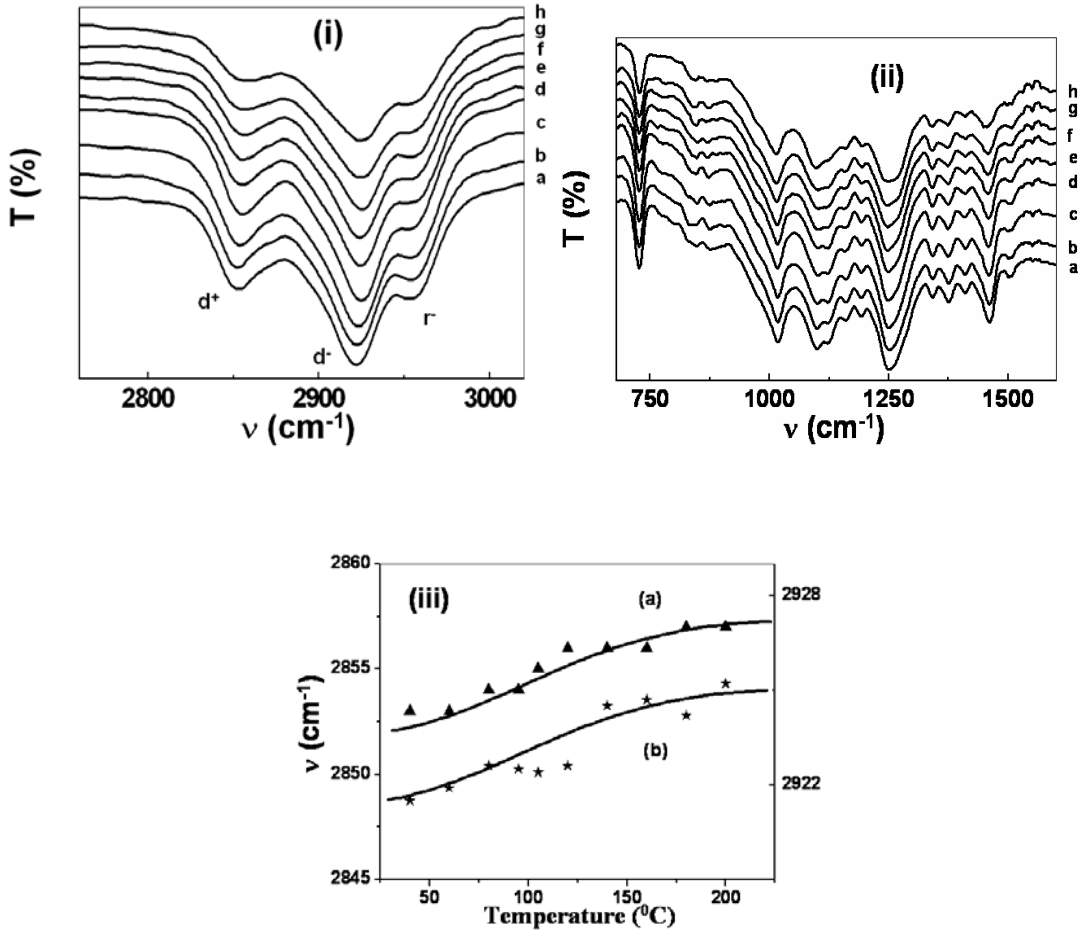

Figure 2.14 (i) High and (ii) low frequency region of the infrared spectra of these MPCs in a pressed KBr pellets heated *in-situ* at 40, 60, 95, 120, 140, 160, 180 and 200 °C corresponding to curves (a-h), where the positions of the characteristic peaks for aliphatic alkane as drastically shifted to lower energy side permanently at higher frequency region above 100 °C. (iii) Variation of symmetric (a) and antisymmetric (b) peak positions with temperatures are shown, where the change of the methylene local environment suggests a temperature induced phase transition.

All other bands are assigned on the basis of n-alkane vibrations [Figure 2.14 (ii)], where peaks corresponding to the methylene wagging and rocking and a large number of progression bands are observed. For the spectrum in the region 1400-1500 cm^{-1}, all-

trans scissoring mode is observed, like methylene scissoring at ~1460 cm^{-1} and CH_2-S methylene scissoring at ~1410 cm^{-1}. The peak at 1376 cm^{-1} is attributed to the symmetric bending vibration of CH_3 groups. The presence of a large number of bands between 1200-1400 cm^{-1} corresponding to either twisting-rocking or wagging progression modes, gives a strong evidence for the micro-environment of the alkanethiol monolayer on Au clusters.[24,33] The band at 1341 cm^{-1} in the spectrum is attributed to the end gauche conformation, while the bands at 1125 and 1095 cm^{-1} are assigned as $(c\text{-}c)_T$ and $(c\text{-}c)_g$ stretching modes respectively. In particular, these prominent progression bands are indicative of the presence of higher order in the monolayers (column like), which might be one of the reasons for the absence of superstructure melting in DSC. The 700-800 cm^{-1} region comprises of two sets of bands, the first one is due to methylene rocking (726 cm^{-1}), while the remaining one is due to C-S stretching.[24,33]

Upon successive heating, interestingly, the high frequency region shows drastic change on the symmetric (d^+) and antisymmetric (d^-) CH_2 stretching peaks as compared to that of the methylene vibrations. In particular, the CH_2 stretching peaks are found to be shifted to higher values at a temperature range of 105-120 °C, indicating disorder. Figure 2.14 (iii) depicts the variation of symmetric (a) and antisymmetric (b) peak positions with temperature, where the change of the methylene local environment is evident. However, the presence of unaffected progressions bands (1200-1400) above the DSC melting temperature suggests higher ordering due to intra-chain packing (can be viewed as bundled columns of alkyl chains),[24.f] which increases as a result of repeated annealing. It is also possible that some of these chains near the metal core are not likely to be molten and hence gets more ordered during repeated annealing. This clearly suggests that in this temperature range phase transition of the superstructures do happen, which cause the destruction of the order. In contrast, in the low frequency region, the C-H stretching does not show any characteristic shift, although partial narrowing of the peaks with heating is observed, indicating increased order in the alkyl chain. However, splitting is not observed in the methylene rocking mode in any of these spectra, which manifests that the interchain interactions are less as compared to that previously reported for Ag or AuAg alloy MPCs.[24]

2.5 Discussion

The complete characterization of these MPCs shows effective capping of DDT on the particles surface, where the order of the monolayer is reflected by the NMR, DSC and FTIR studies. Further, effective van der Waal's attraction among the monolayers of adjacent MPCs causes spontaneous superlattice formation as revealed by these results. *In-situ* temperature controlled low angle XRD and FTIR studies indicate irreversible phase transition of these ordered assemblies to a disordered state as shown in scheme 2.1, where the alkyl chains are considered as ordered columns along with some disordered chains.[24.f]

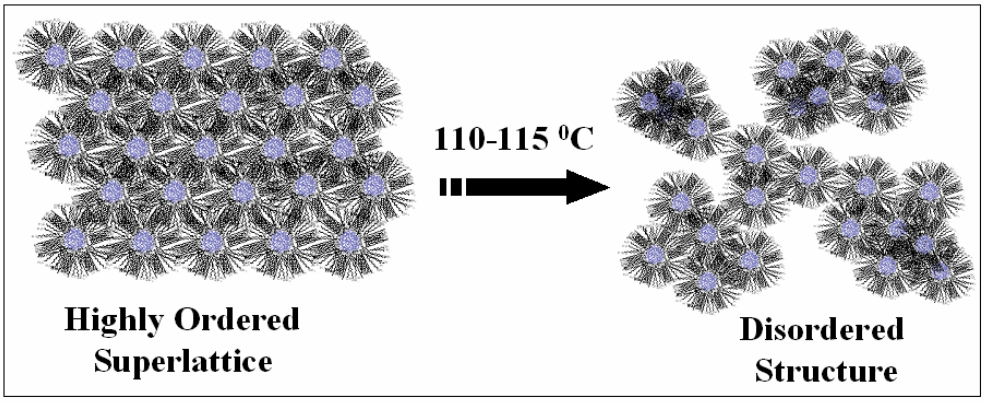

Scheme 2.1 Schematic representation of irreversible phase transition of Au MPCs from ordered assemblies into a disordered state in accordance with the results of i*n-situ* temperature controlled XRD and FTIR studies.

The superlattice stability could be understood well with the help of a model of Ohara and coworkers, where the stability is dependent on the degree of the attractive van der Waal's interactions due to the passivated alkyl chain.[21] The attractive potential for this interaction is given for two finite volume spheres as

$$V(L_{SS}) = -A_H/12[r_r/L_{SS}\{1+ L_{SS}/2(r_a + r_b)\} + 1/(1+ L_{SS}/r_r + D^2/4r_ar_b) +$$

$$2\ln[L_{SS}\{1+ L_{SS}/2(r_a + r_a)\}/\{r_r(1+ L_{SS}/r_r + L_{SS}^2/4r_ar_b)\}] \quad (2.3)$$

The A_H is the material dependent Hamaker constant (= 1.95 eV for Au-Au attraction), r_a and r_b are the radius of two particles A and B respectively, r_r is the reduced radius as $2r_ar_b/(r_a+r_b)$ and L_{SS} is the separation between the nearest surfaces of adjacent spheres. Further, $V(L_{SS})$ is comparable with k_BT and it behaves differently at both $L_{SS} >> r_r$ and $L_{SS} << r_r$ limits. Accordingly, if $V(L_{SS}) >> k_BT$, the enhanced attraction causes aggregation to a nonequilibrium structure (fractal), which is governed by the diffusion limited aggregation model.[21,34]

In the present case, the heating causes increment in the ordering of the passivated monolayers of each MPCs, facilitating the coalescence with its surrounding neighbours. Further, the energy require to form these small aggregates may be less than the energy required to form long range superlattices, thus leading to the destruction of the superlattice order. The loss of crystallinity has been evident from both the low angle XRD and FTIR results, where many subtle changes are observed above 100 °C. Thus our results are in good agreement with the above theoretical predictions of temperature induced diffusion limited phase transition involving nonequilibrium fractal structures.

2.6 Conclusions

Size selective synthesis of Au MPCs in the range of 3.7 – 8 nm is described by a simple route without involving the use of quaternary-ammonium salts or any tedious separation steps. The size distribution of these particles is calculated from the results of TEM and XRD, whereas optical properties of these particles are examined with UV-visible spectroscopic studies. The ^{1}H NMR and FTIR studies are used to address their surface passivation, which show that the ordering of the passivating alkyl chains decrease with increasing Au core size. The effect of temperature on 3.72 nm sized Au MPCs superstructures is demonstrated with the help of *in-situ* XRD and FTIR studies in conjunction with TEM and TG-DSC analysis. More specifically, these Au MPCs form long range, ordered assemblies due to the attractive van der Waal's interactions among the passivated alkyl chains, which upon heating causes an irreversible phase transition to a disordered state. The low angle XRD data shows the disappearance of the Bragg's peaks corresponding to a larger unit cell of highly ordered superlattices due to this phase transition. This has also accounted in FTIR results, which show the shift in antisymmetric

and symmetric stretching frequencies of the methylene vibrations due to the disordered structure. These results are in good agreement with the theoretical prediction that the increment of attractive interactions could cause the formation of diffusion limited non-equilibrium structures. Our study shows that a decrease of temperature sufficiently below the thermal degradation of monolayer from the surface could cause destruction of these superlattices of Au MPCs, thus predicting the effective temperature window for any device application of these artificial solids.

2.7 References

1. (a) Colvin, V. L.; Schlamp, M. C.; Alivisatos, A. P. *Nature* **1994**, *370*, 354. (b) Schmid, G.; Baumle, M.; Greekens, M.; Heim, I.; Osemann, C.; Sawitwoski, T. *Chem. Soc. Rev.* **1999**, *28*, 179. (c) Shipway, A. N.; Katz, E.; Willner, I. *Chem. Phys. Chem.* **2000**, *1*, 18. (d) Mirkin, C. A. *Inorg. Chem.* **2000**, 39, 2258. (e) Rao, C. N. R.; Kulkarni, G. U.; Thomas, P. J.; Edwards, P. P. *Chem. Soc. Rev.* **2000**, *29*, 27. (f) Schmid, G.; Chi, L. F. *Adv. Mater.* **1998**, *10*, 515. (g) Ahmadi, T. S.; Wang, Z. L.; Green, T. C.; Henglein, A.; El-Sayed, M. A. *Science* **1996**, *272*, 1924.
2. Collier, C. P.; Vossmeyer, T.; Heath, J. R. *Annu. Rev. Phys.Chem*. **1998**, *49*, 371 and references therein.
3. Daniel, M.-C.; Astruc, D. *Chem. Rev.* **2004**, *104,* 293.
4. (a) Yin, J. S.; Wang, Z. L. *Phy. Rev. Lett.* **1997**, *79*, 2570. (b) Kim, S.-H.; Medeiros-Ribeiro, G.; Ohlberg, D. A. A.; Williams, R. S.; Heath, J. R. *J. Phys. Chem.B* **1999**, *103*, 10341. (c) Collier, C. P.; Saykally, R. J.; Shiang, J. J.; Henrichs, S. E.; Heath, J. R. *Science* **1997**, *277*, 1978. (d) Markovich, G.; Collier, C. P.; Heath, J. R. *Phys. Rev. Lett.***1998**, *80*, 3807. (e) Snow, A. W.; Wohltjen, A. *Chem. Mater.* **1998**, *10*, 947.
5. (a) Tanori, J.; Pileni, M. P. *Adv. Mater.* **1995**, *7*, 862. (b) Lisiek, I.; Pileni, M. P. *J. Phy. Chem.* **1995**, *99*, 5077. (c) Pileni, M. P. *J. Phy. Chem.B* **2001**, *104*, 3358.
6. (a) Dorogi, M.; Gomez, J.; Osifchin, R.; Andres, R. P.; Reifenberger, R. *Phy. Rev. B* **1995**, *52*, 9071. (b) Amman, M.; Wilkins, R.; Ben-Jacob, E.; Maker, P. D.; Jaklevic, R. C. *Phy. Rev. B* **1991**, *43*, 1146.
7. (a) Thomas, P. J.; Kulkarni, G. U.; Rao, C. N. R. *Chem. Phys. Lett.* **2000**, *321*, 163. (b) Ancona, M. G.; Kruppa, W.; Rendell, R. W.; Snow, A. W.; Park, D.; Boos, J. B. *Phy. Rev. B* **2001**, *64*, 033408.
8. Schaaff, T. G.; Shafigullin, M. N.; Khoury, J. T.; Vezmar, I.; Whetten, R. L. *J. Phys. Chem. B* **1997**, *101*, 7885.
9. (a) Aslam, M.; Mulla, I. S.; Vijayamohanan, K. *App. Phy. Lett.* **2001**, *79*, 689. (b) Aslam, M.; Chaki, N. K.; Mulla, I. S.; Vijayamohanan, K. *Appl. Surf. Sci.* **2001**, *182*, 338. (c) Aslam, M.; Gopakumar, G.; Shoba, T. L.; Mulla, I. S.; Vijayamohanan, K.; Kulkarni, S. K.; Urban, J.; Vogel, W. *J. Colloid Interface Sci.* **2002**, *255*, 79. (d)

Quinn, B. M.; Prieto, I.; Haram, S. K.; Bard, A. J. *J. Phys. Chem. B* **2001**, *105*, 7474.

10. (a) Arakawa, Y.; Takahashi, T. *Optoelectronics* **1988**, *3*, 155. (b) Ugajin, R. *J. Appl. Phys.* **1994**, *76,* 2833. (c) Orlov, A. O.; Amlani, I.; Bernstein, G. H.; Lent, C. S.; Snider, G. L. *Science* **1997**, *277*, 928. (d) Dabbousi, B. O.; Bawendi, M. G. Onitsuka, O.; Rubner, M. F. *Appl. Phys. Lett.* **1995**, *66*, 1316. (e) Greenham, N. C.; Peng, X. G.; Alivisatos, A. P. *Phys. Rev. B* **1996**, *54*, 17628.
11. Brust, M.; Walker, M.; Bethell, D.; Schiffrin, D. J.; Whyman, R. *J. Chem. Soc. Chem. Commun.* **1994**, 801.
12. (a) Templeton, A. C.; Wuelfing, W. P.; Murray, R. W. *Acc. Chem. Res*. **2000**, *33*, 27. (b) Terrill, R. H.; Postelethwaite, T. A.; Chen, C.; Poon, C. D.; Terzis, A.; Chen, A.; Hutchison, J. E.; Clark, M. R.; Wignall, G.; Londono, J. D.; Superfine, R.; Falvo, M.; Johnson, C. H., Jr.; Samulski, E. T.; Murray, R. W. *J. Am. Chem. Soc.* **1995**, *117*, 12537. (c) Chen, S.; Murray, R. W. *Langmuir* **1999**, *15*, 682. (d) Hostetler, M. J.; Wingate, J. E.; Zhong, C.-J.; Harris, J. E.; Vachet, R. W.; Clark, M. R.; Londono, J. D.; Green, S. J.; Stokes, J. J.; Wignall, G. D.; Glish, G. L.; Porter, M. D.; Evans. N. D.; Murray, R. W. *Langmuir* **1998**, *14*, 17.
13. (a) Leff, D. V.; Brandt, L.; Heath, J. R. *Langmuir* **1995**, *12*, 4723. (b) Vijaya Sarathy, K.; Kulkarni, G. U.; Rao, C. N. R. *Chem. Commun.* **1997**, 537. (c) Shenhar, R.; Rotello, V. M. *Acc. Chem. Res.* **2003**, *36*, 549. (d) Cliffel, D. E.; Zamborini, F. P.; Gross, S. M.; Murray, R. W. *Langmuir* **2000**, *16*, 9699. (e) Schaaff, T. G.; Shafigullin, M. N.; Khoury, J. T.; Vezmar, I.; Whetten, R. L. *J. Phys. Chem. B* **2001**, *105*, 8785.
14. (a) Vijaya Sarathy, K.; Raina, G.; Yadav, R. T.; Kulkarni, G. U.; Rao, C. N. R. *J. Phys. Chem. B* **1997**, *101*, 9876. (b) Chen, S.; Sommers, J. M. *J. Phys. Chem. B* **2001**, *105*, 8816. (c) Zamborini, F. P.; Gross, S. M.; Murray, R. W. *Langmuir* **2001**, *17*, 481. (d) Crispin, X.; Bureau, C.; Geskin, V.; Lazzaroni, R.; Brédas, J. *Eurp. J. Inorg. Chem.* **1999**, *1999*, 349. (e) Balogh, L.; Tomalia, D. A. *J. Am. Chem. Soc.* **1998**, *120*, 7355. (f) Yeh, M.; Yang, Y.; Lee, Y.; Lee, H; Yeh, Y.; Chen-Sheng, Y. *J. Phys. Chem. B* **1999**, *103*, 6851. (g) Hostetler, M. J.; Zhong, C.-J.; Yen, B. K. H.; Anderegg, J.; Gross, S. M.; Evans, N. D.; Porter, M.; Murray, R. W. *J. Am. Chem. Soc.* **1998**, *120*, 9396.

15. (a) Manna, A.; Kulkarni, B. D.; Bandyopadhyay, K.; Vijayamohanan, K. *Chem. Mater.* **1997**, *9*, 3032. (b) Manna, A.; Imae, T.; Iida, M.; Hisamatsu, N. *Langmuir* **2001**, *17*, 6000. (c) Wang, W.; Chen, X.; Efrima, S. *J. Phys. Chem. B* **1999**, *103*, 7238. (d) Kim, S.-W.; Park, J.; Jang, Y.; Chung, Y.; Hwang, S.; Hyeon, T.; Kim, Y. W. *Nano Lett.* **2003**, *3*, 1289. (e) Wilcoxon, J. P.; Williamson, R. L.; Baughman, R. *J. Chem. Phys.* **1993**, *98*, 9933.
16. (a) Lin, X. M.; Wang, G. M.; Sorensen, C. M.; Klabunde, K. J. *J. Phys. Chem. B* **1999**, *103*, 5488. (b) Prasad, B. L. V.; Stoeva, S. I.; Sorensen, C. M.; Klabunde, K. J. *Chem. Mater.* **2003**, *15*, 935. (c) Teranishi, T.; Kiyokawa, I.; Miyake, M. *Adv. Mater.* **1998**, *10*, 596.
17. (a) Jana, N. R.; Peng, X. G. *J. Am. Chem. Soc.* **2003**, *125*, 14280. (b) Hiramatsu, H.; Osterloh, F. E. *Chem. Mater.* **2004**, *16*, 2509. (c) Green, M.; O'Brien, P. *Chem. Commun.* **2000**, 183.
18. Waters, C. A.; Mills, A. J.; Johnson, K. A.; Schiffrin, D. J. *Chem. Commun.* **2003**, 540.
19. (a) Alvarez, M. M.; Khoury, J. T.; Schaaff, T. G.; Shafigullin, M. N.; Vezmar, I.; Whetten, R. L. *J. Phys. Chem. B* **1997**, *101*, 3706. (b) Lin, X. M.; Jaegar, H. M.; Sorensen, C. M.; Klabunde, K. J. *J. Phys. Chem. B* **2001**, *105*, 3353. (c) Prasad, B. L. V.; Stoeva, S. I.; Sorensen, C. M.; Klabunde, K. J. *Langmuir* **2002**, *18*, 7515.
20. (a) Harfenist, S. A.; Wang, Z. L.; Alvarez, M. M.; Vezmar, I.; Whetten, R. L. *J. Phys. Chem.* **1996**, *100*, 13904. (b) Wang, Z. L. *Adv. Mater*. **1998**, *10,* 13. (c) Wang, Z. L.; Harfenist, S. A.; Vezmar, I.; Whetten, R. L.; Bently, J.; Evans, N. D.; Alexander, K. B. *Adv. Mater*. **1998**, *10*, 808. (d) Harfenist, S. A.; Wang, Z. L.; Whetten, R. L.; Vezmar, I.; Alvarez, M. M. *Adv. Mater*. **1997**, *9*, 817. (e) Korgel, B. A.; Fullam, S.; Connolly, S.; Fitzmaurice, D. *J. Phys. Chem. B* **1998**, *102*, 8379. (f) Wang, Z. L.; Harfenist, S. A.; Whetten, R. L.; Bently,J.; Evans, N. D. *J. Phys. Chem. B* **1998**, *102*, 3068. (g) Korgel, B. A.; Fitzmaurice, D. *Phys. Rev. B* **1999**, *59*, 14191.
21. (a) Ohara, P. C.; Leff, D. V.; Heath, J. R. Gelbart W. M. *Phys. Rev. Lett.* **1995**, *75*, 3466. (b) Hamaker, H. C. *Physica (Utrecht)* **1937**, *75*, 1058.
22. (a) Luedtke, W. D.; Landman, U. *J. Phys. Chem.* **1996**, *100*, 13323. (b) Whetten, R. L.; Khoury, J. T.; Alvarez, M. M.; Murthy, S.; Vezmar, I.; Wang, Z. L.; Stephens, P. W.; Cleveland, C. L.; Luedtke, W. D.; Landman, U. *Adv. Mater*. **1996**, *8*, 428.

23. Heath, J. R.; Knobler, C. M.; Leff, D. V. *J. Phys. Chem. B* **1997**, *101*, 189.
24. (a) Sandhyarani, N.; Resmi, M. R.; Unnikrishnan, R.; Vidyasagar, K.; Ma, S.; Antony, M. P.; Selvaam, G. P.; Visalakshi, V.; Kumar, N. C.; Pandian, K.; Tao, Y. T.; Pradeep, T. *Chem. Mater* **2000**, *12*, 104. (b) Sandhyarani, N.; Pradeep, T.; Chakrabarti, J.; Yousuf, M.; Sahu, H. K. *Phys. Rev. B* **2000**, *62*, 739. (c) Sandhyarani, N.; Pradeep, T. *Chem. Mater* **2000**, *12*, 1755. (d) Mitra, S.; Nair, B.; Pradeep, T.; Goyal, P. S.; Mukhopadhyay, R. *J. Phys.Chem. B* **2002**, *106*, 3960. (e) Sandhyarani, N.; Pradeep, T.; Antony, M. P.; Selvam, G. P. *J. Chem. Phys.* **2000**, *113*, 9794. (f) Pradeep, T.; Mitra, S.; Nair, A. S.; Mukhopadhyay, R. *J. Phys. Chem. B* **2004,** *108*, 7012.
25. El-Sayed, M. A. *Acc. Chem. Res.* **2001**, *34*, 257 and references therein.
26. Mie, G. *Ann. Physik* **1908**, *25*, 377.
27. Kreibig, U.; Vollmer, M. *Optical Properties of Metal Clusters;* Springer: Berlin, 1995.
28. (a) Papavassiliou, G. C. *Prog. Solid State Chem.* **1980**, *12*, 185. (b) Kerker, M. *The Scattering of Light and Other Electromagnetic Radiation;* Academic Press: New York, 1969. (c) Bohren, C. F.; Huffman, D. R. *Absorption and Scattering of Light by Small Particles;* Wiley: New York, 1983. (d) Creighton, J. A.; Eadon, D. G. *J. Chem. Soc. Faraday Trans.* **1991**, *87*, 3881.
29. Link, S.; El-Sayed, M. A. *J. Phys. Chem. B* **1999**, *103*, 4212.
30. Templeton, A. C.; Pietron, J. J.; Murray, R. W.; Mulvaney, P. *J. Phys. Chem. B* **2000**, *104*, 564.
31. Aiken III, J. D.; Finke, R. G. *J. Mol. Cata. A: Chem.* **1999**, *145*, 1.
32. Guinier, A. *X-ray Diffraction in Crystals, Imperfect Crystals and Amorphous Bodies*; Dover: New York, 1994.
33. Hostetler, M. J.; Stokes, J. J.; Murray, R. W. *Langmuir* **1996**, *12*, 3604.
34. Ball, R. C. *Phys. Rev. Lett.* **1987**, *58*, 274.

Chapter 3

Single Electron Charging Features of Monolayer Protected Gold Clusters*

The electron transfer features of *ca.* 3.72 nm sized Au MPCs have been investigated using combined electrochemical and scanning tunneling microscopic (STM) studies. In particular, the calculated capacitance is in good agreement with experimentally obtained values from both of these techniques. Further, various parameters, like diffusion coefficients and electron transfer rate constants, are calculated from the results of chronoamperometry and impedance techniques. Adsorption phenomena of these MPCs on electrode surfaces have also been discussed along with an elementary discussion of the determination of electron transfer rate constants of adsorbed MPCs.

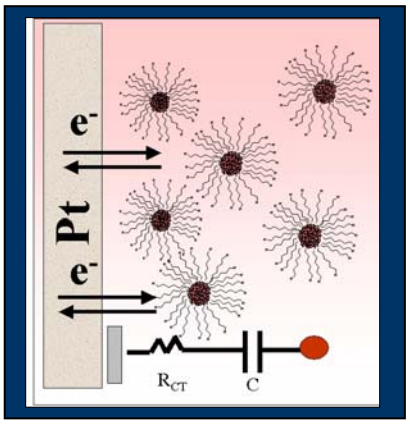

---

* A part of the work has been published in "***J. Appl. Phys.* 2004**, 6, 5032" and another part in "***Langmuir* 2004**, 20, 10208".

3.1 Introduction

In recent years, there has been a large effort to understand the structure and properties of metallic and semiconducting monolayer protected nanoclusters (MPCs) due to their stability coupled with several attractive size dependent properties.[1,2] Further, the ordered arrays of such metallic and semiconducting MPCs are of special interest for harnessing their attractive properties for a large number of potential applications, like single electron devices in molecular electronics.[3]

As discussed in chapter 1 (Section 1.3), electron transfer behaviour in such ordered arrays has shown that, when such metallic nanoclusters are organized at a small spatial distance of ~ 1 nm in one, two or three dimensions, a typical example of the double barrier tunnel junction (DBTJ) is formed in series with the nanoparticles at the centre to manifest single-electron tunneling.[3-9] In particular, the passivated organic molecules enable several magnificent illustrations in controlling the electron transfer through these tunnel junction systems, where the discreteness of electronic charge of these MPCs plays an important role.[3-7] These MPCs have a tiny capacitance (sub-atto farad), C, in such a way that the charging energy ($E_C = e^2/2C$) is always greater than the thermal energy (k_BT), where e is the fundamental charge unit and k_B is the Boltzmann's constant. For example, if the capacitance is few atto farads (10^{-18} F) the charging energy turns out to be 100-150 meV, while thermal energy is only ~ 26 meV. Consequently, in the presence of an external field, the system shows steps in the I-V characteristics due to this capacitive nature, popularly known as Coulomb blockade or Coulomb staircase.[6-7] An interesting consequence of the Coulomb blockade behaviour of these MPCs is the manifestation of multivalent redox property in several electrolytic solutions, which arises due to the coupling of the charge storage capability with consecutive electron transfer events as evidenced by voltammetric measurements, known as quantized double layer (QDL) charging.[10] As mentioned in the first chapter the double layer capacitance (C_{CLU}) of MPCs is so small (sub-atto farad) that even room temperature resolution of single electron charging become possible, analogous to scanning tunneling microscope/spectroscopic (STM/STS) based "Coulomb staircase" or "Coulomb blockade" behaviour.[10] Such QDL charging has been reported for both metal

(i.e., Au, Ag, Cu and Pd) and semiconductor (i.e., CdS, PbS, Si etc.) MPCs, although a majority of the study is concerned with Au MPCs due to their enhanced stability.[10-12] There are extensive reports on the electrochemical behaviour of these smaller sized (1.1- 3 nm diameter) MPCs, while no detailed study is available for larger (> 3 nm diameters) Au MPCs.[10-12]

To date, several experimental illustrations of Coulomb blockade for ensembles of metal nanoparticles anchored on substrates through covalent and electrostatic interactions or superlattices have been reported earlier.[5-9] In comparison, in this chapter, we describe an elementary theoretical model to explain the effect of variation of the chain length and cluster size on the charging energy for such Coulomb blockade nanostructures, assuming the cluster to be a curved metallic surface embedded in a soft medium of organic molecules. Further, the single electron charging features of dodecanethiol (DDT) protected 3.72 nm sized Au MPCs $[Au_{1415}(DDT)_{328}]$ in dichloromethane (CH_2Cl_2) using combined electrochemical and STM studies have been investigated in order to unravel such phenomena in relatively larger sized MPCs. In the preceding chapter (2), we have discussed their synthesis and characterization details along with the effect of temperature on their superstructure. Most importantly, our voltammetric and STM studies summarize that these particles are accessible for single electron charging. For instance, the I-V behaviour obtained from the STM measurements on a single particle shows a clear Coulomb blockade effect, whereas the voltammetry reveals a large population of QDL charging events. These MPCs are found to have high tendency to adsorb on the electrode surface, which is also characterized by cyclic voltammetry (CV) and differential pulse voltammetry (DPV). The electron transfer rate constant calculated using the Laviron's approach for immobilized electroactive species on electrode surface is found to be *ca.* 2 s^{-1}, which is slower as compared to the value for its smaller analogues. We believe that the understanding of the single electron transfer features of these larger sized MPCs would help to rationalize the effect of size on single electron transfer phenomena with its attendant applications in molecular electronics and nanotechnology.

3.2 A Simplified Model to Understand the Charging Behaviour in Coulomb Blockade Nanostructure

Tunneling conductance, $G(V) \cong dI/dV$ of a metal-molecule-metal tunneling junction is a direct measure of the single particle density of state in metal nanoclusters. Landauer has given an elegant description of the size dependent electron tunneling in quantum dots (Q-dots) in terms of transmittivity (reflectivity) of a barrier. When an electron in a nanoparticle experiences a barrier due to the surrounding dielectric medium, the transmission probability (T_P) is given by,

$$\ln T_P \sim [-2(m_e E_g)^{1/2}.L_B]/\hbar \qquad (3.1)$$

where E_g is the barrier potential (conductance gap in eV) and L_B is the length of the barrier as can be typically the length (d) of the passivating chain, m_e is the rest mass of the electron and $\hbar = h/2\pi$, where h is the Plank's constant.[13] We propose a new model for the tunnelling barrier by assuming that the cluster (i.e., a group of metallic or non-metallic atoms) having a curved metallic surface, is embedded in a medium of soft organic moiety. The cluster-organic moiety-interface (metal-molecule interface) can have a charge distribution with an isotropic dielectric constant, enabling them to behave as tiny capacitors.[14] Another key assumption is regarding the spacing between clusters, where twice the chain length is considered for intercluster separation, which may not be strictly true. Accordingly, the capacitance (C_{IC}) of the cluster can be calculated by modifying the simple electrostatic model of 'parallel plate capacitor', to 'curved metallic sheets' separated by a distance of L_{BB}, as,

$$C_{IC} = 2\pi\varepsilon_o\varepsilon_m r^2/L_{BB} \qquad (3.2)$$

where, ε_o is the permittivity of free space, ε_m is the dielectric constant of the medium, r is the radius of the cluster and L_{BB} is the effective distance between two clusters. This effective distance between the clusters is the summation of twice the length of the organic molecule and the distance contribution due to the curved surface of the cluster, i.e., 2(d + dx), where dx is the variation of the distance due to curvature of the surface, as demonstrated in the inset of Figure 3.1. Therefore, dx is given by,

$\Sigma_{(0 \rightarrow r)}\, dx/n = r/2,$

i.e., $L_{BB} = 2(d + r/2),$

where, d represents the length of the organic molecule used for capping the clusters.

Hence, the capacitance (C_{IC}) becomes;

$$C_{Ic} = 2\pi\varepsilon_o\varepsilon_m r/(1 + 2d/r) \qquad (3.\ 3)$$

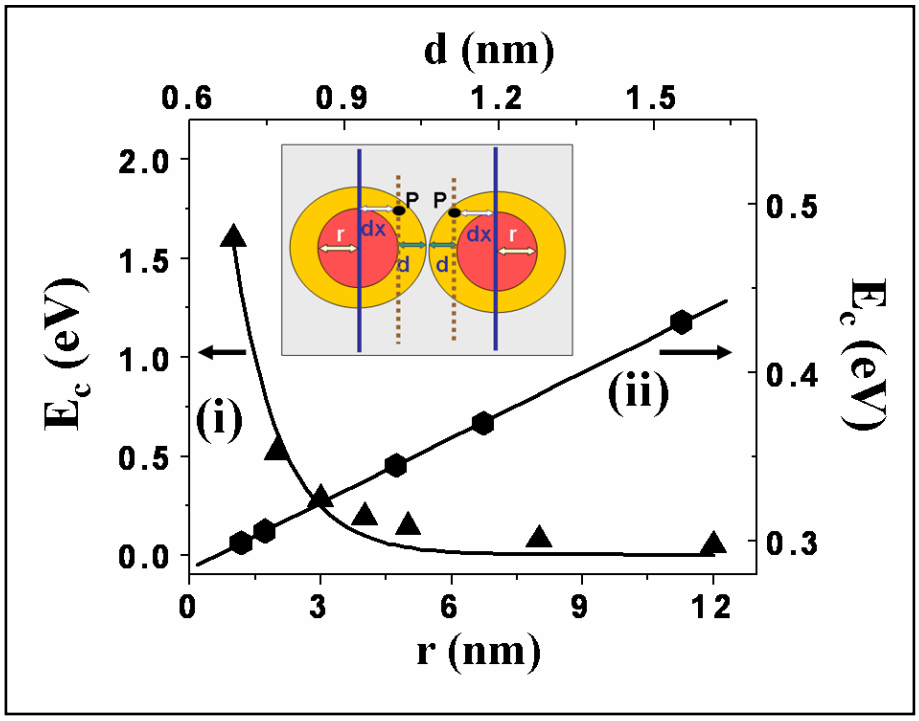

Figure 3.1 (i) Variation of charging energy (E_c) with nanocluster radius (r), calculated by assuming clusters as spherical metal sheets embedded in organic medium (exponential fitting is also seen in the figure as solid line); inset shows the dimensional parameters used to calculate the effective distance between the clusters; r is the radius of the cluster core, d is the length of organic chain and dx is the contribution due to curvature of the cluster surface at a certain point P to the capacitance (C_{IC}). (ii) Variation of electrostatic charging energy (E_c) with chain length (d) for clusters with an average size of 5 ± 0.5 nm with above approximations (linear fitting is also shown as solid line).

Since the distance between clusters can change with size (r) and also with the length of the organic molecule (d), we need to consider the intercluster distance as the primary variable with a minor approximation. When cluster size is very large compared to the length of the organic chain, i.e., d/r is very small, then (1 +2d/r) will be approximately equal to unity. On the contrary, when $r \rightarrow \infty$ the capacitance depends only on the cluster radius and not on the organic chain length. The approximate value of the capacitance at high radius is given by $C_{lc} = 2\pi\varepsilon_o\varepsilon_m r$, while, on the other hand when the organic chain length is very large (i.e., $d \rightarrow \infty$) the capacitance will become zero. For example, experimentally changing either the size of particle or the chain length can lead insulator-to-metal transitions in these Coulomb blockade nanostructures due to the change in the charging energy of the system.[9]

Table 3.1 Variation of calculated capacitances and charging energies of Au MPCs (5 ± 0.5 nm) with various chain lengths of organic passivating molecules

Organic molecule	Length of organic molecule (nm)	Calculated Capacitance (aF)	Calculated Charging Energy (eV)
C_{12} SH	1.56	0.19	0.43
C_8 SH	1.17	0.22	0.37
PhC_2SH	1.00	0.23	0.35
C_5 SH	0.75	0.26	0.31
PhSH	0.70	0.27	0.30

As the charging energy (E_c) is inversely related to the capacitance, we further investigate the nature of charging energy with respect to the length of the organic moiety (Table 3.1). The Electrostatic charging energy for the cluster is derived as,

$$E_c = (e^2/4\pi\varepsilon_o\varepsilon_m r) + (de^2/2\pi\varepsilon_o\varepsilon_m r^2) \qquad (3.4)$$

and therefore,

$$dE_c/dd = (e^2/2\pi\varepsilon_o\varepsilon_m r^2) \quad (3.5)$$

which gives the change in the charging energy with chain length. Consequently, the variation of electrostatic charging energy with cluster radius and chain length for different clusters can be experimentally verified using the above equation. For example, the charging energy varies (E_c) exponentially with cluster radius (r) [Figure 3.1 case (i)], which can be fitted to $E_c = A\ e^{-(r-1)/K'}$, where K′ is constant and A equals to 3.98 eV, corresponding to the charging energy for clusters of 1 nm radius. The above equation also easily predicts the charging behaviour of clusters at boundary conditions of cluster radius; as for instance, the charging energy will become zero only for a very big cluster, i.e., having infinite radius. On the other hand, the charging energy for a zero radius cluster is shown as infinity, i.e., the charging of a cluster with zero diameter is not possible. This equation also reveals that at the limiting condition of the cluster i.e., at zero dimension, interestingly, the model collapses to the case of the point atom. In addition, the charging energy (E_c) calculated by the above equation for 5 $\pm$ 0.5 nm clusters with different capping agents reveals a linear decrease with the decrease in chain length (d) [Figure 3.1 case (ii)]. Simultaneously, the calculated value of intercept (i.e., $e^2/4\pi\varepsilon_o\varepsilon_m r$ = 192 meV) using 5 nm sized clusters can be considered as the charging energy, when the chain length (d) becomes zero (i.e., bare cluster). More significantly, this implies that in the absence of organic moiety, clusters can thus act as capacitors with a charge, $Q = 2\pi\varepsilon_o\varepsilon_m rV$. This has profound implications on the electronic structure of small clusters in deciding the limits of metallicity with respect to size and Kubo gap.[15]

3.3 Experimental Section

3.3.1 Materials

Dodecanethiol (99%), $NaBH_4$ and tetrabutylammoniumhexaflurophosphate (TBAHFP) and $HAuCl_4.3H_2O$ were obtained from Aldrich, whereas toluene, acetone and dichloromethane are of AR grade from Merck and were used after further purification. In all these experiments deionized water (16 MΩ) from Milli-Q system was used.

3.3.2 Synthesis of Au MPCs

Synthesis and characterization details of $Au_{1415}(DDT)_{328}$ MPCs have been already described in chapter 2 (section 2.2.2) along with the appropriate determination of composition.

3.3.3 Scanning Tunneling Microscope/Spectroscopic (STM/STS) Measurements

One of the most widely used test samples for STM investigations is highly oriented pyrolytic graphite (HOPG) substrates due to its reasonable flatness in the sub-nanometer range and non-reacting nature. HOPG was used after cleaving off surface layers of graphite using good quality tape to create a fresh, atomically flat surface, with cleavage steps. Later, they were cleaned with acetone and ultrasonically agitated in methanol to remove impurities and adhered particles, if any. The sample for STM analysis was prepared by putting a very dilute drop of nanoparticle solution on HOPG substrate followed by drying for 5 min. STM studies were subsequently carried out immediately after the deposition. The STM tips were made from 0.25 mm diameter polycrystalline Pt - Rh wire by mechanically cutting them at an angle.

A home-built STM based on fine mechanical-screw-lever arrangement assembly with a compact, four-quadrant, three dimensional scanner was used for this investigation.[16] Details of the system and the general procedure for imaging are discussed elsewhere.[17] The images were processed using SPIP software.[18] The STM imaging was carried out in air with an optimum values of tunnel current (0.15 nA) and bias voltage (100 mV) in constant current mode. The time between imaging and sample preparation was kept minimum (5 m) and once the particles were located with some difficulties they were imaged repeatedly.

3.3.4 Electrochemical Measurements

All the electrochemical measurements were carried out in CH_2Cl_2 using tetrabutylammoniumhexaflurophosphate (TBAHFP) as supporting electrolyte in an ice bath (273 – 276 K) using a standard three electrode cell comprising Pt micro electrode

(50 μm) as the working electrode, a Pt wire as counter electrode and another Pt wire as quasi reference electrode (calibrated independently with an internal standard of ferrocene/ferrocenium cation redox couple) unless mentioned separately. Differential pulse (modulation time 0.02 s, interval time 0.1 s, step potential 0.025 V and modulation amplitude 0.02 V), cyclic voltammograms and chronoamperometry experiments were performed on an Autolab PGSTAT30 (ECO CHEMIE) instrument, whereas electrochemical impedance measurements were carried out in an impedance analyzer (Autolab PGSTAT 30 with FRA software). The ac signal amplitude was 5 mV and the frequency range employed was 1 Hz to 50 kHz and the data were recorded with averaging over 3 cycles for each frequency. The chronoamperometry and impedance measurements were carried out employing a Pt disc (0.5 mm diameter) working electrode under identical conditions as mentioned above.

3.4 Single Electron Charging Features of $Au_{1415}(DDT)_{328}$

3.4.1 STM/STS Measurements

Figure 3.2 (a) shows a typical STM image of Au nanoparticles on HOPG surface, where few isolated particles are located. The particle size is estimated to be ≈ 4.5 nm from STM image as shown in Figure 3.2 (b), which is comparable to the size obtained from the TEM analysis (Figure 3.2c). STS was performed by positioning Pt-Rh tip over an isolated Au MPC (marked by an arrow in Figure 3.2a) by disabling the feedback control and measuring I-V characteristics. The I-V characteristics were always repeated several times and the final signal was averaged over tens of runs. The derivative, dI/dV vs. V was obtained by the numerical differentiation of measured I-V curves.

Figure 3.3 shows typical I-V characteristics of an isolated nanoparticle marked in Figure 3.2 (a), along with its dI/dV variation with voltage (left inset). In particular, curve (a) describes the experimental I-V behaviour, while (b) shows the theoretically fitted curve using equations 3.1 and 3.2, based on orthodox theory.[19] These curves are highly non-linear with the zero conductance region of around 0.2 eV, which could be due to the Coulomb blockade effect. More specifically, the comparison of (a) with (b) depicts that the experimental curve deviates from theoretical one, especially, at higher positive and negative biases.

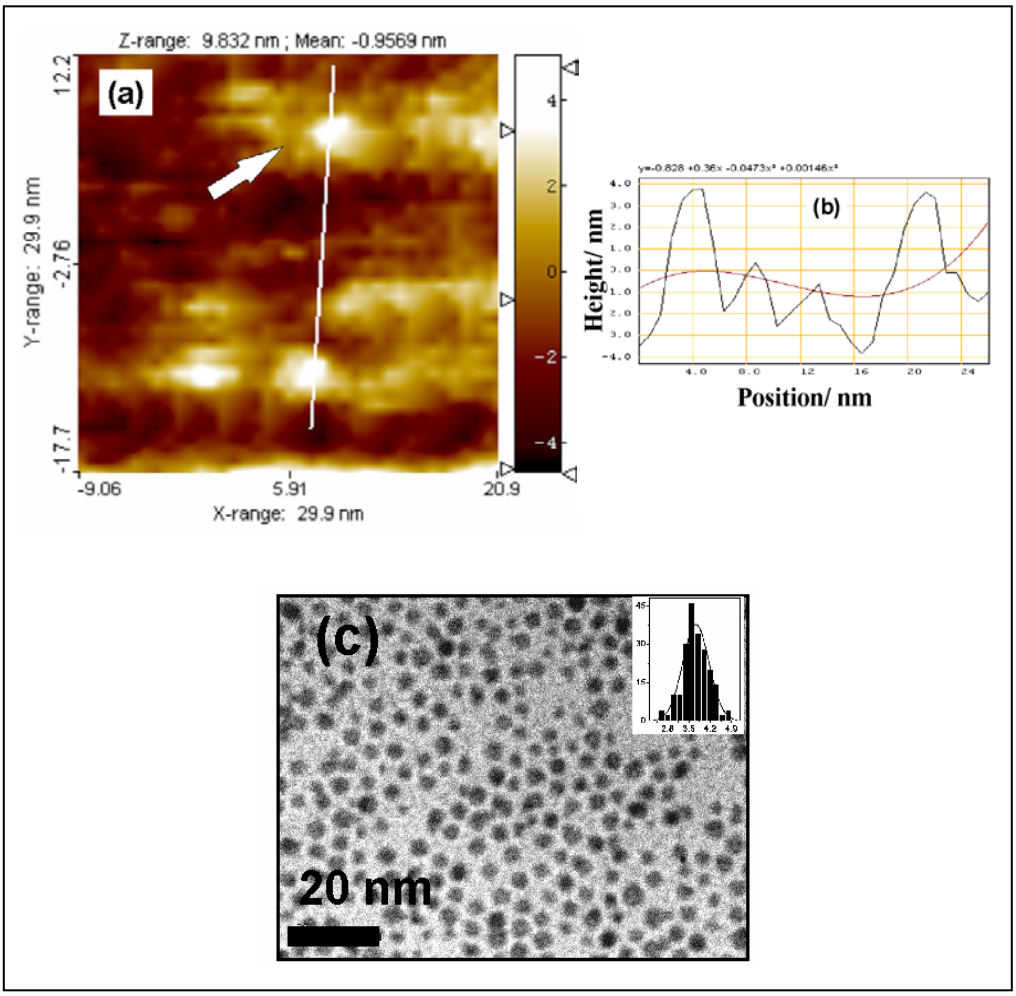

Figure 3.2 (a) Constant current STM image of Au nanoparticles (scan area: 300 Å x 300 Å) with important parameters, like I = 0.15 nA and V = 100 mV; (b) Line profile of two nanoparticles are marked by the line in (a). (c) TEM image of the same particle for comparison showing fairly uniform Gaussian distribution with an average particle size of 3.72 ± 0.4 nm (inset).

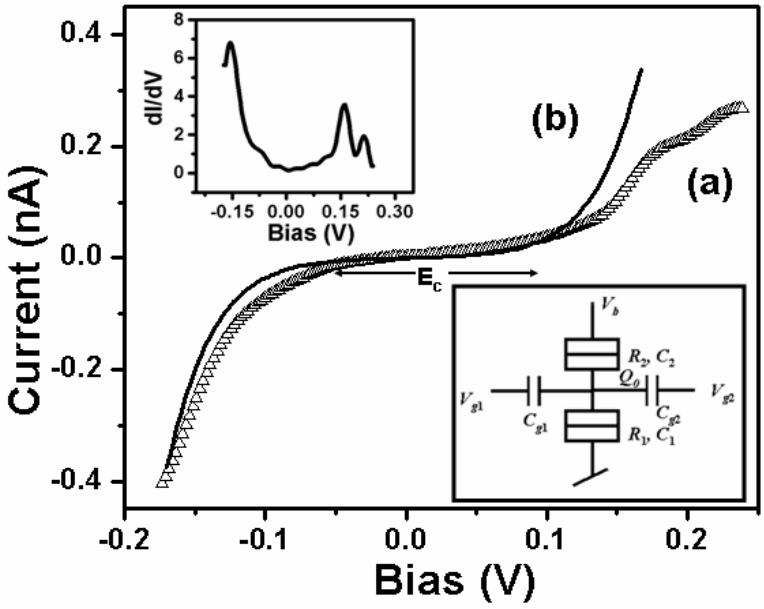

Figure 3.3 I-V characteristics of the isolated Au particle marked in Figure 3.2 (a) showing single electron charging features as illustrated by (a) experimental plot along with (b) its theoretically fitted curve using equations (3.1 and 3.2). The dI/dV vs. V is shown in left inset, whereas the schematic diagram of the theoretical model used to fit with the experimental curve is shown in the right inset. Comparison of experimental and theoretical plot gives the best-fit parameters as R_1 = 10^8 ohms, C_1 = 1 x 10^{-19} F, R_2 = 10^6 ohms, C_2 = 2.5 x 10^{-20} F, Cg_1 = 2.8 x 10^{-19} F, Vg_1 = 0 V, Cg_2 = 0 F, Vg_2 = 0 V, Q_0 = 0, V_b = 0.17 V, E_c = 0.19 eV, kT/E_c = 0.1307 and T = 300 K.

The detailed explanation for single electron tunneling[6] can be provided by the orthodox theory of Hanna and Tinkham,[6c] where two-junction system is treated with fractional charge Q_o on the central electrode without an external electrode. In particular, the theory gives an expression for current (I) in the following form:

$$I = \sum_{N=-\infty}^{N=\infty} e[r_1(N,V) - l_1(N,V)]\rho(N,V) \qquad (3.6)$$

Where r_1 (N, V) and l_1 (N, V) are the electron tunneling rates from the right and left respectively, on the first junction and ρ (N, V, t) is the probability that there are N extra electrons on the middle electrode at time t with applied voltage V.[6b] According to Amman

et. al.[6b] if it is assumed that the charge distribution completely relaxes during the tunneling event (i.e., the time of tunneling is much longer than the relaxation time of the system but shorter than the time between tunneling events), the resultant electron tunneling rate turns out to be,

$$r_1(N,V) = \frac{1}{e^2 R_1} \frac{eV_1(N,V) - E_c}{[1 - e^{\{-eV_1(N,V)+E_c\}/k_B T}]} \qquad (3.7)$$

From the above equation (3.2) it is clear that at T = 0 K tunneling is suppressed for $eV_1 < E_{C,}$ where E_C corresponds to the charging energy of the junction.

Right inset of Figure 3.3 shows the schematic diagram of the equivalent circuit of DBTJ used to fit the experimental curve, where (R_1, C_1) is the resistance and capacitance of tip/nanoparticle junction, (R_2, C_2) is the resistance and capacitance of nanoparticle/substrate junction, ($C_{g1,}V_{g1}$) and (C_{g2},V_{g2}) are the capacitance and voltage on the tip with respect to ground potential, Q_0 is the fractional charge, E_c is the Coulomb blockade energy and T is the temperature.[19] Although the theory is defined for three electrode system (right inset of Figure 3.3), we simplify it here for the two electrode system, considering V_{g1}, V_{g2} = 0 and V_b as the sample bias voltage. Since there is no third electrode C_{g1} and C_{g2} are parallel to C_1 and this combination represents the tunnel junction capacitance between the tip and the nanoparticle. The best fit parameters obtained are R_1=10^8 ohms, C_1 = 1 x 10^{-19} F, R_2 = 10^6 ohms, C_2 = 2.5 x 10^{-20} F, Cg_1 = 2.8 x 10^{-19} F, Vg_1 = 0 V, Cg_2 = 0 F, Vg_2 = 0 V, Q_0 = 0, V_b = 0.17 V, E_c=0.19 eV, kT/E_c = 0.1307 and T= 300 K.

The capacitance (C_S) and E_c are found to be 7.495 x 10^{-19} F and 0.106 eV respectively considering a spherical particle coated with dielectric layer, where $C_S = 4\pi\varepsilon_0\varepsilon_m r$; with r ≈ 2.25 nm as the radius of the nanoparticle (from STM), ε_0 (=8.85 x 10^{-12} $F.m^{-1}$) as the permittivity of free space, ε_m as dielectric constant as 3[14] and E_C the charging energy ($E_C = e^2/2C_S$). In particular, the value of E_C obtained from the fitted parameters of the experimental plot is slightly higher than that of the value calculated theoretically. However, it is possible that simple orthodox model is inadequate in this region or a model based on electron transport in metal-organic molecule-metal may be

required to understand the electron transport in the present case.[20] Inspite of these deviations, the STM studies show that these larger particles are accessible for single electron charging in air despite their higher capacitance values.

3.4.2 Electrochemical Behaviour

3.4.2.1 Quantized Double Layer Charging

The consecutive one electron QDL peaks observe in solution are analogous to current peaks seen in traditional redox reactions.[10] Thus, MPCs in solution can be viewed as mixed-valent ensembles of clusters with adjacent state of core charges, where the QDL charging process is diffusion controlled and obeys the Nernst equation with respect to the average core potential.[10] Accordingly, these peak potentials can be taken as the formal redox potential $E^{0'}$ for each (z/z ± 1) "redox couple or charge state couple" and is given by the DPV peak potentials.[10d] The formal redox potential $E^{0'}$ can be described by:

$$E^{0'}_{z/z+1} = E_{PZC} + (z-{}^{1}/_{2})e/C_{CLU} \qquad (3.8)$$

where E_{PZC} is the potential of zero charge (i.e., z = 0) of the MPC and z is assigned such that z > 0 and z < 0 corresponding to core "oxidation" and "reduction" respectively and C_{CLU} is the capacitance of the MPC. More specifically, the C_{CLU} is associated with the ionic space charge formed around an MPC dissolved in the electrolyte solution, upon electronic charging of the core, whose charging is controlled by electrostatic (i.e., double layer) principles.[10] The above equation predicts a linear plot of $E^{0'}_{z/z+1}$ vs. charge state (popularly known as "Z-plot"), which can be used to determine C_{CLU} from the slope.[10-12]

Figure 3.4 (a) shows the superimposed DPV response of 2 mg Au MPC/ml in (i) 0.1 and (ii) 0.05 M TBAHFP in CH_2Cl_2, where a large population of evenly spaced current peaks are observed (charging states are marked in Figure 3.4 following z/z ± 1 fashion).[11] The blank response (iii) is also superimposed with these curves recorded in an identical condition at 0.1 M TBAHFP. Further, (b) shows the response of 2 mg Au MPC/ml in 0.1 M TBAHFP upon cathodic scan direction. Figure 3.4 (c) shows superimposed DPV response (graph i-ii) of these MPCs (2 mg Au MPC/ml in 0.05 M

TBAHFP) using 10 and 5 mV pulse amplitude respectively. Here, as prepared Au MPCs are assigned the charge state of z = -1, which is reasonable since a very strong reducing agent, like $NaBH_4$, is used for MPC preparation and thus one expects the MPC formed to be in the reduced form.[11a] Hence, -1/0 and -2/-1 are the first oxidation and reduction processes respectively; the -1/0 and 0/1 charge steps are marked in all graphs for comparison with respect to the potential measured using a Pt quasireference electrode. The corresponding potentials for individual charge steps of each DPV plots have been summarized in Table 3.2.

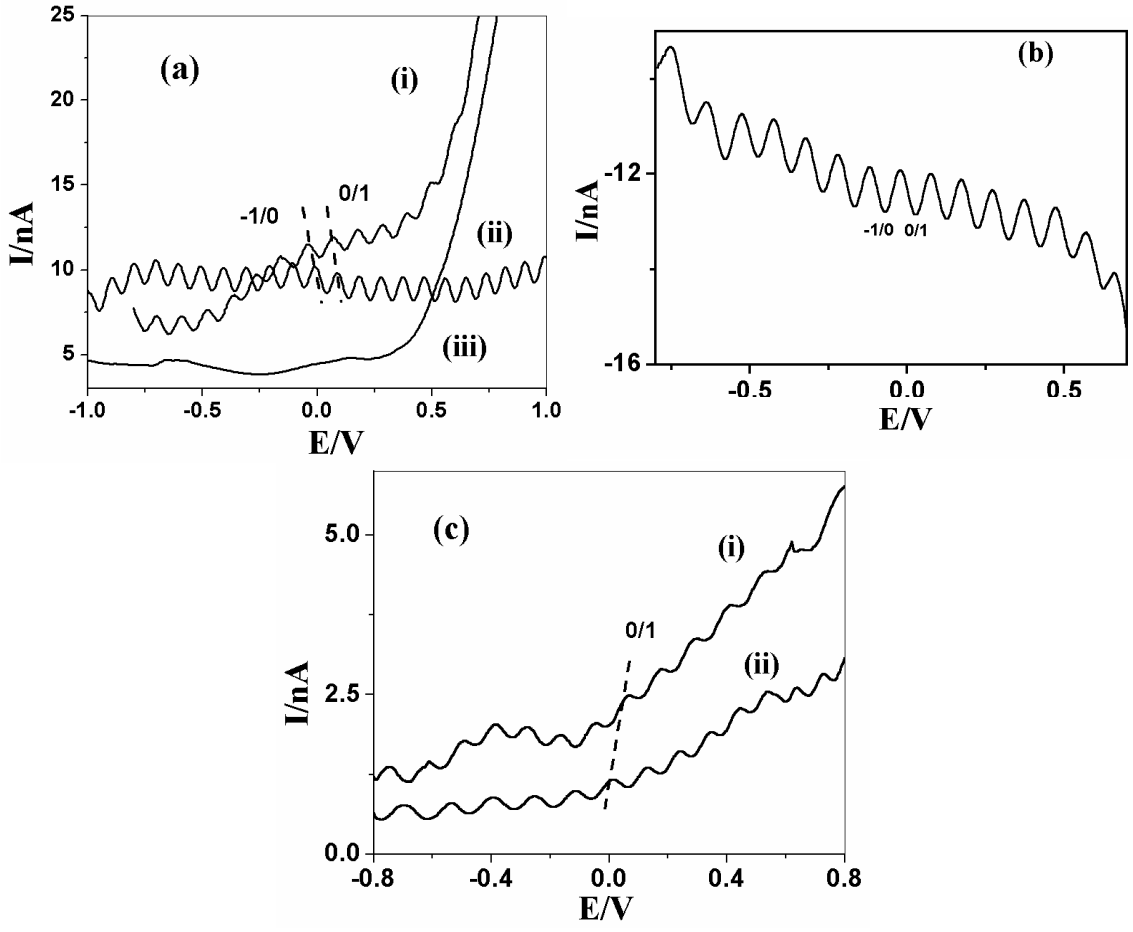

Figure 3.4 (a) Superimposed DPV responses of 2 mg Au MPC/ml with (i) 0.1 M and (ii) 0.05 M TBAHFP concentration at 20 mV pulse amplitude in CH_2Cl_2 on a Pt microelectrode (50 μm) along with the (iii) blank response; (b) response of 2 mg Au MPC/ml in 0.1 M TBAHFP upon cathodic scan direction in identical conditions and (c) responses using (i) 10 and (ii) 5 mV pulse amplitude at 0.05 M TBAHFP. The -1/0 and 0/+1 charge steps are marked for comparison in all cases.

Table 3.2 Peak positions and corresponding charge states for the DPV responses as shown in Figure 3.4

Charge State	Fig. 3.4. a.(i)	Fig. 3.4. a.(ii)	Fig. 3.4.b	Fig. 3.4. c.(i)	Fig. 3.4. c.(ii)
-9/-8	---	-0.90	---	---	---
-8/-7	---	-0.80	---	---	---
-7/-6	-0.70	-0.70	-0.69	---	---
-6/-5	-0.60	-0.60	-0.58	-0.76	---
-5/-4	-0.48	-0.51	-0.48	-0.62	---
-4/-3	-0.37	-0.41	-0.37	-0.50	-0.71
-3/-2	-0.27	-0.31	-0.27	-0.39	-0.54
-2/-1	-0.16	-0.21	-0.17	-0.29	-0.39
-1/0	-0.05	-0.11	-0.07	-0.18	-0.26
0/+1	0.07	-0.01	0.024	-0.05	-0.12
+1/+2	0.18	0.09	0.13	0.06	0.01
+2/+3	0.29	0.19	0.22	0.17	0.13
+3/+4	0.40	0.28	0.32	0.28	0.23
+4/+5	0.49	0.37	0.42	0.41	0.34
+5/+6	0.58	0.47	0.53	0.53	0.44
+6/+7	0.70	0.56	0.61	0.61	0.54
+7/+8	---	0.65	---	0.69	0.63
+8/+9	---	0.74	---	---	0.73
+9/+10	---	0.82	---	---	---
+10/+11	---	0.90	---	---	---

Interestingly, the full width at half maximum (FWHM) of each peak is found to be of ca. 50-55 mV particularly signifying the QDL process for these larger MPCs, which differs from the earlier reports of smaller sized Au MPCs (110-115 mV) or ideal (90.6 mV) one electron transfer process for conventional redox species.[10,21] This anomalous FWHM might be attributed to several complex interactions of these charged MPCs in the vicinity of electrode surface. For example, these MPCs can be viewed as assembly of mixed valent redox centers at the electrode solution interfaces during electrochemical process.[22] This resembles the case of conducting polymers, where the occupied site interaction energies (in the order of k_BT) substantially cause change in redox capacity with the magnitude and types of interactions. This type of interaction is also widely known for electroactive films or adsorption electrochemistry, where depending on the degree of the adsorbate-adsorbate interaction substantial broadening or sharpening of the voltammetric peaks are observed.[22] Another possibility is the interdigitation of the hydrocarbon chains effectively leading to closer distance between MPCs as if there is an attractive interaction caused by the soft organic matrix. Furthermore, there are also possibilities for the reorganization of charges among clusters by electron self-exchange or disproportionation. In contrast, the smaller sized MPCs show broadened FWHM values, which could be attributed to their negligibly weak interactions originating from their semiconducting nature.[10]

Figure 3.5 (a-e) represents the "Z plot" for Au MPCs corresponding to the DPV response shown in Figure 3.4a (i-ii), Figure 3.4b and Figure 3.4c(i-ii) respectively, where linear ($R^2 > 0.99$) behaviour can be seen as expected for the ideal QDL behaviour.[10-12] The C_{CLU} calculated from the slope of the "Z plots" as summarized in Table 3.3, are in good agreement with the theoretically estimated capacitance value of 1.4 aF using a concentric sphere capacitance model, as

$$C_{CLU} = 4\ \pi\varepsilon_o\varepsilon_m\ (^r/_d)\ (r + d) \qquad (3.9)$$

where, ε_o is the permittivity of free space, ε_m is the dielectric constant of the medium (taken as 3)[14], r is the radius of the MPC core (1.86 nm) and d is the length of the capping agent (1.52 nm).[10d] According to this model, the charging energy,

$$E_c = e^2/2C_{CLU} = (e^2d) / [8\pi\varepsilon_o\varepsilon_m\ r(r + d) \qquad (3.10)$$

for the same MPC is found to be of 52 meV confirming the criteria for single electron charging ($E_c >> k_BT_{273}$).

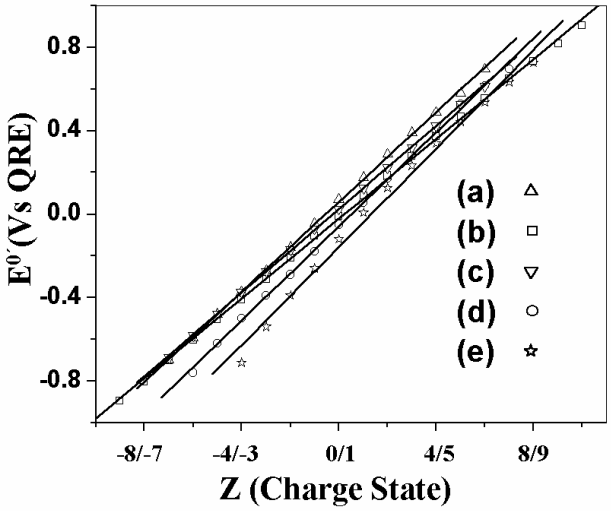

Figure 3.5 Superimposed "Z plot; i.e., $E^{0'}$ vs. redox couple charge state (Z/Z ± 1)" for Au MPCs (graphs a-e) of the DPV response corresponding to graphs Figure 3.4a (i-ii), Figure 3.4b and Figure 3.4c (i-ii) respectively, where a linear (R^2 > 0.99) behaviour can be seen as expected for the ideal QDL behaviour.

Table 3.3 Comparison of the Capacitance calculated from the slopes of the Z plots (Figure 3.5) and the Concentric Sphere Capacitance Model

Z plots from Figure 3.5	R^2	Experimental Capacitance (aF)	Capacitance from Concentric Sphere Capacitance Model (aF)
(a)	0.999	1.57	
(b)	0.999	1.76	
(c)	0.999	1.68	1.4
(d)	0.999	1.50	
(e)	0.996	1.43	

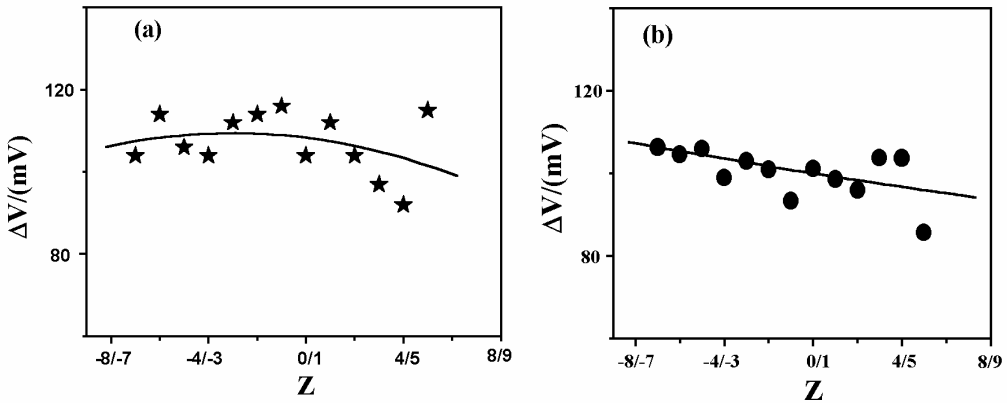

Figure 3.6 (a-b) Plot of ΔV vs. charge state (Z) obtained from the DPV responses shown in Figure 3.4a (i) and Figure 3.4b respectively, revealing more regular voltage spacing at negative potential.

However, plot of ΔV vs. *Z* (Figure 3.6) reveals relatively more regular voltage spacing at negative potential, although there is a variation in the intermediate potential, perhaps due to the relative polydispersity of samples. The ΔV values in Figure 3.6 (a) and (b) correspond to the DPV response shown in Figure 3.4a (i) and Figure 3.4b respectively.

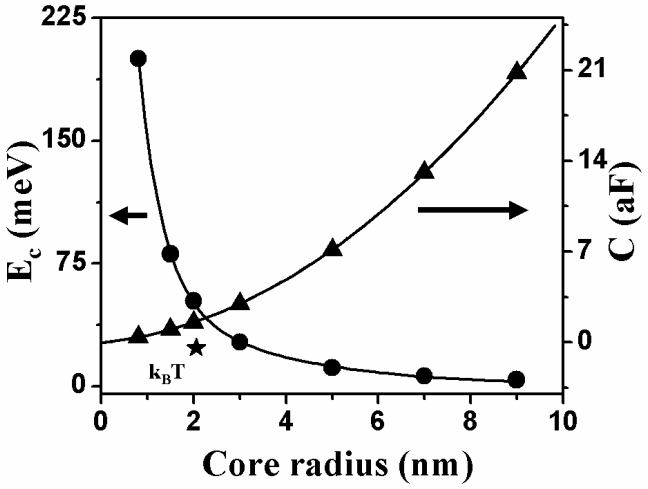

Figure 3.7 Theoretical prediction of the variation of capacitance (▲) and charging energy (•) with size according to the concentric sphere capacitance model for DDT protected Au MPCs [Energy position of k_BT_{273} is marked as (★)].

Interestingly, Figure 3.7 shows the variation of capacitance (▲) and charging energy (•) with the core radius using same capping molecule (DDT) and could be fitted to non-linear and exponential curve fitting respectively. Accordingly, when the size is small, fewer charging events are possible at smaller potential window with higher ΔV value due to the larger E_c. In contrast, smaller E_c of the large sized MPC causes highly populated charging events with smaller ΔV value at a shallow potential window. This simple plot predicts that 5-7 nm is the limit for observing QDL behaviour, although lowering the temperature can further change the limit by 1-2 nm.

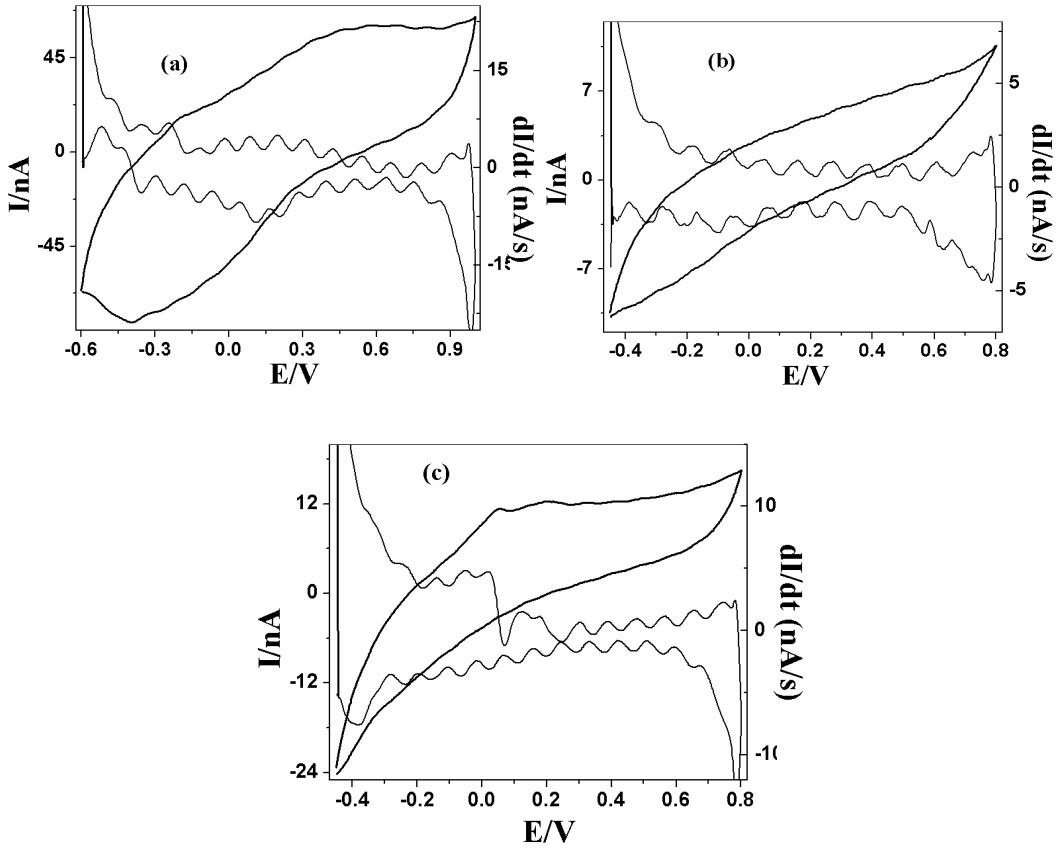

Figure 3.8 Cyclic voltammetric response of Au MPCs at (a) 50 and (b) 100 mV/s superimposed with its derivative response showing a series of QDL charging steps; (c) shows the same superimposed response at 100 mV/s, where electrode fouling due to specific adsorption is evident.

In comparison to DPV, CV also resolves this high population of charge steps, where the derivative response is particularly comparable with DPV results. Figure 3.8 shows the cyclic voltammetric response of Au MPCs at (a) 50 and (b) 100 mV/s scan rate along with its derivative responses. Since these larger sized particles essentially have higher capacitance values as indicated also by the DPV peak to peak spacing (*ca.* 100 mV), this could in principle prevent better resolution by CV. Interestingly, Figure 3.8 (c) shows the CV response at 100 mV/s scan rate, where electrode fouling is observed due to the adsorption of these MPCs. This observation is taken into consideration in later sections during the discussion of the electrochemical features of these adsorbed MPCs.

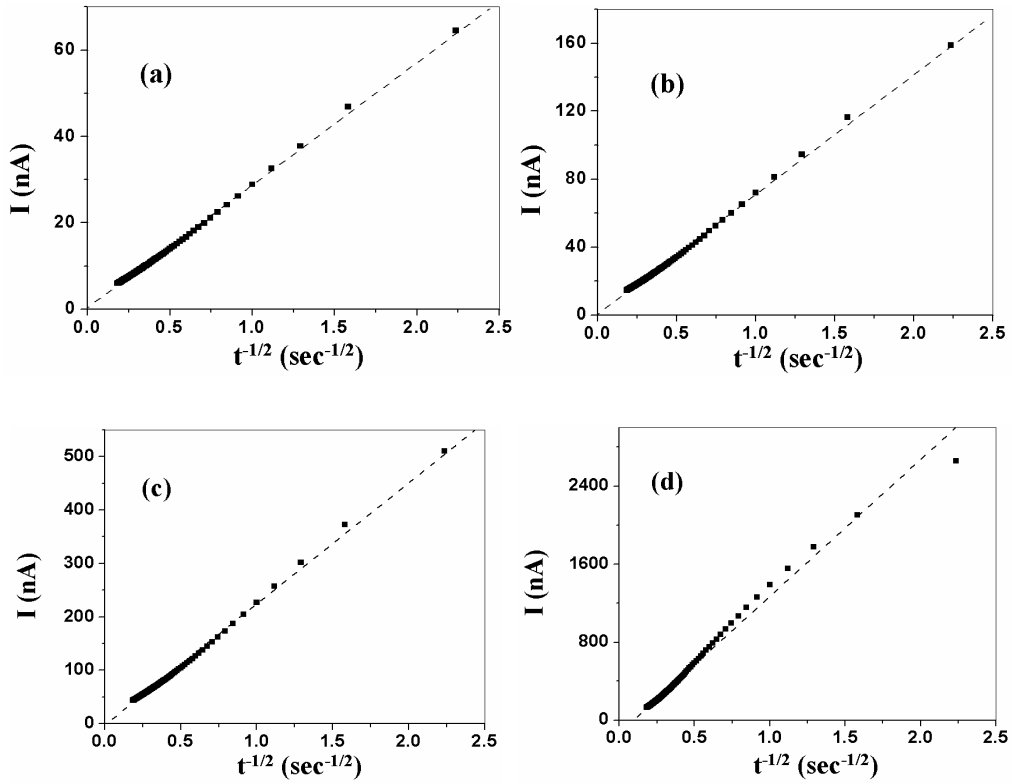

Figure 3.9 (a-d) Linearly fitted I vs. $t^{-½}$ plots, obtained under four applied anodic potentials corresponding to (+1), (+2), (+4) and (+6) charge states.

The diffusion coefficient (D_C) of Au MPCs has also been calculated by chronoamperometry technique using Cottrell equation (3.11).[21] Assuming that linear

semi-infinite diffusion is applicable for freely diffusing MPCs in solution, the current (I) - time (t) response can be written as,

$$I_d(t) = n\,F\,A\,C_n\,D_C^{\frac{1}{2}}\,\pi^{-\frac{1}{2}}\,t^{-\frac{1}{2}} \qquad (3.11)$$

where, n is the change in core charge state, C_n is the MPC concentration in the solution (8.7×10^{-7} mol.cm^{-3}), A is the area of the electrode (0.5 mm diameter = 1.96×10^{-3} cm^2), F is the Faraday constant, t (0.2 s ≤ t ≤ 30 s) is the time duration of the measurement of current after applying the respective constant potential corresponding to individual charge step in DPV response as shown in Figure 3.4 and D_C is the diffusion coefficient of the charged clusters in the electrolyte solution under applied potential.

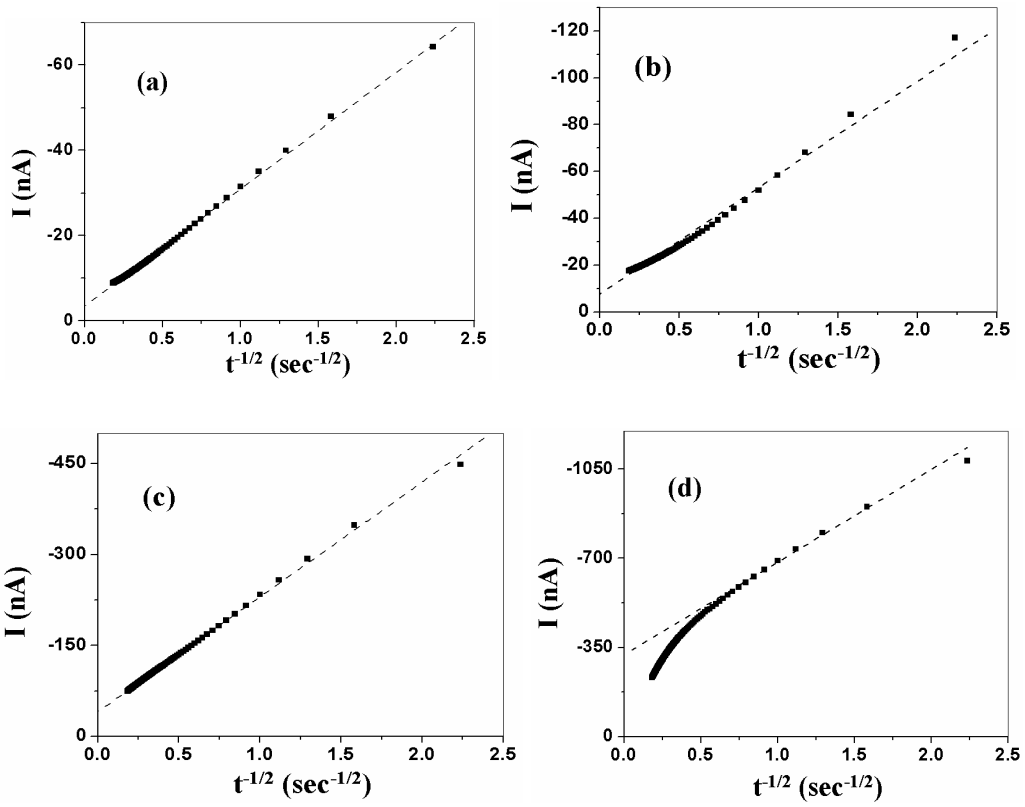

Figure 3.10 (a-d) Linearly fitted I vs. $t^{-\frac{1}{2}}$ plots, obtained under four different applied cathodic potentials corresponding to (-1), (-2), (-4) and (-6) charge states.

The D_C of cluster is calculated by analyzing the slope of the linearly fitted I vs. $t^{-\frac{1}{2}}$ plots. These I vs. $t^{-\frac{1}{2}}$ plots were obtained under various applied potentials corresponding

to the valleys (between two peaks) of the DPV response shown in graph (i) of Figure 3.4, where MPCs are assumed to be roughly in monovalent charge states. For example, Figure 3.9 (a-d) and Figure 3.10 (a-d) show the individual linearly fitted I - $t^{-½}$ behaviour under different anodic and cathodic potentials corresponding to (+1), (+2), (+4), (+6), (-1), (-2), (-4) and (-6) charge states respectively. The terms anodic and cathodic are used to indicate that the applied bias is either anodic or cathodic with respect to the E_{PZC}. Table 3.4 summarizes various parameters, such as applied potential, corresponding charge states, slope of the plots and the calculated diffusion coefficient using equation (3.11).

The experimentally observed D_C values are compared with the theoretically calculated diffusion coefficient (D_{SE}) using modified Stokes-Einstein equation (3.12),

$$D_{SE} = k_B T / 2\pi\eta d_H \qquad (3.12)$$

where, D_{SE} is the diffusion coefficient of neutral MPCs, k_B is the Boltzman constant, T is absolute temperature (here 273 K), η is solvent viscosity (viscosity of CH_2Cl_2 at 273 K is 0.533 cp) and d_H is the hydrodynamic diameter of the MPC. The hydrodynamic diameter (d_H) has been assumed to be twice the chain length added to the diameter of the Au MPC.[10e,2g,h] The calculated value of D_{SE} by above equation is 16.6 x 10^{-7} $cm^2.s^{-1}$, which is comparable with the experimentally observed values.

Interestingly, the calculated D_C values for these clusters increase with applied potential, despite being smaller to those calculated (D_{SE}) using modified Stokes-Einstein equation. This potential dependent variation of D_C can be attributed several to factors, like the charged nature of MPCs, contribution due to migration and interactions with other charged or uncharged MPCs, electrode surface, presence of supporting electrolyte anions or cations and solvent molecules.[23] Moreover, the hydrophobic nature of the capping monolayer also provides strong interaction between adjacent clusters, which may drastically affect the motion of MPCs in solution under the applied potential. These types of interactions could be explained on the basis of DLVO (Derjaguin-Landau-Verwey-Overbeek) theory, where both hydrophobic (attractive) and electrostatic (repulsive) interactions are considered.[24] More specifically, in solution there is always a competition between these two forces, where a change in any of them may affect the

motion of these MPCs. The above reasons justify the deviation of experimental diffusion coefficient values from the theoretical ones, primarily arising from the larger dimension of these MPCs.

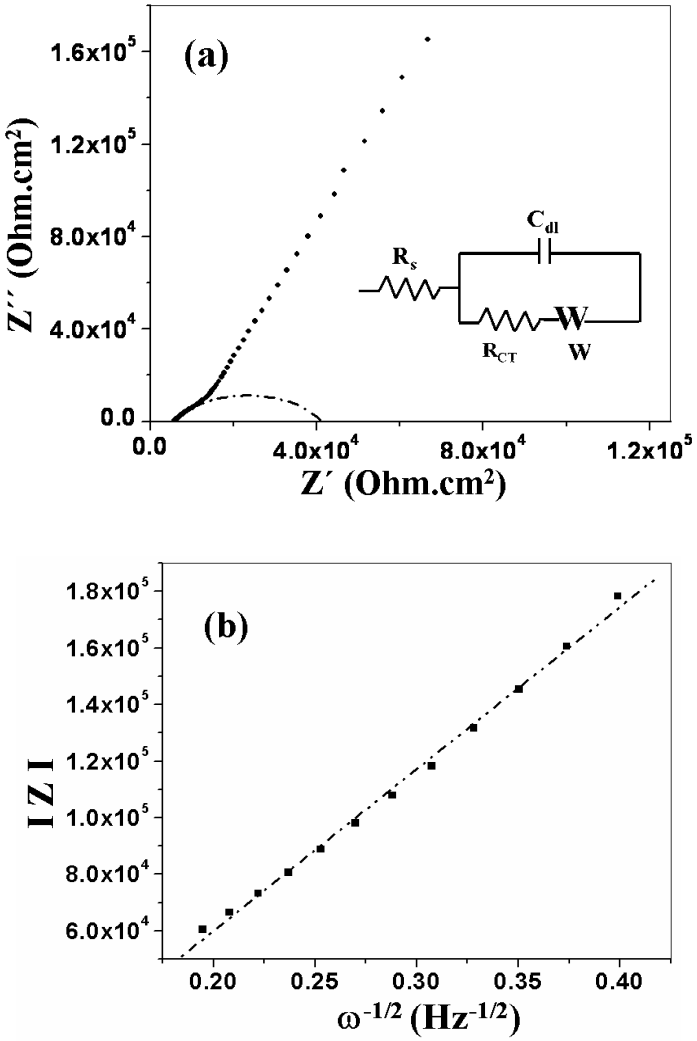

Figure 3.11 (a) Complex plane impedance plot of Au MPCs in CH_2Cl_2 on a Pt disc (0.5 mm diameter), where the suppressed semicircle at the higher frequency domain is fitted and analyzed with a Randles equivalent circuit. The low frequency region is particularly governed by the mass transfer as a straight line at more than 45° to the real axis is observed. The Randles equivalent circuit is shown as inset, where R_S is solution resistance, R_{CT} is charge transfer resistance, C_{dl} is double layer capacitance and W is Warburg impedance. (b) Diffusion coefficient is estimated from the slope (σ) of the linearly fitted ($R^2 > 0.99$) modulus of the real and imaginary part of impedance data (4.19 Hz to 1 Hz) with $\omega^{-1/2}$.

Impedance technique is particularly useful to understand the electron transfer dynamics and the mass transport features of the electroactive materials in solution.[21] Figure 3.11 (a) shows complex plane impedance plots of Au MPCs in CH_2Cl_2 on a Pt disc (0.5 mm diameter), where a suppressed semicircle at the higher frequency domain and a straight line with more than 45° inclination angle to the real axis in the low frequency region are observed. Subsequently, this plot has been divided into high and low frequency regions for the convenience of interpretation before analysis using the Randles equivalent circuit, considering that the charging of an MPC to an individual charge step from its adjacent number is a one-step, one electron process.[21]

Table 3.4 Various parameters and calculated diffusion coefficient values from chronoamperometry (Figure 3.9 and 3.10)

Chronoam-perometry graphs	Charge State (DPV)	Applied Potential (V)	Slope (x 10^{-9} A.$s^{1/2}$)	Num ber of elect-ron	D_C from Chronoam-perometry (x 10^{-7} $cm^2.s^{-1}$)	D_C from Impedan -ce (x 10^{-7} $cm^2.s^{-1}$)	D_{SE} (x 10^{-7} $cm^2.s^{-1}$)
Fig. 1.9 (a)	+1	0.13	28	1	0.93	**1.24**	**16.6**
Fig. 1.9 (b)	+2	0.25	70	2	1.43		
Fig. 1.9 (c)	+4	0.45	227	4	3.71		
Fig. 1.9 (d)	+6	0.65	1402	6	63.00		
Fig. 1.10 (a)	-1	-0.11	28	1	0.87		
Fig. 1.10 (b)	-2	-0.22	45	2	0.60		
Fig. 1.10 (c)	-4	-0.43	189	4	2.60		
Fig. 1.10 (d)	-6	-0.65	582	6	10.86		

The high frequency data could be fitted to a semicircle, which give rise to charge transfer resistance (R_{CT}) and solution resistance (R_S) as 3.51 x 10^4 and 5.87 x 10^4 ohm.cm^2 respectively. The double layer capacitance (C_{dl}) 2.4 μF.cm^{-2}, is calculated using the frequency maxima (ω_{max} = 11.89 Hz) of this semicircle, as [$C_{dl} = 1 / R_{CT}\ \omega_{max}$] suggesting the interfacial capacitive contribution of ensembles of these MPCs at the electrode-solution interface. This seems to be reasonable as the value is one order of magnitude less as compared to the value for a bare electrode. The standard rate constant of one electron QDL charging process has been calculated using the following relationship:

$$k = RT / n^2 F^2 R_{CT} C_n \qquad (3.13)$$

assuming n = 1, $C_n = C^*(O) = C^*(R) = (8.7 \times 10^{-7}$ mol.cm$^{-3})$, $\alpha = 0.5$, T = 273 K. The k is found to be of 7.97 x 10^{-6} cm.s^{-1}, which suggests that the QDL charging process is kinetically very sluggish as compared to a normal redox reaction, such as $Fe(CN)_6^{3-}$/ $Fe(CN)_6^{4-}$ couple on a gold electrode ($k \approx 2.3 \pm 0.7 \times 10^{-2}$ cm.s^{-1}).[25] Low frequency region is particularly informative about the mass transport features, which we consider as solely due to diffusion. We have linearly fitted the modulus of the real and imaginary part of impedance data (4.19 Hz to 1 Hz) with $\omega^{-1/2}$ to calculate (σ) from the slope of the graph (5.73 x 10^5 ohm.cm^2.s$^{-1/2}$) as shown in Figure 3.11 (b). In particular the low frequency component (Warburg impedance),

$$W = \sigma\omega^{-1/2} - j\sigma\omega^{-1/2} \qquad (3.14)$$

where σ is a constant. The diffusion coefficient (D_C) can be calculated from the following relationship as,

$$\sigma = \sqrt{2}\, RT / A\, n^2 F^2 D_C^{1/2} C_n \qquad (3.15)$$

assuming n = 1, A = area of the electrode (1.96 x 10^{-3} cm^2), $D_O = D_R = D_C$, $C_n = C^*(O) = C^*(R) = (8.7 \times 10^{-7}$ mol.cm$^{-3})$ and T = 273 K. The D_C is found to be of 1.24 x 10^{-7} cm^2.s^{-1}, which is comparable with the value obtained from chronoamperometry.

3.4.2.2 Adsorption features

Ordered arrays of MPCs are particularly useful for several technological and fundamental applications.[26] Recent reports show that smaller MPCs can be organized on an electrode surface either by place exchanging with bifunctional ligand molecules present on the Au MPCs surface or by direct covalent linkage through a bridge of metal ion to a carboxylate terminal SAMs on gold electrode.[27] These preformed MPC layers have been used in recent times for several electrochemical and solid state electrical measurements, which show single electron transfer phenomena.[2c,26,27] In addition, these MPCs show a strong tendency to physisorb on the electrode surface during voltammetry, presumably due to the interaction among charged MPCs and supporting electrolytes ions.[11a] These adsorption phenomena could be revealed by both CV and DPV results and it is possible to extract the electron transfer (ET) kinetics.[27]

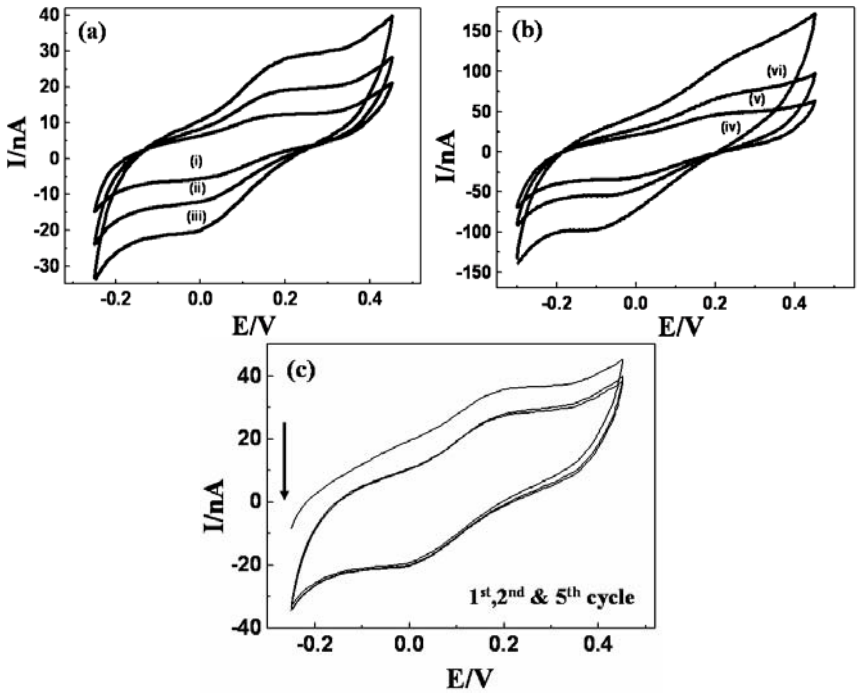

Figure 3.12 Scan rate dependent cyclic voltammetric behaviour of adsorbed Au MPCs on Pt microelectrode in CH_2Cl_2 at (a) (i) 10, (ii) 25 and (iii) 50 mV/s and (b) at (iv) 100 and (v) 200 and (vi) 500 mV/s scan rates (all are in second cycles). (c) Superimposed CV response of these particles for first five cycles at 50 mV/s scan rate.

We have also observed the signature for the electrode film formation of Au MPCs upon prolonged cycling during CV and DPV experiments. For example, Figure 3.12 (a and b) represents the scan rate dependent cyclic voltammograms of these MPCs in CH_2Cl_2 at (i-vi) 10, 25, 50, 100, 200 and 500 mV/s scan rates (all at second cycle), where 0/1 and -1/0 charging peaks become prominent. The appearance of peaks is more significant at lower scan rates and the magnitude of ΔE_p for the case of 10 mV/s is in good agreement with the DPV peak spacing for 0/1 to -1/0 charge state. Figure 3.12 (c) depicts the effect of cycling at 50 mV/s, where the peak current and spacing are almost invariant after second cycle. Accordingly, Figure 3.13 shows such superimposed response of the MPCs during various courses of the DPV experiments. For example, (i) shows the initial response as depicted in Figure 3.4, while (ii-iii) represent after several cycles along with (iv) indicating a response after sustained cycling (> 25 cycles) as revealed by the CV.

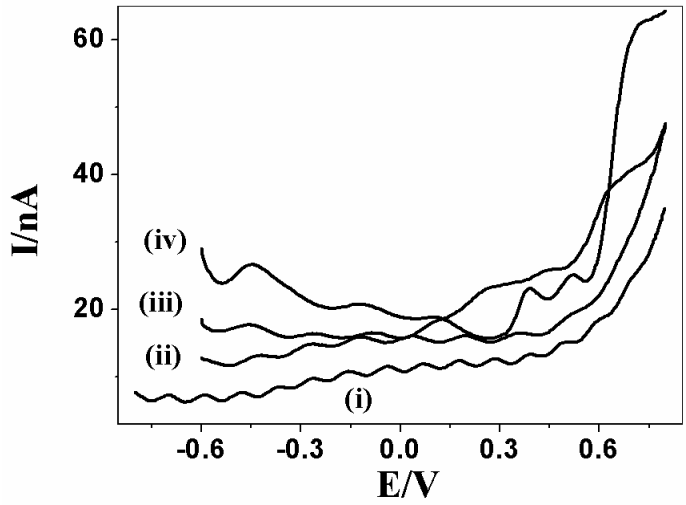

Figure 3.13 The superimposed DPV response of the MPCs in various course of the experiment; (i) initial responses as depicted in Figure 3.4, (ii-iii) after several scanning and (iv) the same features are depicted by the CV analysis in Figure 3.12, demonstrating surface immobilization after prolong scanning, probably due to interaction among charged MPCs and with counter ions of the supporting electrolytes.

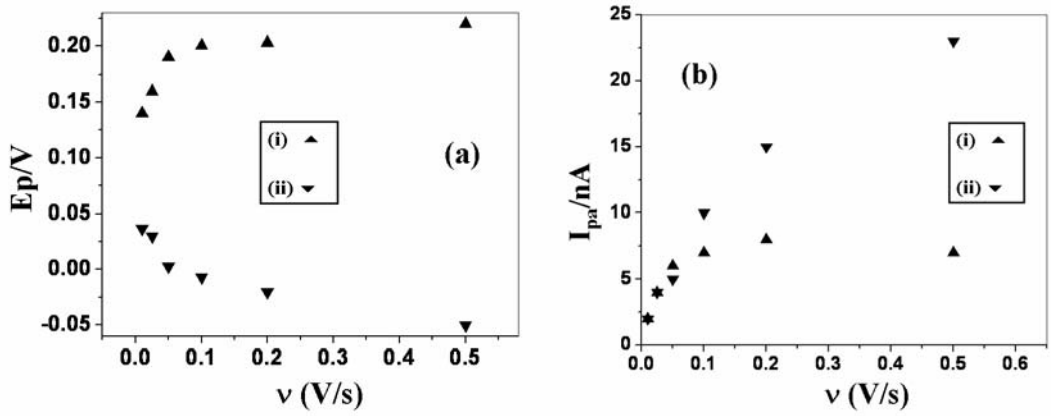

Figure 3.14 The superimposed plots of (a) peak potential and (b) peak currents with scan rates from the cyclic voltammograms in Figure 3.12, where (i) and (ii) represents anodic and cathodic peaks respectively. The variation of peak potential and current with scan rates is indicative of irreversible one electron transfer process of immobilized electroactive species on electrode surface.

The superimposed variation of peak potential and current with scan rate reveals that adsorbed redox species undergoes electron transfer in the form of a totally irreversible one electron process.[21] For example, the variation of peak potential with scan rate is more at higher scan rates compared to that at its lower ones, indicating that the process becomes charge-transfer limited on the time scale corresponding to higher scan rates (Figure 3.14a). For instance, this diagnostic feature can also be seen from the variation of peak currents with scan rate, where a prominent nonlinearity is observed particularly at higher scan rates (Figure 3.14b). However, the deviation at low scan rates might possibly originate due to the convolution of currents of diffusing species with those strictly due to the adsorption on the electrode surface. Furthermore, several additional factors, such as insulating nature due to monolayer capping, inhomogeneity of the film, finite mass and charge transport through the film, structural and resistive changes in the film during oxidation/reduction process and finally changes in the dielectric constant of the film and solution may also cause deviations from the ideal behaviour.

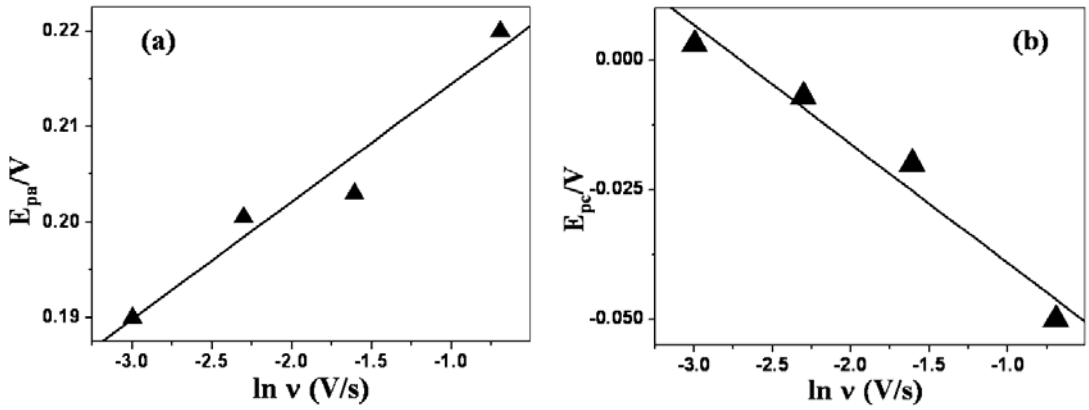

Figure 3.15 Variation of ln *v* vs. E_p for both (a) anodic and (b) cathodic peaks respectively from the CV shown in Figure 3.12. The value of α is estimated to be of 0.35 as obtained from the slope of these graphs according to equation (3.18).

In an attempt to determine the energy transfer coefficient α and the rate constant k_{ads}, we used Laviron's approach, which is valid for totally irreversible reactions for an electroactive species immobilized on the electrode surface.[28] Realistically, this can be approximated, when the difference in cathodic and anodic peak potentials is (ΔE_p) > 200/n mV. We have used the ΔE_p values of -1/0 to 0/1 charging peaks at 50, 100, 200 and 500 mV/s scan rate in the CVs illustrated in Figure 3.12 for the ET analysis, where (ΔE_p) > 200/n mV. The anodic (E_{pa}) and the cathodic (E_{pc}) peak potentials are expressed by this approach as follows:

$$E_{pc} = E^{0'} - (RT/\alpha nF)\ \ln(\alpha nF/kRT) - (RT/\alpha nF)\ \ln v \qquad (3.16)$$

$$E_{pa} = E^{0'} + [RT/(1-\alpha)nF]\ \ln[(1-\alpha)nF/kRT] - [RT/(1-\alpha)nF]\ \ln v \qquad (3.17)$$

where $E^{0'}$ is the formal potential and R, T, F and n have their normal significance. Thus plots of E_{pc} and E_{pa} vs. ln v should have two straight lines with slopes s_c and s_a as [-(RT/αnF)] and [RT/(1-α)nF], respectively.

Table 3.5 Peak Potentials of anodic (E_{pa}), cathodic (E_{pc}) processes, peak separation (ΔE_p) and other relevant parameters, such as α and k_{ads} calculated from the CV data (Figure 3.12)

Scan Rate ($V.s^{-1}$)	0.010	0.025	0.050	0.100	0.200	0.500	α	Rate Constant (k_{ads}) (s^{-1})	Average ET (k_{ads}) (s^{-1})
E_{pa} (V)	0.140	0.160	0.190	0.200	0.203	0.220		2.8	
E_{pc} (V)	0.037	0.030	0.003	-0.007	-0.020	-0.050			
							0.35	1.5	2.2
ΔE_p (V)	0.103	0.130	0.187	0.207	0.223	0.270			

Thus α and k_{ads} can be determined from the following relationships,

$$\alpha = s_a/(s_a - s_c) \quad (3.18)$$

$$k_{ads} = (\alpha n F v_c/RT) \text{ or } [(1-\alpha)nFv_a/RT] \quad (3.19)$$

where, v_c and v_a are the cathodic and anodic sweep rates at $E_p = E^{0'}$ respectively. Accordingly, Figure 3.15 (a and b) shows the linear variation of ln v vs. E_p for both anodic and cathodic directions respectively. The estimated value of α is 0.35, which shows that the energy barrier for QDL charging is not symmetric and the rate constant k_{ads} is approximately 2.2 s^{-1} (values from v_a and v_c are 2.8 and 1.5 s^{-1} respectively). Table 3.5 summarizes the anodic (E_{pa}), cathodic (E_{pc}) peak potentials, anodic to cathodic peak separations (ΔE_p) from the CV data as shown in Figure 3.12 at various scan rates and the calculated relevant parameters, such as α and k_{ads} using Laviron's approach. The calculated rate constant of these larger sized particles are found to be smaller as compared to recently reported values for similar covalently attached smaller sized Au MPCs.

3.5. Conclusions

In this chapter, we analyze the variation of capacitance and charging energy with cluster size and length of organic molecules using a simple model to understand the electronic behaviour of Coulomb blockade nanostructures. Further, we show for the first time that the relatively larger sized Au MPCs can also act as multivalent redox species (QDL behaviour) despite their higher capacitance values (1.4 aF). Various electrochemical techniques, such as CV, DPV, chronoamperometry and impedance measurements have been utilized to unravel their electron transfer features. Independent STM studies also have been used to support their accessibility for single electron transfer, where Coulomb blockade effects are evident at room temperature. In particular, the current-voltage (I-V) characteristics of these Au particles on highly oriented pyrolytic graphite (HOPG) surface are nonlinear with a large central gap (around 0.2 eV) and are in good agreement with the orthodox theory for DBTJ systems. The capacitance calculated from both these two experimental techniques are in good agreement with the results of the theoretical calculations. Further, the electrochemical techniques (chronoamperometry and impedance measurements) have been used to calculate their diffusion coefficients (x 10^{-7} $cm^2.s^{-1}$), which show evidence for the effect of charge on these values. The electron transfer rate constant (7.97 x 10^{-6} $cm.s^{-1}$) also has been estimated from the impedance measurement as well as from voltammetry using Laviron's approach for adsorbed MPCs (*ca.* 2 s^{-1}).

3.6 References

1. (a) Rao, C. N. R.; Kulkarni, G. U.; Thomas, P. J.; Edwards, P. P. *Chem. Soc. Rev.* **2000**, *29*, 27. (d) Schmid, G.; Baumle, M.; Greekens, M.; Heim, I.; Osemann, C.; Sawitwoski, T. *Chem. Soc. Rev.* **1999**, *28*, 179. (c) Daniel, M.-C.; Astruc, D. *Chem. Rev.* **2004**, *104*, 293.
2. (a) Brust, M.; Walker, M.; Bethell, D.; Schiffrin, D. J.; Whyman, R. *J. Chem. Soc. Chem. Commun.* **1994**, 801. (b) Templeton, A. C.; Wuelfing, W. P.; Murray, R. W. *Acc. Chem. Res.* **2000**, *33*, 27. (c) Aslam, M.; Mulla, I. S.; Vijayamohanan, K. *Langmuir* **2001**, *17*, 7487. (d) Wilcoxon, J. P.; Martin, J. E.; Provencio, P. *J. Chem. Phys.* **2001**,*115*, 998.
3. (a) Kuzmin, L. S.; Likharev, K. K. *Jpn. J. Appl. Phys.* **1987**, *26*, 1387. (b) Averin, D. V.; Likharev, K. K. In *Single Electron Tunneling*; Grabert, H.; Devoret, M. H.; Eds.; Plenum: New York, 1992, p. 311. (c) Remacle, F.; Levine, R. *J. Am. Chem. Soc.* **2000**, *122,* 4084. (d) Nakanishi, T.; Ohtani, B.; Uosaki, K. *J. Phys. Chem. B* **1998**, *102*, 1571. (e) McConnell, W. P.; Novak, J. P.; Brousseau III, L. C.; Fuierer, R. R.; Tenent, R. C.; Feldheim, D. L. *J. Phy. Chem. B* **2000**, *104*, 8925.
4. (a) Klein, D. L.; Roth, R.; Lim, A. K. L.; Alivisatos, A. P.; McEuen, P. L. *Nature* **1997**, *389*, 699. (b) Andres, R. P.; Bein, T.; Dorogi, M.; Feng, S.; Henderson, J. I.; Kubiak, C. P.; Mahoney, W.; Osifchin, R. G.; Reifenberger, R. *Science* **1996**, *272*, 1323. (c) Simon, U. *Adv. Mater.* **1998**, *10*, 1487. (d) Feldheim, D. L.; Keatig, C. D. *Chem. Soc. Rev.* **1998**, *27*, 1. (e) Andres, R. P.; Bielefeld, J. D.; Henderson, J. I.; Janes, D. B.; Kolagunta, V. R.; Kubiak, C. P.; Mahoney, W. J.; Osifchin, R. G. *Science* **1996**, *273*, 1690.
5. (a) Ancona, M. G.; Kruppa, W.; Rendell, R. W.; Snow, A. W.; Park, D.; Boos, J. B. *Phy. Rev. B* **2001**, *64*, 033408. (b) Wang, B.; Wang, H.; Li, H.; Zheng, C.; Hou, J. G. *Phy. Rev. B* **2000**, *63*, 035403.
6. (a) Dorogi, M.; Gomez, J.; Osifchin, R.; Andres, R. P.; Reifenberger, R. *Phy. Rev. B* **1995**, *52*, 9071. (b) Amman, M.; Wilkins, R.; Ben-Jacob, E.; Maker, P. D.; Jaklevic, R. C. *Phy. Rev. B* **1991**, *43*, 1146. (c) Hanna, A. E.; Tinkham, M. *Phys. Rev. B.* **1991**, *44***,** 5919.
7. Thomas, P. J.; Kulkarni, G. U.; Rao, C. N. R. *Chem. Phys. Lett.* **2000**, *321*, 163.
8. Chiquito, A. J.; Pusep, Y. A.; Mergulhao, S.; Galzerani, J. C.; Moshegov, N. T. *Phy.*

Rev. B **2000**, *61*, 5499.

9. (a) Collier, C. P.; Saykally, R. J.; Shiang, J. J.; Henrichs, S. E.; Heath, J. R. *Science*, **1997**, *277*, 1978. (b) Kim, S.-H.; Medeiros-Ribeiro, G.; Ohlberg, D. A. A.; Williams, R. S.; Heath, J. R. *J. Phys. Chem. B* **1999**, *103*, 10341. (c) Aslam, M.; Mulla, I. S. Vijayamohanan, K. *App. Phy. Lett.* **2001**, *79*, 689.
10. (a) Ingram, R. S.; Hostetler, M. J.; Murray, R. W.; Schaaff, T. G.; Khoury, J. T.; Whetten, R. L.; Bigioni, R. L.; Guthrie, D. K.; First, P. N. *J. Am. Chem. Soc.* **1997,** *119*, 9279. (b) Pietron, J. J.; Hicks, J. F.; Murray, R. W. *J. Am. Chem. Soc.* **1999**, *121*, 5565. (c) Chen, S.; Ingram, R. S.; Hostetler, M. J.; Pietron, J. J.; Murray, R. W.; Schaaff, T. G.; Khoury, J. T.; Alvarez, M. M.; Whetten, R. L. *Science* **1998**, *280*, 2098. (d) Chen, S.; Murray, R. W.; Feldberg, S. W. *J. Phys. Chem. B* **1998**, *102*, 9898. (e) Miles, D. T.; Murray, R. W. *Anal. Chem.* **2003**, *75*, 1251.
11. (a) Quinn, B. M.; Lijeroth, P.; Ruiz, V.; Kaaksonen, T.; Kontturi, K. *J. Am. Chem. Soc.* **2003**, *125*, 6644. (b) Li, D.; Li, J. *Chem. Phys. Lett.* **2003**, *372*, 668. (c) Chen, S.; Sommers, J. M. *J. Phys. Chem. B* **2001**, *105*, 8816. (d) Cheng, W.; Dong, S.; Wang, E. *Electrochem. Commun.* **2002**, *4*, 412. (e) Yang, Y.; Chen, S. *Nano Lett.* **2003**, *3*, 75.
12. (a) Haram, S. K.; Quinn, B. M.; Bard, A. J. *J. Am. Chem. Soc.* **2001**, *123*, 8860. (b) Ding, Z.; Quinn, B. M.; Haram, S. K.; Pell, L. E.; Korgel, B. A.; Bard, A. J. *Science* **2002**, *296*, 1293. (c) Chen, S.; Truax, L. A.; Sommers, J. M. *Chem. Mater.* **2000**, *12*, 3864.
13. (a) Landauer, R. *I. B. M. J. Res. Dev.* **1957**, *1*, 223. (b) Landauer, R. *Phys. Lett. A* **1981**, *8*, 91.
14. (a) Holmlin, R. E.; Haag, R.; Chabinyc, M. L.; Ismagilov, R. F.; Cohen, A. E.; Terfort, A.; Rampi, M. A.; Whitesides, G. M. *J. Am. Chem. Soc.* **2001**, *123*, 5075. (b) Rampi, M. A.; Schueller, O. J. A.; Whitesides, G. M. *Appl. Phys. Lett.* **1998**, *72*, 1781.
15. Issendorff, B. v.; Cheshnovsky, O. *Annu. Rev. Phys. Chem.* **2005**, *56*, 549.
16. (a) Kaiser, W. J.; Jaklevic, R. C. *Surf. Sci.* **1987**, *181*, 55. (b) Binning, G.; Smith, D. P. E. *Rev. Sci. Instrum.* **1986**, *57*, 1688. (c) Dharmadhikari, C. V. In *Encyclopedia of Analytical Chemistry: Instrumentation and Applications;* Meyers, R. A.; Eds.; John Wiley: UK, 2000.

17. Datar, S.; Kumar, M.; Sastry, M.; Dharmadhikari, C. V. *Colloids and Surfaces A* **2003**, *232/1*, 11.
18. SPIP stands for Scanning Probe Image Processor, which is software for Scanning Probe Microscopy and other Microscopy Techniques developed by Image Metrology, Denmark.
19. The experimental I-V has been fitted using the program available in website *http://qt.tn.tudelft.nl/research/set/asymIV/SETIV.html.*
20. Stratton, R. *J. Phys. Chem. Solids* **1962**, *23*, 1177.
21. Bard, A. J.; Faulkner, L. R. *Electrochemical Methods, Fundamentals and Applications; 2nd ed,* John Wiley & Sons: New York, 2001.
22. (a) Hicks, J. F.; Zamborini, F. P.; Osisek, A. J.; Murray, R. W. *J. Am. Chem. Soc.* **2001**, *123*, 7048. (b) Chidsey, C. E. D.; Murray, R. W. *J. Phys. Chem.* **1986**, *90*, 1479. (c) Laviron, E. *J. Electroanal. Chem.* **1981**, *122*, 37.
23. Guidelli, R. *Electrified Interfaces in Physics, Chemistry and Biology;* Kluwer Academic Publishers, 1992.
24. (a) Derjaguin, B. V.; Landau, L. *Acta Physicochimica. URSS* **1941**, *14*, 633. (b) Verwey, E. J. W.; Overbeek, J. T. G. *Theory of the Stability of Lyophobic Colloids;* Elsevier: Amsterdam, 1948. (c) Verwey, E. J. W.; Overbeek, J. T. G. *J. Chem. Soc., Faraday Trans.* **1946**, *I, 42B*, 117. (d) Overbeek, J. T. G. *Pure Appl. Chem.* **1980**, *52*, 1151.
25. Tokuda, K; Gueshi, T.; Matsuda, H. *J. Electroanal. Chem.* **1979**, *102*, 41.
26. (a) Freeman, R. G.; Grabar, K. C.; Allison, K. J.; Bright, R. M.; Davis, J. A.; Guthrie, A. P.; Hommer, M. B.; Jackson, M. A.; Smith, P. C.; Walter, D. G.; Natan, M. J. *Science* **1995**, 267, 1629. (b) Baum, T.; Bethell, D.; Brust, M. Schiffrin, D. J. *Langmuir* **1999**, *15*, 866.
27. (a) Chen, S.; Murray, R. W. *J. Phys. Chem. B* **1999**, *103*, 9996. (b) Gittins, D. I.; Bethell, D.; Schiffrin D. J.; Nichols, R. J. *Nature* **2000**, *408*, 67. (c) Chen, S. *J. Phys. Chem. B* **2000**, *104*, 663. (d) Zamborini, F. P.; Hicks, J. F.; Murray, R. W. *J. Am. Chem. Soc.* **2000**, *122,* 4514. (e) Hicks, J. F.; Zamborini, F. P.; Murray, R. W. *J. Phys. Chem. B* **2002**, *106*, 7751.
28. Laviron, E. *J. Electroanal. Chem.* **1979**, *101*, 19.

Chapter 4

Interactions of Charged Monolayer Protected Gold Clusters in Electrolyte Solution *

In this chapter, the quantized double layer (QDL) charging features of 4.63 nm sized monolayer protected Au nanoclusters [$Au_{2869}(DDT)_{541}$] have been investigated using electrochemical and scanning tunneling microscopy (STM)/ spectroscopy (STS) studies. These particles show clear accessibility for single electron charging, despite their higher capacitance (1.95 aF). Further, the diffusion coefficients have been estimated for various charge state particles using chronoamperometry and impedance techniques, which subtly reflect the interactions between the charged MPCs. These results show that higher core charge facilitates higher diffusion coefficients, indicating the importance of repulsive interaction compared to that of the neutral MPCs.

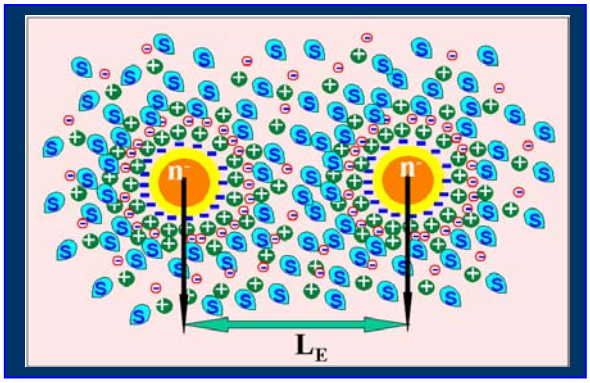

---

* A part of the work has been published in "***Electrochem. Commun.*** **2004**, *6,* 661" and another part has been communicated to ***"Langmuir 2005"***.

4.1 Introduction

Interparticle interaction of colloids, especially for nanometer sized colloidal dispersions of solid particles suspended in a liquid solvent, play a crucial role for numerous industrial applications, like advanced coatings, drug carriers and colloidal crystals preparation.[1-2] This has also a pivotal role for hierarchical self-assembly of nanostructured materials, which is believed to be a central process for nanotechnology.[3-7] Accordingly, the interactions of monolayer protected nanoclusters (MPCs) are often dictated by their size selective preparation, separation and especially their self-assembly depending on their shape, size, nature of solvent and other ions present in solution.[3-7] Interestingly, MPCs and their assemblies show fascinating single electron transfer property, which renders them as potential building blocks for nanoelectronic circuit components as discussed in chapter 1.[3,8-11]

Conventionally, STM is used to assess single electron transfer features of smaller MPCs at low temperature, which often show "Coulomb staircase.[12-14] Furthermore, the voltammetric measurements of smaller sized MPCs in solution or self-assembled on electrode surface also show quantized double layer charging (QDL) analogous to Coulomb blockade as discussed in chapter 1 and 3.[15-20] Due to this double layer charging, the smaller sized particles ($2r < 1.3$ nm, where 'r' is the radius of particles) behave like molecular redox system, where bonding interactions (electron orbital-shell effects or pairing effects, or both) are dominated over electrostatic charging of the metal cores, covered with a dielectric film.[17] This has been reflected as a large separation of potential (ΔV) in the potential of zero charge (i.e., E_{PZC}) regions in $1.1 < 2r < 1.9$ nm size regime, termed as "Electrochemical Band Gap" and is comparable with HOMO-LUMO (Highest Occupied Molecular Orbital-Lowest Unoccupied Molecular Orbital) gap.[17] However, the electrostatic principles govern the electronic charging of the core larger than 1.9 nm, i.e., double layer principles dominated over bonding interactions. More specifically, the capacitance is associated with the ionic space charge around MPCs dissolved in the electrolyte solution.[15-20]

To date, several important issues related to the core-charged MPCs have been reported, like (a) charge equilibration upon mixing of different core charged MPCs,

described by the stoichiometry of the mixture and the Nernst relation,[16] (b) relation of core charge with the surface plasmon resonance (SPR),[21] FTIR absorption and narrow band-edge photoluminescence (for semiconducting particles)[22] and (c) effect on chemical reactivities, like ligand place-exchanges on MPCs.[23] Further, several theoretical and experimental efforts have been put forward to understand MPC-MPC and MPC-solvent interactions,[6,7,24,25] although no adequate reports are available for the interactions of charged MPCs. Since the QDL process is diffusion controlled,[15-20] the effective interaction between MPCs can in principle affect both mass transfer (diffusion coefficients) and electron transfer processes in different ways. Consequently, measurement of diffusion coefficients at various charge steps could provide some valuable insight on the interaction between the charged MPCs, where the delicate balance of van der Waals interaction and electrostatic repulsion could change their motion in solution.

In this chapter, single electron charging feature of 4.63±0.04 nm sized Au nanoparticles passivated with dodecanethiol (DDT) has been investigated using both STM/STS and voltammetric techniques. In particular, STM/STS measurements of these particles were carried out on a highly oriented pyrolytic graphite (HOPG) substrate at room temperature in air to obtain topography, current-voltage (I-V) and dI/dV versus V characteristics. The experimental I-V has been fitted with the theoretical I-V based on the orthodox model.[26,27] The voltammetric measurements were performed in dichloromethane using differential pulse voltammetry (DPV) and cyclic voltammetry (CV). More importantly, our study summarizes that Au MPCs show highly nonlinear I-V characteristics, while the QDL charging property is evident in voltammetric measurements as a large population of charging events with an equidistant ΔV spacing. The capacitances of these MPCs obtain from both STS and voltammetric measurements are found to be in good agreement with the theoretical values. To explore the effective interactions of charged MPCs, the diffusion coefficient values are calculated for various charged particles using chronoamperometry and impedance techniques. These results show that the presence of higher charge enables these particles to diffuse faster along with concomitant enhancement in their electron transfer rates.

4.2 Experimental Section

4.2.1 Materials

Materials used in these experiments were same as mentioned in chapter 3 (section 3.3.1).

4.2.2 Synthesis of Au MPCs

Synthesis and characterization details of $Au_{2869}(DDT)_{541}$ MPCs have been already described in chapter 2 (section 2.2.2) along with the appropriate determination of composition.

4.2.3 Scanning Tunneling Microscope/Spectroscopic (STM/STS) Measurements

The samples for STM analysis were prepared by putting a drop of nanoparticle solution on HOPG substrate and used after drying it for 5 min. STM studies were carried out immediately after the deposition using tips made from 0.25 mm diameter polycrystalline Pt - Rh wire by mechanically cutting them at an angle. A home-built STM based on fine mechanical-screw-lever arrangement assembly[28] with a compact, four-quadrant, three-dimensional scanner was used for this investigation.[29] Details of the system and the general procedure for imaging are discussed elsewhere.[30] Images were prepared using SPIP software.[31] The STM imaging was carried out in air with optimum values of tunnel current (I = 0.2 nA) and bias voltage (V = 100 mV) in constant current mode. The time between imaging and sample preparation was kept minimum. Once the particles were located with some difficulties they could be imaged repeatedly and tunneling spectroscopy was performed by positioning Pt-Rh tip over an isolated Au-nanoparticle by disabling the feedback control and measuring I-V characteristics. The I-V characteristics were always repeated several times and finally the signal was averaged over tens of runs. The dI/dV vs. V characteristics were obtained by numerical differentiation of measured I-V curves.

4.2.4 Electrochemical Measurements

All electrochemical measurements were carried out in dichloromethane using 0.1 M tetrabutylammoniumhexaflurophosphate (TBAHFP) supporting electrolyte in an ice bath (273-276 K) using a standard three electrode cell comprising Pt micro electrode (50 μm) as the working electrode, a Pt wire as counter electrode and another Pt wire as a quasireference electrode (calibrated independently with an internal standard ferrocene/ferrocenium couple) unless mentioned separately. Differential pulse (modulation time 0.02 s, interval time 0.1 s, step potential 0.025 V and modulation amplitude 0.02 V) and cyclic voltammetric experiments were performed on an Autolab PGSTAT30 (ECO CHEMIE) instrument. Electrochemical impedance measurements were carried out in an impedance analyzer (Autolab PGSTAT 30 with FRA software) employing a Pt disc (0.5 mm diameter) working electrode. The ac signal amplitude was 5 mV rms within 1 Hz to 50 kHz frequency range and the data was recorded with averaging over 3 cycles for each frequency. Similarly, chronoamperometry experiments were carried out employing a Pt disc (0.5 mm diameter) working electrode under identical conditions as mentioned above.

4.3 Single Electron Charging Features of $Au_{2869}(DDT)_{541}$

Although many reports are available on the electrochemical behaviour of smaller (1-2 nm) diameter Au MPCs, only few studies are available for the combined investigations using electrochemical and STM techniques.[15] In particular, the low temperature I-V measurements using STM at 93 K revealed "Coulomb staircase" with six regularly spaced charging steps for 1.64 nm diameter Au MPCs.[15] In the preceding chapter (Chapter 3) we have discussed the combined experimental evidence (STM and voltammetric) for single electron charging features of larger sized Au MPCs (3.72 nm); consequently it is necessary to explore whether more larger particles do also show this property or not. Accordingly, the single electron charging features of these MPCs have been compared using STM and electrochemical techniques and these results show that 4.63 nm sized particles also depict similar behavior despite their higher capacitances. More importantly, the presence of high population of charging events in these larger

particles would make them useful for nanoelectronic device construction due to the simplicity of their preparation as compared to that of smaller sized particles. [32-34]

4.3.1 STM/STS Results

Due to their highly monodispersed nature, Au MPCs form ordered structures on HOPG surface as revealed by STM (Figure 4.1a-b) as well as by TEM (Figure 4.1d). The particle size estimated from STM image is ≈ 4 nm from Figure 4.1 (b-c), which is smaller than the size from TEM results, indicating that tip convolution effects are minimum and perhaps that an asperity smaller than nanoparticle is responsible for imaging.

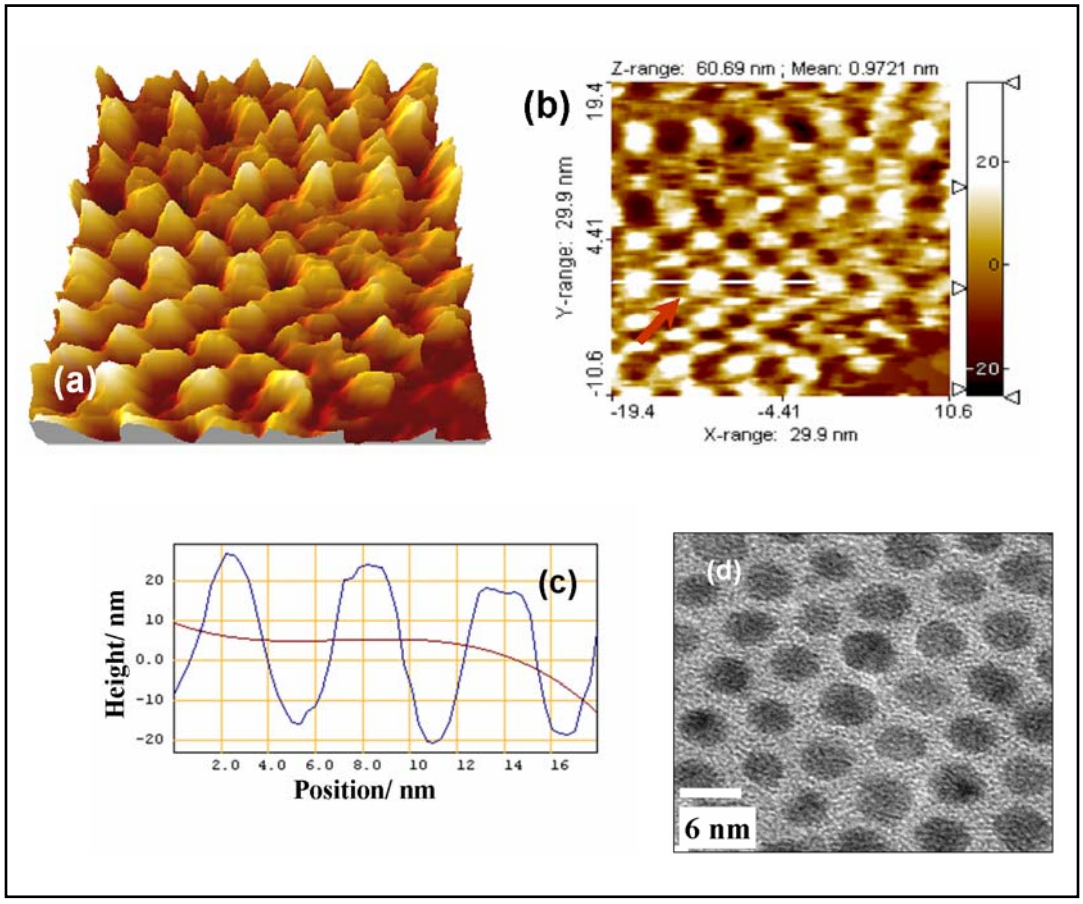

Figure 4.1 (a) 3D view of the STM image of the ordered structures of DDT capped Au nanoparticles (300 x 300 Å), scan Area (300 x 300 Å), I = 0.2 nA, V = 100 mV. (b) Plane view and (c) line profile of three marked Au nanoparticles; (d) TEM also reveals similar features.

Figure 4.2 shows typical I-V and dI/dV vs. V characteristics (inset 1) of these particles, where curve (a) shows the experimental I-V response taken on an isolated nanoparticle as indicated by an arrow in Figure 4.1 (b). An attempt to fit this data with orthodox theory fails, which on closer examination, reveals that these curves are asymmetric with a d.c. shift along the X-axis. Removal of the offset of 0.05 V from experimental data results into a fairly good fit with the theoretical curve, which is shown in curve (b) of Figure 4.2. These I-V curves show fairly non Coulomb blockade regime (zero current region), which can be explained by the orthodox theory of single electron.[26,27]

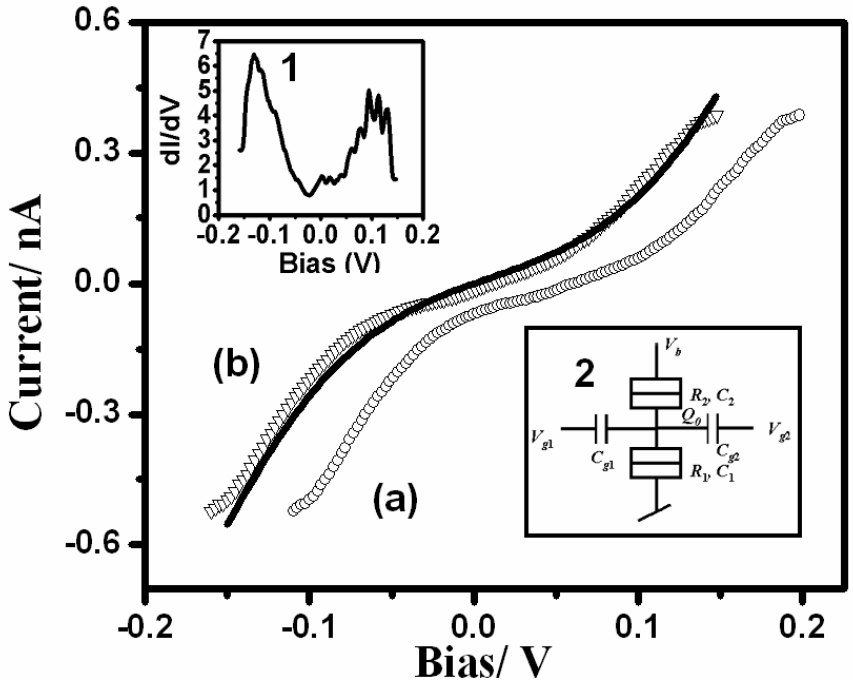

Figure 4.2 Curve (a) marked by "○" symbol shows the experimental I-V of isolated Au nanoparticle marked by an arrow in Figure 4.2b with d.c. offset of 0.05 V. Curve (b) marked by "▽" symbol shows the offset-corrected I-V. Left inset (1) shows the dI/dV versus V of curve (b). Right inset (2) [45] shows the schematic diagram of the theoretical model used to fit the experimental curve. Comparison of offset-corrected experimental I-V [curve (b)] and theoretical plot (solid line) gives the best fit parameters as $R_1=10^8$ ohms, $C_1 = 5 \times 10^{-20}$ F, $R_2 = 10^6$ ohms, $C_2 = 7 \times 10^{-19}$ F, $Cg_1 = 1 \times 10^{-22}$ F, $Vg_1 = 0$ V, $Cg_2 = 0$ F, $Vg_2 = 0$ V, Q_0 (e) = -0.05 e, $V_b = 0.15$ V, $E_c = 0.11$ eV, $k_BT/E_c = 0.2421$ and T = 300 K.

We have performed curve fitting[35] of the I-V plots based on the orthodox theory. According to Hanna and Tinkham[27] the current is given by,

$$I(V) = e[\Gamma_2^+(n_0) - \Gamma_2^-(n_0)] \tag{4.1}$$

where n_0 is the most probable number of electrons on the center electrode and Γ_2^+ and Γ_2^- are the tunneling rates for the second junction $\Gamma_j^{\pm}(n)$ is given by,

$$\Gamma_j^{\pm}(n) = \frac{1}{R_j e^2}\left(\frac{-\Delta E_j^{\pm}}{1-\exp(\Delta E_j^{\pm}/k_B T)}\right) \tag{4.2}$$

where the +/- refers to the electrons tunneling on/off the center electrode ($n \rightarrow n \pm 1$), ΔE is the energy change of the system when the electron tunnels across the barrier and R_j is the tunneling resistance of the j^{th} junction. For the case of low temperature, when $|\Delta E_2^{\pm}(n_0)| >> k_B T$, $\Gamma_2(n_0)$ can be simplified as,

$$\Gamma_2^{\pm} = \left\{ \begin{array}{c} \frac{1}{R_2 C_\Sigma}\left[-\frac{1}{2} \mp (n_0 - Q_0/e) \pm C_1 V/e\right], for \Delta E_2^{\pm} \langle 0 \\ 0, for \Delta E_2^{\pm} \rangle 0 \end{array} \right\} \tag{4.3}$$

Where $C_\Sigma = C_1 + C_2$, C_1 and C_2 are the capacitance of the first and the second junction and Q_0 is the fractional electron charge present on the particle.

This means that I(V) = 0 when

$$(-e/2 + n_0 e - Q_0)/C_1 \leq V \leq (e/2 + n_0 e - Q_0)/C_1 \tag{4.4}$$

This is so called “Coulomb blockade”. Outside of this voltage range I(V) is given by:

$$I(V) = \frac{1}{R_2 C_\Sigma}\left[-(n_0 e - Q_0) + C_1 V - \frac{e}{2}\mathrm{sgn}(V)\right] \tag{4.5}$$

The sgn(V) is the signum function of (V) often used to define a function of real number, which is 1 for positive numbers, −1 for negative numbers and 0 for zero. Although the

theory is strictly defined for a three electrode system [right inset (2) of Figure 4.2], it can be extended for the case of two electrode system by considering V_{g1} and V_{g2} equal to zero and taking V_b as the sample bias voltage. Since there is no third electrode, C_{g1} and C_{g2} are parallel to C_1 and the combination represents the tunnel junction capacitance between the tip and a typical nanoparticle. The schematic diagram[35] of the equivalent circuit of double barrier tunnel junction to fit the experimental curve is shown in the inset 2 of Figure 4.2, where (R_1, C_1) is the resistance and capacitance of tip/nanoparticle junction, (R_2, C_2) is the resistance and capacitance of nanoparticle/substrate junction, (C_{g1},V_{g1}) and (C_{g2},V_{g2}) are the capacitance and voltage on tip with respect to the ground potential, Q_0 is the fractional charge, E_C is the charging energy or Coulomb blockade energy and T is the temperature.

The best fit parameters for the offset-corrected I-V data, that result into a fairly good fit with the theoretical curve are $R_1 = 10^8$ ohms, $C_1 = 5 \times 10^{-20}$ F, $R_2 = 10^6$ ohms, $C_2 = 7 \times 10^{-19}$ F, $Cg_1 = 1 \times 10^{-22}$ F, $Vg_1 = 0$ V, $Cg_2 = 0$ F, $Vg_2 = 0$ V, Q_0 (e) = -0.05 e, $V_b = 0.15$ V, $E_c = 0.11$ eV, $k_BT/E_C = 0.242$ and T = 300 K. The capacitance (C_S) of the particle can be estimated using a simple model involving spherical particles coated with a dielectric layer as $4\pi\varepsilon_0\varepsilon_m r = 6.67 \times 10^{-19}$ F, where r (≈ 2 nm, from STM) is the radius of the nanoparticle, ε_0 (= 8.85×10^{-12} F.m^{-1}) is the permittivity of free space and ε_m is the dielectric constant (= 3 for DDT). Accordingly, the E_C (= $q^2/2C_S$) comes out to be 0.12 eV, which is in reasonable agreement considering the uncertainty involved in the measured parameters.

Interestingly, there is no zero current region in these I-V curves and only a suppression of current over the region of the order of 0.1 eV is observed, which can also be seen in inset 1 of Figure 4.2. These results are significantly different from our earlier results with 3.72 nm particles measured at lower concentration (chapter 3), indicating the coupling of nanoparticles in self-assembled areas leading to a smaller tunneling current in the zero bias region. The presence of charge, Q_0(e) = 0.05 e also suggests the possibility of reorganization of charges between the clusters in the presence of electrode surface. Similar results have been observed for the STM/STS measurements of titanium dioxide nanoparticle film on Au(111), where the increase in the particle density results in a change in the shape of I-V curves.[36]

4.3.2 Voltammetric Results

The consecutive one electron QDL peaks observed in solution are analogous to current peaks seen in traditional redox reactions, where the QDL charging process is diffusion controlled and obeys the Nernst equation with respect to the average core potential.[20] Accordingly, these peak potentials can be taken as the formal redox potential $E^{0'}$ for each (z/z ± 1) "redox couple or charge state couple" and is given by the DPV peak potentials. The formal redox potential $E^{0'}$ can be described by:

$$E^{0'}_{z/z+1} = E_{PZC} + (z-{}^{1}/_{2})e/C_{CLU} \qquad (4.6)$$

where E_{PZC} is the potential of zero charge (i.e., z = 0) of the MPC and z is assigned such that z > 0 and z < 0 corresponding to core "oxidation" and "reduction" respectively and C_{CLU} is the capacitance of the MPC. The above equation predicts a linear plot of $E^{0'}_{z/z+1}$ vs. charge state (popularly known as "Z-plot"), which can be used to determine C_{CLU} from the slope.[20]

Figure 4.3 (a) shows the superimposed DPV response of these larger sized Au MPCs protected with DDT in dichloromethane on a Pt microelectrode (50 μm) at 1.6, 0.96 and 0.8 mg/ml concentrations (i-iii respectively) along with the blank Pt (50 μm) response under identical conditions. For example, DPV plots (Figure 4.3a) reveal highly populated evenly spaced current peaks (80-90 mV), whereas Figure 4.3 (b) shows the linear variation of base line corrected DPV peak currents of (i) -1/0 and (ii) 0/1 charge state with MPC concentration. Accordingly, Figure 4.3 (c) shows the superimposed DPV response of these larger sized Au MPCs protected with DDT in dichloromethane on a Pt microelectrode (50 μm) at 0.96 mg/ml concentrations at i) 30, ii) 20 and iii) 10 mV pulse amplitude. These DPV plots reveal a highly populated evenly spaced (*ca.* 80-90 mV) current peaks, where the (–1/0) and (0/1) charging peaks are marked following z/z ± 1 fashion for comparison (corresponding potentials are expressed vs. Pt quasireference electrode). The corresponding potentials for individual charge steps of each DPV plots have been summarized in Table 4.1. Interestingly, the full width at half maximum (FWHM) of each peak is found to be of ca. 40-45 mV, particularly signifying the QDL process for these larger MPCs, which differ from the earlier reports for smaller sized Au MPCs (110-115 mV) or ideal (90.6 mV) one electron transfer process for conventional

redox species.[15-20,37] This anomalous FWHM value might be attributed to several complex interactions among these assemblies of mixed-valent redox centers at the electrode-solution interface during the electrochemical process.[38-40]

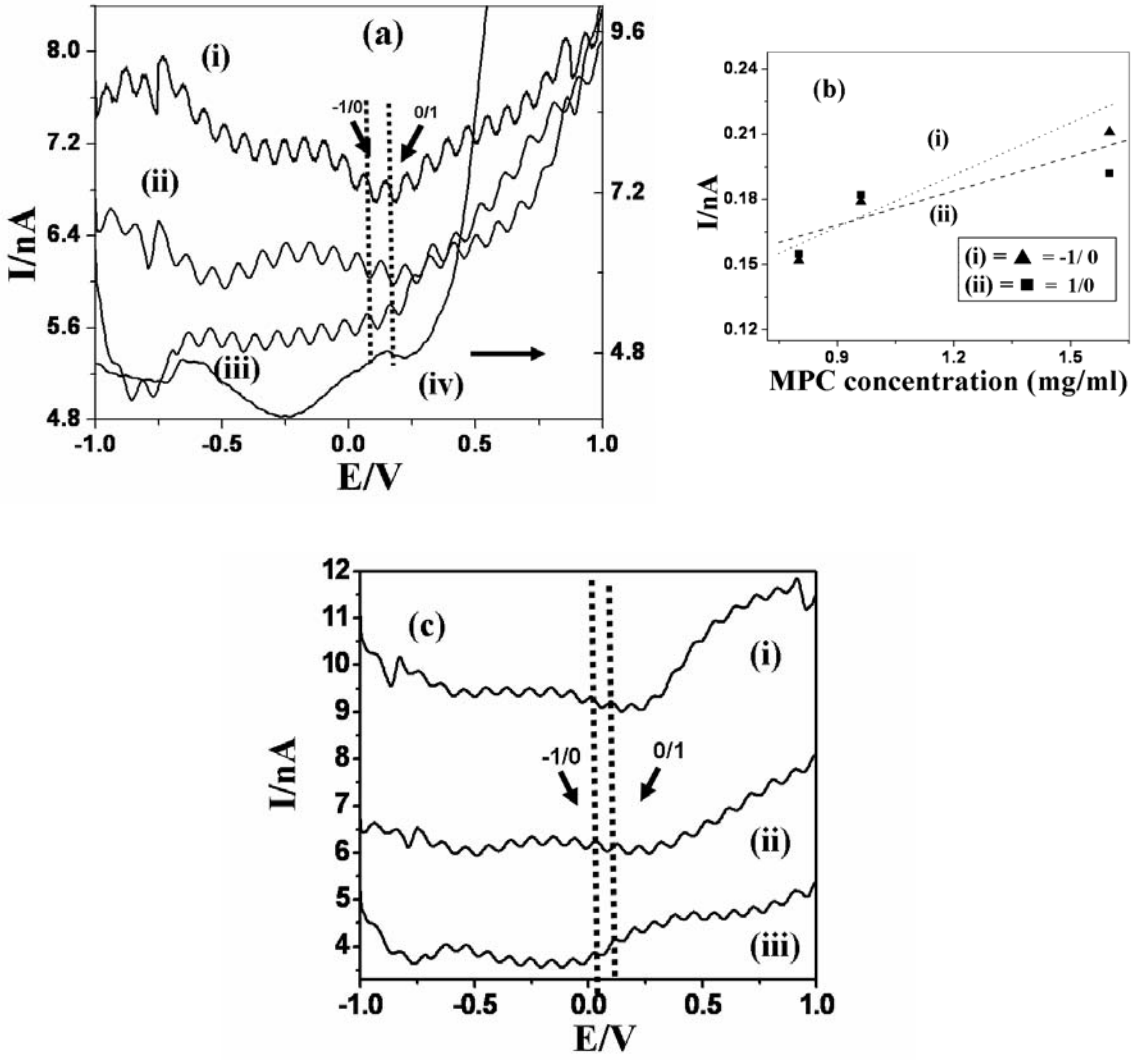

Figure 4.3 (a) DPV response of (4.63 ± 0.04 nm) DDT passivated Au MPCs, at 1.6, 0.96 and 0.8 mg/ml concentrations corresponding to graph (i-iii) respectively along with the blank response (iv); (b) nonlinear increment of the DPV base line corrected peak currents at (-1/0) and (0/+1) charging peaks with MPC concentration and (c) the superimposed DPV response of Au MPCs at i) 30, ii) 20 and iii) 10 mV pulse amplitude using 0.96 mg MPCs/ml, showing highly populated QDL charging. These figures reveal a highly populated evenly spaced current peaks, where the (–1/0) and (0/+1) charging peaks are marked for comparison.

Table 4.1 Peak positions and corresponding charge states for the DPV response shown in Figure 4.3. (Columns have been named according to the individual DPV graphs as shown in Figure 4.3)

Charge State	Figure 4.3. a. i (V)	Figure 4.3. a. ii (V)	Figure 4.3. a. iii (V)	Figure 4.3. c. i (V)	Figure 4.3. c.ii (V)	Figure 4.3. c. iii (V)
11/12	0.93	---	---	---	---	---
10/11	0.85	---	0.93	0.91	---	0.90
9/10	0.77	0.91	0.86	0.83	0.91	0.82
8/9	0.70	0.81	0.78	0.74	0.81	0.72
7/8	0.62	0.71	0.67	0.65	0.72	0.64
6/7	0.55	0.62	0.58	0.56	0.62	0.55
5/6	0.47	0.52	0.50	0.47	0.52	0.45
4/5	0.39	0.42	0.41	0.37	0.42	0.38
3/4	0.30	0.32	0.33	0.29	0.32	0.29
2/3	0.27	0.22	0.26	0.19	0.22	0.20
1/2	0.15	0.13	0.16	0.10	0.13	0.12
0/1	0.06	0.04	0.07	0.01	0.04	0.03
-1/0	-0.02	-0.06	-0.07	-0.07	-0.06	-0.07
-2/-1	-0.09	-0.15	-0.02	-0.16	-0.15	-0.16
-3/-2	-0.18	-0.25	-0.11	-0.26	-0.25	-0.25
-4/-3	-0.26	-0.34	-0.20	-0.36	-0.34	-0.34
-5/-4	-0.33	-0.44	-0.28	-0.45	-0.44	-0.44
-6/-5	-0.41	-0.54	-0.37	-0.55	-0.54	-0.53
-7/-6	-0.49	-0.64	-0.46	-0.65	-0.65	-0.62
-8/-7	-0.57	-0.75	-0.55	-0.75	-0.75	-0.72
-9/-8	-0.65	-0.84	-0.63	-0.83	-0.84	-0.82
-10/-9	-0.74	-0.94	-0.7	-0.92	-0.94	-0.92
-11/-10	-0.80	---	-0.81	---	---	---
-12/-11	-0.88	---	-0.91	---	---	---
-13/-12	-0.96	---	---	---	---	---

In conjunction with the results of DPV, these high populations of charge steps are also accessible by cyclic voltammetry. For example, Figure 4.4 (a) shows the superimposed response of these MPCs at 50 mV/s scan rate using 0.96 and 0.8 mg/ml concentrations (graphs i and ii respectively) along with the blank Pt (50 μm) response under identical conditions, where a high population of evenly space sigmoidal waves are visible, indicating successive one electron process. Since these larger sized particles essentially have higher capacitance values as indicated by the DPV peak to peak spacing (*ca.* 80-90 mV), this could in principle lead to poor resolution by CV. In particular, the derivative (graphs i and ii respectively) of these CV responses is comparable with the DPV results, as shown in Figure 4.3. Further, Figure 4.4 (c) shows the superimposed CV response of these MPCs at i) 100 and ii) 50 mV/s scan rates using 0.96 mg/ml MPC concentration, where the corresponding derivatives (iii and iv) are comparable with the DPV results. Interestingly, these MPCs do not show any signature of the "Electrochemical Band Gap" as observed for smaller sized particles, indicating that the process is particularly governed by the double layer charging principles.

Table 4.2 Capacitance values calculated from the Z plots (Figure 4.5)

Z plot	R^2	Capacitance (aF)
(3.a. i)	0.99	2.13
(3. a. ii)	0.99	1.75
(3. a. iii)	0.99	2.07
(3. c. i)	0.99	1.86
(3. c. ii)	0.99	1.75
(3. c. iii)	0.99	1.87

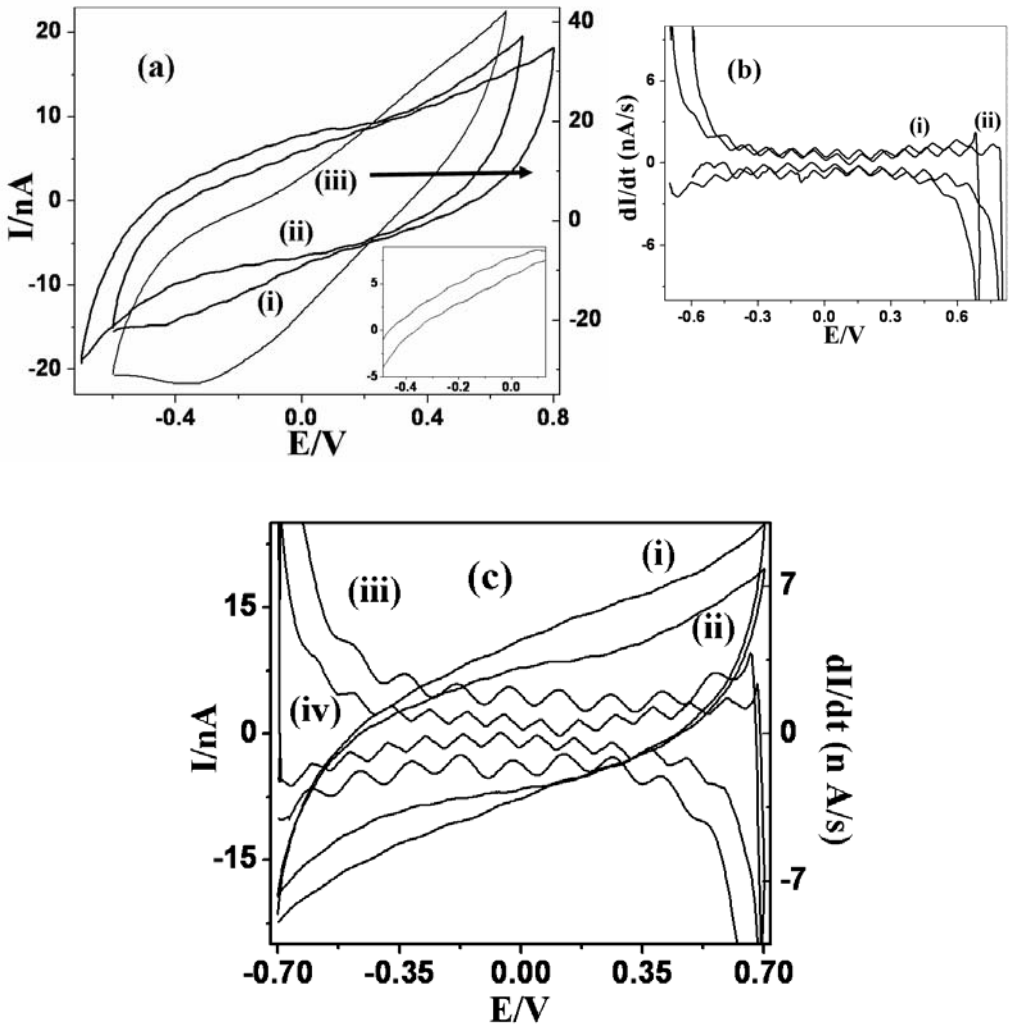

Figure 4.4 (a) CV response at 50 mV/s scan rate for 0.96 and 0.8 mg/ml concentrations (graphs i-ii respectively) along with the blank response (iii), where the QDL behaviour is clearly visible in the enlarged view of the CV curves shown as an inset, (b) derivative response of the CV shown in (a) and (c) superimposed CV response at i) 100 and ii) 50 mV/s scan rate for 0.96 mg MPCs/ml concentrations along with their derivative response (iii and iv respectively).

Figure 4.5 (a-f) represents the corresponding "Z plot" for these Au MPCs obtained form the DPV analysis at Figure 4.3 (a and c), where linear (R^2 > 0.99) behaviour can be seen as expected for the ideal QDL behaviour.[15-20] The capacitance (C_{CLU}) values calculated (Table 4.2) from the slope of the "Z plot" are 2.13, 1.75 and 2.07 aF from Figure 4.5 (a-c) corresponding to graphs at Figure 4.3 (a. i-iii), while 1.86, 1.75

and 1.87 aF form Figure 4.5 (d-f) corresponding to graphs at Figure 4.3 (c. i-iii). These experimentally determined capacitances of 4.63 nm sized Au MPCs are in good agreement with the corresponding theoretical value (1.95 aF), estimated with the help of a concentric sphere capacitance model.[20]

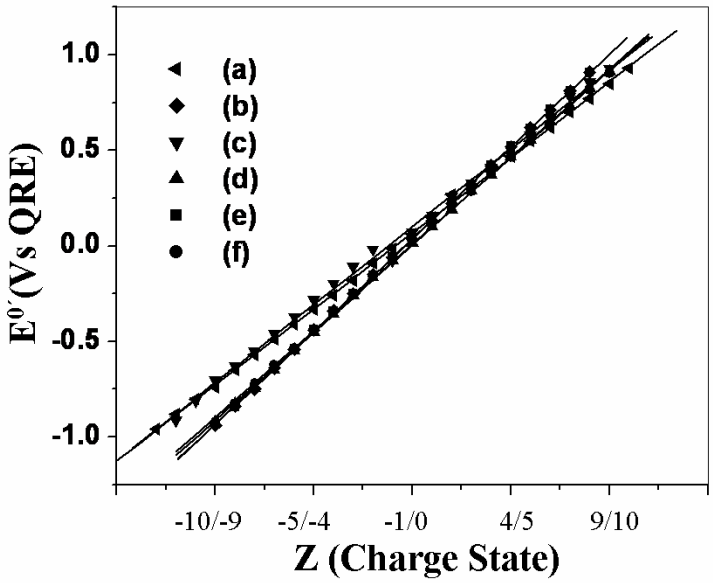

Figure 4.5 Superimposed "Z plots" of $E^{0'}$ vs. redox couple charge state (Z/Z ± 1) of Au MPCs at (a) 1.6, (b) 0.96 and (c) 0.8 mg/ml concentrations using 20 mV pulse amplitude; graphs (d – f) correspond to DPV response at 30, 20 and 10 mV pulse amplitude using 0.96 mg MPCs/ml suggesting ideal QDL behaviour.

So far we have discussed the electron transfer features of these particles using STM/STS and voltammetric techniques, where both of these techniques depict their single electron transport features. More specifically, multiple peaks have been observed in voltammetric experiments, whereas STS measurements only show evidence for Coulomb blockade near zero bias without any signature of the Coulomb staircase. In particular, STM analysis considers particles to form double barrier tunnel junctions (DBTJ), where the interfacial capacitances of both sides contribute to the real capacitance of the particle. The capacitance from STM measurement is estimated to be

of 7.5 x 10^{-19} F, which is in good agreement with the theoretical prediction. However, supporting electrolyte ions and solvent molecules always surround the particles and consequently they can diffuse together to the electrode surface prior to electron transfer. Although the processes are same in both STM and voltammetry (i.e., the electrode is used to donate and subtract electron from the particle to detect the current), STM has an advantage of unraveling geometrical and electronic structure of isolated particles as well as particles within self-assembled films. In sharp contrast, electrochemistry provides phenomena of averaged sized particles (ensemble) in the proximity of the solution environment. Despite these differences, Coulomb blockade observed in both voltammetry and STM experiments are fairly in good agreements with a common origin of their capacitive contribution, notwithstanding the difference between the environments.

4.4 Interaction of Au MPCs

There are numerous experimental studies to account interparticle interactions between dispersed MPCs,[24] which include osmometry and small angle X-ray scattering (SAXS) measurements of trioctylphosphine (TOP) and trioctylphosphineoxide (TOPO)-capped CdSe[24c] and DDT protected Au MPCs[6c]. Furthermore, few theoretical studies are also available, which account both the MPC-MPC and MPC-solvent interactions quantitatively.[25] These results show that the interparticle interaction is followed by simple steric stabilization model (in the order of thermal energy), where the core-core van der Waals attraction is modified by an osmotic repulsion between adsorbed chains.[6c,24,25] More specifically, the larger sized particles (i.e., > 5 nm diameter) are less attractive than that of smaller core sized particles, possibly due to the less number of ligand surface coverage than that of larger one.[6c] The potentials of van der Waals attraction (E_{vdw}) and steric repulsion (E_{steric}) are described by the following relations:

$$E_{vdw} = -A/12[(4r^2/L_{CC}^2-4r^2) + (4r^2/X^2) + 2\ln(L_{CC}^2-4r^2/ L_{CC}^2)] \quad (4.7)$$

$$E_{steric} = [100r\delta_{SAM}^2/(L_{CC}-2r)\pi\sigma_{thiol}^3] k_B T\exp[-\pi(L_{CC}-2r)/ \delta_{SAM}] \quad (4.8)$$

where, A is the Hamaker constant, r is the radius and L_{CC} is the center to center distance between spheres, δ_{SAM} is the chain length of capping molecule and σ_{thiol} is the diameter of the area occupied by the capping molecule on the particle surface.[41] Furthermore, the

strength of the interparticle interaction also could be modulated by changing the nature of solvent i.e., by tuning the degree of solvation.[25b]

Scheme 4.1 Schematic representation of the interaction of the MPCs in electrolyte solution for (a) neutral and (b) charged MPCs, where "L_N" and "L_E" are the core to core separation ($L_N < L_E$) for respective cases; (c) the schematics of individual entities, like Au MPCs, solvent molecules, supporting electrolyte cations and anions to demonstrate these interactions

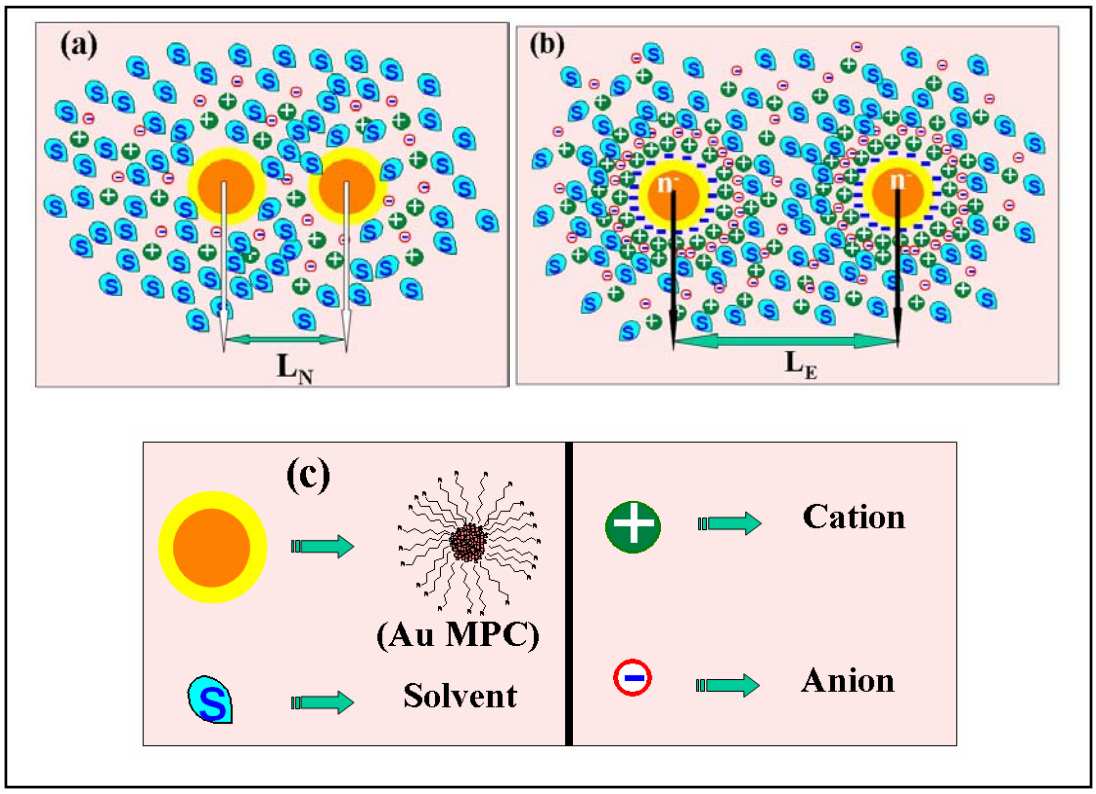

The interparticle interactions of MPCs in electrolyte solution are described by Derjaguin-Landau-Verwey-Overbeek (DLVO) principle,[1,2] where there is a delicate balance between steric repulsion, long range van der Waals attraction and electrostatic repulsion due to the electrical double layer. The repulsive electrostatic potential between like-charged colloidal particles suspended in a polar solvent is expressed by

$$E_{el} = 2\pi\varepsilon\varepsilon_0 r\, \xi^2 \ln[1 + \exp(-\kappa L_{SS}')] \qquad (4.9)$$

where, r is the radius of particles, ξ is the surface potential, ε is the relative permittivity of the solution, ε_0 is the permittivity of vacuum, κ^{-1} is the Debye length and L_{SS}' is the surface separation distance in electrolytic solution.[1,2] One of the important issues is how the charge present on the MPCs affects these interactions. Since the width of the double layer would be expected to be increased with the increment of the core charge, it is likely that the higher charge present on the MPCs could enhance the repulsion. Accordingly, scheme 4.1 shows the interaction of MPCs in electrolyte solution for (a) neutral and (b) charged MPCs, where "L_N" and "L_E" are the core to core separation for (a) and (b) respectively. It is clear from this argument that "L_N" should be less than "L_E" due to the increase of repulsion as a result of the increment of core charge. Since the QDL phenomenon is diffusion controlled process, the electrochemical measurement of diffusion coefficient of MPCs at various charge steps could easily justify this prediction. Consequently, diffusion coefficient values have been measured for various charge steps using two independent electrochemical techniques chronoamperometry and impedance technique. Furthermore, impedance measurements also allow us to put insight onto the charge step dependent electron transfer features along with diffusion coefficient measurements.

4.4.1 Chronoamperometric Results

The diffusion coefficients (D_C) of Au MPCs have been calculated by chronoamperometry using Cottrell equation (4.10).[37] Assuming that linear semi-infinite diffusion is applicable for freely diffusing MPCs in solution, the current (I) - time (t) response can be written as follows:

$$I_d(t) = n F A C_n D_C^{1/2} \pi^{-1/2} t^{-1/2} \qquad (4.10)$$

where, n is the change in core charge state, C_n is the MPC concentration in the solution (9.5×10^{-7} mol.cm^{-3}), A is the area of the electrode (0.5 mm diameter = 1.96×10^{-3} cm^2), F is the Faraday constant, t ($0.2 \text{ s} \leq t \leq 20 \text{ s}$) is the duration for the measurement of current after applying the respective constant potential corresponding to individual charge step in DPV response as shown in Figure 4.3 and D_C is the diffusion coefficient of the charged clusters in the electrolyte solution under applied potential.

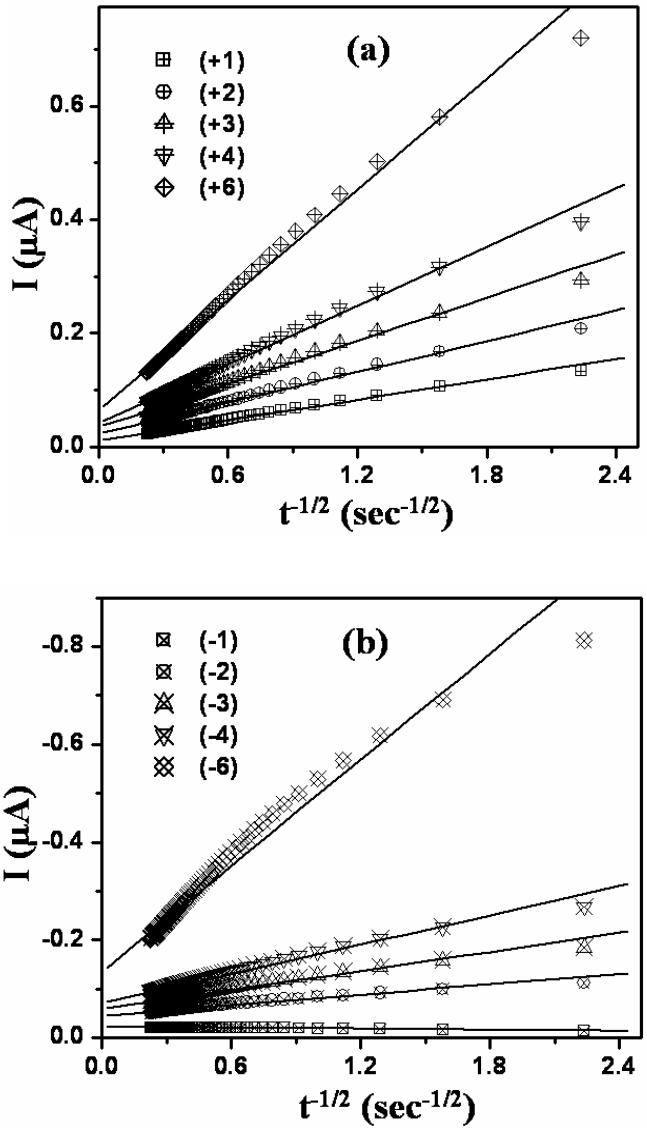

Figure 4.6 Superimposed linearly fitted I vs. $t^{-½}$ plots, under five applied (a) anodic potentials corresponding to (+1), (+2), (+3) (+4) and (+6) charge states and (b) cathodic potentials corresponding to (-1), (-2), (-3), (-4) and (-6) charge states.

The D_C of cluster is calculated by analyzing the slope of the linearly fitted I vs. $t^{-½}$ plots. These I vs. $t^{-½}$ plots were obtained under various applied potentials corresponding to the valleys (between two peaks) of the DPV response as shown in graph (i) of Figure 4.3, where all MPCs are assumed to be approximately in monovalent charge states. For example, Figure 4.6 (a and b) shows the superimposed linearly fitted I - $t^{-½}$ behaviour

under different anodic and cathodic potentials corresponding to [(+1), (+2), (+3), (+4) and (+6)] and [(-1), (-2), (-3), (-4) and (-6)] charge states respectively. The terms anodic and cathodic are used to indicate that the applied bias is either anodic or cathodic with respect to the E_{PZC}. Table 4.3 summarizes various parameters such as applied potential, corresponding charge states, slope of the plots and the calculated diffusion coefficient using equation (4.10).

Table 4.3 Various parameters and calculated diffusion coefficient values using equation 4.10 from chronoamperometry data (Figure 4.6)

Charge State (DPV)	Applied Potential (V)	Slope $\mu A.s^{1/2}$	Number of Transferred Electron	D_C $cm^2.s^{-1}$	D_{SE} ($x\ 10^{-7}\ cm^2.s^{-1}$)
+1	0.19	0.06	1	3.50×10^{-7}	
+2	0.27	0.09	2	1.98×10^{-7}	
+3	0.35	0.13	3	1.74×10^{-7}	
+4	0.43	0.17	4	1.80×10^{-7}	
+6	0.59	0.32	6	2.84×10^{-7}	14.7
-1	0.02	0.003	1	1.40×10^{-9}	
-2	-0.09	0.04	2	3.10×10^{-8}	
-3	-0.16	0.07	3	4.60×10^{-8}	
-4	-0.23	0.10	4	6.00×10^{-8}	
-6	-0.48	0.36	6	3.50×10^{-7}	

4.4.2 Impedance Results

Figure 4.7 (a) shows the superimposed complex plane impedance plots of Au MPCs in CH_2Cl_2 on a Pt disc (0.5 mm diameter) working electrode under open circuit potential (OCP) and various anodic dc bias corresponding to various charge steps (+1),

(+2), (+4) and (+6), where a suppressed semicircle at the high frequency domain and a straight line with more than 45° angle to the real axis in the low frequency region are observed. Subsequently, the impedance data have been divided into high and low frequency regions for the convenience of interpretation and analyzed using the Randles equivalent circuit, considering the electrode reaction to be a single-step, one electron process.[37] The high frequency part of these plots has been fitted to a semicircle using complex nonlinear least square (CNLS) procedure and has been superimposed in Figure 4.7 (b).

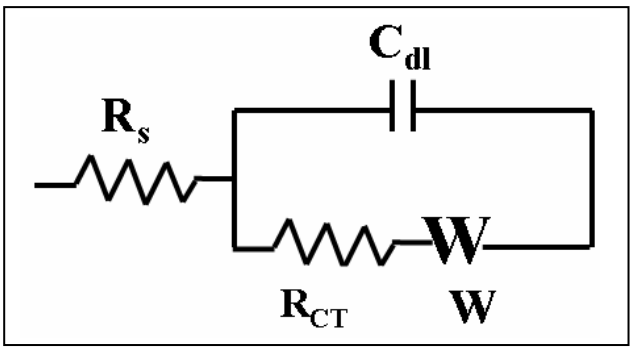

Scheme 4.2 Schematic representation of Randles equivalent circuit used for analyzed impedance data, where R_S is solution resistance, R_{CT} is charge transfer resistance, C_{dl} is double layer capacitance and W is Warburg impedance.

Accordingly, Figure 4.8 (a) shows the superimposed complex plane impedance plots of these Au MPCs under OCP and various cathodic dc bias corresponding to various charge steps (-1), (-2), (-4) and (-6), whereas the semicircle fitted with the high frequency part has been indicated in Figure 4.8 (b). The schematic representation of Randles equivalent circuit used for analyzed impedance data is shown in Scheme 4.2, where R_S is solution resistance, R_{CT} is charge transfer resistance, C_{dl} is double layer capacitance and W is Warburg impedance. Various parameters calculated from these plots along with corresponding charge steps have been summarized in Table 4.4. Furthermore, Figure 4.9 (a) shows the plot of applied potentials vs. IZI, which accounts for lowering of the impedance at higher charge, possibly due to the presence of surface

states on lower charge state particles. Accordingly, Figure 4.9 (b) shows the superimposed variation of R_{CT}, R_s and C_{dl} with applied potentials, which indicate that R_{CT} decreases while C_{dl} increases with increase of applied potentials.

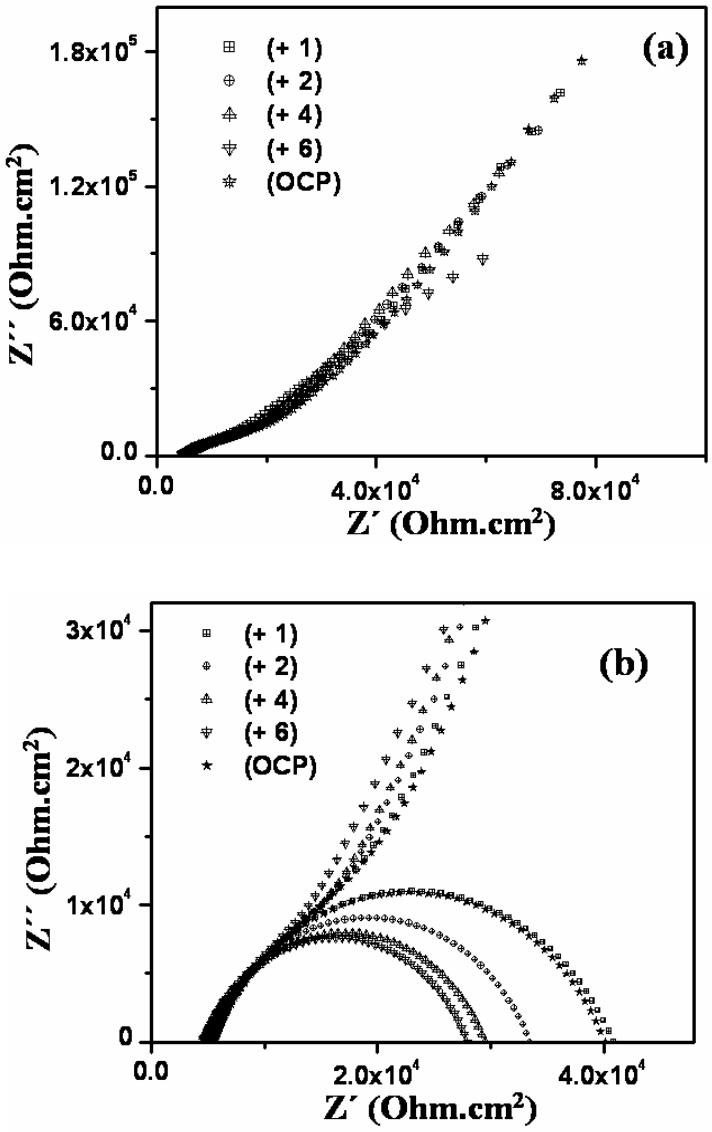

Figure 4.7 (a) Complex plane impedance plots of Au MPCs in CH_2Cl_2 on a Pt disc (0.5 mm diameter under OCP and various anodic dc bias corresponding to various charge steps (+1), (+2), (+4) and (+6); (b) the superimposed high frequency part of these plots, after fitting with the Randles equivalent circuit.

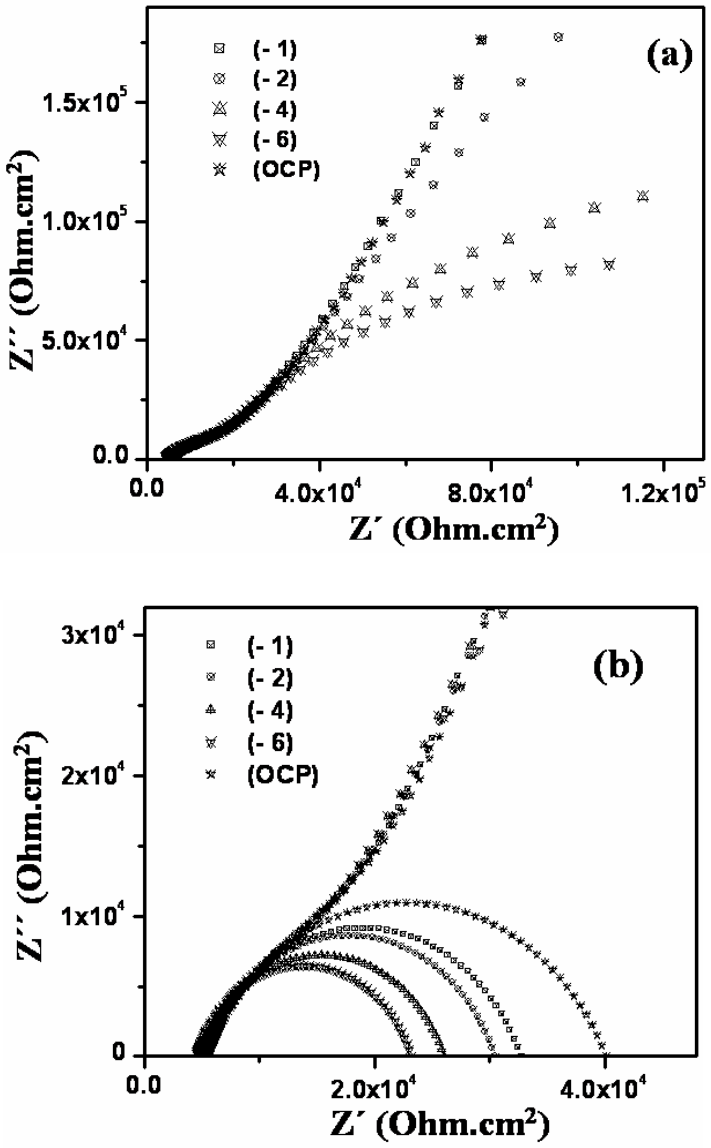

Figure 4.8 Complex plane impedance plots of Au MPCs in CH_2Cl_2 on a Pt disc (0.5 mm diameter) under (a) OCP and various cathodic dc bias corresponding to various charge steps (-1), (-2), (-4) and (-6); (b) the superimposed high frequency part of these plots, after fitting with the Randles equivalent circuit.

The calculated standard rate constants of the one electron QDL charging process at various charge states also have been summarized in Table 4.4 using the following relationship,

$$k = RT / n^2 F^2 R_{CT} C_n \qquad (4.11)$$

assuming n = 1, $C_n = C^*(O) = C^*(R) = (9.5 \times 10^{-7}$ mol.cm$^{-3})$, $\alpha = 0.5$, T = 273 K and the value of R_{CT} has been obtained from the fitted semicircle in the real axis as shown in Table 4.4. The variation of the standard rate constant (k) with applied potential has been plotted in Figure 4.9 (c), where higher charge state particles reveal higher rate constant. However, the reversible features observed in voltammetry (Figure 4.4) especially for scan rates below 100 mV/s do not agree with this sluggish nature and this could be justified due to various deviations from the ideal semi-infinite diffusion boundary condition due to adsorption, assumption of symmetric energy barrier, involvement of complex interactions between these MPCs, additional migrational contribution due to the charged nature of MPCs etc. Further studies are desired to unravel the exact reasons for this discrepancy.

The diffusion coefficients are estimated for various charge state particles by analyzing the lower frequency part of the impedance plots (Warburg impedance), considering, diffusion as the sole mode of mass transport. The linearly fitted modulus of the real and imaginary part of the impedance data (3.76 Hz to 0.464 Hz) with $\omega^{-1/2}$ are superimposed in Figure 4.10 (a) and (b) for anodic and cathodic processes respectively. The estimated diffusion coefficient (D_C) values at various charge states have been summarized in Table 4.4, after extracting from the slope (σ) of the linearly fitted modulus of the real and imaginary part using the following relationship (4.12):

$$\sigma = \sqrt{2}\, RT / A\, n^2 F^2 D_C^{1/2} C_n \qquad (4.12)$$

assuming n = 1, A = area of the electrode (1.96×10^{-3} cm^2), $D_O = D_R = D_C$, $C_n = C^*(O) = C^*(R) = (9.5 \times 10^{-7}$ mol.cm$^{-3})$ and T = 273 K.

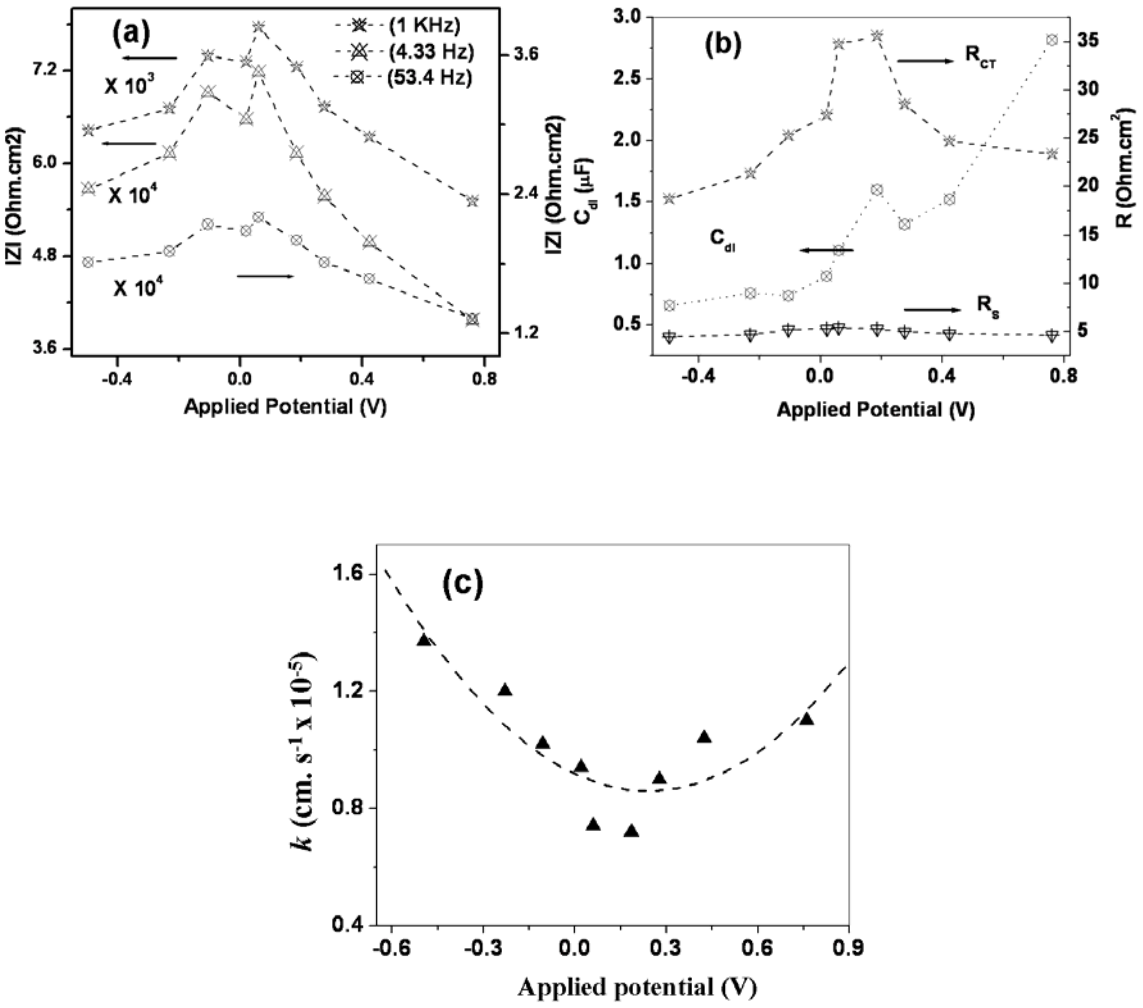

Figure 4.9 (a) Plots of applied potential vs. IZI at three different frequencies (*viz.* 1 KHz, 53.4 Hz and 4.33 Hz), showing the decrease of impedance at higher charge, possibly due to the presence of surface states on lower charge state particles. (b) The superimposed variation of R_{CT}, R_s and C_{dl} with applied potentials, showing a decrease of R_{CT} and increase of C_{dl} with increased of applied potentials. (c) The variation of the standard rate constant (k) with applied potential suggesting higher rate constant for particles with higher charge states.

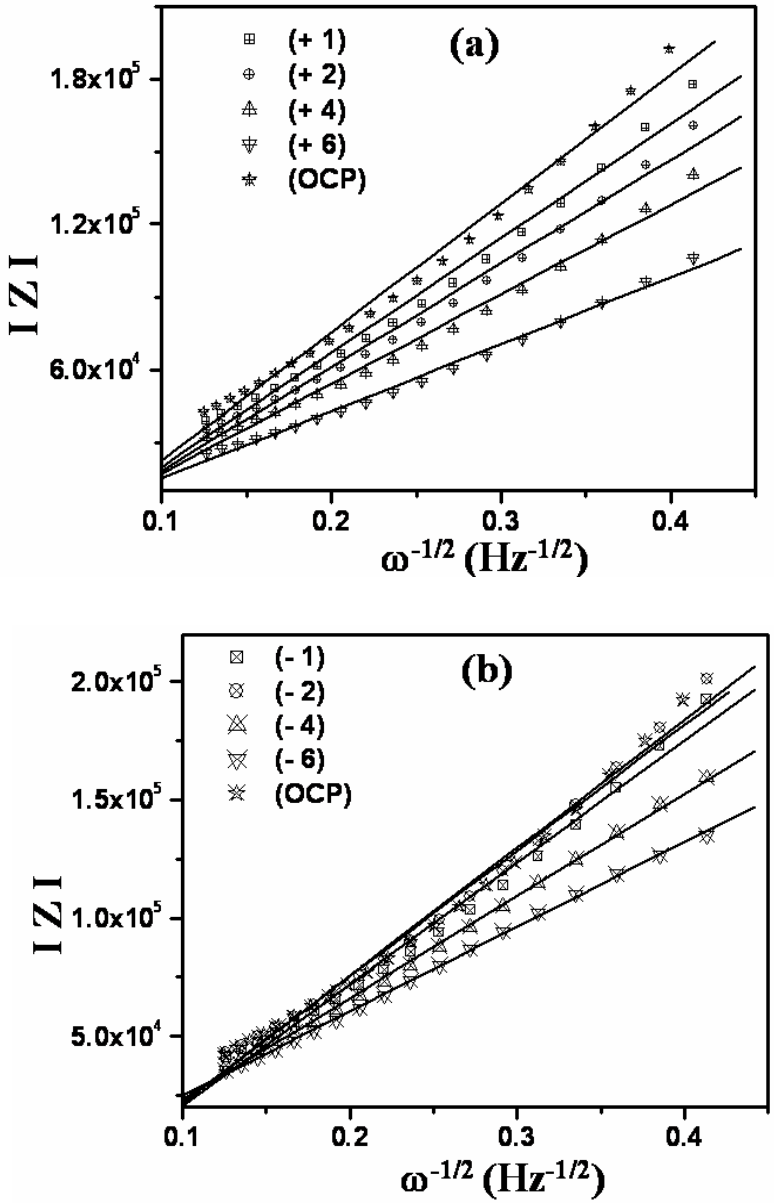

Figure 4.10 Superimposed linearly fitted (R^2 > 0.99) modulus of the real and imaginary part of impedance data (3.76 Hz to 0.464 Hz) with $\omega^{-1/2}$ under (a) anodic and (b) cathodic applied dc bias potentials as shown in Table 4.4.

Table 4.4 Various parameters, such as solution resistance (R_S), charge transfer resistance (R_{CT}), double layer capacitance (C_{dl}), standard rate constant (k) and diffusion coefficient (D_C) calculated from the impedance measurements along with Stokes-Einstein equation. The diffusion coefficient values are comparable with values shown at Table 4.3

Charge State (DPV)	Applied Potential	R_{CT} (Ohm. cm^{-2}) x 10^3	R_S (Ohm. cm^{-2}) x 10^3	C_{dl} (μF)	k (cm. s^{-1}) x 10^{-5}	σ (Ohm. $cm^{-2}.s^{-1/2}$)	D_C ($cm^2.s^{-1}$) x 10^{-7}	D_{SE} (x 10^{-7} $cm^2.s^{-1}$)
+6	0.70	23.35	4.63	2.82	1.10	277126.5	2.67	
+4	0.42	24.71	4.80	1.52	1.04	369729.0	1.84	
+2	0.28	28.52	5.00	1.32	0.90	428002.2	1.87	
+1	0.19	35.62	5.28	1.60	0.72	472642.4	1.53	
OCP	0.06	34.76	5.40	1.11	0.74	531373.4	1.21	14.7
-1	0.02	27.42	5.29	0.90	0.94	515216.0	1.29	
-2	-0.11	25.27	5.20	0.74	1.02	541246.0	1.16	
-4	-0.23	21.37	4.70	0.76	1.20	431390.0	1.84	
-6	-0.50	18.72	4.47	0.66	1.37	357823.8	2.67	

4.4.3 Effect of Charge Steps on Diffusion Coefficient

Interestingly, the experimentally calculated D_C values using chronoamperometry and impedance have been found to increase with the increment of the core charges as shown in Figure 4.11 (a and b). However, the experimentally calculated D_C values are found to be smaller compared to the estimated diffusion coefficient (D_{SE} = 14.7 x 10^{-7} $cm^2.s^{-1}$) using modified Stokes-Einstein equation [$D_{SE} = k_BT/2\pi\eta d_H$]. The D_{SE} is the diffusion coefficient of MPCs in the solution assuming no charge on it, where, k_B is the Boltzman constant, T absolute temperature (here 273 K), η the solvent viscosity

(viscosity of CH_2Cl_2 at 273 K is 0.533 cp) and d_H the hydrodynamic diameter of the MPC (twice the chain length added to the diameter of the Au MPCs, i.e., 7.67 nm).[42,43] This anomaly of theoretical diffusion coefficient value with experimental results might be due to the weakly attractive nature of the MPCs, which has not been considered in the Stokes-Einstein equation. Several other factors, like contribution due to migration and interactions with other charged or uncharged MPCs, effect of interdigitation of chains on MPC surface, supporting electrolyte anions or cations and solvent molecules, might possibly slow down the experimental D_C values.[44]

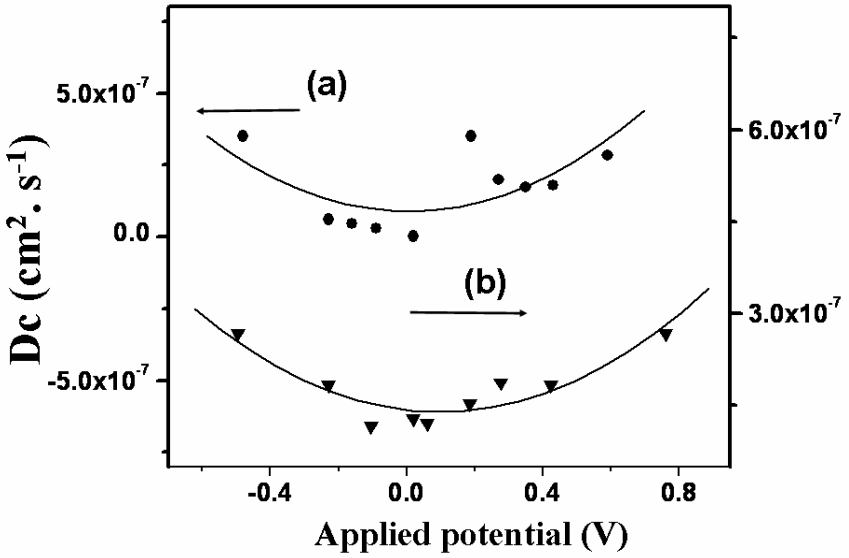

Figure 4.11 Variation of diffusion coefficients (D_C) with applied potentials as estimated from (a) chronoamperometry and (b) impedance analysis causing an increase in Dc with increment of core charges.

The potential dependent variation of D_C is the direct evidence for the presence of interparticle interactions, where the lower charge state particles are more attractive than the one with higher charge states. The highly charged particles might be repulsive due to the effective overlap of double layers, which is expected to increase with increasing the core charge. Thus for the case of MPCs possessing a lower charge state, there is a

balance between van der Waals (attractive) and electrostatic (repulsive) interactions, whereas MPCs having higher charge state can experience repulsive force as the major effective interaction. These reasons justify the preliminary experimental evidence for the interparticle interaction of charged MPCs as demonstrated by the charge state dependent variation of diffusion coefficients.

4.5 Conclusions

Our electrochemical and STM results demonstrate that the single electron transfer features of larger sized Au MPCs are accessible, despite their higher capacitance values. More specifically, voltammetry reveals high population of charging events, whereas STS exhibits highly nonlinear I-V as an evidence for the single electron transport. We believe that these unique single electron transfer features of these Au MPCs along with their preparative simplicity will have attendant applications for designing nanoelectronic devices. The effective interactions of the charged MPCs have been evidenced from the estimation of diffusion coefficient values of various charged particles, illustrating that the higher core charge enables these MPCs to move fast along with an increase in electron transfer rate constant. This charge state dependent variation of diffusion coefficient indicates that the repulsive forces are more dominant compared to attractive ones at higher core charge states, whereas there is a delicate balance between both attractive and repulsive forces at lower core charge particles. We believe that these results would help to understand the interactions of charged MPCs in solution, essential for several important applications.

4.6 References

1. Hunter, R. J. *Introduction to Modern Colloid Science;* Oxford University Press: Oxford; 1993
2. Israelachvili, J. *Intermolecular & Surface Forces*, 2nd ed.; Academic Press: London, 1991.
3. Daniel, M.-C.; Astruc, D. *Chem. Rev.* **2004**, *104*, 293.
4. (a) Whitesides, G. M. Grzybowski, B. *Science* **2002**, *295*, 2418. (b) Collier, C. P.; Vossmeyer, T.; Heath, J. R. *Annu. Rev. Phys.Chem*. **1998**, *49*, 371 and references therein.
5. (a) Boncheva, M., Bruzewicz, D. A.; Whitesides, G. M. *Pure Appl. Chem.* **2003**, *75*, 621. (b) Murray, C. B.; Kagan, C. R.; Bawendi, M. G. *Annu. Rev. Mater. Sci.* **2000**, *30*, 545.
6. (a) Murray, C. B.; Norris, D. J.; Bawendi, M. G. *J. Am. Chem. Soc.* **1993**, *115*, 8706. (b) Shah, P. S.; Holmes, J. D.; Johnston, K. P.; Korgel, B. A. *J. Phys. Chem. B* **2002**, *106*, 2545. (c) Saunders, A. E.; Korgel, B. A. *J. Phys. Chem. B* **2004**, *108*, 16732. (d) Rabani, E.; Reichman, D. R.; Geissler, P. L.; Brus, L. E. *Nature* **2003**, *426*, 271. (e) Korgel, B. A.; Fullam, S.; Connolly, S.; Fitzmaurice, D. *J. Phys. Chem. B* **1998**, *102*, 8379.
7. (a) Ge, G.; Brus, L. E. *J. Phys. Chem. B* **2000**, *104*, 9573. (b) Sigman, M. B., Jr.; Saunders, A. E.; Korgel, B. A. *Langmuir* **2004**, *20*, 978. (c) Shah, P. S.; Holmes, J. D.; Doty, R. C.; Johnston, K. P.; Korgel, B. A. *J. Am. Chem. Soc.* **2000,** *122*, 4245.
8. Schmid, G.; Baumle, M.; Greekens, M.; Heim, I.; Osemann, C.; Sawitwoski, T. *Chem. Soc. Rev.* **1999**, *28*, 179.
9. Schmid , G.; Corain, B. *Eur. J. Inorg. Chem.* **2003**, *2003*, 3081.
10. Gittins, D. I.; Bethell, D.; Schiffrin, D. J.; Nichols, R. J. *Nature* **2000**, *408*, 67.
11. Andres, R. P.; Bein, T.; Dorogi, M.; Feng, S.; Jenderson, J. I.; Kubiak, C. P.; Mahoney, W.; Osifchin, R. G.; Reifenberger, R. *Science* **1996**, *272*, 1323.
12. Dorogi, M.; Gomez, J.; Osifchin, R.; Andres, R. P.; Reifenberger, R. *Phy. Rev. B* **1995**, *52*, 9071.
13. Feldheim, D. L.; Keatig, C. D. *Chem. Soc. Rev.* **1998**, *27*, 1.
14. Thomas, P. J.; Kulkarni, G. U.; Rao, C. N. R. *Chem. Phys. Lett.* **2000**, *321*, 163.

15. Ingram, R. S.; Hostetler, M. J.; Murray, R. W.; Schaaff, T. G.; Khoury, J. T.; Whetten, R. L.; Bigioni, R. L.; Guthrie, D. K.; First, P. N. *J. Am. Chem. Soc.* **1997,** *119*, 9279.
16. Pietron, J. J.; Hicks, J. F.; Murray, R. W. *J. Am. Chem. Soc.* **1999**, *121*, 5565.
17. Chen, S.; Ingram, R. S.; Hostetler, M. J.; Pietron, J. J.; Murray, R. W.; Schaaff, T. G.; Khoury, J. T.; Alvarez, M. M.; Whetten, R. L. *Science* **1998**, *280*, 2098.
18. Quinn, B. M.; Lijeroth, P. Ruiz, V.; Kaaksonen, T.; Kontturi, K. *J. Am. Chem. Soc.* **2003**, *125*, 6644.
19. Hicks, J. F.; Templeton, A. C.; Chen, S.; Sheran, K. M.; Jasti, R.; Murray, R. W.; Debord, J.; Schaaff, T. G.; Whetten, R. L. *Anal. Chem.* **1999**, *71*, 3703.
20. Chen, S.; Murray, R. W.; Feldberg, S. W. *J. Phys. Chem. B* **1998**, *102*, 9898.
21. Templeton, A. C.; Pietron, J. J.; Murray, R. W.; Mulvaney, P. *J. Phys. Chem. B* **2000**, *104,* 564.
22. (a) Shim, M.; Guyot-Sionnest, P. *Nature* **2000**, *407*, 981. (b) Wang, C. J.; Shim M.; Guyot-Sionnest, P. *Science* **2000**, *291,* 2390.
23. (a) Song, Y.; Murray, R. W. *J. Am. Chem. Soc.* **2002**, *124,* 7096. (b) Guo, R.; Song, Y.; Wang, G.; Murray, R. W. *J. Am. Chem. Soc.* **2005**, *127,* 2752.
24. (a) Mattoussi, H.; Cumming, A. W.; Murray, C. B.; Bawendi, M. G.; Ober, R. *Phys. Rev. B* **1998**, *58*, 7850. (b) Striolo, A.; Ward, J.; Prausnitz, J. M.; Parak, W. J.; Zanchet, D.; Gerion, D.; Milliron, D.; Alivisatos, A. P. *J. Phys. Chem. B* **2002**, *106*, 5500.(c) Korgel, B. A.; Fitzmaurice, D. *Phys. Rev. B* **1999**, *59*, 14191. (d) Henderson, D.; Duh, D. M.; Chu, X.; Wasan, D. *J. Colloid Interface Sci.* **1997**, *185*, 265.
25. (a) Rabani, E.; Egorov, S. A. *J. Chem. Phys.* **2001**, *115*, 3437. (b) Rabani, E.; Egorov, S. A. *Nano Lett.* **2002**, *2*, 69.
26. Amman, M.; Wilkins, R.; Ben-Jacob, E.; Maker, P. D.; Jaklevic, R. C. *Phy. Rev. B* **1991**, *43*, 1146.
27. Hanna, A. E.; Tinkham, M. *Phys. Rev. B.* **1991**, *44*, 5919.
28. Kaiser, W. J.; Jaklevic, R. C. *Surf. Sci.* **1987**, *181*, 55.
29. Binning, G.; Smith, D. P. E. *Rev. Sci. Instrum.* **1986**, *57*, 1688.

30. Dharmadhikari, C. V. Final Consolidated Report on the project entitled, *"Development of Scanning Tunneling Microscope for Surface Studies"*, BRNS, Department of Atomic Energy, Govt. of India, 1996.
31. SPIP stands for Scanning Probe Image Processor, which is software for Scanning Probe Microscopy and other Microscopy Techniques developed by Image Metrology, Denmark.
32. Whetten, R. L.; Khoury, J. T.; Alvarez, M. M.; Murthy, S.; Vezmar, I.; Wang, Z. L.; Stephenes, P. W.; Cleveland, C. L.; Luedtke, W. D.; Landman U. *Adv. Mater*. **1996,** *8*, 428.
33. Wilcoxon, J. P.; Martin, J. E.; Provencio, P. *J. Chem. Phys.* **2001**,*115*, 998.
34. Templeton, A. C.; Wuelfing, W. P.; Murray, R. W. *Acc. Chem. Res.* **2000**, *33*, 27.
35. http://qt.tn.tudelft.nl/research/set/asymIV/SETIV.html
36. Datar, S.; Kumar, M.; Sastry, M.; Dharmadhikari, C. V. *Colloids and Surfaces A* **2003**, *232/1*, 11.
37. Bard, A. J.; Faulkner, L. R. *Electrochemical Methods, Fundamentals and Applications; 2nd ed.* John Wiley & Sons: New York, 2001.
38. Hicks, J. F.; Zamborini, F. P.; Osisek, A. J.; Murray, R. W. *J. Am. Chem. Soc.* **2001**, *123*, 7048.
39. Chidsey, C. E. D.; Murray, R. W. *J. Phys. Chem.* **1986**, *90*, 1479.
40. Laviron, E. *J. Electroanal. Chem.* **1981**, *122*, 37.
41. (a) Ulman, A. *J. Mater. Ed.* **1989**, *11*, 205. (b) Porter, M. D.; Bright, T. B.; Allara, D. L.; Chidsey, C. E. D. *J. Am. Chem. Soc.* **1987**, *109*, 3559. (c) Hamaker, H. C. *Physica IV* **1937**, 1058.
42. Terrill, R. H.; Postelethwaite, T. A.; Chen, C.; Poon, C. D.; Terzis, A.; Chen, A.; Hutchison, J. E.; Clark, M. R.; Wignall, G.; Londono, J. D.; Superfine, R.; Falvo, M.; Johnson Jr., C. H.; Samulski, E. T.; Murray, R. W. *J. Am. Chem. Soc.* **1995**, *117*, 12537.
43. (a) Miles, D. T.; Murray, R. W. *Anal. Chem.* **2003**, *75*, 1251. (b) Wuelfing, W. P.; Templeton, A. C.; Hicks, J. F.; Murray, R. W. *Anal. Chem.* **1999**, *71*, 4069.
44. Guidelli, R. *Electrified Interfaces in Physics, Chemistry and Biology*; Kluwer Academic Publishers, 1992.

Chapter 5

Electrochemical Investigation of Monolayer Protected Silver Nanoclusters*

In this chapter, the redox feature of dodecanethiol protected silver nanoparticles (size regime of 2-7 nm) films on a Pt electrode have been compared using the results from cyclic voltammetry (CV) in aqueous medium. In particular, these particles show irreversible voltammograms and the redox behaviour is indeed affected by the size as in agreement with the theoretical calculations of Kubo gap. Further, an alternate one step method for the preparation of Ag nanoparticles in nonaqueous medium using an electron transfer agent triethylamine (TEA) has been depicted along with their electrochemical features.

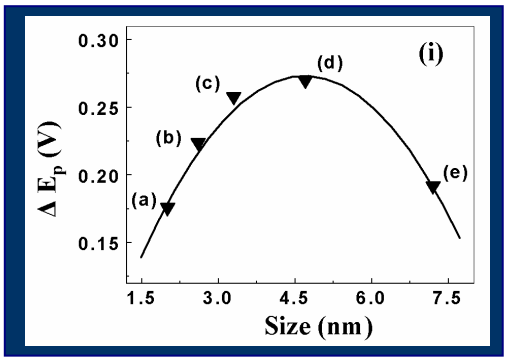

---

* A part of the work has been published in "***Phys. Chem. Chem. Phys.*** **2004**, *6*, 1304" and another part in "***Chem. Commun.*** **2002**, 76".

5.1 Introduction

The size and shape dependent properties of metal nanoparticles (smaller than 15 nm or so) are often different from that of the bulk, leading to the expectation that the electrochemistry of nanometer scale particles should also differ from that of their bulk analogues.[1-6] For example, in case of silver, the lattice constant of the fcc unit cell is contracted by as much as 9% for nanoparticles,[7] while the melting point is depressed by as much as 700 °C.[7-9] Moreover, electronic properties including the photoelectron yield[10-12] and the energy of the plasmon resonance absorption also exhibit similar remarkable size dependence.[13] These observations lead to the expectation that the electrochemical properties of silver nanoparticles should also be size dependent. Accordingly, as discussed in chapter 1, the standard redox potential (E^0) of the nanoparticles shifts negatively from the corresponding bulk E^0, provided that the surface free energy is same for both.[14-16] This is further confirmed by the pulse radiolysis experiments, where a single Ag atom exhibits an E^0 of -1.8 V vs. normal hydrogen electrode (NHE) while the silver trimer (i.e., Ag_3) is found to have an E^0 near –1.0 V as compared to + 0.799 V for bulk Ag.[17-20] The silver clusters are therefore predicted to be stronger reducing agent than zinc ($E^0_{Zn/Zn2+}$ = -0.76V), as they can readily reduce many inorganic and organic compounds.[21-23] Spectroelectrochemical study of small polyacrylic acid coated silver particles in an aqueous solution using an optically transparent thin layer electrode reveals that the position of the surface plasmon band is blue shifted during electron accumulation, depending on the applied potential.[24]

In preceding chapters (2-4), we have discussed several aspects of monolayer protected Au nanoclusters (Au MPCs) and due to similarities of Au and Ag, it is important to extend these studies to silver. Accordingly, this chapter is devoted to the discussion of synthesis, characterization and electrochemical features of monolayer protected silver nanoclusters (Ag MPCs) due to their immense importance in catalysis, photochemistry and nanoelectronics.[24-26] In the first part of this chapter, the size dependent redox features of dodecanethiol (DDT) protected Ag nanoparticles in aqueous medium have been investigated as the redox property of silver is well known due to their potential applications in catalysis, photography, optical property manipulation

or anti-microbial and other biological activities.[24,25] We find that the redox behaviour of Ag core is affected by size as in agreement with the theoretical calculations on the basis of Kubo gap. More specifically the separation between oxidation and reduction peaks (ΔE_p) in cyclic voltammograms, increases with increase in size and after reaching a maxima (3.5-6 nm), decreases with further increase in size despite the presence of dielectric capping layers of organic molecules. As kinetic parameters are directly related with ΔE_p value, our results suggest that the electron transfer facility should decrease with increase in size in a similar manner. Further, in the last section, an alternate one step method of the preparation of Ag MPCs in nonaqueous medium using a reducing agent triethylamine (TEA) has been demonstrated along with their electrochemical features. TEA has been selected on the basis of its unique properties as reducing agent in photochemical reactions, miscibility in most of the organic solvents and the use of amine group for stabilizing nanoclusters.[27] DDT and tridecylamine (TDA) have been used along with TEA to enhance the monodispersity and stability. These particles exhibit redox activity depending on the nature of capping molecules, which can be effectively utilized in suitable electrocatalytic reactions.

5.2 Experimental Section

5.2.1 Materials

Dodecanethiol (99%), tridecylamine, $NaBH_4$, $LiClO_4$ and KCl obtained from Aldrich and $AgNO_3$ from Merck were used as received, while triethylamine, toluene and acetonitrile are of AR grade and were used after further purification. In all these experiments deionized water from Milli-Q system was used. Ag-benzoate was prepared by using silver nitrate and benzoic acid and use used after recrystallization from water as a pure crystalline solid.

5.2.2 Synthesis of Different Sized Ag MPCs

Ag nanoparticles of different sizes were synthesized by a modified Brust's method.[28] In brief, 100 ml of 1 mM aqueous $AgNO_3$ solution was reduced by 0.4 M $NaBH_4$ aqueous solution in the presence of 100 ml of 3 mM DDT in toluene under vigorous stirring. Yellow color initially appeared in the aqueous layer was gradually

transferred into dark brown in the organic layer. Different sized particles (a-e) were obtained by tuning the reaction temperature and the metal salt to DDT ratio. More specifically, two types of particles, (a) and (c) were synthesized at 0 °C, keeping the metal to DDT ratio as 1 : 3 and 1 : 1.5 respectively, whereas, particles (b), (d) and (e) were synthesized at room temperature by varying the metal to DDT ratio as 1 : 3, 2 : 3 and 1 : 1.5 respectively. Particles were concentrated under vacuum using a rotary pump (10^{-2}- 10^{-3} torr) at 40 °C and precipitated by the addition of acetonitrile and the resultant brown powder was collected by centrifugation. All the samples were further redispersed in toluene for solution phase investigations.

5.2.3 Characterization Techniques

Optical measurements were recorded using Shimadzu UV-2101 PC spectrophotometer using a quartz cell (10 mm path). The spectra were background subtracted using the same solvent.

Transmission electron microscopic (TEM) measurements were carried out on a JEOL model 1200EX instrument operated at an accelerating voltage of 120 kV. A drop of toluene containing Ag nanoparticles was placed on an amorphous carbon film (400 mesh), deposited on a commercial copper grid for electron microscopy. After slow evaporation of toluene at room temperature, the grid was introduced in the electron microscope chamber and the images were recorded.

Fourier transform infrared spectroscopic (FTIR) measurements were carried out on a Shimadzu PC-8201 instrument in the diffuse reflectance mode at a resolution of 2 cm^{-1} using KBr pellet.

X-ray photoelectron spectroscopic (XPS) measurements of Ag nanoparticles were carried out as dropcasted film on glass slide by using VG MicroTech ESCA 3000 instrument at a pressure >1 × 10^{-9} torr. The general scan and Ag 3 d, C 1s and S 2p core-level spectra were recorded with unmonochromatized Mg $K\alpha$ radiation (photon energy = 1253.6 eV) at a pass energy of 50 eV and an electron takeoff angle (angle between electron emission direction and surface plane) of 60°. The overall resolution

was ~ 1 eV for the XPS measurements. The core-level binding energies (B.E.s) were aligned taking the adventitious carbon binding energy as 285 eV.

Cyclic voltammetric experiments (CV) were performed on an Autolab PGSTAT30 (ECO CHEMIE) instrument using a standard three electrode cell, comprising Ag nanoclusters organized [few drops of Ag MPCs (≈1 mg/ml) were dropcasted and dried at ambient condition] on a Pt disc (4 mm diameter) as the working electrode, a large platinum flag as counter electrode and saturated calomel electrode (SCE) as reference.

5.3 Size Dependent Redox Features of Ag MPCs

5.3.1 Particle Characterization

Since the number of atoms present in the clusters influences almost all physical and chemical properties of nanoclusters, uncertainties in size dispersion often causes irreproducibility of cluster properties. One way to solve this problem is by carrying out precise fractionation with a variety of complex methods, such as solubility fractionation, chromatography, capillary electrophoresis and mass spectrometry.[29-31] Nevertheless, a complete characterization using various techniques is essential in order to get information about their structure, morphology and composition prior to any investigation of their size-dependent property. In the present study, the particles are characterized initially from their surface plasmon resonance by UV-visible spectroscopy, whereas TEM along with selected area electron diffraction (SAED) gives the size dispersion and crystal structure. FTIR and XPS techniques are also used to characterize these particles, in particular to get the information about surface composition and oxidation state.

Figure 5.1 (a-e) shows UV-visible spectra of differently sized particles [corresponding to particle (a-e)] in toluene, demonstrating that the plasmon absorption of metal particles is strongly affected by its size distribution. The peak position of different Ag nanoparticles (a-e) are significantly broadened and more importantly there is a blue shift (24 nm), suggesting an increase in size as reported recently.[30] The UV-visible peak positions are summarized in Table 5.1. Although particle size can be calculated from the UV-visible absorption maxima using Mie theory, the results need not always agree because several changes occur in the surface structure due to the adsorption of the

capping agents.[13,32,33] A plot of the plasmon peak position vs. particle size (from TEM measurements) suggests significant nonlinearity (Inset of Figure 5.1). The peak broadening and shift observed in the UV-visible spectra are attributed to the aggregation or the formation of a superlattice type of structure, which is in good agreement with TEM results. For example, the peak broadening and shift are well known for the MPC superlattices due to intercluster plasmon coupling.[34]

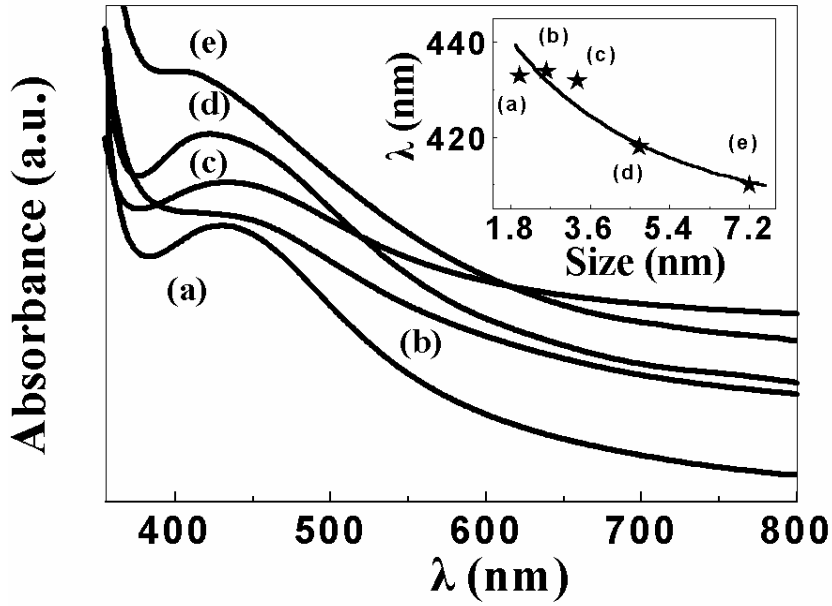

Figure 5.1 (a-e) UV-visible absorption spectra of different sized DDT protected Ag nanoparticles corresponding to (a-e) in toluene; inset showing the nonlinear variation of the peak position with particle size.

Figure 5.2 (a-e) shows TEM images along with their particle size distribution of different Ag nanoparticles (a-e). In particular, Figure 5.2 (a) shows the TEM image of the smallest sized particle (a) of the series with an average particle size of 2±0.4 nm, with reasonable monodispersity. Similarly, Figure 5.2 (b, c and d) reveals nearly monodispersed particles (b), (c) and (d) with an average particle size of 2.6, 3.3 and 4.7±0.4 nm. In contrast, TEM image of particle (e) shows [Figure 5.2 (e)] some degree of

polydispersity with an average particle size of 7.2±0.4 nm, perhaps arising from unfavorable experimental conditions, like low capping agent to metal salt ratio and preparation at relatively higher temperature.

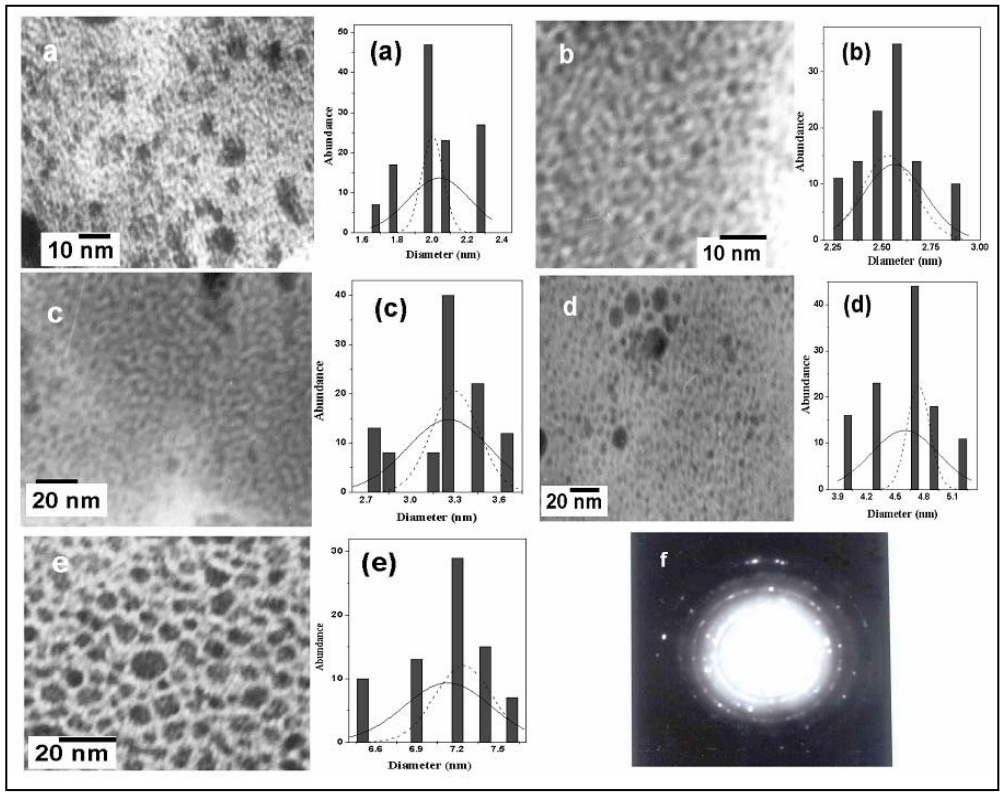

Figure 5.2 (a-e) TEM images of the "as prepared" different sized Ag MPCs (a-e) along with their respective particle size distribution. The representative SAED patterns of DDT capped Ag particles shown in (f) for particle (c), revealing bulk fcc crystalline structure with a lattice constant of 4.079 ^{0}A. For electron microscopy, a drop of toluene containing nanoparticles was placed on an amorphous carbon film of nearly 3 nm thickness, deposited on a commercial copper grid and dried at room temperature in air.

Interestingly, particles (a-c) show close packed superlattice type structure as illustrated in Figure 5.2 (a-c) due to their small and monodispersed nature, with an inter-cluster spacing of *ca.* 2.5 nm, corresponding to roughly double the chain length of the DDT, assuming some degree of chain interdigitation.[34-36] This array like features are

absent for particles (d-e), which may be due to larger size and polydispersity of particles as reported earlier.[37] Moreover, the crystallinity is restored in particles as illustrated by the representative selected area electron diffraction (SAED) pattern of the sample (c) in Figure 5.2 (f), which reveals fcc bulk crystal structure with a lattice constant of 4.079 ^{0}A; the planes are identified as (111), (220), (311), (331) and (422).

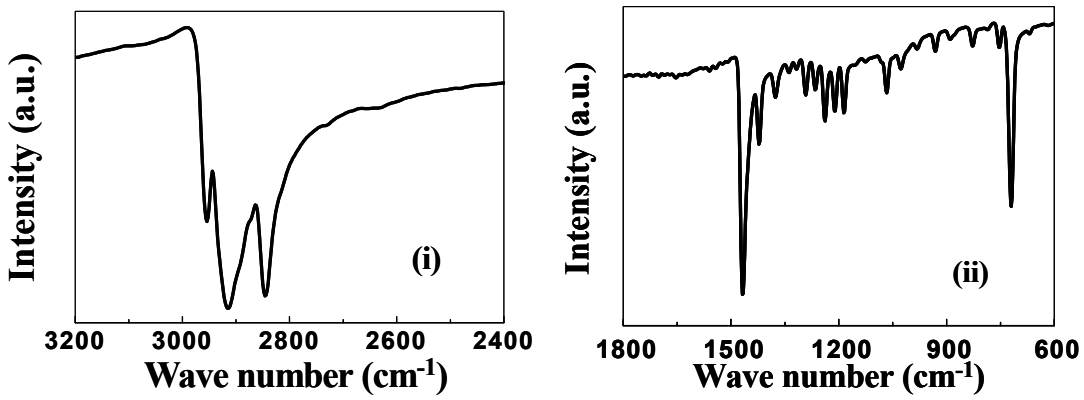

Figure 5.3 Representative FTIR spectrum of DDT capped Ag MPCs corresponding to particle (c) in the (a) 4000 to 450 cm^{-1} range, indicating C-H starching region and (b) n-alkane vibration region. The spectrum was recorded with diffuse reflectance mode using KBr pellet dispersion with a 2 cm^{-1} resolution.

In order to get a molecular level understanding of the surface passivation of these particles, FTIR spectra were recorded. The spectrum of DDT passivated surface shows several clearly resolved peaks indicating ordered and dense crystalline bulk alkane, especially for all the C-H stretching regions [Figure 5.3 (i)] as reported previously.[35,38] The high degree of conformational order is best evidenced by the position of the symmetric (d^+) and antisymmetric (d^-) CH_2 stretching peaks. Average values of 2849±1 and 2923±1 cm^{-1} for these peaks indicate an extremely high percentage of all-trans conformations. Disordered systems, such as liquid alkanes, display much higher values (2856 and 2928 cm^{-1} respectively), which have been convoluted to higher number of gauche defects.[38] The r^+ and r^- bands for methylene vibration have been identified as 2893±1 and 2956±1 cm^{-1} respectively.

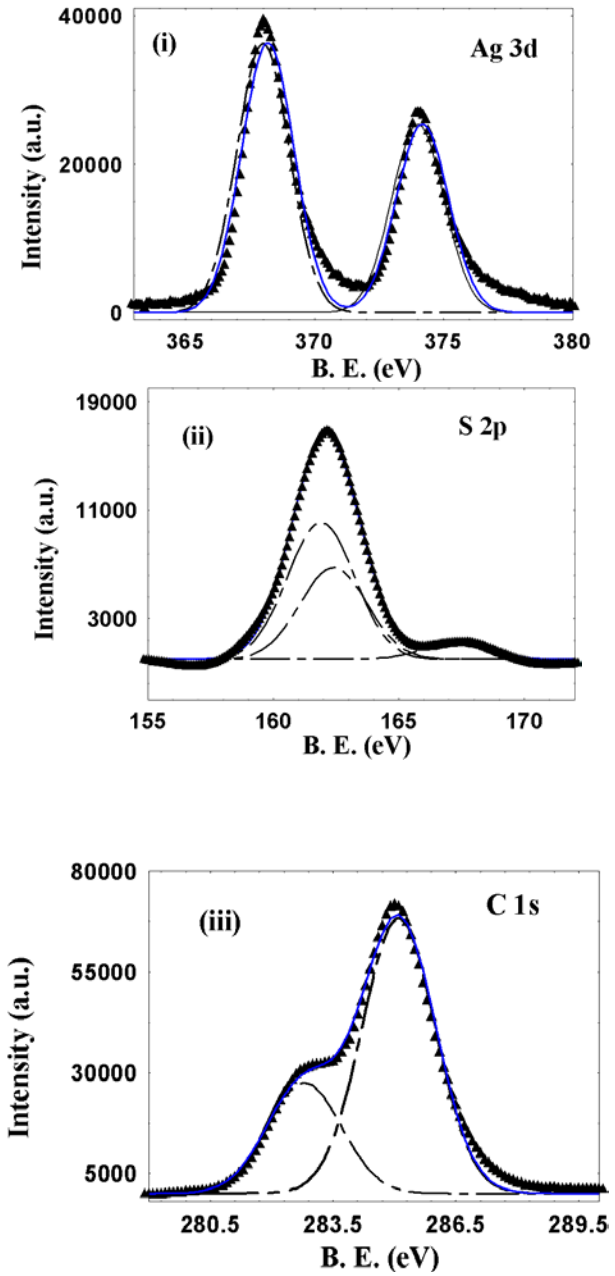

Figure 5.4 Representative X-ray photoelectron spectra of DDT capped Ag nanoparticles corresponding to particle (c), revealing core level information of (a) Ag 3d, (b) S 2p and (c) C 1s (experimental data points are shown as up triangle, resultant fitting curve as continuous line and individual fitted curves as dashed lines).

All other bands were assigned on the basis of n-alkane vibrations [Figure 5.3 (ii)]. For the spectrum in the region 1400-1500 cm^{-1}, all-trans scissoring modes have been observed, like methylene scissoring at ~1466 cm^{-1} and CH_2-S methylene scissoring at ~1424 cm^{-1}. The peak at 1379 cm^{-1} is attributed to the symmetric bending vibration of CH_2 groups, while the presence of large number of bands between 1200-1400 cm^{-1} corresponding to either twisting-rocking or wagging progression modes, is a strong evidence for the micro-environment of the alkanethiol monolayer on silver clusters.[39] The band at 1339 cm^{-1} in the spectrum is attributed to the end gauche conformation, while the bands at 1122 and 1070 cm^{-1} are assigned as $(c\text{-}c)_T$ and $(c\text{-}c)_g$ stretching modes respectively. The 700-800 cm^{-1} region comprises of two sets of bands, the first one due to methylene rocking and the other remaining due to C-S stretching. The intense peak at 720 cm^{-1} is assigned as the methylene-rocking mode, where a small shoulder near 720 cm^{-1} may be due to C-S stretching.[35, 38,39]

The XPS analysis of core level spectra of C 1s, Ag 3d and S 2p confirms the formation of Ag nanoparticles with the surface passivation of DDT. The peak position, line shape and peak to peak separation (≈ 6 eV) are the standard measure of the Ag oxidation state [Figure 5.4 (i)].[35]The B.E. for Ag 3d doublet (368.2 and 374.2 eV) is consistent with Ag^o oxidation state.[35] The S 2p doublet appears at 161.9 and 163.2 eV respectively [Figure 5.4 (ii)], which is in good agreement with those of previously reported values for chemically bound thiolate sulfur. [40,41]The shift in B.E. is neither due to the presence of free alkylthiol nor disulfide, as their B.E.s is expected to be much larger than 163 eV. Although there is a mild signature for the peak corresponding to thiolate moiety at 167.8 eV, it is possible to be originated from the beam induced damage as reported earlier for 2D SAM and for Au MPCs.[42] Figure 5.4 (iii) shows C 1s XP spectrum, where the deconvolation of the peak with respect to Gaussian fitting shows two distinct peaks at 282.8 and 285 eV respectively.[42] We have taken 285 eV peak as the reference peak, while peak at 282.8 eV may be due to the presence of carbide species, originating from differential sample charging. Since the peak positions were assigned on the basis of the C 1s peak at 285 eV, it does not affect the other B.E. values. The XPS result is in good agreement with FTIR results, which confirms the presence of DDT molecules on the surface of Ag particles.

5.3.2 Electrochemical Measurements

In order to understand the electrochemical behaviour of these differently sized Ag MPCs, samples were dropcasted on the Pt disc electrode from toluene dispersion and dried at room temperature in air prior to cyclic voltammetric experiments. Figure 5.5 (a-e) shows the scan rate dependent voltammograms of Ag MPCs corresponding to particles (a-e) in 0.1 M aqueous KCl upon anodic scanning, where nearly irreversible nature with varying peak to peak separation is evident. Accordingly, Figure 5.6 (a-e) shows representative cyclic voltammograms of these particles (a-e) at 100 mV/s scan rate and Table 5.1 summarizes the detailed analysis of the electrochemical parameters such as anodic (E_{Pa}) and cathodic (E_{Pc}) peak potentials, ΔE_P and $E_{1/2}$ from these voltammograms at 100 mV/s scan rate for all particles along with their surface plasmon peak positions (UV-visible) and their average size (TEM). For example, Figure 5.6 (a) shows the voltammograms of particle (a), revealing broad and prominent anodic peak as compared to cathodic peak, whereas Figure 5.6 (b-e) corresponding to particle (b-e), shows nearly irreversible behaviour.

The current peaks observed in the cyclic voltammetry (CV) are quite small, as MPC films are highly resistive; nevertheless, peaks are neither due to oxidation of thiol nor any electrochemical reaction of the supporting electrolyte as the potential window is quite small. In addition, these peaks are missing when base line voltammograms are taken under identical condition without Ag nanoclusters. Consequently, the electrochemical data suggests that, as prepared particles are more prone to oxidation compared to reduction, as the anodic peak is more distinct. The electrochemical reactions can be rationalized as, $Ag_n^0 \rightarrow Ag_n^+ + e^-$, followed by, $Ag_n^+ + Cl^- \rightarrow Ag_{n-1}^+ + AgCl + e^-$, whereas, the cathodic peak could be due to the possible reaction, $Ag_n^+ + e^- \rightarrow Ag_n^0$. The anodic peak of the couple is better resolved especially at higher scan rates and there is a slight dependence of scan rate on the peak potential, perhaps due to the insulating nature of the DDT layer on the metal cluster surface. The broad nature of redox peaks can also be due to the distribution of redox potentials corresponding to cluster dispersion,[43] while the plateau type behaviour of both oxidation and reduction peaks can be attributed to the microelectrode type behaviour.

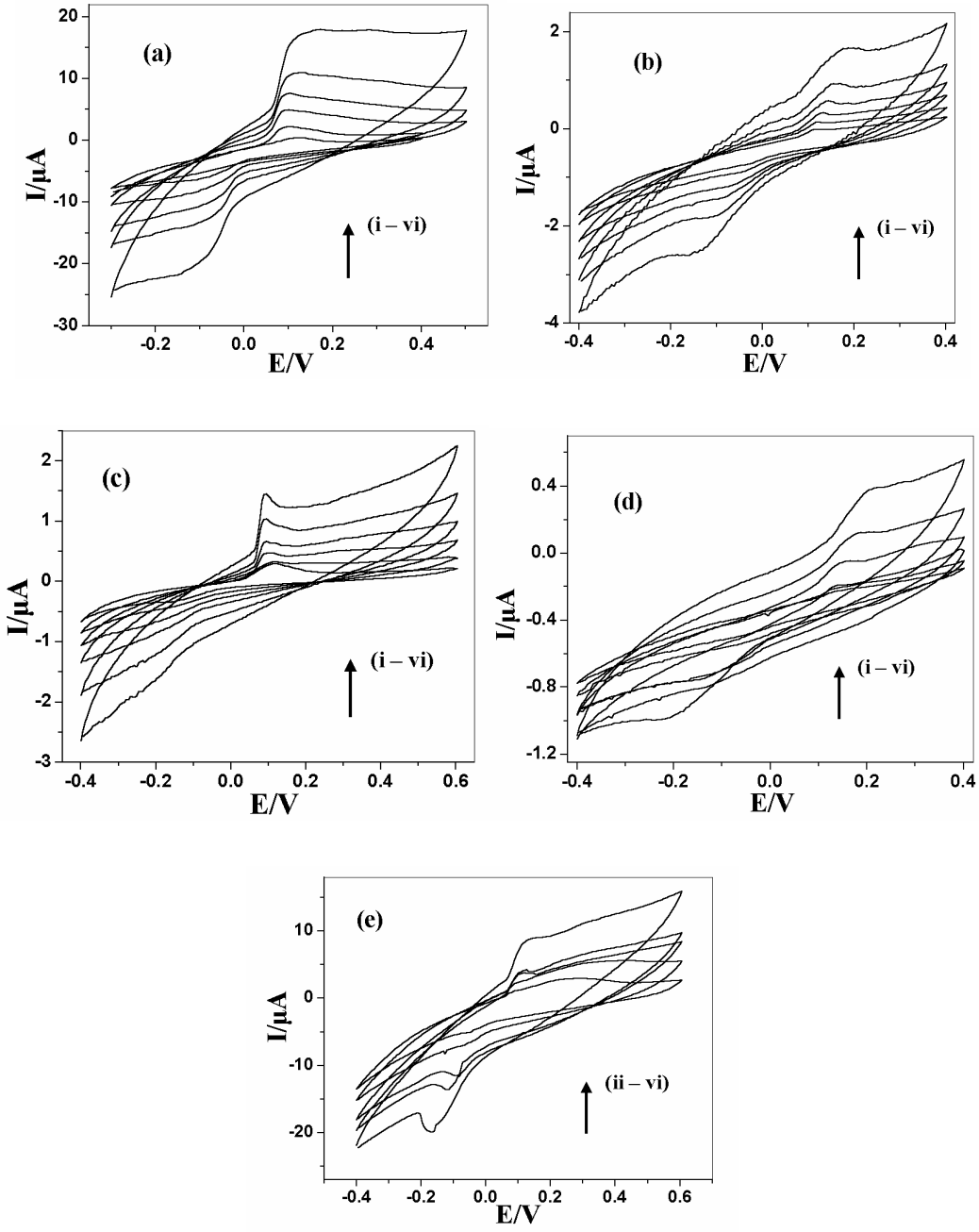

Figure 5.5 (a-e) Superimposed voltammograms corresponding to particles (a-e) at 10, 20, 50, 100, 200 and 500 mV/s scan rate (all in 2nd scan) in 0.1 M aqueous KCl using a modified Pt as working electrode, Pt flag as counter and SCE as reference. The anodic peak of the couple is better resolved especially at higher scan rates and there is a slight dependence of scan rate on the peak potentials, perhaps due to the insulating nature of the DDT layer on the metal cluster surface.

The difference in some of the features of voltammograms could be attributed to effectiveness of the capping agent and the population of the surface defects, like pinholes, grain boundaries, trapped solvents and high resistance of the MPC films.[43] Nevertheless, the presence of these alkyl chains does not obstruct electron transfer behaviour from the core as indicated by the capped nanoclusters, although the anodic peak is sharper than the cathodic one due to more facile oxidation process. The oxidation process after several cycles (> 50) causes a partial destruction of monolayer integrity and this reorganization is seen for all cases as a prominent anodic peak in comparison with the cathodic one. For example, Figure 5.7 shows both peaks significantly sharpened, suggesting the destruction of monolayers during the oxidative sweep of CV measurements.

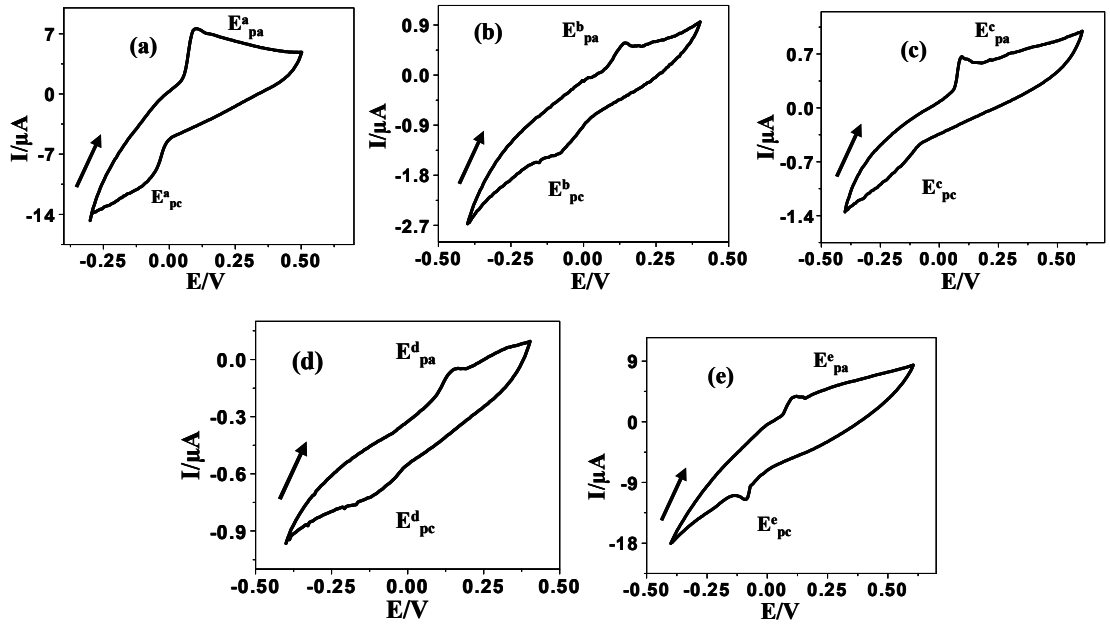

Figure 5.6 Representative cyclic voltammograms (a-e) of different sized DDT protected Ag nanoparticles (a-e) at 100 mV/s scan rate in 0.1 M aqueous KCl using a modified Pt as working electrode (all are in 2nd scans).

Table 5.1 Variations of surface plasmon peak positions and electrochemical parameters, such as E_{Pa}, E_{Pc}, ΔE_P and $E_{1/2}$ for 2-7 nm sized (from TEM) DDT capped Ag nanoclusters (a-e)

Cluster Type	Position of the plasmon peak (nm)	Size (TEM; ±0.4 nm)	E_{pa} (V)	E_{pc} (V)	ΔE_p (V)	$E_{1/2}$ (V)
(a)	433	2	0.096	-0.08	0.176	0.008
(b)	434	2.6	0.144	-0.080	0.224	0.032
(c)	432	3.3	0.094	-0.164	0.258	-0.350
(d)	418	4.7	0.150	-0.120	0.270	0.015
(e)	410	7.2	0.105	-0.087	0.192	0.009

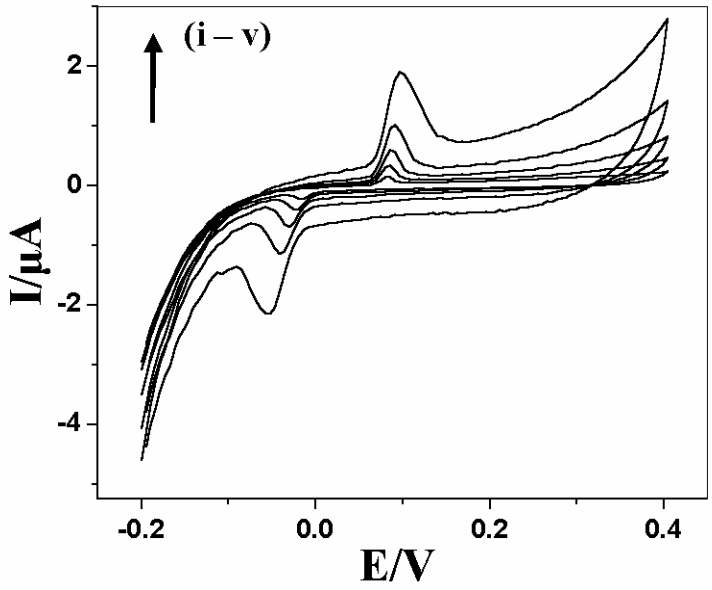

Figure 5.7 Representative cyclic voltammetric response of particle (c) at 20, 50, 100, 200 and 500 mV/s scan rate after 50 scans 0.1 M aqueous KCl using a modified Pt as working electrode, Pt flag as counter and SCE as reference, where both the peaks are sharpened enough, suggesting the destruction of monolayers during oxidative sweep of CV measurements.

The peak nature or position of voltammograms does not change significantly, if the supporting electrolyte, KCl, is replaced by (a) KNO_3 or (b) Na_2SO_4 as shown in Figure 5.8 for particle (c). The electrochemical reaction is believed to occur via electron tunneling across the particle and the electrode through organic capping molecules.[24] The mechanism of electron transfer has been speculated to include contact electrification, nanosparking or multielectron tunneling across the Helmholtz layers between the two metal surfaces etc.[24]

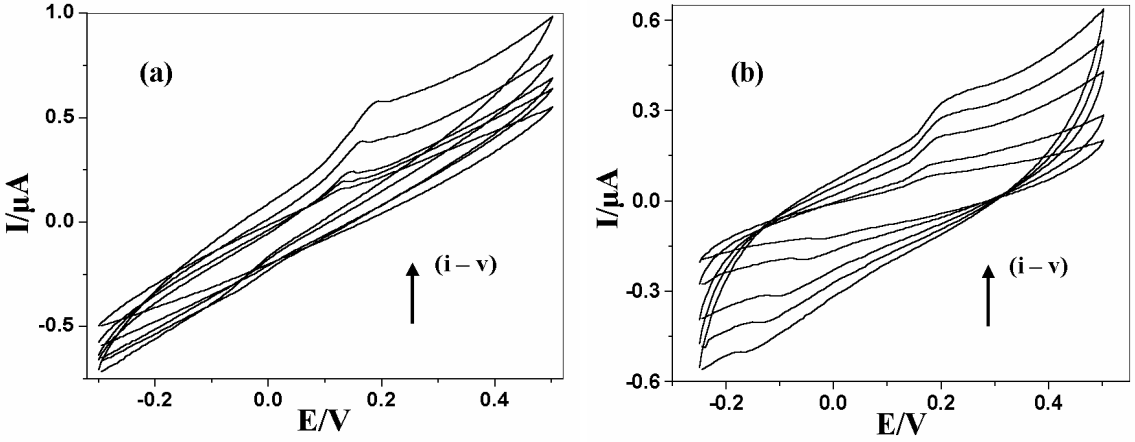

Figure 5.8 The superimposed voltammograms of particle (b) at 20, 50, 100, 200 and 500 mV/s scan rate in 0.1 N aqueous KNO_3 (a) and at 10, 20, 50, 75 and 100 mV/s in 0.1 N aqueous Na_2SO_4 using a modified Pt as working electrode, Pt flag as counter and SCE as reference (all are in 2nd scan). The peak nature or position is unaffected with the change of supporting electrolyte KCl to KNO_3 or Na_2SO_4.

In order to understand the effect of particle size on the electrochemical behaviour of DDT capped Ag nanoparticles, we intend to correlate the separation between anodic to cathodic peak potentials (ΔE_P) and $E_{1/2}$ with size. Accordingly, a representative plot of ΔE_P vs. particle size is shown in Figure 5.9 (i), where an increase of ΔE_P with increase in size is clear till 3.5-6 nm. Interestingly, Figure 5.9 (ii) shows the plot of $E_{1/2}$ vs. particle size revealing an almost constant value of $E_{1/2}$ throughout this size regime as observed for conventional materials. Further, as ΔE_P value is directly related to the kinetic

parameters, we hope the electron transfer facility may decrease with increase in size in a similar manner. Nevertheless, we have not carried out the calculation of rate constants by using dimensionless parameters, since there are several ambiguities such as large ΔE_P separation or unknown diffusion coefficients, transfer coefficients for this colloidal systems.[44] Perhaps electrochemical scanning tunneling microscopy (ESTM) can resolve the problem with its higher sensitivity compared to CV. Despite these limitations, this is the first attempt for a systematic study of size dependent redox property of Ag MPCs.

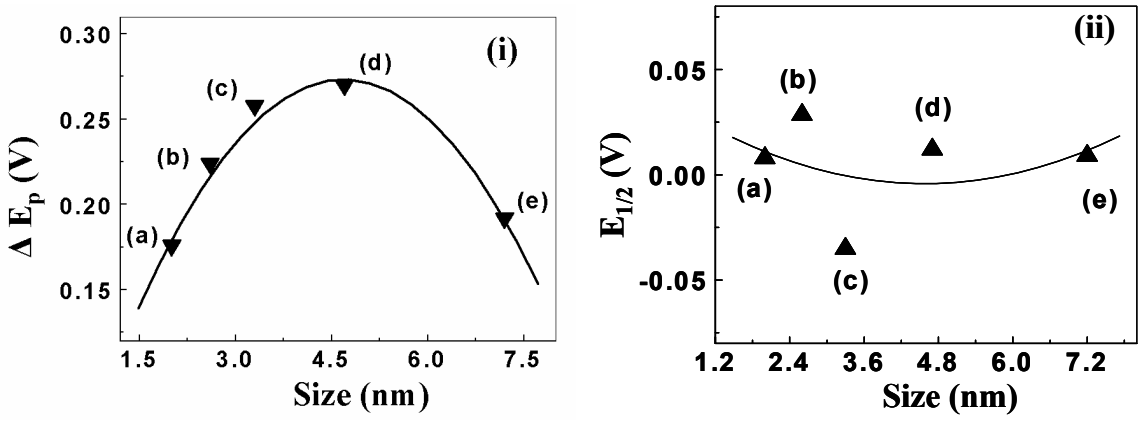

Figure 5.9 Variation of (i) ΔE_P with size of the Ag MPCs showing the maxima around 3.5-6 nm followed by a further reduction and (ii) $E_{1/2}$ vs. particle size for similar clusters ($E_{1/2}$ was calculated by averaging the cathodic and anodic peak potentials of voltammograms).

Similar correlation of size-dependent redox properties of gold nanoparticles is also important for understanding their role in catalysis.[45] For example, a recent report shows that positively charged Au_n particles are the active catalytic species for the production of water gas, while metallic gold particles are mere spectators.[45a] In this regard, we do not observe any redox activity of Au MPC films in neutral aqueous medium for variety of supporting electrolytes, like KCl, Na_2SO_4 and KNO_3, while bare gold particles show redox activity in acidic medium.[3,46] Since desorption of organic monolayer is known in such harsh conditions,[47] eventually leading to the agglomeration

of uncapped particles by electrochemical Ostwald ripening,[48] it may not be suitable for investigating such sensitive features.

5.4 Synthesis of Ag Nanoparticles Using Triethylamine

Since the physical and photophysical properties of nanoclusters are influenced by the number of atoms present in the clusters (size, shape control), size dispersion often cause large irreproducibility of cluster properties.[5,33,49] Thus a minor variation in the size distribution can cause a large discernible effect in many of the properties and consequently, one of the principal objectives of various synthetic strategies is to achieve precise control over their size, shape and dispersion.[50] Metallic nanoclusters stabilized by self-assembled monolayers (SAMs) are generally prepared by the well known Brust's synthesis.[28] In brief this method consists of a biphasic system where a reducing agent such as $NaBH_4$ along with an appropriate capping agent in an organic phase is used to generate metal nanoclusters.[28] Since $NaBH_4$ can cause sudden pH change of the aqueous phase subsequent to the generation of cluster nuclei, its adverse effect on the growth rate of the clusters can be avoided by the use of a mild reducing agent. Furthermore, the high diffusion coefficient of silver ions in water (dielectric constant, $\varepsilon \approx 80$) can accelerate the growth of the particle size and hence the use of low dielectric constant solvent is important to restrict the growth.[51]

Researchers have tried so far several routes to get precise size distribution by following various strategies including, 1) use of metal complex that serves both metal ion provider and nanocluster stabiliser,[52] 2) different solvent systems with low dielectric constant (eg. supercritical water, CO_2 and ethane),[53] 3) use of different types of capping agents, like aliphatic or aromatic thiols, amines, acids to restrict clusters growth[54] along with the use of different templates, such as miceller solutions, cavities of zeolites and pores of alumina, to restrict the clusters growth.[55] In this regard, we have carried out the synthesis of silver nanoparticles in toluene (monophasic system with low dielectric constant) with the help of a unique electron transfer agent triethylamine (TEA). Silver benzoate as a homogeneous soluble salt is selected as a metal ion provider as well to stabilize initially formed clusters by the adsorption of benzoate anions. Simultaneous use of DDT or TDA along with TEA reveals monodispersed silver nanoclusters, whereas use

of only TEA produces polydispersed clusters in the same synthetic strategy. Accordingly, cyclic voltammetric results of these clusters suggest different electrochemical properties.

5.4.1 Synthetic Procedure

Briefly, the capped nanoclusters were synthesized in toluene using TEA as an electron transfer agent and Ag-benzoate as the metal ion provider. Briefly, 1 mM Ag-benzoate was dissolved in toluene by vigorous stirring followed by addition of DDT or TDA such that metal ion to DDT/TDA concentration ratio kept 1 : 1. After half an hour vigorous stirring, 100 mM TEA (in toluene) was added dropwise and stirred overnight. The resulting colorless solution was shaken with 10 mM $NaHCO_3$ solution to remove excess benzoic acid and then the resulting toluene solution was dried under N_2 atmosphere. The particles without capping in toluene were also synthesized by using the same synthetic protocol, except using any external capping agents during synthesis.

5.4.2 Characterization of Ag Nanoparticles

The reducibility of TEA has been demonstrated by UV-visible spectroscopy (Figure 5.10a), which reveals the presence of a charge-transfer absorption band between 517 and 308 nm. This shows an orange coloration (lasting for few minutes ≈ 5-10 min) as shown by the photograph in inset 1 of Figure 5.10 (a). However, the absorption intensity in the visible region has diminished with time along with a concomitant rise of the peak intensity in the ultraviolet region (colorless solution; photograph in inset 2 of Figure 5.10a). Significantly, this later absorption at 308 nm corresponds to the surface plasmon characteristic of very smaller silver nanoclusters, which perhaps adsorbed with TEA and benzoic acid on its surface.[6,17,56] The quiescent solution produces silver mirror (≈ 7 days) due to the growth of particles of chemically identical silver clusters as shown by the photograph as inset 3 of Figure 5.10 (a).

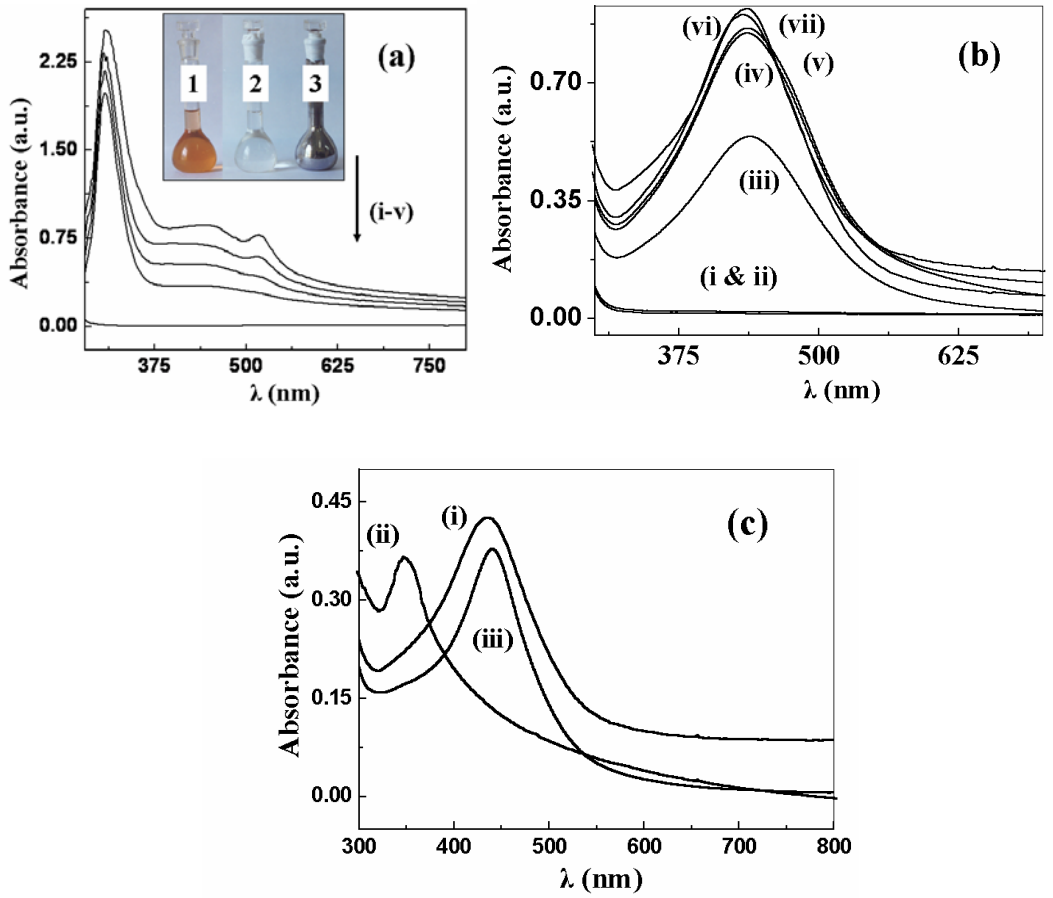

Figure 5.10 (a) Time dependent UV-visible spectra of the reduction of Ag-benzoate by triethylamine at (i) 1 min, (ii) 5 min, (iii) 10 min, (iv) 15 min superimposed with (v) UV-visible spectra of aqueous 1,4-dioxan mixture of triethylamine. (b) Time dependent reduction of Ag-benzoate by TEA in toluene without using any external capping agent at (i) 10 min, (ii) 30 min, (iii) 295 min, (iv) 385 min, (v) 450 min, (vi) 28 h and (vii) 49 h, suggesting slow growth process of these particles. (c) Superimposed UV-visible absorbance spectra of Ag nanoclusters prepared by (i) only TEA, (ii) TEA along with DDT and (iii) TEA along with TDA.

The reduction in toluene is comparatively slower than that of in neat TEA as revealed in Figure 5.10 (b), which shows the time dependent UV-visible spectra of the Ag particles synthesized in toluene without using any external capping agent. More specifically, spectra (i-vii) corresponding to 10 min, 30 min, 295 min, 385 min, 450 min, 28 h and 49 h, show the growth process of these particles. In presence of external

capping agent, like DDT or TDA, the process is much faster as shown in the superimposed UV-visible spectra in Figure 5.10 (c), where graphs (i-iii) corresponding to bare, DDT and TDA capped particles. Silver nanoclusters prepared using TEA alone (i) display a broad and unsymmetrical surface plasmon band at 434 nm with a full width at half minimum (FWHM) of *ca.* 96 nm. More significantly, this plasmon band shows a slight red shift with time (*ca.* 4 nm shift after keeping for 1 week) concomitant with a broadening, which indicates increase of the cluster size. In sharp contrast, the simultaneous use of DDT and TEA (ii) exhibits an intense and symmetric plasmon band at 348 nm with a FWHM of *ca.* 68 nm, whereas use of TDA (iii) shows plasmon peak at 440 nm with FWHM of *ca.* 67 nm.[6,17,57] In addition, these plasmon characteristics are found to be invariant for two months. The unusual shift of surface plasmon peak for the DDT capped nanoparticles might be attributed to their self-assembled nature, which can be seen clearly from the TEM micrographs.

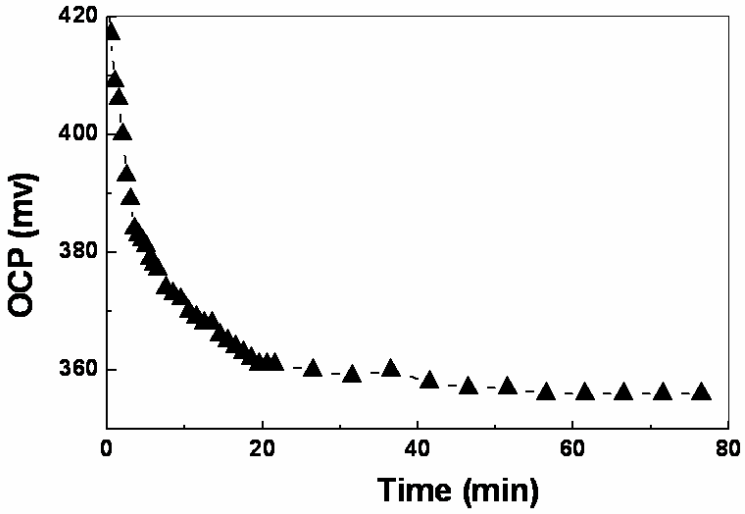

Figure 5.11 Variation of the open circuit potential (OCP) as a function of time, between the Ag/AgCl reference electrode and Ag-benzoate coated Pt working electrode, after the addition of the TEA, confirming the reducing capability of TEA.

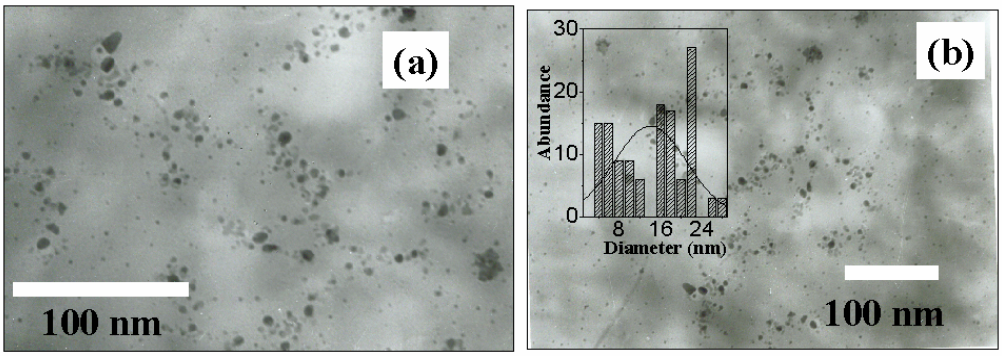

Figure 5.12 (a) and (b)TEM images of the resultant polydispersed Ag nanoparticles as a consequence of the mixing of Ag-benzoate with a broad size distrubtion (3 - 30 nm) having an average particle size of 14 ± 1 nm, inset (b) showing the corresponding histograms.

The reducing capability of TEA has also been proved by the open circuit potential (OCP) measurement experiments, where the change of OCP as a function of time is monitored between the Ag/AgCl reference electrode and Ag-benzoate coated Pt working electrode, after the addition of TEA at room temperature in 0.1 M $LiClO_4$/acetonitrile. The change of OCP with time has been shown in Figure 5.11, where the negative potential drop (60 mV) within 20 min upon the addition of 1 ml TEA to the system signifies reducing capability of TEA.[56] However, no such changes are observed in presence of either Ag-benzoate coated Pt working electrode in presence of acetonitrile or blank Pt in presence of TEA.

The formation of nanoparticles from the reaction of neat TEA and Ag-benzoate has also been confirmed from the TEM analysis as shown in Figure 5.12, which indicates polydispersed nature with a broad size distrubtion (3-30 nm) having an average particle size of 14 ±1 nm. Possibly, both TEA and benzoic acid act as weak stabilizing agents during the reduction, which causes this polydispersity. However, Figure 5.13 shows a typical TEM image of clusters prepared with TEA alone in toluene, where a polydispersed size distribution (1.4 ±0.2 to 28.6 ±0.2 nm) with an average

particle size of 4.5±0.2 nm can be seen. Perhaps, the slow reduction due to less dielectric nature of toluene could reduce the average particle size.

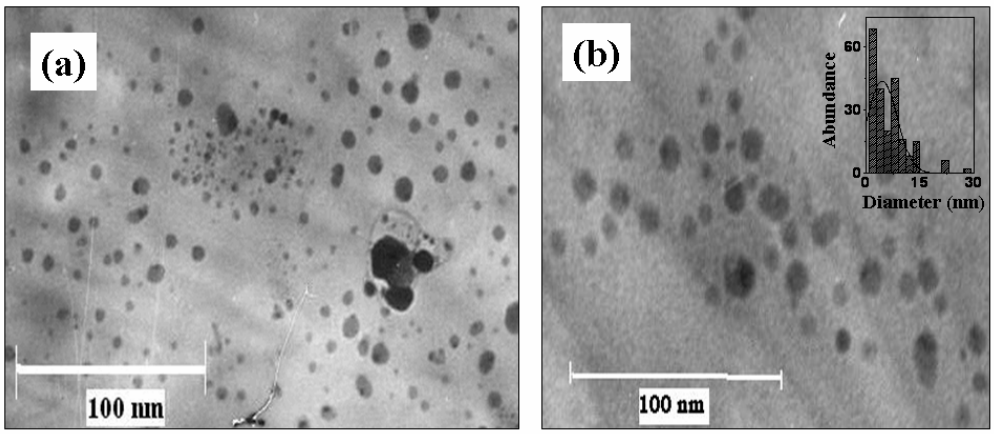

Figure 5.13 TEM images of Ag nanoclusters prepared only with TEA in tolune, showing polydispersed nature (size distribution 1.4 ± 0.2 to 28.6 ± 0.2 nm) with an average particle size of 4.5 ± 0.2nm; inset (b) showing the corresponding histograms.

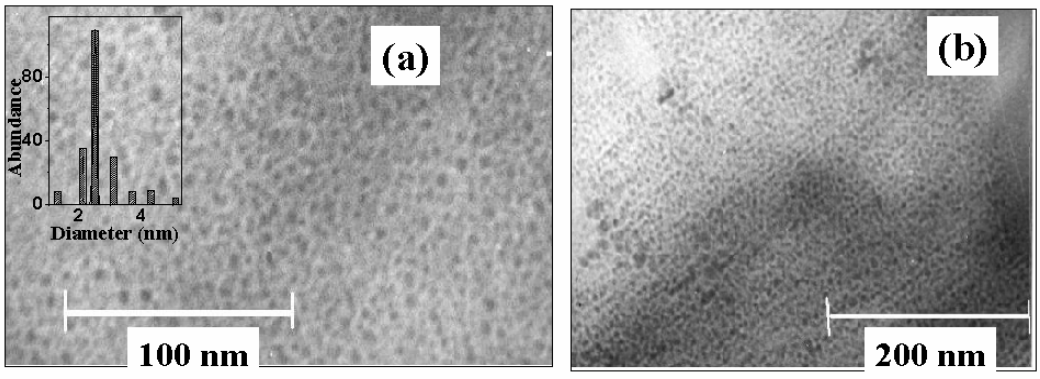

Figure 5.14 (a) TEM images of Ag nanoparticles prepared by the simultaneous use of TEA along with DDT (Inset shows the corresponding histograms), showing an average particle size of 2.5 ± 0.3 nm. (b) TEM image of the self-assembled array of Ag nanoclusters prepared by TEA along with DDT.

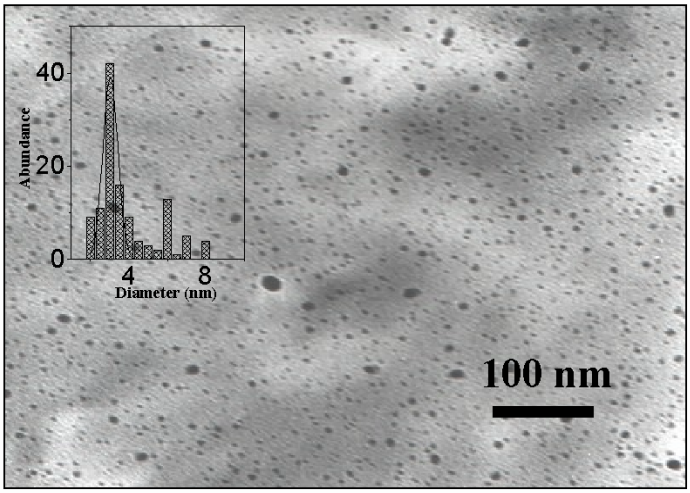

Figure 5.15 TEM images of Ag nanoparticles prepared by the simultaneous use of TEA along with TDA (Insets show the corresponding histograms), showing an average particle size of 3 ± 0.7 nm.

In comparison to these bare particles, the TEM image of clusters prepared using DDT and TEA (Figure 5.14a) simultaneously reveals the presence of a highly monodispersed distribution with an average particle size of 2.5 ±0.3 nm. Interestingly, Figure 5.14 (b) illustrates array like features for these clusters with an intercluster spacing of *ca.* 2.5 nm due to the hydrophobic interaction of long alkyl chains.[35] More specifically, the facetting observed for such arrays is attributed to the formation of highly ordered superstructures, which perhaps causes the drastic blue shift of surface plasmon peak of these particles. However, such array like features have not been observed for the case of TDA capped particles, which also reveals a nearly monodispersed nature with an average particle size of 3 ±0.7 nm (Figure 5.15).

5.4.3 Electrochemical Properties

The cyclic voltammograms (Figure 5.16) of various Ag nanoparticles in aqueous acetonitrile (10 : 100; v : v) solution of $LiClO_4$ reveals the presence of a distinct redox couple possessing unique electron transfer properties as a function of scan rate. The cyclic voltammograms are recorded by dropcasting the Ag MPCs (≈ 1mg/ml) on the Pt disc electrode (4 mm) from toluene dispersion and dried at room temperature in air prior

to experiments. For example, voltammograms shown in Figure 5.16 (a) of Ag nanoclusters prepared with TEA alone under identical conditions exhibit nearly an irreversible oxidation peak, signifying that these clusters prefer to exist in the oxidized form in solution.

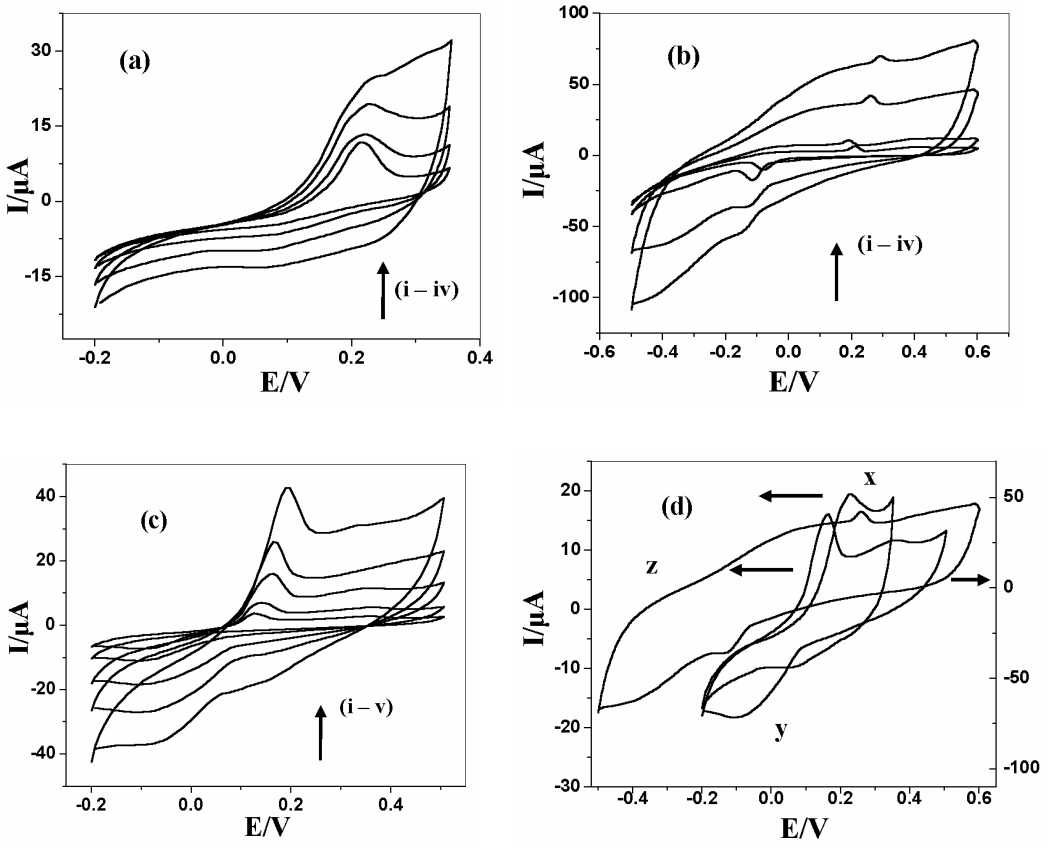

Figure 5.16 Superimposed cyclic voltammograms of silver nanoclusters of (a) bare Ag particles prepared in toluene at 10, 25, 50, 100 mv/s scan rate, (b) DDT capped Ag nanoparticles at 4, 10, 50 and 100 mV/s, (c) AgTDA particles at 10, 20, 50, 100, 200 mV/s and (d) all these three particles at 50 mV/s for comparison, showing capping dependent redox accessibility of these particles.

Table 5.2 Variations of electrochemical parameters, such as E_{Pa}, E_{Pc}, ΔE_P and $E_{1/2}$ for Ag bare, DDT and TDA capped Ag nanoclusters prepared using TEA

Ag Nanoparticles Figure 5.16 (d)	**E_{Pa} (V)**	**E_{Pc} (V)**	**ΔE_P (V)**	**$E_{1/2}$ (V)**
Bare particles (x)	0.23	0.07	0.16	0.15
TDA capped particles (y)	0.16	-0.09	0.25	0.035
DDT capped particles (z)	0.26	-0.13	0.39	0.065

Nevertheless, the presence of the alkyl chains does not obstruct the electron transfer behaviour from the core as indicated by the superimposed cyclic voltammograms in Figure 5.16 (b and c) for DDT and TDA capped clusters respectively. For example, cyclic voltammograms (b) of Ag clusters protected with DDT show a quasi-reversible couple, whereas the oxidation peak is prominent for (c) TDA capped particles. The anodic (E_{Pa}) and cathodic (E_{Pc}) peak potentials, peak separations (ΔE_P) and $E_{1/2}$ have been summarized in Table 5.2 for the CV at 50 mV/s scan rate [Figure 5.16 (d)]. Since ΔE_P is directly related to the feasibility of donation and acceptance of electrons to the Fermi level, the nature of the capping agent is perhaps responsible for such a behaviour. More specifically, the ΔE_P increases in the order of bare particles (x) < TDA capped particles (y) < DDT capped particles (z), which might be attributted to the stronger Ag-S bond as compared to the Ag-N bonds. The highly packed nature of DDT capped Ag particles as observed in UV-visible and TEM might also be responsible for such higher ΔE_P values due to the interlinking of clusters. These unique differences in the redox features of silver nanoclusters by simple tuning of capping agent can be effectively utilised in suitable electrocatalytic reactions with Ag_n /Ag_n^+ mediators.

5.5 Conclusions

We have demonstrated the size dependent electrochemical behaviour of DDT protected silver nanoclusters. Our study reveals that the redox behaviour is affected by size as in agreement with the theoretical calculations based on the Kubo gap. More specifically, the separation between oxidation and reduction peaks (ΔE_P) increases with the increase in size and after reaching a maxima (3.5-6$\pm$0.5 nm) followed by a further decline. As the kinetic parameters are directly related with ΔE_P values, the electron transfer facility decreases with the increase in size in a similar manner. Further, we have also demonstrated the reducing capability of TEA to form highly monodispersed silver nanoclusters in an anhydrous organic medium, which shows that the selection of the capping agent plays a critical role in controlling the redox accessibility. These unique redox features of capped silver nanoclusters can be effectively utilized in suitable electrocatalytic synthesis with Ag_n /Ag_n^+ mediators.

5.6 References

1. Colvin, V. L.; Schlamp, M. C.; Alivisatos, A. P. *Nature* **1994**, *370*, 354.
2. Schmid, G.; Baumle, M.; Greekens, M.; Heim, I.; Osemann, C.; Sawitwoski, T. *Chem. Soc. Rev.* **1999**, *28*, 179.
3. Shipway, A. N.; Katz, E.; Willner, I. *Chem. Phys. Chem.* **2000**, *1*, 18.
4. Rao, C. N. R.; Kulkarni, G. U.; Thomas, P. J.; Edwards, P. P. *Chem. Soc. Rev.* **2000**, *29*, 27.
5. Schmid, G.; Chi, L. F. *Adv. Mater.* **1998**, *10*, 515.
6. Henglein, A. *Chem. Rev.* **1989**, *89*, 1861.
7. Montano, P. A.; Purdum, H.; Shenoy, G. K.; Morrison, T. I.; Schulze, W. *Surf. Sci.* **1985**, *156*, 228.
8. Buffat, P.; Borel, J.–P. *Phys. Rev. A* **1976**, *13*, 2287.
9. Castro, T.; Reifenberger, R.; Choi, E.; Andres, R. P. *Phys. Rev. B* **1990**, *42*, 8548.
10. Mueller, U.; Schmidt-Ott, A.; Burtscher, H. Z. *Phys. B* **1988**, *73*, 103.
11. Schleicher, B.; Burtscher, H.; Siegmann, H. C. *Appl. Phys. Lett.* **1993**, *63*, 1191.
12. Schmidt-Ott, A.; Schurtenberger, P., Siegmann, H. C. *Phys. Rev. Lett.* **1980**, *45*, 1284.
13. Link, S.; El-Sayed, M. *Annu. Rev. Phys. Chem.* **2003**, *54*, 331.
14. Plieth, W. J. J. *Phys. Chem.* **1982**, *86*, 3166.
15. Plieth, W. J. *Surf. Sci.* **1985**, *156*, 530.
16. Fisher, L. R.; Israelachvili, J. N. *J. Colloid Interface Sci.* **1981**, *80*, 528.
17. Henglein, A. *J. Phys. Chem.* **1993**, *97*, 5457.
18. Henglein, A. *Top. Curr. Chem.* **1988**, *141*, 113.
19. Henglein, A.; Mulvaney, P.; Linnert, T. *Faraday Dis. Chem. Soc.* **1991**, *92*, 31.
20. Henglein, A. *In Modern Trends of Colloid Science in Chemistry and Biology*; Eicke, H.-F., Ed.; Berkhäuser-Verlag: Basel, Switzerland, 1985; p 126.
21. Henglein, A. *Ber. Bunsen-Ges. Phys. Chem.* **1977**, *81*, 556.
22. Henglein, A. *Chem. Phys. Lett.* **1989**, *154*, 473.
23. Tausch-Treml, R.; Henglein, A.; Lilie, J. *Ber. Bunsen-Ges. Phys. Chem.* **1978**, *82*, 1335.

24. Ung, T.; Giersig, M.; Dunstan, D.; Mulvaney, P. *Langmuir* **1997**, *13*, 1773.
25. (a) Sudrik, S. G.; Maddanimath, T.; Chaki, N. K.; Chavan, S. P.; Chavan, S. P.; Sonawane, H. R.; Vijayamohanan, K. *Org. Lett.* **2003**, *5*, 2355. (b) Ung, T.; Liz-Marzan, L. M.; Mulvaney, P. *J. Phys. Chem. B* **1999**, *103*, 6770. (c) Fan, F-R. F.; Bard, A. J. *J. Phys. Chem. B* **2002,** *106*, 279.
26. (a) Petit, C.; Lixon, P.; Pileni, M. P. *J. Phys. Chem.* **1993**, *97*, 12974. (b) Heath, J. R.; Knobler, C. M.; Leff, D. V. *J. Phys. Chem. B* **1997**, *101*, 189. (c) Quinn, B. M.; Prieto, I.; Haram, S. K.; Bard, A. J. *J. Phys. Chem. B* **2001**, *105*, 7474. (d) Sampaio, J. F.; Beverly, K. C.; Heath, J. R. *J. Phys. Chem. B* **2001**, *105*, 8797.
27. Cohen, S. G.; Parola, A.; Parsons Jr., G. H. *Chem. Rev.* **1973**, *73*, 141.
28. Brust, M.; Walker, M.; Bethell, D.; Schiffrin, D. J.; Whyman, R. *J. Chem. Soc. Chem. Commun.* **1994**, 801.
29. Whetten, R. L.; Khoury, J. T.; Alvarez, M. M.; Murthy, S.; Vezmar, I.; Wang, Z.; Stephens, P. W.; Cleveland, C. L.; Luedtke, W. D.; Landman, U. *Adv. Mater.* **1996**, *8*, 428.
30. Wilcoxon, P.; Martin, J. E.; Provencio, P. *J. Chem. Phys.* **2001**, *115*, 998.
31. Templeton, A. C.; Wuelfing, W. P.; Murray, R. W. *Acc. Chem. Res.* **2000**, *33*, 27.
32. Mie, G. *Ann. Phys. (N.Y.)* **1908**, *25*, 377.
33. Link, S.; El-Sayed, M. *J. Phys. Chem. B* **1999**, *103*, 4212.
34. (a) Prasad, B. L. V.; Stoeva, S. I.; Sorensen, C. M.; Klabunde, K. J. *Langmuir* **2002**, *18*, 7515. (b) He, S.; Yao, J.; Jiang, P.; Shi, D.; Zhang, H.; Xie, S.; Pang, S.; Gao, H. *Langmuir* **2001**, *17*, 1571. (c) Sakata, J. K.; Dwoskin, A. D.; Vigorita, J. L.; Spain, E. M. *J. Phys. Chem. B* **2005**, *109*, 138. (d) Harfenist, A.; wang, Z. L.; Alvarez, M. M.; Vezmar, I.; Whetten, R. L. *J. Phys. Chem.* **1996**, *100*, 13904.
35. Sandhyarani, N.; Resmi, M. R.; Unnikrishnan, R.; Vidyasagar, K.; Ma, S.; Antony, M. P.; Selvaam, G. P.; Visalakshi, V.; Kumar, N. C.; Pandian, K.; Tao, Y. T.; Pradeep, T. *Chem. Mater*. **2000**, *12*, 104.
36. Aslam, M.; Mulla, I. S.; Vijayamohanan, K. *Langmuir* **2001**, *17*, 7487.
37. Brown, L. O.; Hutchison, J. E. *J. Phys. Chem. B* **2001**, *105*, 8911.
38. Snyder, R. G.; Strauss, H. L.; Elliger, C. A. *J. Phys. Chem.* **1982**, *86*, 5145.
39. Hostetler, M. J.; Stokes, J. J.; Murray, R. W. *Langmuir* **1996**, *12*, 3604.

40. Bain, C. D.; Troughton, E. B.; Tao, Y. T.; Eval, J.; Whitesides, G. M.; Nuzzo, R. G. *J. Am. Chem. Soc.* **1989**, *111*, 321.
41. Bourg, M.-C.; Badia, A.; Lennox, R. B. *J. Phys. Chem. B* **2000**, *104*, 6562.
42. Colvin, V. L.; Goldstein, A. N.; Alivisatos, A. P. *J. Am. Chem Soc.* **1992**, *114*, 5229.
43. (a) Sabatini, E.; Rubinsten, I. *J. Phys. Chem.* **1987**, *91,* 2974. (b) Green, S. J.; Pietron, J. J.; Jennifer, J. S.; Hostetler, M. J.; Vu, H.; Wuelfing, W. P.; Murray, R. W. *Langmuir* **1998**, *14*, 5612.
44. Bard, A. J.; Faulkner, L. R. *Electrochemical Methods, Fundamentals and Applications; 2nd ed.* John Wiley & Sons: New York, 2001.
45. (a) Fu, Q.; Saltsburg, H.; Flytzani-Stephanopoulos, M. *Science* **2003,** *301*, 935. (b) Jin, Y.; Shen, Y.; Dong, S. *J. Phys. Chem. B* **2004**, *108*, 8142.
46. (a) Bharathi, S.; Nogami, M.; Lev, O. *Langmuir* **2001**, *17*, 2602. (b) Jin, Y.; Dong, S. *J. Phys. Chem. B* **2003**, *107*, 13969.
47. (a) Quinn, B. M.; Kontturi, K. *J. Am. Chem. Soc.* **2004**, *126*, 7168. (b) Kakiuchi, T.; Usui, H.; Hobara, D.; Yamamoto, M. *Langmuir* **2002**, *18*, 5231.
48. Redmond, P. L.; Hallock, A. J.; Brus, L. E. *Nano Lett.* **2005**, *5*, 131.
49. (a) Kim, S.-H.; Medeiros-Ribeiro, G.; Ohlberg, D. A. A.; Williams, R. S.; Heath, J. R. *J. Phys. Chem. B* **1999**, *103*, 10341. (b) Mirkin, C. A. *Inorg. Chem.* **2000**, *39*, 2258.
50. (a) Alvarez, M. M.; Khoury, J. T.; Schaaff, T. G.; Shafigullin, M. N.; Vezmar, I.; Whetten, R. L. *J. Phys. Chem. B* **1997**, *101*, 3706. (b) Ahmadi, T. S.; Wang, Z. L.; Green, T. C.; Henglein, A.; El-Sayed, M. A. *Science* **1996**, *272*, 1924.
51. Ziegler, K. J.; Doty, R. C.; Johnston, K. P.; Korgel, B. A. *J. Am. Chem. Soc.* **2001**, *123*, 7797.
52. (a) Manna, A.; Imae, T.; Iida, M.; Hisamatsu, N. *Langmuir* **2001**, *17*, 6000. (b) Bunge, S. D.; Boyle, T. J.; Headley, T. J. *Nano Lett*. **2003**, *3*, 901. (c) Jana, N. R.; Peng, X. G. *J. Am. Chem. Soc.* **2003**, *125*, 14280.
53. (a) Shah, P. S.; Holmes, J. D.; Doty, R. C.; Johnston, K. P.; Korgel, B. A. *J. Am. Chem. Soc.* **2000**, *122*, 4245. (b) Ziegler, K. J.; Doty, R. C.; Johnston, K. P.; Korgel, B. A. *J. Am. Chem. Soc.* **2001**, *123*, 7797. (c) Cason, J. P.; Khambaswadkar, K.; Roberts, C. B. *Ind. Eng. Chem. Res.* **2000**, *39*, 4749. (d) Cason, J. P.; Roberts, C. B. *J. Phys. Chem. B* **2000**, *104*, 1217. (e) Ohde, H.;

Rodriguez, J. M.; Ye, X.-R.; Wai, C. M. *J. Chem. Soc. Chem. Commun.* **2000**, 2353. (f) Dimitrijevic, N. M.; Bartels, D. M.; Jonah, C. D.; Takahashi, K.; Rajh, T. *J. Phys. Chem. B* **2001**, *105*, 954. (g) Sun, Y. P.; Guduru, R.; Lin, F.; Whiteside, T. *Ind. Eng. Chem. Res.* **2000**, *39*, 4663.

54. Daniel, M.-C.; Astruc, D. *Chem. Rev.* **2004**, *104*, 293.
55. (a) Manna, A.; Kulkarni, B. D.; Bandyopadhyay, K.; Vijayamohanan, K. *Chem. Mater.* **1997**, *9*, 3032. (b) Jacobs, G.; Ghadiali, F.; Pisanu, A.; Borgna, A.; Alvarez, W. E.; Resasco, D. E. *Appl. Catal. A* **1999**, *188*, 79. (c) Yoo, J. W.; Hathcock, D.; El-Sayed, M. A. *J. Phys. Chem. A* **2002**, *106*, 2049.
56. Creighton, J. A.; Eadon, D. G. *J. Chem. Soc. Faraday Trans* **1991**, *87*, 3881.
57. Paik, W.-k.; Eu, S.; Lee, K.; Chon, S.; Kim, M. *Langmuir* **2000**, *16*, 10198.

Chapter 6

Conclusions and Future Prospects

This last chapter deals with the significant conclusions of the present study. It also outlines several general limitations of such monolayer protected hybrid materials along with the suggestions for their improvements. Several other promising areas and challenges are also discussed to stretch the applications of nanoscale materials in view of the fundamental and technological interests of physicists, chemists, biologists and engineers. Finally, some of the future prospects and precautions of the nanotechnology are presented within the broad perspective of fabricating the next generation devices.

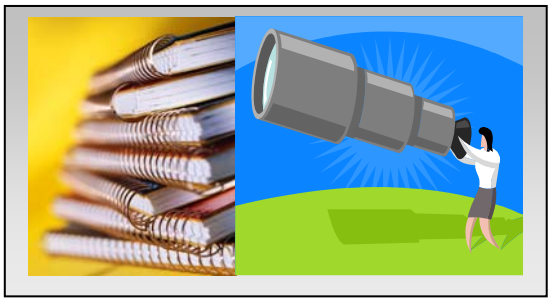

The recent progress in the understanding of size-dependent properties of functionalized metallic nanoparticles has been phenomenal in achieving the novel functions as revealed in this study and also by several other reports.[1-3] Monolayer protected nanoclusters (MPCs), especially of Au and Ag, are ideal in this respect, since they offer tremendous flexibility to modulate their structures and properties.[1-3] Apart from the core size manipulation, the ability to tune the organic capping molecule's properties renders these hybrid materials as indispensable functional units for nanotechnology.[1-3] Accordingly, an array of such clusters is considered as the closest experimental systems to justify quantum theories in low-dimensions, fascinating many material scientists to "create" designer materials for the rapidly emerging applications in molecular electronics.[1-3]

Although plenty of methods are available for the synthesis of Au MPCs, several limitations still persist. For example, the most widely used Brust's method[4] is only effective for synthesizing 1 - 5 nm sized particles, while several other limitations, like the presence of large polydispersity, the use of quaternary-ammonium salts as phase transfer catalysts (troublesome to remove, which may contaminate the particle surface), higher costs for the phase transfer agents and necessary tedious methods for purification and size sieving, need to be improved. In this regard, we have developed a low cost process excluding the use of any quaternary-ammonium salts as phase transfer catalysts for the size selective preparation of moderately monodispersed, larger Au MPCs. These particles are capable of forming large area superstructures as evident from TEM and the effect of temperature on such ordered assemblies (3.72 nm sized Au MPCs) have revealed temperature induced diffusion limited phase transition, involving nonequilibrium fractal structure.

Single electron transfer behaviour or quantized double layer charging (QDL) of MPCs has been identified as one of the key features for their use as building blocks for nanoelectronic circuit components.[3b,5] Although, QDL feature has been vastly investigated for smaller MPCs ($2r < 3$ nm, where 'r' is radius) using STM/STS and voltammetric techniques, no such reports are available to understand such behaviour for larger sized MPCs. Subsequently, we are the first to demonstrate the single electron

charging behaviour of larger sized Au MPCs (3.72 nm and 4.63 nm) using several electroanalytical and other techniques.

Although several experimental and theoretical reports of MPC-MPC and MPC-solvent interactions are known,[2-3] no adequate studies have been performed to illustrate the interaction of charged MPCs. Accordingly, the diffusion coefficients are calculated for 4.63 nm sized Au MPCs at its various charge state using chronoamperometry and impedance techniques. Interestingly, these results demonstrate that the presence of higher charge enables these particles to diffuse faster along with concomitant enhancement in their electron transfer rates, indicating the importance of repulsive interaction as compared to that of the neutral MPCs. These initial results could add new useful information for understanding the interactions of charged MPCs in solution under electric field, where the steric interaction is also active due to long aliphatic chains.

The electrochemical features of five differently sized Ag MPCs (2-7 nm) have been investigated to correlate size effect on the redox activity of nanometer scale particles. This study reveals that the redox behaviour of Ag core is affected by size, showing an initial increase of the separation between oxidation and reduction peaks (ΔE_p) in cyclic voltammograms with increasing size till a maxima (3.5-6 nm) followed by further decrease. Further, a single-step method of the preparation of Ag MPCs in nonaqueous medium has been demonstrated along with their electrochemical features.

How can soft and subtle organic molecules help to form order in inorganic nanomaterials, like metallic and semiconducting clusters? The answer to this question mainly lies in their ability to form self-assembled monolayers (SAM) on selected structures by their adsorption characteristics.[6] This gives remarkable stability to MPCs of many noble metals and semiconductors, facilitating their use in real device applications. A unified understanding of the electromagnetic interaction of nanoclusters with tunable size-scales would unravel several fundamental questions of photon-solid interactions within a fully quantum electrodynamics framework.[1] In addition, investigations of resonant absorption phenomena as a function of material dimensionality, symmetry and excitonic structure would give several surprising photonic and electronic applications in the coming years. With such new nanostructures containing artificially designed ligands acting as molecular interconnectors, even supplementing some of the cluster properties,

the prospect for the field should continue to be bright in the next decade, leading eventually more and more applications of monolayer protected clusters.

Despite steady progress during the couple of years, several key questions and challenges remain to be addressed, as illustrated bellow:

1) Adequate strategies have to be developed to create or modulate nanostructures in a predefined fashion.

2) A proper understanding of the role of commonly used materials for the preparation of nanostructures as well as the interface of nanoparticle/organic or biomolecules need to be evaluated. Since the toxicity is also expected to increase for nanomaterials compared to its bulk, these assessments may help to extend their applications in several social sectors.

3) Suitable methods to prepare shape selective nanostructures, composites of organic-inorganic or inorganic-bio materials are to be developed, since they often have novel functions.

4) Assembling various shaped and high aspect ratio nanostructures in well defined domain to understand their coupled optical, electrical or magnetic response is still a daunting challenge.

5) The understanding of the nucleation, growth, kinetics and thermodynamics of these structures are necessary to resolve several fundamental issues related to the structural manipulation of these materials.

In addition to these challenges, several issues related to the limitations of these hybrid materials, like stability, dynamics of organic monolayer in presence of external stimulations and structural modulation due to change of field gradient, have to be further understood thoroughly before their utilization. Accordingly, the understanding of the properties of high aspect ratio or various shaped nanostructures is also necessary to unravel the electron transfer features at reduced dimensions, especially, for electronic applications. Additionally, special initiation is also required to create bio-hybrid materials, which is expected to find immense utility in bio-nanotechnology, especially, if they are

coupled with suitable biomolecules.

A detailed understanding of the fundamental aspects of these materials would enable several fascinating nanoelectronic circuitry, while composites would be used as materials for making smart devices. Several technologies would be expected to revolutionize including, information technology, computer technology, biotechnology and energy technology along with their impact on social sectors, like health, food, water and medicine concerning our daily life.[7] However, the social and environmental issues of nanotechnology have to be critically examined before delivering technology as several frightening consequences are proposed recently.[8] Accordingly, the cost and energy conservation for creating nanoarchitectures have also to be reduced along with ensuring their reproducibility. Finally, as a consequence of nanotechnology, we would hope an unprecedented change in our socio-economic scenario in the coming decades.

References

1. (a) Schmid, G.; Baumle, M.; Greekens, M.; Heim, I.; Osemann, C.; Sawitwoski, T. *Chem. Soc. Rev.* **1999**, *28*, 179. (b) Rao, C. N. R.; Kulkarni, G. U.; Thomas, P. J.; Edwards, P. P. *Chem. Soc. Rev.* **2000**, *29*, 27. (c) Burda, C.; Chen, X.; Narayanan, R.; El-Sayed, M. A. *Chem. Rev.* **2005**, *105*, 1025.
2. (a) Daniel, M.-C.; Astruc, D. *Chem. Rev.* **2004**, *104*, 293 and references therein. (b) Shenhar, R.; Rotello, V. M. *Acc. Chem. Res.* **2003**, *36*, 549 and references therein. (c) Templeton, A. C.; Wuelfing, M. P.; Murray, R. W. *Acc. Chem. Res.* **2000**, *33*, 27 and references therein. (d) Thomas, K. G.; Kamat, P. V. *Acc. Chem. Res.* **2003**, *36*, 888.
3. (a) Collier, C. P.; Vossmeyer, T.; Heath, J. R. *Annu. Rev. Phys. Chem*. **1998**, *49*, 371 and references therein. (b) Chen, S.; Ingram, R. S.; Hostetler, M. J.; Pietron, J. J.; Murray, R. W.; Schaaff, T. G.; Khoury, J. T.; Alvarez, M. M.; Whetten, R. L. *Science* **1998**, *280*, 2098. (c) Collier, C. P.; Saykally, R. J.; Shiang, J. J.; Henrichs, S. E.; Heath, J. R. *Science* **1997**, *277*, 1978.
4. Brust, M.; Walker, M.; Bethell, D.; Schiffrin, D. J.; Whyman, R. *J. Chem. Soc. Chem. Commun.* **1994**, 801.
5. (a) Chen, S.; Murray, R. W.; Feldberg, S. W. *J. Phys. Chem. B* **1998**, *102*, 9898. (b) Hicks, J. F.; Templeton, A. C.; Chen, S.; Sheran, K. M.; Jasti, R.; Murray, R. W.; Debord, J.; Schaaff, T. G.; Whetten, R. L. *Anal. Chem.* **1999**, *71*, 3703.
6. Love, J. C.; Estroff, L. A.; Kriebel, J. K.; Nuzzo, R. G.; Whitesides, G. M. *Chem. Rev.* **2005**, *105*, 1103 and references therein.
7. *Societal Implications of Nanoscience and Nanotechnology*; Roco, M. C., Bainbridge, W. S. Eds. National Science Foundation Report: Arlington, VA; Kluwer Academic Publishers: Boston, MA, 2001.
8. Roco, M. C., Karn, B. *Environ. Sci. Technol. A - Pages* **2005**, *39*, 106A and reference there in.

List of Publications

1. *"Preparation and electrical characterisation of dodecanethiol monolayer protected silver nanoclusters"*

   M. Aslam, **N. K. Chaki**, I.S. Mulla and K. Vijayamohanan, ***Appl. Surf. Sci.*** 2001, 182, 338.

2. *"Application of self-assembled monolayers in materials chemistry"*

   N. K. Chaki, M. Aslam, J. Sharma and K. Vijayamohanan, ***Proc. Indian Acad. Sci. (Chem. Sci.)*** 2001, 113, 659.

3. *"Self-assembled monolayers as a tunable platform for biosensor applications"*

   N. K. Chaki and K. Vijayamohanan, ***Biosens. Bioelectron.*** 2002, 17, 1.

4. *"Single phase preparation of monodispersed silver nanoclusters using a unique electron transfer and cluster stabilising agent, triethylamine"*

   N. K. Chaki, S. G. Sudrik, H. R. Sonawane and K. Vijayamohanan, ***Chem. Commun.*** 2002, 76.

5. *"Device applications of self-assembled monolayers and monolayer Protected Nanoclusters"*

   M. Aslam, **N. K. Chaki**, J. Sharma and K. Vijayamohanan, ***Curr. Appl. Phys.*** 2003, 3, 115.

6. *"Monolayer-coated Au and Ag nanoclusters"*

   N. K. Chaki, T. G. Gopakumar, M. Aslam and K. Vijayamohanan, ***Encyclopedia of Nanoscience and Nanotechnology (ENN)***, *American Scientific Publishers, Vol. 5*, 861.

7. *"Evidence for the involvement of silver nanoclusters during the Wolff rearrangement of α –diazoketones"*

   S. G Sudrik, T. Maddanimath, **N. K. Chaki**, S. P. Chavan, S. P. Chavan, H. R. Sonawane and K. Vijayamohanan, ***Org. Lett.*** 2003, 5, 2355.

8. *"Effect of chain length on the tunneling conductance of gold quantum dots at room temperature"*

   N. K. Chaki, T. G. Gopakumar, T. Maddanimath, M. Aslam, and K. Vijayamohanan, ***J. Appl. Phys.*** 2003, 94, 3663. (Erratum: in *J. Appl. Phys.* 94, 7379*)*

9. *"Effect of chain length and the nature of the monolayer on the electrical behaviour of hydrophobically organized gold clusters"*

   N. K. Chaki, M. Aslam, I. S. Mulla and K. Vijayamohanan, ***J. Phys. Chem. B*** 2003, *107,* 13567.

10. *"Controlled interlinking of Au and Ag nanoclusters using 4-aminothiophenol as Molecular Interconnects"*

J. Sharma, **N. K. Chaki**, A. B. Mandale, R. Pasricha and K. Vijayamohanan, ***J. Colloid Interface Sci.*** 2004, 272, 145.

11. *"Size dependent redox behavior of monolayer protected silver nanoparticles (2-7 nm) in aqueous medium"*

    N. K. Chaki, J. Sharma, A. B. Mandle, I. S. Mulla, R. Pasricha and K. Vijayamohanan, ***Phys. Chem. Chem. Phys.*** 2004, 6, 1304.

12. *"Tuning the aspect ratio of silver nanostructures: The effect of solvent mole fraction and 4-aminothiophenol concentration"*

    J. Sharma, **N. K. Chaki**, S. Mahima, R. G. Gonnade, I. S. Mulla and K. Vijayamohanan, ***J. Mater. Chem.*** 2004, 14, 970.

13. *"Quantized double layer charging of dodecanethiol protected larger Au nanoclusters: Combined investigations using differential pulse voltammetry, cyclic voltammetry and impedance technique"*

    N. K. Chaki, B. Kakade and K. P. Vijayamohanan, ***Electrochem. Commun.*** 2004, *6*, 661.

14. *"Highly resolved quantized double layer charging of relatively larger dodecanethiol passivated gold quantum dots"*

    N. K. Chaki, B. Kakade, J. Sharma, S. Mahima, S. K. Haram and K. P. Vijayamohanan, ***J. Appl. Phys.*** 2004, 96, 5032.

15. *"Single electron charging features of larger dodecanethiol protected gold nanoclusters: electrochemical and STM studies"*

    N. K. Chaki, P. Singh, C. V. Dharmadhikari and K. P. Vijayamohanan, ***Langmuir*** 2004, 20*,* 10208.

16. *"Temperature induced phase transitions of the ordered superlattice assembly of Au nanoclusters"*

    N. K. Chaki and K. Vijayamohanan, ***J. Phys. Chem. B*** 2005, 109, 2552.

17. *"Silver-nanocluster redox-couple promoted non-classical electron transfer: an efficient electrochemical generation of a-ketocarbene intermediates from a-diazoketones"*

    S. G. Sudrik, **N. K. Chaki**, V. B. Chavan, S. P. Chavan, T. Maddanimath, S. P. Chavan, H. R. Sonawane and K. Vijayamohanan, (Submitted to *Chem. Eur. J.)*.

18. *"Interactions of relatively larger (4.63 nm) monolayer protected gold clusters during quantized double layer charging"*

    N. K. Chaki, B. Kakade, K. P. Vijayamohanan, P. Singh and C. V. Dharmadhikari, (Submitted to *Langmuir*).

19. *"Electrochemical organization of monolayer protected gold nanoclusters on single-walled carbon nanotube bundles"*

    Mahima S., **N. K. Chaki**, J. Sharma, B. Kakade, R. Pasricha, Lakshminarayanan V., A. M. Rao and K. Vijayamohanan, (Submitted to *Langmuir*).

Erratum